Developing combination therapy to improve viral vector cancer vaccine efficacy



Laurine Noblecourt

Linacre College

University of Oxford

A thesis submitted for the degree of

Doctor of Philosophy

Hilary Term 2023



LUDWIG CANCER RESEARCH

To Dr David Fournand

Developing combination therapy to improve viral vector cancer vaccine efficacy

Abstract

The development of effective cancer immunotherapies presents several major challenges that must be considered. Notably, it requires the generation of specific immune responses against cancer cells whilst counteracting the highly immunosuppressive mechanisms of the tumour microenvironment. Vaccination strategies consisting of heterologous prime/boost with recombinant chimpanzee adenovirus (ChAdOx1) and modified vaccinia Ankara (MVA) has been shown to induce high magnitude of specific cytotoxic $CD8^+$ T cell responses against cancer antigens. Despite these specific anti-tumour immune responses, in therapeutic pre-clinical studies, ChAdOx1/MVA vaccination has shown limited tumour control. Undeniably, it is necessary to develop treatment combination strategies to overcome the multitude of mechanisms that cancer cells use to escape the immune system. However, to successfully combine therapies and generate synergy, research is needed to comprehend their respective therapeutic mechanisms, and determine the optimal sequence of treatment administration. In this study, we tested a novel combination of three treatments comprising of ChAdOx1/MVA vaccines, a chemotherapy regimen based on Carboplatin and Paclitaxel (CarboTaxol) and anti-programmed cell death protein-1 (PD1) therapy. We discovered that this triple combination therapy exhibited strong therapeutic effects in murine tumour models, outperforming corresponding double-treatment combinations. Importantly, we demonstrated that, at a specific therapeutic window, CarboTaxol increased the magnitude of the specific $CD8^+$ T cell response induced by ChAdOx1/MVA. We explored the mechanisms behind the adjuvant effect of CarboTaxol and discovered that this chemotherapy induced T cell factor 1 (TCF1) in $CD8^+$ T cells in both mouse models and human samples. Lastly, we showed the importance of the timing of anti-PD1 administration, relative to vaccination, and established that CarboTaxol allowed more flexibility for anti-PD1 administration. This study brings into light new roles for CarboTaxol and holds promises for testing this combination strategy in clinical trials.

Acknowledgments

Firstly, I would like to thank my supervisors Prof. Benoit Van Den Eynde and Dr Carol Leung for their support throughout my PhD. Thank you for giving me the amazing opportunity to work and learn under your guidance. Thank you for believing in me, I will be forever grateful for what you allowed me to achieve during those 4 years. Thank you, Dr Carol Leung, I would not be the scientist that I am today without the teaching and time you granted me.

I was immensely privileged to work with incredible and passionate lab-mates who also shaped the scientist that I am today. Thank you for being the source of incredible discussions and for having been there for me no matter what (e.g. through an apocalyptic COVID-19 pandemic). Thank you, Dr James McAuliffe, for your teaching, your unconditional support, all the laughs you brought into the lab when it was mostly us against DBA/2 mice, at the beginning. Thank you, Dr Vineeth Chandrasekar, for all the great conversations we had and the moral support you offered me. Thank you, Vinny Pereira-Almeida, for your infinite kindness, your consistent help and for all the pens I stole from you. Thank you, Amanda Wicki, for your incredible help in and out of the lab, I will always seek for more of our morning gossips during blood sampling. Thank you, Emily Steffke and Julia McCarthy, for your help but also for the absolute joy and happiness you brought into the VDE lab! Lastly arrived but not least, thank you, Dr Silvia Panetti, for having helped so much already and for adding your fire to our science debate. I am grateful for the bond we share and will forever keep with me the multitude of happy memories in the lab and around Oxford!

Outside my lab, I had the chance to meet, Joseph Chadwick, Lucija Fleisinger and Ashvina Segaran, on the day we all started our PhDs. Thank you all for being these amazing friends, it has been such a force having you by my side.

Merci à mes amis, en France ou autour du monde, particulièrement Mathilde, Camille et Anna, savoir que vous êtes toujours là pour moi après toutes ces années est une chance absolue, merci pour votre incroyable soutien. Merci, Félicien, de toujours demander

les dernières nouvelles pour t'assurer que je tenais bon ! Thank you, Mona, for the kind messages and all our road trips around the UK.

Thank you, Carolyn and Paul Cass, for your support and kindness during the tough months of writing this thesis! Special thanks to Milly and Alfie for the many drooling hugs!

Thank you, Dr Steven Cass for being this bright, beautiful, safe island, which gave me strength when needed and kept me happy despite everything. You are an inspiration to excel, and you indubitably made me progress beyond what you realise. Thank you for your unconditional patience and kindness, I would not have finished this PhD with all my sanity without you!

Merci à ma famille qui a été mon ancre durant ces années de thèse. Avoir été loin les uns-des-autres aura été difficile mais ne vous a pas empêché de m'offrir votre soutien et amour inconditionnel. Tout particulièrement, merci Alain et Jocelyne Fournand, mon papi et ma petite mamie, d'avoir été les merveilleuses personnes que vous êtes, toujours là malgré la distance. Merci à Emma, ma sœur, pour ton énergie et ta joie de vivre que je reçois même de loin, mais surtout merci pour ta patience. Merci à Kilian, mon petit frère, pour ta constante et incroyable gentillesse. Et par-dessus tout, un incommensurable merci à ma petite maman, Sandra Noblecourt, merci d'avoir cru en moi aussi inconditionnellement, je ne pourrais jamais mettre sur page ce que je te dois, mais cette thèse, si elle est là, c'est grâce à toi.

Merci Dr David Fournand, mon parrain, l'aspiration à faire de grandes choses, de toujours questionner, de me surpasser, je te la dois. Tu nous as quitté trop tôt, et pourtant, tu as été là pour chacun des choix que j'ai effectués dans ma vie, incluant la décision de venir à Oxford, travailler sur ce fabuleux projet. Cette thèse, elle est pour toi.

Thank you, Dr David Fournand, my godfather, the aspiration to do wonderful things, to always question, to do my best, I owe it to you. You left us too early, and yet, you have been there for every single choice I have made in my life, including the decision to come here, in Oxford, working on this incredible project. This thesis is for you.

Table of Contents

Abstract ..... **ii**

Acknowledgments ..... **iii**

List of figures ..... **ix**

List of tables ..... **xiv**

List of abbreviations ..... **xv**

Chapter I: Introduction **1**

1.1 Tumour immunology 2

1.1.1 Brief history behind tumour immunology 2

1.1.2 Tumour Elimination 5

1.1.3 Tumour equilibrium 24

1.1.4 Tumour escape 25

1.2 Cancer Treatments 32

1.2.1 Standard of care 32

1.2.2 Immunotherapy 36

1.3 Thesis Aims 48

Chapter II: Materials and methods **49**

2.1 Materials 50

2.1.1 Reagents and kits 50

2.1.2 Buffers and media 51

2.1.3 Cell lines 53

2.1.4 Vaccines 53

2.1.5 Therapeutic monoclonal antibodies 53

2.1.6 Chemotherapies 54

2.1.7 Mice 54

2.1.8 Peptides 54

2.1.9 Flow cytometry antibodies 55

2.1.10 Tetramer 61

2.1.11 Instruments and software 61

2.2 Methods 63

2.2.1 ChAdOx1 and MVA viral vectors 63

2.2.2 Cell culture 63

2.2.3 Collection of tissues 64

2.2.4 ELISAs 67
2.2.5 Co-culture 68
2.2.6 In vivo mouse studies 70
2.2.7 Staining for flow cytometry 73
2.2.8 Flow cytometry panel gating strategy 75
2.2.9 Statistical analysis 81
Chapter III: ChAdOx1/MVA vaccines synergise with CarboTaxol and anti-PD1 for enhanced immunogenicity, tumour control and survival. 83
3.1 Introduction 84
3.2 Chapter aims 88
3.3 Improving ChAdOx1/MVA efficacy against 15V4T3 syngeneic tumour model in DBA/2 mice 89
3.3.1 15V4T3 tumour model: Experimental design 89
3.3.2 Tumour growth and mouse survival evaluation 90
3.3.3 Evaluation of ChAdOx1/MVA-P1A immunogenicity and its modulation by the combination of treatments 93
3.4 Impact of the triple combination of treatments on the TME, spleen and blood 100
3.4.1 Evaluation of the TME infiltrated $CD8^+$ T cells 100
3.4.2 Investigation of long-term impact on systemic $CD8^+$T cells 103
3.5 Improving ChAdOx1/MVA-E6-E7 mediated tumour control and immunogenicity against TC-1 syngeneic tumour model in C57BL/6 mice 106
3.5.1 TC-1 tumour model: experimental design 106
3.5.2 TC-1 tumour growth evaluation and mouse survival 107
3.5.3 ChAdOx1/MVA-E6-E7 immunogenicity and modulation by CarboTaxol 109
3.6 Discussion 111
3.6.1 Synergy of a novel combination therapy 111
3.6.2 Impact of the triple combination therapy on $CD8^+$ T cell phenotypes 112
Chapter IV: Effects of CarboTaxol on the immune system and tumour microenvironment 115
4.1 Introduction 116
4.2 Chapter Aims 120
4.2 CarboTaxol has early effects on the systemic and tumour-infiltrated innate immune cells in tumour bearing mice 121
4.2.1 Chemotherapy has short-term impact on myeloid cells 121

4.2.2 In vivo depletion of PMN-MDSCs using in vivo anti-GR1 antibody does not improve tumour control nor vaccine immunogenicity 129

4.3 CarboTaxol impacts $CD8^+$ and $CD4^+$T cells in tumour bearing and tumour free mice 135

4.3.1 TCF1 expressing $CD8^+$ and $CD4^+$T cells are increased after CarboTaxol treatment in tumour bearing mice 135

4.3.2 CaboTaxol-treated tumour free mice show an expansion of $CD8^+$ and $CD4^+TCF1^+$ cells 144

4.4 Potential link between TCF1 expression in $CD8^+$ T cells and $CD11b^+Ly6G^+$ cell depletion after CarboTaxol treatment 148

4.4.1 A strong correlation exists between TCF1 expression in $CD8^+$ T cells and $CD11b^+Ly6G^+$ cell depletion 148

4.4.2 Anti-GR1 antibody does not induce TCF1. 153

4.5 CarboTaxol acts as an adjuvant for ChAdOx1/MVA vaccine platform: importance of the timing of treatments 156

4.5.1 CarboTaxol improves vaccine immunogenicity in tumour free mice 156

4.5.2 CarboTaxol induces activation of cDC2 but not cDC1 159

4.6 Viral vector vaccines induce expansion of $CD11b^+$ $Ly6G^+$ cells 163

4.7 CarboTaxol impacts on the cytokine environment 168

4.7.1 CarboTaxol decreases systemic level of IL12/23(p40) 168

4.7.2 CarboTaxol-treated groups showed decreased basal IL12/23(p40) production by blood monocytes 172

4.7.3 Investigation of IL12/23(p40) impact on TCF1 expression in T cells 174

4.8 Discussion 176

4.8.1 Short-term effects of CarboTaxol 176

4.8.2 CarboTaxol is an adjuvant for viral vector vaccines 179

4.8.3 Link between TCF1 expression and $CD11b^+Ly6G^+$ cell depletion 182

Chapter V: Translational aspect of the triple combination therapy: emphasis on the importance of timing of treatment 185

5.1 Introduction 186

5.2 Chapter aims 189

5.3 Investigating different time points for anti-PD1 treatment 190

5.3.1 Tumour control and survival upon different time points of anti-PD1 treatment combined with ChAdOx/MVA and CarboTaxol 190

5.3.2 Evaluating the impact of anti-PD1 treatment timing on the magnitude of the P1A specific response 193

5.4 Impact of CarboTaxol on the triple combination with pre-vac anti-PD1 195

5.4.1 CarboTaxol induces TCF1 expression in $CD8^+$ T cells regardless of the anti-PD1 treatment timing 195

5.4.2 Evaluation of potentially sub-primed $CD8^+$ T cells 198

5.4.3 Depletion of $Ly6G^+$ $CD11b^+$ cells occurs in the new regimen of triple combination of treatments 201

5.5 *TCF7* expression is increased after 3 cycles of Carboplatin and Paclitaxel in ovarian cancer patients 202

5.6 Discussion 206

5.6.1 New triple combination regimen efficacy and potential mechanism of action 206

5.6.2 Ovarian cancer patients display higher *TCF7* expression and increase proportion of *TCF7*+ $CD8^+$ T cells after 3 cycles of CarboTaxol 209

Chapter VI: Summary and future work 212

6.1 Synergy of a triple combination of treatments: ChAdOx1/MVA, anti-PD1 and CarboTaxol 213

6.1.1 Summary 213

6.1.2 Limitations and future plans 214

6.2 CarboTaxol is an adjuvant for ChAdOx1/MVA: mechanism investigation. 215

6.2.1 Summary 215

6.2.2 Limitations and future plans 219

6.3 Importance of CarboTaxol in extending anti-PD1 therapeutic window: translational aspect of the triple combination 220

6.3.1 Summary 220

6.3.2 Future plans and limitations 221

6.4 Project limitation: complexity of translating drugs to the clinic. 222

Appendix 224

REFERENCES 229

List of figures

Figure 1.1 Cancer Immunity Cycle adapted from Chem and Mellman, Immunity, 2013. **p7**

Figure 2.1 Gating strategy for intracellular cytokine staining by flow cytometry. **p75**

Figure 2.2 Gating strategy for general phenotyping panel. **p76**

Figure 2.3 Gating strategy for T cell phenotyping panel. **p77**

Figure 2.4 Gating strategy for T cell exhaustion and tetramer panel. **p78**

Figure 2.5 Gating strategy for potential MDSCs with the Myeloid cell panel. **p78**

Figure 2.6 Gating strategy for DC phenotyping staining. **p79**

Figure 2.7 Gating strategy for IL12/23(p40) expression in different innate cells. **p80**

Figure 3.1 Timeline of tumour study and harvest and treatment regimens of each group tested. **p89**

Figure 3.2 Tumour growth control efficacy of ChAdOx1/MVA-P1A vaccination in combination with chemotherapy and anti-PD1 treatments. **p91**

Figure 3.3 Survival of mice vaccinated with ChAdOx1/MVA-P1A in combination with chemotherapy and anti-PD1 treatments. **p92**

Figure 3.4 P1A-specific $CD8^+$ T-cell responses 12 days post ChAdOx1/MVA P1A vaccination**. p95**

Figure 3.5 P1A-specific $CD8^+$ T-cell responses 5 days post ChAdOx1/MVA P1A vaccination. **p97**

Figure 3.6 P1A-specific $CD4^+$T-cell responses 5 days post ChAdOx1/MVA P1A vaccination. **p98**

Figure 3.7 T cell infiltration and $CD8^+$ T cell phenotype in the TME of 15V4T3 tumour bearing mice. **p102**

Figure 3.8 $CD8^+$ T cell activation phenotype in the spleen and blood of 15V4T3 tumour bearing mice. **p104**

Figure 3.9 Stemness status of total and P1A-specific $CD8^+$ T cell in the spleen and blood of 15V4T3 tumour bearing mice. **p105**

Figure 3.10 Timeline of tumour study and treatment regimens of each group tested in C57BL/6 mice. **p106**

Figure 3.11 Tumour growth control efficacy of ChAdOx1/MVA-E6/E7 vaccination in combination with chemotherapy and anti-PD1 treatments. **p107**

Figure 3.12 Survival of mice vaccinated with ChAdOx1/MVA-E6/E7 in combination with chemotherapy and anti-PD1 treatments. **p108**

Figure 3.13 P1A-specific $CD8^+$ T-cell responses 10 days post ChAdOx1/MVA-E6/E7 vaccination. **p110**

Figure 4.1 Timeline of tumour harvest and treatment regimens of every group tested. **p121**

Figure 4.2 Myeloid cells gating strategy in blood of 15V4T3 DBA/2 tumour bearing mice. **p122**

Figure 4.3 Myeloid cells in blood of 15V4T3 DBA/2 tumour bearing mice. **p123**

Figure 4.4 Myeloid cells in BM, spleen and tumour of 15V4T3 DBA/2 tumour bearing mice. **p125**

Figure 4.5 $CD11b^+$GR1hiLy6G+ in blood of TC-1 C57BL/6 tumour bearing mice. **p126**

Figure 4.6 $CD11b^+Ly6G^+$ cell immunosuppressive functions on $CD8^+$ T cell proliferation. **p128**

Figure 4.7 Timeline of tumour harvest and treatment regimens of every group tested. **p129**

Figure 4.8 One injection of anti-GR1 combined with ChAdOx1/MVA-P1A in tumour bearing DBA/2 mice. **p130**

Figure 4.9 Timeline of tumour harvest and treatment regimens of every group tested. **p131**

Figure 4.10 Combination of ChAdOx1/MVA-P1A with anti-GR1 injections in tumour bearing DBA/2 mice. **p132**

Figure 4.11 $CD11b^+Ly6G^+$ depletion after sequential injections of anti-GR1.**p133**

Figure 4.12 CarboTaxol impacts $CD8^+$ T cell phenotype in the blood, spleen and TME of 15V4T3 DBA/2 tumour bearing mice. **p136**

Figure 4.13 CarboTaxol impacts stem-like progenitor-exhausted $CD8^+$ T cell phenotype in the TME of 15V4T3 DBA/2 tumour bearing mice. **p138**

Figure 4.14 CarboTaxol impacts $CD4^+$T cell phenotype in the blood, spleen and TME of 15V4T3 DBA/2 tumour bearing mice. **p140**

Figure 4.15 CarboTaxol impacts $TCF1^+PD1^+CD4^+$ T cell phenotype in the TME of 15V4T3 DBA/2 tumour bearing mice. **p141**

Figure 4.16 CarboTaxol impact on central memory and effector memory $CD8^+$ an $CD4^+$T cells of 15V4T3 DBA/2 tumour bearing mice. **p143**

Figure 4.17 CarboTaxol impacts $CD8^+$ T cell phenotype in the blood, spleen and TME of tumour free DBA/2 mice. **p145**

Figure 4.18 CarboTaxol impacts $CD4^+$T cell phenotype in the blood, spleen and TME of tumour free DBA/2 mice. **p146**

Figure 4.19 CarboTaxol impacts central memory $CD8^+$ an $CD4^+$T cells in the spleen and BM of tumour free DBA/2 mice. **p147**

Figure 4.20 Myeloid cells in spleen, BM, and blood after CarboTaxol treatment of tumour free DBA/2 mice. **p148**

Figure 4.21 Correlation between $CD11b^+Ly6G^+$ cells proportion and TCF1 expression in $CD8^+$ T cells in 15V4T3 tumour model. **p150**

Figure 4.22 Correlation between $CD11b^+Ly6G^+$ cells proportion and TCF1 expression in $CD8^+$T cells in tumour free DBA/2 mice. **p151**

Figure 4.23 Anti-GR1 does not significantly expand $TCF1^+$ $CD8^+$ T cells in the spleen, blood and TME of 15V4T3 DBA/2 tumour bearing mice. **p155**

Figure 4.24 Combination of ChAdOx1/MVA-P1A with CarboTaxol in tumour free DBA/2 and C57BL/6 mice. **p157**

Figure 4.25 The timing of CarboTaxol treatment is of major importance to improve the priming and boosting of the ChAdOx1/MVA-P1A vaccines. **p158**

Figure 4.26 Dendritic cell populations in tumour free and tumour bearing mice after CarboTaxol. **p160**

Figure 4.27 cDC phenotype in tumour free and tumour bearing mice after CarboTaxol. **p162**

Figure 4.28 Effect of ChAdOx1 and MVA viral vectors on the immune system at 12-, 24- and 28-hours post injection in DBA/2 mice. **p163**

Figure 4.29 Effect of CarboTaxol on viral-vector vaccine granulocytes recruitment in DBA/2 tumour free mice. **p165**

Figure 4.30 Effect of CarboTaxol on viral-vector vaccine granulocytes recruitment and vaccine immunogenicity in C57BL/6 tumour free mice. **p167**

Figure 4.31 IL12/23(p40) levels after CarboTaxol in tumour free and tumour bearing DBA/2 mice. **p169**

Figure 4.32 IL-1β and IFNα levels after CarboTaxol in tumour free and tumour bearing DBA/2 mice. **p171**

Figure 4.33 IL12/23(p40) basal production in the blood is decreased after CarboTaxol in $CD11b^+$ $Ly6C^+$ and $CD11b^+Ly6G^+$ cells in DBA/2 mice. **p173**

Figure 4.34 Anti-IL12/23(p40) in vivo antibody does not expand $TCF1^+$ cells in $CD8^+$ T cells. **p174**

Figure 5.1 Timeline and treatment groups for the evaluation of the pre-vac anti-PD1 new regimen in 15V4T3 tumour model. **p190**

Figure 5.2 The pre-vac anti-PD1 treatment improves tumour growth control only when combined with CarboTaxol+ChAdOx1/MVA-P1A vaccination in 15V4T3 tumour bearing DBA/2 mice. **p191**

Figure 5.3 The pre-vac anti-PD1 treatment improves mouse survival only when combined with CarboTaxol+ChAdOx1/MVA-P1A vaccination in 15V4T3 tumour bearing DBA/2 mice. **p192**

Figure 5.4 The pre-vac anti-PD1 treatment increases P1A-specific $CD8^+$ T cells only when combined with CarboTaxol+ ChAdOx1/MVA-P1A vaccination in 15V4T3 tumour bearing DBA/2 mice. **p193**

Figure 5.5 Timeline and treatment groups for harvest to investigate the pre-vac anti-PD1 new regimen in 15V4T3 tumour model. **p195**

Figure 5.6 TME of mice treated with the triple combination with pre-vac anti-PD1 show expanded TCF1 expressing cells due to the CarboTaxol treatment. **p197**

Figure 5.7 Mice treated with the triple combination with pre-vac anti-PD1 display increase of TCF1 expressing cells in the spleen and blood due to the CarboTaxol treatment. **p198**

Figure 5.8 Pre-vac anti-PD1 expands $CD38^+PD1^+$ $CD8^+$ T cells in the TME of tumour bearing mice. **p200**

Figure 5.9 $CD11b^+Ly6G^+$ cells are depleted in the triple combination with pre-vac anti-PD1. **p201**

Figure 5.10 Carboplatin and paclitaxel increase TCF1 expression in epithelial ovarian cancer patients. **p203**

Figure 5.11 Carboplatin and paclitaxel increase TCF1 expression in Central memory $CD8^+$ T cells in epithelial ovarian cancer patients. **p205**

Figure 6.1 Potential mechanisms for CarboTaxol adjuvant function. **p218**

Appendix Figure 1. Evolution of the magnitude of the P1A specific CD8 response overtime: comparison between Vaccine+CarboTaxol and Triple combination groups. **p224**

Appendix Figure 2. Prophylactic ChAdOx1/MVA-P1A combined with CarboTaxol promotes a better protection than vaccine alone against 15V4T3 in DBA/2 mice. **p225**

Appendix figure 3. Evolution of innate cell population after ChAdOx1 and CarboTaxol. **p226**

List of tables

Table 1. List of reagents and kits 50
Table 2. ACK lysis buffer for mouse blood (10X, ph7.3) 51
Table 3. Tumour dissociation buffer 51
Table 4. Complete RPMI 51
Table 5. 15V4T3 culture media 52
Table 6. T cell media for co-culture 52
Table 7. FACS buffer 52
Table 8. MACS buffer 53
Table 9. Cell lines 53
Table 10. Viral vector vaccines 53
Table 11. Monoclonal antibodies 53
Table 12. chemotherapies 54
Table 13. Mouse strains 54
Table 14. Cytokine panel 55
Table 15. General panel 56
Table 16. T cell panel for Harvest 57
Table 17. T cell exhaustion panel and tetramer for late Harvest 58
Table 18. Myeloid cell panel for Harvest 59
Table 19. Dendritic cell panel for Harvest 60
Table 20. IL12/23(p40) panel 61
Table 21. Instruments 61
Table 22. Software 62
Table 23: Peptide sequences in P1A library used for T-cell stimulation assays. 227

List of abbreviations

APC	Antigen-presenting cell
BLIMP-1	B-lymphocyte-induced maturation protein 1
CarboTaxol	Carboplatine+Paclitaxel
ChAdOx1	Chimpanzee adenovirus Oxford 1
CIC	Cancer immunity cycle
CM	Central memory
CPI	Checkpoint inhibitor
DAMP	Damage associated molecular pattern
DC	Dendritic cell
DNA	Deoxyribonucleic acid
EM	Effector memory
ER	Endoplasmic reticulum
ERAAP	ER aminopeptidase associated with antigen processing
FACS	Flourescence activated cell sorting
g	Gram
i.m.	Intramuscular
i.p.	Intraperitoneal
ICB	Immune checkpoint blockade
ICS	Intracellular cytokine staining
IFN	Interferon
Ii	Invariant chain
IL	interleukin
IMDM	Iscove's modified Dulbecco's medium
IU	Infectious units
MAGE	melanoma-associated antigen
MDSC	Myeloid derived suppressor cell
mg	Milligram
MHC	Major histocompatibility complex
MVA	Modified vaccinia Ankara
NYESO-1	New York oesophageal squamous cell carcinoma 1
PAMP	Pathogen associated molecular pattern
PBMC	Peripheral blood mononuclear cells
PBS	Phosphate buffered saline
PD1	Programmed cell death protein 1
PDL1	Programmed death ligand 1
PFU	Plaque forming units
PRR	Pattern recognition receptor
RNA	Ribonucleic acid
RPMI 1640	Roswell Park Memorial Institute 1640
s.c	Subcutaneous

SEM	Standard error of the mean
STAT	Signal transducer and activator of transcription
TAP	Transporter associated with antigen presentation
TAPBP	TAP binding protein
TAPBPR	TAP binding related protein
TCF1	T cell factor 1
TCR	T cell receptor
Tet	Tetramer
TiLs	Tumour infiltrating lymphocytes
Tim3	T cell immunoglobulin and mucin domain-containing protein 3
TMD	Transmembrane domain
TME	Tumour microenvironment
TNF	Tumour necrosis factor
tPA	Tissue plasminogen activator
Treg	Regulatory T cell
WHO	World Health Organization

Chapter I: Introduction

1.1 Tumour immunology

1.1.1 Brief history behind tumour immunology

Cancer is one of the leading causes of death worldwide, representing nearly 1 out of 6 deaths in 2020, according to the world health organisation[1,2]. This can be accounted for the fact that cancer carries multi-dimensional dysfunctions, making it extremely challenging to treat[3]. Cancer was first described as a genetic disease which develops from the acquisition of random genetic mutations in somatic cells. These mutations lead to the loss of cellular functions and contribute to an acquired uncontrolled proliferation and expansion. Thereby, cancer cells invade healthy tissue at the primary site of growth, but eventually can colonise other parts of the body in a spreading process known as metastasis. This metastatic process is usually the cause of patient death due to the failure of multiple organ functions[4,5]. However, cancer is not only a genetic disease, and its expansion as well as its evolution also depends on its environment. Hence, due to its genetic and environmental variables, cancer presents an extreme intra- and inter-individual heterogeneity. This heterogeneity makes this disease particularly challenging to treat and still requires for the expansion of very diverse treatment strategies.

Because cancer cells are an expansion of the body's cells, they are considered part of the individual "self" which, by definition, protect them from recognition by the immune system[6]. Hence, for a long time, the immune system was not considered part of the environmental factors that shape cancer. In fact, the concept of tumour immunology which encompasses the complex interactions between the immune system and cancer cells, has been understood relatively recently[6]. Although this tumour immunology concept is complex, its full understanding will allow the development of better anti-cancer strategies.

Long before the first experiment investigating the concept of tumour immunology, clinical evidence had brought to light a role for the immune system in cancer resolution. In the late 19th century, the surgeon William Coley noticed that patients with erysipelas (a streptococcal skin infection) displayed remission of sarcomas. Based on this observation, he injected patients with a mixture of heat-inactivated *Streptococcus pyogenes* and *Bacillus prodigious*, which resulted in long-term cancer remission[7]. This highlighted the potential role of the immune system, which, activated against the infection, indirectly contributed to cancer remission. However, it took a century to the scientific community to prove the existence of anti-tumour immunity. In fact, the possibility of an immune response specific against cancer cells was mostly ignored until critical experiments were done in the 1950s. Among those, Foley, Prehn, and Main highlighted for the first time the involvement of the immune system in protecting from tumour development. Briefly, in chemically induced sarcomas in murine models, the animals resected from a first tumour challenge showed increase resistance to tumour development after a second challenge; highlighting a protection from the first challenge [8–11]. In 1957, based on these early experiments, Burnet and Thomas attributed this protection to the immune system and postulated the concept of immunosurveillance for the first time[12]. Later, observations were made in HIV and immunosuppressed patients, where the immune system is compromised. The occurrence of tumours in those patients was greater than in healthy individuals, highlighting the active role of the immune system in preventing tumour development, hence the existence of immunosurveillance[13,14]. One breakthrough in tumour immunology, was the publication by the Schreiber group in 2001, which confirmed the importance of adaptive immune cells, and the inflammatory cytokine interferon (IFN)γ as extrinsic tumour suppressor[15]. Importantly, this study also highlighted for the first time the role of the immune system in the selection of more aggressive cancer cells, called immunoediting[16]. Hence, highlighting

the conflicted role of the immune system which can be pro-tumorigenic by shaping the tumour cells into more aggressive neoplasia. This research led to the theory of the three Es, published in 2004, which is still accepted today[17]. The three Es refers to the three steps of tumour progression in relation to the interactions between immune cells and tumour cells. These 3 phases consist of:

-Elimination, where immunosurveillance and elimination of tumour cells occur.

-Equilibrium, where the process of immunoediting starts.

-Escape, where the tumour cells hide from immunosurveillance and start metastasising.

Finally, in 2011, a paper highlighting the hallmarks of cancer included immunoediting and the escape of immunosurveillance as a contributor of tumour progression[3]. In the following sections, I will expand on how the conflicted interactions between cancer cells and the immune cells function and evolve throughout the 3 Es stages.

1.1.2 Tumour Elimination

Tumour elimination is the process also known as immunosurveillance. It occurs when the immune system prevents the development of malignancies by the early detection of lesions and clearance of any abnormal cells. Tumour cell elimination involves the activation of both innate and adaptive immunity. The steps leading to the tumour elimination by the immune system are finely regulated in a spatio-temporal manner that have been described as the cancer immunity cycle (CIC)[16,18].

1.1.2.1 Cancer Immunity Cycle: Overview

In a review published in 2013, Chen and Mellman depicted for the first time the CIC. The CIC describes in seven steps the mutual feeding cycle between cancerous cell killing and immune cell activation (see figure 1.1). At the origin of the CIC lies the genetic instability of abnormal cells which die or become dysfunctional with uncontrolled proliferation [4,5]. This uncontrolled expansion of abnormal cells in the surrounding tissue along with spontaneous cell deaths cause the production of inflammatory signals named damaged associated molecular pattern (DAMPs)[18]. Moreover, DAMPs recruit innate cells among which are natural killer (NK) cells. NK cells are essential actors in early immunosurveillance with their innate ability to directly kill cancer cells which feed these inflammatory signals[19]. This cell death process and DAMP production will lead to the initiation of the CIC. Briefly, this cycle involves the following steps[18]:

1- Recruitment of innate cells, attracted by DAMPs, and the release of tumour associated antigens (TAA).
2- The recruited innate cells consist of antigen presenting cells (APC): dendritic cells (DC) and macrophages. These cells, predominately DCs, uptake TAAs.

3- APCs are the main actors in antigen presentation and T cell activation. They relate the information of the presence of aberrant cells to the adaptive immune system: CD8+, $CD4^+$T cells and by extension, B cells.
4- These adaptive immune cell types then traffic to the tumour sites.
5- The activated lymphocytes subsequently infiltrate the tumour microenvironment (TME).
6- Lymphocytes and particularly $CD8^+$T cells specifically recognise cancer cells.
7- $CD8^+$ T cells directly kill cancer cells, supported by $CD4^+$T cells and B cells.

This expansion of tumour cell death in the TME will in turn lead to more DAMP signals and TAA spreading, starting this CIC from step 1 over again (fig 1.1). In the following sections, I will discuss in detail all the steps of the CIC to fully comprehend the mechanisms that are in place during the tumour elimination phase.

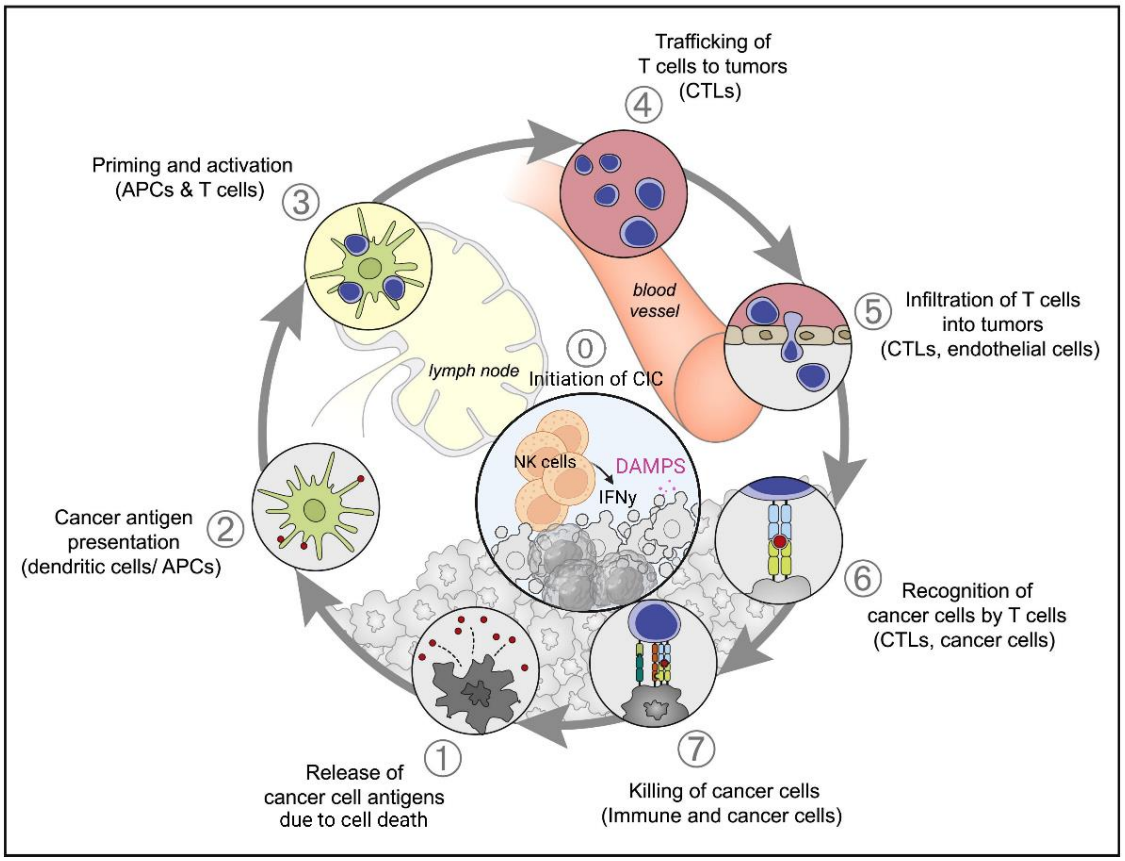


Figure 1.1 Cancer Immunity Cycle adapted from Chem and Mellman, Immunity, 2013. At the origin of the interaction between cancer cells and immune cells there is cell death and DAMPs. Mutated body cells either die from the acquired mutations or are recognised by NK cells and killed through direct killing or IFNγ. This leads to the production of DAMPs which in turn recruits innate cells including DCs (0). Due to the cell death process, there is a release of TAA (1). The APCs uptake and present TAA (2). Specific T cells are selected, primed, and activated through DCs presentation (3). T cells migrate to the tumour sites (4) and infiltrate the TME (5). Due to their specific TCR, they are able to recognise TAA presented through MHCI or MHCII molecules on tumour cell surface (6). T cell can be directly or indirectly cytotoxic to cancer cells after recognition (7).

1.1.2.2 Innate immunity: steps 0 to 3 of the CIC

NK cells and IFNγ : involvement in the initiation of the CIC (step 0,1)

NK cells are one of the first lines of defence after a cancer lesion occurs[19]. They will be attracted by DAMPs to the tumour site. NK cells get activated by the downregulation of major histocompatibility complex I (MHCI) and the upregulation of inducible MHCI-related (MIC)-A and MIC-B, ligands for the activating receptor NKG2D [20]. Once activated, NK cells can directly kill cancer cells by the release of perforin/granzyme, or the expression of Fas ligand (Fas-L) which trigger apoptosis of the tumour cells expressing Fas receptor. NK cells also produce IFNγ which is toxic to cancer cells [15,21]. IFNγ directly promotes apoptosis in tumour cells expressing IFNγ receptor-Janus pathway, by inducing caspase-1 and -8 through signal transducer and activator of transcription 1 (STAT1) signaling[15,22]. IFNγ also acts indirectly by activating other innate cells[21]. These first lines of defence will enhance DAMP signals by expanding tumour cell death. The DAMPs will then recruit other innate cells named APCs, particularly important to activate T cells.

DCs and macrophages: major actors from step 1 to 3 of the CIC

Macrophages and DCs are involved in the acquisition, processing, and presentation of TAAs to T cells. They are recruited to the TME via the increasing inflammatory signals which occur in the tumour bed. DCs and macrophages recognise DAMPs such as DNA, RNA released from dying cells through pattern recognition receptors (PRRs) which leads to their activation[23,24].

Dendritic Cells

DCs will differentiate from antigen-capture focused immature DCs, with high phagocytic activity, to activated mature DCs that have better migratory ability and higher

expression of MHC and co-stimulatory signals (i.e CD80/CD86 and cytokines). This maturation process will be dependent on the environmental cues present in the tissue of origin (e.g TME)[25]. Once activated, DCs are the main innate population to present antigen and activate T cells through their expression of MHC molecules and co-stimulatory signals. Four major DC subsets have been described[26]:

- Conventional DCs (cDC) are distinguished between cDC1 and cDC2. cDC2s are involved in CD4 helper T (Th) cell type 2 (Th2) differentiation as well as Th17 responses, but their overall role in cancer immunity is not fully understood, partly due to their very limited number in the TME[27]. Opposingly cDC1s, have been shown to have a major role in anti-tumour responses. Indeed, cDC1s have been correlated with increase patient survival and better response to therapy[28,29]. They are responsible for the priming of $CD8^+$ T cells due to an ability to cross-present antigens. Cross presentation is the process where external antigen in peripheral tissue (usually loaded on MHCII) are loaded and presented onto MHCI[26]. However, there is evidence that a crosstalk between DC subsets occurs and that cDC1s alone are not sufficient in promoting the anti-tumour response[27].
- Monocytic DCs (mDC) are derived from monocytes ($Ly6C^+$ in mice). They have been shown to have the highest capacity in antigen uptake, giving them an advantage for antigen presentation[30]. Furthermore, blockade of monocytes entry into the lymph node (LN) and tumour sites by immunostimulatory agent monosodium urate crystals, completely abrogated mDC differentiation and anti-tumour response [31]. Interestingly, $Ly6C^+$CD103+ mDCs have been shown to have the ability to cross-present to $CD8^+$ T cells[32]. Finally, mDCs have been shown to promote T cell survival and proliferation in the tumour bed[31].

- Plasmacytoid DCs (pDC): their role in anti-tumour immunity is less established. They mostly express MHCII and cannot cross-present [28]. They have been correlated with poor prognosis in breast cancer patients and ovarian carcinoma due to the generation of IL-10 producing $CD8^+$ regulatory T cells[28,33]. Interestingly, they are known to produce inflammatory cytokines in response to viral threats such as type I IFNs (such as IFNα). This ability to produce IFNs has been shown to improve cDC1 cross presentation to T cells[29].

Collectively, the main subsets involved in anti-tumour response are cDC1s and mDCs which can both colonise the tumour initiation site, uptake antigens, migrate to draining lymph node (dLN) as well as activating $CD8^+$ T cells, a major cell subset in the anti-tumour response.

Macrophages

There are two origins of macrophages: embryonic, which will give rise to tissue resident macrophages, and, later in life, bone marrow derived monocytes which circulate in the blood and colonise tissue to become macrophages. Macrophages are found throughout the body and act as major sentinels against external threats and cancer cell [34]. Importantly, another characteristic of macrophages is their plasticity. Indeed, macrophages can adapt their phenotype according to their environment. Therefore, we can describe a broad range of macrophage phenotypes [23,34]. However, two main types of macrophages have been characterised: ‘M1’ or pro-inflammatory macrophages and ‘M2’ or anti-inflammatory macrophages. M1 macrophages are the main actors in targeting tumour or infected cells by phagocytosis or by producing pro-inflammatory signals such as DAMPs and cytokines. These pro-inflammatory signals recruit other immune cells such as NK cells and DCs, promoting the CIC. M2 macrophages are involved in inflammation resolution

processes and tissue repair making them particularly important in reducing the intense immune response and in avoiding the development of autoimmunity[35].

Like DCs, macrophages can express MHC molecules and co-stimulatory signals to prime and activate T cells in case a threat is detected. Although cross presentation has been thought to be the specificity of DCs, it has become more evident that macrophages, especially M1, are able to cross-present and stimulate $CD8^+$ T cells[36]. Cross-presentation in macrophages is less understood than in DCs, but macrophages can stimulate both naïve and memory $CD8^+$ T cells. Therefore, the role of macrophages in inducing an adaptive anti-tumour response and in sustaining the CIC is not neglectable. Of note, once the tumour is more developed, macrophages can also colonise the TME, becoming tumour associated macrophages (TAMs). TAMs have conflicted roles in tumour progression, probably due to their high plasticity, they can either delay or promote the tumour development depending on the signals present in the TME [34,37].

Antigen processing and presentation

Two major pathways of antigen processing and presentation can be differentiated based on the origin of the antigens.

Antigens that are intracellular (i.e viral proteins, mutated proteins) will be processed and presented onto MHCI. Any nucleated cells can present through MHCI which can be seen as a sentinel for dysfunctions in our body's cells[38]. Briefly, intracellular proteins are degraded by the cell's proteasome, which under IFNγ signalling will be upgraded to an immunoproteasome, particularly efficient in degrading proteins into short peptides. These peptides will enter the endoplasmic reticulum (ER) through transporter associated with antigen presentation TAP. In the ER, those peptides would be cut further

into 8-10 amino acids peptides in order to fit in the binding pocket of MHCI by ER aminopeptidase associated with antigen processing (ERAAP). ERAAP-deficient mouse models showed impaired CD8 response due to the instability of their MHCI-peptides complexes[39]. In the ER, MHCI is surrounded by a peptide loading complex (PLC) made of several chaperones and enzymes (TAP included)[38]. Among the PLC components, tapasin (or TAP binding protein TAPBP) acts as a bridge between TAP and MHCI, stabilizing the transporter while promoting the localisation of MHCI next to it, hence next to a peptide enriched milieu. Importantly, tapasin will be of major importance to select high affinity peptides and load them onto MHCI, process known as peptide editing[38,40]. Of note, the importance of tapasin is true for any MHCI allotypes but variable as some MHCI will be more prone to bind highly affine peptides than others[40]. MCHI-loaded complex then travels to the cell membrane. Through that process, the complex can be further edited by tapasin-related protein TAPBPR, which further select high affinity peptide-MHCI complexes and can return suboptimal complexes into the ER[41]. MHCI-peptide complexes expressed at the cell surface will be recognized by CD8 expressing T cells[38].

MHCII is involved in the presentation of engulfed antigens, hence it is expressed on cells able to capture pathogens or dying cells, such as APCs. The phagocytosed components in endosomes will be lysed due to the acidification of the milieu after the fusion of the endosomes with lysosomes, forming phagolysosomes[38,42]. MHCII chains are assembled in the ER such as MHCI. Because the MHCII specific peptides are located in phagolysosomes, MHCII stays bound to a chaperone called invariant chain (Ii) to prevent any binding with peptides in the ER. Ii also guides MHCII into the endosomal compartment where it will eventually fuse with a phagolysosome containing the phagocytosed degraded antigens. The acidification of the milieu will degrade most of the li chain, letting class II-associated invariant chain peptide (CLIP) in the MHCII binding pocket. Peptides from

engulfed antigens will be loaded onto MHCII instead of CLIP in a process regulated by DM (HLR/H-DM) which, like tapasin, promotes peptide editing[38,42]. The li chain has been used as a molecular adjuvant for cancer vaccines and its effects, as a molecular adjuvant, will be described later. Once loaded with the right peptide, MHCII-peptide complexes are expressed at the cell surface where they will be recognized by CD4 expressing T cells[42].

Very importantly engulfed antigens can escape the phagocytosis pathway into the cytoplasm, be degraded by the immunoproteasome, and enter the ER where they will be loaded onto MHCI molecules[38,43]. Alternatively, engulfed antigens have been shown to be loaded directly onto MHCI into the endosomes[43]. This process is called cross-presentation, and, as stated above, can only be performed by some APCs[43]. Which cross presentation pathway is used for a particular antigen is not completely understood but some evidence suggests that the size of the engulfed particles rather than the nature of the antigen determines the cross-presentation pathway for loading onto MHCI[44]. This pathway is particularly important for the priming of naïve $CD8^+$ T cells to TAAs[43].

1.1.2.3 Adaptive immune response to cancer: step 4 to 7 of the CIC

$CD4^+$and $CD8^+$ T cells activation and differentiation: step 3

Signals for an efficient priming

T lymphocytes are characterised by the acquisition of a T cell receptor (TCR) which is the association of CD3ε, CD3δ, CD3ζ subunits and α and β chains during thymic development. Due to the recombination of V(D)J genes which encode for the α and β chains, there is an extremely broad repertoire of TCRs. Each T cell expresses a unique type of TCR that is highly specific to one antigen. T cell activation is restricted to this antigen being presented through MHCI and MHCII molecules. The expression of CD8 and CD4 molecules is defined by the ability of the T cells to stabilise its interaction with MHCI

or MHCII on structural cells in the thymus. CD4 stabilises MHCII interaction while CD8 stabilises MHCI interaction[18]. T cells with a TCR showing affinity for self-antigens will be eliminated in the thymus. Both types of T cells also express the co-stimulatory receptor CD28 which binds to stimulatory signals CD80/CD86 expressed on DCs and macrophages. The CD80/CD86-CD28 interaction is as necessary as MHC-antigen recognition to achieve T cell activation [45]. Furthermore, the environmental cues such as cytokines that are produced by APCs support complete T cell activation. Importantly, the specific cytokines released by APCs define T cell differentiation into cellular subsets with specific functions for the problem/lesion encountered by the APCs[46]. Finally, the activated T cells will undergo rapid clonal expansion. T cell proliferation is supported by additional activation signals from the DCs such as OX40L and 4-1BBL ligands that interact with receptors OX40 and 4-1BB on the T cell surface, which promote greater expansion of activated T-cells[47,48].

Importance of T cell subset phenotypes

$CD8^+$ and $CD4^+$T cell differentiation and final phenotypes need to be coherent for fighting the threat encountered by APCs. Hence, they are defined during priming by the environmental cues produced by APCs. For an efficient anti-tumour response, it is preferrable to have highly cytotoxic $CD8^+$ T cells, cytotoxic $CD4^+$T cells and inflammatory $CD4^+$Th1 cells [49,50], hence these cell types will be described in more detail in the following sections.

There are seven different subsets of $CD4^+$T cells: Cytotoxic $CD4^+$, Th1, Th2, Th9, Th17, T follicular helper (Tfh), regulatory T (T regs) cells. Different cytokine signals will trigger the expression of different transcription factors, specific to each $CD4^+$subtypes which will activate downstream genes associated to the various and specific functions of

these subsets. Among those, the presence of cytotoxic $CD4^+$T cells has been correlated with better prognosis in melanoma patients[51] . Cytotoxic $CD4^+$ T cells can be differentiated from helper $CD4^+$T cells, as they express RUNX3 and EOMES, such as cytotoxic $CD8^+$ T cells, and have been shown to produce both IFNγ and granzyme B [51]. Their differentiation relies partly on BLIMP-1 transcriptional activity which antagonise the Tfh development, in the context of both viral infection and cancer[52,53]. Indeed, BLIMP-1 is repressed by T cell factor 1 (TCF1) which promote Tfh differentiation [54]. In parallel, Th1 $CD4^+$cells differentiation is induced by T-BET which will promote the production of IFNγ, among other inflammatory cytokines[55]. Moreover, Th1 cells have been shown to upregulate CD40L which will bind to its cognate receptor CD40 expressed on DCs. This interaction will sustain DC activation, enhancing $CD8^+$ T cell priming and activation[56].

The maturation state of DCs and the cytokine signal during priming will also impact $CD8^+$T cell phenotypes. Indeed, $CD8^+$ T cell can become short-live effector cells (SLEC) or memory precursor effector cells (MPEC). T-bet transcription factor induction has been shown to promote SLEC while the transcription factor Eomes will drive MPEC[57]. More recently, Eomes has been shown to be induced by TCF1 signalling[58]. TCF1 is a transcription factor involved in stemness maintenance and development[59]. Ideally, the maintenance of stem-like factor will promote better proliferation and differentiation of cytotoxic $CD8^+$ T cells. In fact, recent research has shown the importance of TCF1 expression in $CD8^+$ T cells to support anti-tumour response by conferring stem-like properties to these cells[60]. Indeed, activated $TCF1^+$ $CD8^+$ T cells present improved survival[61]. Moreover, TCF1 promotes the maintenance of $CD8^+$ T cell effector function once they are confronted by TME immunosuppressive mechanisms[62]. In many cancer types, these $TCF1^+$ $CD8^+$ T cells are not the major subset and most $CD8^+$ T cells present

SLEC phenotype, which will rapidly become terminally differentiated and potentially lose their cytotoxic functions either in the periphery or in the TME[61].

T cell migration and infiltration of the tumour sites: step 4 and 5

Once activated, T cells leave the secondary lymphoid organs (LNs, spleen) to migrate to the tumour site. Several actors are in place in this spatio-temporally regulated process. T cells will be led to the TME due to chemokines and adhesion molecules. Activated T cells downregulate homing molecules such CD62L or CCR7 which enables them to leave the lymphoid tissues[63,64]. Activated T cells also upregulate CXCR3, a receptor for CXC chemokines. Upon their entry in the vascular system, activated T cells follow the gradient of chemokines in the blood stream or presented via glycosaminoglycans by endothelial cells[65]. Particularly, CXCL9 and CXCL10, ligands for CXCR3, have been associated with T cell infiltration different cancer types such as melanoma and ovarian cancers[66,67]. T cells follow this increasing gradient of chemokines to the tumour site where they will extravasate due to adhesion molecules, high chemokines concentration and cytokine signals[68,69]. Indeed, these signals allow the process of rolling, tethering, and binding of endothelial cells that lead to extravasation. In fact, CXCR3 was shown to play an important role in the extravasation process by stabilising intravascular T cell adhesion[70,71]. Furthermore, cytokines such as IL-6 and tumour necrosis factor (TNF)-α will increase adhesion molecule on the endothelium of the TME[68]. Once their entry into the tumour extracellular matrix, T cells can stay motile and migrate within the TME using adhesion molecules and chemokine signals. Interestingly, T cells can also move through “simple” frictional force which will promote enough shear force for the movement through high density, adhesion molecule-deficient tissue such as tumours[72].

T cell recognition of cancer cells: step 6

Upon entry in the TME, T cells will need to interact with cancer cells. The recognition of tumour cells by $CD8^+$ and $CD4^+$T cells is restricted to the presentation of TAAs onto MHCI and MHCII respectively. TAAs can be distributed into different families of antigens with different expression patterns. Hence, there are TAAs defined as either neoantigens, viral antigens, overexpressed antigens, melanoma-associated antigen (MAGE)-type antigens, or antigens that are derived from the unusual expression of non-coding genetic elements (retrotransposon, non-coding RNA, unusual open reading frame among others)[73].

Overexpressed antigens.

TAAs can rise from the overexpression of tissue specific proteins. These proteins are naturally expressed in the original healthy tissue but are expressed in higher level in the tumour cells. These antigens are usually poorly immunogenic as T cells specific for self-proteins would have been eliminated out as part of central or peripheral tolerance processes[73]. However, the change in the density of these peptides presented at the surface of malignant cells can break the tolerance and lead to T cell activation and tumour cell killing. For example, the melanocyte specific antigens Melan-A has shown to induce cytotoxic T cell response in melanoma patients[74]. Importantly, these antigens can lead to off-target effects, hence autoimmune activity.

Neoantigens.

Neoantigens are derived from mutated genes which occurs in the process of cancer cell uncontrolled growth. These mutated genes lead to the expression of mutated proteins. These proteins can greatly differ from the initial protein found in healthy tissue and therefore become immunogenic. However, the expression of neoantigens is dependent on

the mutation profile of every individual, hence one patient will have a very different profile of neoantigen expression than another patient for a similar type of cancer. Therefore, although potentially very immunogenic, neoantigens cannot be used as target for the development of universal treatments and are mostly used as part of personalised medicine strategies [75]. Interestingly, a commonality of antigen expression is found and shared across patients for a similar type of cancer and sometimes across different types of cancer. This is the case for viral antigens, unusual expression of non-coding elements and MAGE-type antigens.

Viral Antigens.

Viral antigens, as their name suggest, are derived from viral proteins. Indeed, seven viruses such as Human Papillomavirus (HPV) and Hepatitis B virus (HBV) have been shown to be oncogenic (i.e induce cancer). HPV is the cause of most cervical cancers while HBV infection has been correlated with hepatocellular carcinoma. The most well studied HPV viral antigens are E6 and E7, which directly contribute to the growth of HPV derived neoplasia[74]. Due to their external nature, viral antigens can be highly immunogenic and therefore be a very accessible target for T cells. However, viral-induced cancers only represent 15% of all type of cancers worldwide[76].

MAGE-type antigens.

MAGE-type antigens are a family of tumour antigens that are encoded by cancer germline genes, mostly located in the X chromosome. These genes are not expressed in healthy somatic cells. Indeed, cancer germline genes are tightly regulated through epigenetic regulation which repressed their expression in somatic tissues. The only healthy tissues expressing MAGE-type antigens are male germline cells, the placenta, and cells in

the developing trophoblast. These sites are "immune privileged" which are defined by the lack of MHCI expression, hence they cannot be targeted by $CD8^+$ T cells. Therefore, T cells do not display any tolerance against these cancer germline genes, which make them perfect targets for cancer elimination when they are expressed by cancer cells[77]. There is evidence that MAGE-type antigens can be highly immunogenic and expressed in many different types of cancers such as lung carcinoma and colorectal cancers[77]. Indeed, tumour cells can express those genes and present them through MHCI to $CD8^+$ T cells[73,78]. Moreover, spontaneous T cell response against MAGE-type antigens have been detected in blood of melanoma patients[79].

MAGE-type antigens are one of the first discovered tumour antigen and have been thoroughly characterised[79–81]. To date, 276 MAGE-type antigens have been defined. Furthermore, many MAGE epitopes and their restriction to the different MHC molecules have been determined [82]. Murine tumour models have shown expression of murine equivalent for MAGE-type antigen, named P1A, encoded by the murine cancer-germline gene *Trap1a*. P1A has the same expression profile as human MAGE-type antigens in healthy tissues and is expressed in murine tumour cells such as 15V4T3 or P815 in DBA/2 background. Indeed, P1A expression was involved in tumour regression due to the induction of $CD8^+$ T-cell responses specific against this TAA[83].

Unusual expression of non-coding genetic elements

This family encompasses many different genetic elements other than coding genes. In normal cells, these elements do not usually code for functional proteins and have mainly a function in genetic and epigenetic regulation.

One of these non-coding genetic elements are retrotransposons, and particularly endogenous retrovirus (ERV). ERVs are mobile genetic elements mostly responsible in DNA structural changes, and gene regulation. They are small sequences of DNA, remnants of an old virus infection that has been incorporated in the genome through evolution and have contributed to gene family diversity[84]. Importantly, ERV have been linked to cancer initiation and progression through insertional mutagenesis by transposition or by the expression of retroviral tumour promoting proteins[85]. Interestingly, the unusual transcription of this section of DNA, and sometimes their translation into retroviral proteins have been shown to be immunogenic[84,86,87]. In a recent study, the presence of ERV has shown to induce tertiary lymphoid structure in both human and mouse tumour models. Moreover, the induced ERV-specific antibody responses improved mouse survival in a mouse lung adenocarcinoma model[88]. Other non-coding elements that can be aberrantly expressed in cancer are non-coding RNAs, which contribute to genetic regulation in physiological condition. Indeed, non-coding RNA can have multiple functions and have been involved in gene transcription and post-transcription regulation. Among those, long non-coding RNA have been shown to comport small open reading frames that give rise to small peptides. The expression of these small peptides can occur upon tumorigenesis. Interestingly, vaccination with viral vectors encoding these small peptides was able to induce an antigen specific $CD8^+$ T cell response which confirmed their immunogenic potential[89]. Alternatively, unusual open reading frames in the untranslated 5'UTR region of mRNAs, or in non-coding exon, or in exon junctions have also shown to be expressed in cancer cells and give rise to TAAs[90]. Altogether, non-coding element is a non-neglectable source of TAAs and have been shown to represent 90% of the tumour specific antigens from various tumour lines both human and mouse. Because they originate from

aberrant expression but not mutation, this type of TAAs can be expressed across patients in a broad ranges of cancer types making them promising targets for vaccination[90].

Recognition of TAA

Once specific T cells have reached the tumour site, they can recognise the TAAs against which they have been activated. It is accepted that the main cytotoxic T cells against tumour cells are $CD8^+$ T cells[91]. Their presence in the TME has been correlated to better prognosis in many cancer types such as lung and breast cancers[92,93]. $CD8^+$ T cell recognition of TAA is restricted to MHCI molecules. Importantly, MHCI molecules are expressed in all nucleated cells to present potential infectious or tumour antigens which will be recognised by $CD8^+$ T cells. Hence, MHCI are also expressed at the surface of tumour cells and will present TAA epitope to $CD8^+$ T cells [50]. MHCII molecules are not expressed on every cell of the body and mostly on professional antigen presenting cells such as macrophages and DCs. Interestingly, tumour cells can present abnormal MHCII expression and be recognised by $CD4^+$T cells. MHCII expression in different human cancers has been correlated with better prognosis[94]. However, $CD4^+$T cells anti-tumour functions often do not involve direct killing of tumour cells but rather indirect mechanisms such as cytokines signals that will help $CD8^+$T cell function and sustain APC recruirment[56].

Cytotoxic mechanisms leading to cancer cell death: step 7

$CD8^+$

Activated $CD8^+$ T cells are cytotoxic through at least 4 major mechanisms. They can perform a direct targeting of tumour cells which requires close contact between the $CD8^+$ T cell and the tumour cell, referred to as the immune synapse. The formation of the TCR-MHC-I synapse polarizes the cytoskeleton of the T cell acting toward the release of vesicles

containing perforin and granzyme B. Perforins are proteins that assemble and create holes in the targeted tumour cells. This allows granzyme B, released by $CD8^+$ T cells, to infiltrate into the cytosol of the tumour cell where it degrades substrates required for normal cell function. Moreover, granzyme B is capable of activating apoptosis through the direct or indirect activation of caspases [50]. Although one T cells can trigger the death of one cancer cell on its own, it has been recently shown that generally one cancer cell will need the targeting of several $CD8^+$ T cells. Specifically, it is the overload of subsequent release of perforin/granzyme B that will trigger tumour cell death[95].

The two next mechanisms that $CD8^+$ T cells used to directly kill cancer cells, consist of the expression of cell death ligands. These membrane-bound proteins trigger apoptosis upon recognition with their cognate receptors on the cell surface of the cancer cell. Hence, $CD8^+$ T cells express Fas-L which recognises Fas receptor expressed on tumour cells. Alternatively, $CD8^+$ T cells produce TNF-related apoptosis-inducing (TRAIL) ligand to engage with TRAIL receptors on tumour cells[50].

Lastly, $CD8^+$ T cells also secrete IFNγ which can have direct and indirect cytotoxic effects on cancer cells[21]. IFNγ can activate caspase-1 or caspase-8 through STAT1 signalling and directly induce tumour cell apoptosis[22,96]. IFNγ can also enhance MHCI and MHCII expression on cancer cells, promoting their recognition by $CD8^+$ and $CD4^+$T cells respectively.

$CD4^+$

As mentioned previously, $CD4^+$T cells can be cytotoxic and display mechanisms to directly kill cancer cells. These cells can present the same cytotoxic mechanisms as cytotoxic $CD8^+$T cells, except their recognition of TAAs is restricted to MHCII

presentation. Concerning helper $CD4^+$ T cells, their cytotoxic role is indirect and dependent on the type of $CD4^+$Th cells. $CD4^+$Th cell role in sustaining and promoting the anti-tumour response is central. Th1 type has abundantly been described in anti-tumour response[56]. Th1 $CD4^+$T cells are inflammatory and have been shown to help the anti-tumour response through the production of IFNγ and TNF-α, potentially directly cytotoxic to certain tumour cells. Particularly, circulating Th1 $CD4^+$T cells have been correlated with better prognosis in non-small cell lung carcinoma (NSCLC) patients[49]. Th1 $CD4^+$cells also help cytotoxic $CD8^+$ T cell activation by the production of IL2 which will promote the proliferation of $CD8^+$ T cell expressing CD25 (IL2 receptor)[56]. Another subset of $CD4^+$T cells that can potentially be important in anti-cancer response, but less described as such, is the Th2 cells. Indeed, Th2 $CD4^+$T cells are involved in activating B cell responses. The anti-tumour role of B cells is still poorly understood and quite controversial, but the presence of tertiary lymphoid structures (lymph-nodes-like structures) has been correlated with better prognosis in cancer patients[97]. Finally, although Tfh cells are not directly cytotoxic to cancer cells, they have been shown to promote $CD8^+$ T cell function and limit their exhaustion in an IL21 dependent manner when infiltrated in the TME[98].

After the induction of tumour cell killing by T cells the tumour cell death will create more inflammatory signals and DAMPs as well as the spreading of TAA that will be captured by APCs. Hence, feeding the CIC and promoting the tumour elimination. However, tumour cells are aggressive and eager to proliferate. Therefore, the failure of this cycle can happen, which will lead to the two other phases of the three Es: Equilibrium and Escape.

1.1.3 Tumour equilibrium

The second E of the three Es concept is the equilibrium phase, where the immune system participates in shaping, editing the growing tumour, concept known as immunoediting [16]. More precisely, a balance between immune recognition and tumour growth is taking place during this phase. This balance allows for elementary evolution processes to take place with the selection of tumour cell clones that can thrive in an environment highly targeted by immune cells. Hence, only cancer cells that cannot be recognised by the immune system will survive and expand. Particularly, tumour cell clones that do not express immunogenic TAAs tend to expand as they avoid immune responses. Moreover, tumour cell clones can also acquire advantages through the acquisition of random mutations. Indeed, tumours grow while acquiring more of the mechanisms that will allow the suppression of immune responses[99]. The first study highlighting the tumour sculpting role of the immune system involved the transplantation of tumours that grew either in wild-type (WT) or T and B cell-deficient RAG2-/- mice into WT immunocompetent host[15]. While the tumour from WT donor mice grew progressively into the host, 40% of the tumour from RAG2-/- mice were rejected by the immunocompetent host. The tumour that first grew into RAG2-/- were less edited due to the absence of the immune system, hence were more immunogenic.

This phase has a blurry start and end, and probably overlaps with the elimination and escape phases [16]. Ultimately, cancer cell evolution will lead to the escape phase where the tumour is out of immune control. Tumour cells can, then, metastasise and thrive in sites away from the primary site, leading to multi-organ dysfunction and patient deaths [17].

1.1.4 Tumour escape

The escape phase occurs when tumour growth is greater than the immune system ability to kill cancer cells. At this stage the CIC is completely disrupted by the acquisition of immune evasion mechanisms from the tumour cells[17]. Tumour cells not only escape immune recognition through the loss of immunogenic signals and antigens but also hijack immune processes and suppressive immune cells for the benefit of their own growth[17]. In fact, the heterogeneity of cancer cells implies that the tumour can escape the immune system through many different mechanisms [16]. Furthermore, immune escape does not only occur in the tumour site but can also target CIC steps such as DC activation, T cell priming or T cell migration which are away from the TME (systemic mechanisms)[100,101].

1.1.4.1 Systemic immune escape mechanisms

Altering innate cell recruitment and activation

The initiation of the CIC is due to cancer cell death which triggers the release of DAMP signals. The cell death that triggers immunogenic signals is called immunogenic cell death (ICD). These inflammatory signals are necessary to recruit NK cells, DCs and macrophages and contribute to their activation. However, tumour cells can also die through physiological tolerogenic form of death, named apoptosis, which does not activate immune responses. Physiological apoptosis will trigger the decrease expression of “don’t eat me” signals such as CD47 and the exposure on the cell surface of “eat me” signals such as phosphatidylserine. These signals will lead to the engulfment of apoptotic cells by tolerogenic macrophages, without the release of DAMPs[102].

Cancer cells can inhibit APCs recruitment and activation through the secretion of cytokines, growth factors, or tumour-derived exosomes. Indeed, tumour cells can send signals that will alter DC maturation. STAT3 overexpression in tumour cells has been

shown to prevent DC maturation through the secretion of inhibitory cytokine such as IL-10 and TGF-β but also the angiogenic vascular endothelial growth factor (VEGF)[103].

Furthermore, tumour cells have been shown to alter the systemic composition of the immune system with decrease proportion of DCs. Increased serum IL-6 in a pancreatic mouse tumour model was shown to promote DC apoptosis[104]. Many cancer types such as ovarian cancer display a reduction in peripheral blood DCs[101]. Cancer cells also induce haematopoiesis with the expansion of aberrant, immature macrophages, monocytes, and neutrophils[101]. These expanded immature cells with immunosuppressive abilities are referred as monocytic (M-) myeloid derived suppressor cells (MDSCs) and granulocytic or polymorphonuclear (PMN-) MDSCs. These cells can act in supressing the immune response in both the system and the TME [105]. Of note, which subset is preferentially expanded, and the immunosuppressive mechanisms they used are gender- and cancer type-dependent[106,107].

Inhibition of T cell priming

Priming of T cells through TAA presentation by immature DCs has been shown to trigger more tolerogenic T cells, hence decreasing their effector functions against tumour cells. Indeed, DCs integrate environmental immunosuppressive cytokines and signals which can lead to impaired T cell activation and differentiation[103].

The immunosuppressive environment can trigger checkpoint molecules. Checkpoint signals control the activation and strength of immune responses in healthy individual which prevent the development of autoimmunity or chronic inflammation. In fact, one checkpoint molecule that can dampen the priming of anti-tumour $CD8^+$ T cell is cytotoxic T-lymphocyte-associated protein-4 (CTLA-4). Indeed, CTLA-4 competes with

CD28 for the binding with CD80/CD86 on APCs and has been shown to weaken anti-tumour response[108].

In parallel, one major subset expanded in many cancer types are $CD4^+$T regs. T regs have been shown to decrease CD80/CD86 expression on APC surface through trans-endocytosis, hence suppressing T cell activation[109]. T regs perform a crucial role in impairing effector T cell response in the system through the production of inhibitory cytokines such as IL-10[110].

One important mechanism of peripheral inhibition of T cell priming is the generation of PMN- and M-MDSCs upon tumorigenesis. Both subsets have been related to impaired T cell homing into lymphoid organs by cleavage of CD62L[111]. Furthermore, both subsets can express high level of arginase 1, an enzyme that will decrease available L-arginine. L-arginine depletion will reduce TCR expression on T cells as well as reduce their proliferation[105]. Some of the immunosuppressive mechanisms are unique to each subset of MDSCs. PMN-MDSC has been shown to express high levels of reactive oxygen species (ROS) through STAT3 activation and NADPH expression. ROS are toxic and decrease T cell activation and proliferation. In contrast, M-MDSCs can express high levels of nitric oxide (NO), the product of L-Arginine metabolism trough iNOS, which impairs T cell expansion and functions [111,112]. Finally, ROS and NO can react with each other and form peroxynitrites which nitrate the TCR on the cell surface, hence preventing the priming and activation of T cells[105].

Inhibition of T cell migration

Tumour cells can decrease their production of chemokines, which are crucial in guiding the migration of T cells into the TME. Tumour angiogenesis is triggered through the expression of VEGF and fibroblast growth factor (FGF). These two factors will

downregulate the expression of adhesion molecules on the tumour endothelium, preventing an efficient extravasation of activated T cells into the tumour sites[113]. Moreover, MDSCs have been related to the increased nitration of chemokines, hence preventing lymphocyte migration in the TME[112]. M-MDSC have been related to NO-mediated downregulation of adhesion molecules such as CD162 and CD44 in the vasculature, decreasing T cell extravasation and entry to the tumour site[114].

1.1.4.2 Immunosuppression in the TME

It is of major importance for T cells to infiltrate the TME, where the last step of the CIC occurs: cancer cell killing. Tumours that are poorly infiltrated are referred as "cold" tumours while tumours that contain infiltrated lymphocytes (TiLs) are referred as "hot" tumours[100].

Escape of immune recognition and immunosuppression induced by tumour cells

When tumour cells grow, the TME becomes denser, making T cell infiltration particularly challenging. Furthermore, the competition for metabolites such as oxygen and amino acids is fierce in the TME. While tumour cells can thrive in a hypoxic environment it is mostly detrimental for T cells[115]. This competition for resources will impair T cell functions hence participating in the escape of immune recognition[116].

Direct mechanisms have been described for tumour cells to escape immune recognition in the TME. Tumour cells can decrease MHCI expression hence diminishing TAA presentation to $CD8^+$ T cells and escape from recognition[20]. One important immunosuppressive mechanism is the expression of checkpoint molecules such as programmed cell death-ligand 1 (PD-L1). The receptor for this ligand, programmed cell death protein 1 (PD1) is expressed on T cells early after their activation. Checkpoint molecules are expressed in healthy tissues and are involved in the resolution of the immune

response by controlling the activity of T cells once they have fulfilled their roles. Tumour cells can hijack this mechanism by presenting PD-L1 or PD-L2 which will bind to PD1 on the T cell surface[117]. In the context of the TME, where T cells can be constantly stimulated against TAAs due to the persistence of the tumour, PD1 expression tends to be increased and sustained on T cells [118]. Additional co-inhibitory receptors such as Tim3 are also induced on over-stimulated T cells as part of the immune control process[119]. The interaction of PD1 and Tim3 with their cognate molecules on the tumour cell surface will trigger T cell exhaustion, which refers to as a decrease in T cell cytotoxic function and proliferation[120].

As previously mentioned, there are different subset of $CD8^+$ T cells, and $TCF1^+CD8^+$ T cells expressing PD1 in the TME are not necessarily exhausted. Indeed, $TCF1^+$ $PD1^+$ $CD8^+$ T cells, defined as progenitor exhausted stem-like cells, displayed high proliferation potential while sustaining their functions in the TME. The presence of $TCF1^+PD1^+$ $CD8^+$ T cells have been correlated to a better prognosis and tumour control[62,121].

Immunosuppression by recruited immune cells

One major strength of the TME is the presence of immune cells that mediate immunosuppression. Immunosuppressive immune cells can be naturally present in healthy conditions and play a crucial role in regulating immune responses, preventing autoimmunity, and resolving immune responses. However, in the TME this is disadvantageous to the host. There are 3 major types of immunosuppressive immune cells hijacked by the TME: $CD4^+$T regs, M2 macrophages and MDSCs[100]. There is a complex crosstalk between these 3 suppressive subsets as well as with tumour cells to suppress immune response in the TME[37,110,122].

MDSCs

The mechanisms used by MDSCs to supress T cell in the TME mostly overlap with the mechanisms found in the periphery[105]. Hence, through ROS and NO production and L-arginine depletion, MDSCs trigger misfunctioning TCRs which will be unable to recognise TAA, preventing T cell to exert their cytotoxic functions toward cancer cells. MDSCs have been shown to induce T cell apoptosis through the secretion of NO and the expression of Fas-L. NO can upregulate Fas expression on T cells and trigger apoptosis upon ligation with Fas-L. Furthermore, both types of MDSCs can upregulate PD-L1 and trigger T cell exhaustion in the TME. Another mechanism through which PMN- and M-MDSCs exert their suppressive function is through the recruitment of immunosuppressive tumour associated macrophages (TAMs) and $CD4^+$T regs [105,111]. Finally, MDSCs can induce de novo $CD4^+$T regs in an IL-10 and IFNγ dependent manner[123].

$CD4^+$T cells

In a similar way, $CD4^+$T regs have been shown to promote MDSC expansion through TGF-β production. Also, $CD4^+$T regs can induce PD-L1 expression on MDSCs, supporting their suppressive functions. Alternatively, $CD4^+$T regs can directly express PD-L1, IL-10 and TGF-β and support T cell exhaustion[110,124].

M2 macrophages

Macrophage characterisation in the TME is complex with a range of phenotypes existing. These phenotypes evolve depending on the environmental cues and interaction with tumour cells. However, it has been accepted that tolerogenic M2 TAMs can present immunosuppressive functions. Like MDSCs and T regs, M2 TAMs can deplete L-arginine and secrete TGF-β and IL-10 and express PD-L1, hence targeting effector T cells[34]. M2

TAMs production of TGF-β and IL-10 will support T regs and MDSCs functions. Furthermore, they will recruit more T regs, through the production of CCL20/22[37].

Altogether, the mechanisms of systemic and TME immunosuppression described here are non-exhaustive and part of a complex integration of signals. To fight cancer progression, the need to support and reinvigorate the CIC is of major importance. The last decades of research have focused on targeting these immunosuppressive mechanisms together with harnessing the anti-tumour response, creating a new type of cancer treatment: cancer immunotherapy.

1.2 Cancer Treatments

1.2.1 Standard of care

Cancer is a challenging disease to treat due to its multi-dimensional aspects. When possible, clinicians will preferentially remove the tumour by surgery. Although quite invasive, physically removing cancer is the most efficient way to treat these aggressive cells. However, surgery is not always possible, especially when the patient is diagnosed late, or the location of the tumour is within critical functional sites of organs. One of the more advance stages in cancer progression is when it has metastasised, invading organs away from the primary site which prevents a possible efficient surgery. Conversely to surgery, treatments that target cell expansion such as chemotherapy and radiation therapy have been the main alternative used to treat patients. These treatments are still widely use to target cancer expansion [4,5]. They can be used alone or in combination, in order to reduce the tumour size, making surgery possible. Because cancer cells can acquire resistance to these treatments, combination of different chemotherapies, targeting different cell division processes, is usually more efficient than single-agent therapy. However, one main drawback of chemotherapy and radiation is their lack of specificity for tumour cells. Healthy cells will also be targeted with these strategies which induce severe side effects[125]. Interestingly, the modulation of chemotherapy and radiation doses and combinations has put into light their immunomodulatory effects. For the focus of the thesis project, we will expand on chemotherapy, not radiotherapy in the following section.

1.2.1.1 Chemotherapy classification

Chemotherapeutic agents are classified in different families depending on their mechanism of action to stop cell division and expansion[125]:

- Alkylating agents: Molecules containing unstable alkyl groups that react with cellular proteins and nucleic acids. They destabilise DNA, inhibiting DNA replication and

transcription and leading to cell death. Platinum-based chemotherapies, such as carboplatin, count among this family commonly used to treat ovarian cancer and NSCLC. One of the most cytotoxic effects of carboplatin is the formation of crosslinks between strands of DNA, which directly stops DNA replication during G2/M phases, eventually leading to apoptosis[126].

-Antimetabolites: molecules that mimic nucleotides such as cytidine, purine, or pyrimidine analogues. They will incorporate as false metabolites into the DNA, blocking its replication. fluorouracil (5-FU), a pyrimidine analogue, and gemcitabine, a cytidine analogue, are commonly used for colorectal and breast cancer respectively[125].

-Antimicrotubular agents: impact the cell cytoskeleton, and particularly microtubules polymerisation. This family counts topoisomerase inhibitors, which inhibits DNA repair by blocking topoisomerase I or II. Taxanes are also part of this family such as paclitaxel which will stabilise microtubules preventing the assembly of a functional mitotic spindle, important for cell division[127]. This will block cell replication and lead to cell apoptosis[128]. Paclitaxel is commonly used to treat ovarian cancer and NSCLC.

-Antibiotics: some antibiotics can inhibit DNA or RNA synthesis such as actinomycin D[125].

Interestingly, although the first purpose in using chemotherapy was to target tumour cell expansion, chemotherapies can also have immunomodulatory effects. These immunomodulatory effects depend on the type and dose of chemotherapy used. However, these effects are promising and start to be exploited as part of anti-cancer strategies[129].

1.2.1.2 Chemotherapy immunomodulatory effects

Chemotherapy can modulate the immune system through two main mechanisms: tumour cell intrinsic or tumour cell extrinsic[130].

Tumour cell intrinsic mechanisms

Chemotherapy drugs can sensitise tumour cells to T cell recognition and T cell killing by the induction of MHCI and TRAIL receptor at the surface of the tumour cells[99]. It is the case of cyclophosphamide which promotes TRAIL receptor in a mouse model of malignant mesothelioma, AB1-HA[131].

Most chemotherapy has been shown to induce apoptosis, a tolerogenic cell death. However, some chemotherapies can induce an immunogenic form of death (ICD), promoting anti-tumour responses. ICD is the main form of tumour cell intrinsic immunomodulatory effects. ICD is induced by a stress response in tumour cells. Briefly, this stress response involves the generation of early "eat-me" signals such as the translocation of calreticulin at the cell surface. These early signals will induce DC maturation[132]. Later, when the tumour cell is dying, the release of high-mobility group box 1 protein (HMGB1) and IL-1β will finalise DC maturation. The matured DCs uptake TAAs of the dying tumour cells and migrate to the LN to stimulate an anti-tumour response. It is the accumulation of all these ICD hallmarks that define whether chemotherapy is immunogenic through ICD. Indeed, while cisplatin can trigger HMGB1, it is not able to induce ICD due to the lack of calreticulin exposure at the cell surface of colon cancer cells[133].

The mechanisms underlying the activation of tumour cell stress and ICD are not fully understood. Different classes of chemotherapies have been shown to induce ICD. However, drugs of the same family can induce either ICD or tolerogenic cell death. Indeed, cyclophosphamide and cisplatin are two alkylating agents, however only cyclophosphamide can induce ICD[134,135]. Similarly, combination of chemotherapy can induce ICD while the use of the same drugs as single-agent treatment cannot[136,137]. Finally, cyclophosphamide has been shown to induce ICD against glioblastoma but not against

KM12 colon tumours although using the same dosage[135,138]. This indicates that ICD induction depends not only on the chemotherapy drug but also on the tumour type. Moreover, the dose of chemotherapy has a major effect on the efficacy of ICD as cyclophosphamide given at metronomic dose has shown to promote tumour regression with long lasting immunity, whilst the maximum tolerated dose (MTD) of cyclophosphamide only induced transient activation of innate immune responses[139]. In parallel, many investigations have highlighted the importance of the dosage and type of chemotherapy in the modulation of tumour-extrinsic immunomodulatory effects[140–142].

Tumour cell extrinsic immunomodulatory effects

Chemotherapies can directly impact the immune system, independently of their impact on tumour cells. Paclitaxel has been shown to stimulate DC activation by acting as an agonist for TLR4[143]. Similarly, enhanced T cell and NK cell functions were observed in breast cancer patients treated with Taxanes[144]. Furthermore, the combination of Paclitaxel and Carboplatin has been shown to improve $CD8^+$ T cell effector functions in the blood of ovarian[145], NSCLC[146], and melanoma patients[147]. Interestingly, metronomic doses of Cisplatin and Paclitaxel in a murine ovarian cancer model showed a better tumour control due to the recruitment of effector $CD8^+$ T cells in the TME as compared to the MTD regimen[142]. Furthermore, in a phase III trial in ovarian cancer patients, metronomic dose of Paclitaxel alongside Carboplatin has shown promising effect with an increase survival compared to the MTD regimen[148]. Alternatively, low dose of cyclophosphamide inhibits the functions of $CD4^+$T regs, hence promoting effector T cell anti-tumour efficacy[149]. This was not observed with high dose of cyclophosphamide where lymphopenia was induced. Again, this emphasises the dose-sensitivity of chemo-mediated immunomodulation mechanisms.

One main effect of several chemotherapies has been the depletion of MDSCs. The combination of Carboplatin and Paclitaxel has been shown to deplete PMN-MDSCs, hence improving vaccination in TC-1 tumour model[150]. Gemcitabine and 5-FU also depletes MDSCs[151,152]. Importantly, the dose has again a major importance on MDSC depletion. Indeed, if gemcitabine was able to deplete M-MDSCs when given in a single injection, this effect was reversed when several injections were performed, and an accumulation of splenic M-MDSC and no reduction in tumour M-MDSCs was observed in a murine breast cancer model[153].

This is a non-exhaustive presentation of the immunomodulatory effects of chemotherapies. However, a common pattern is observable across models and drugs used, where low and metronomic doses seem preferential to MTD. The reason why metronomic and low doses of chemotherapy seem more immunogenic are not fully understood. However, MTD are usually highly toxic with a range of side effects among which lymphopenia and decrease in TiLs have been described[130]. Furthermore, MTD of chemotherapy has been shown to induce cancer stem cells in a cancer-associated-fibroblast dependent mechanism. Cancer stem cells are highly proliferative clones, also named tumour-initiated cells which will reinvigorate tumour growth after chemotherapy[154]. The usage of intermediate dose to find the right balance between immunomodulatory effects and tumour toxicity have been hypothesised but need to be further explored [137].

1.2.2 Immunotherapy

1.2.2.1 What is immunotherapy?

Cancer immunotherapy refers to the therapeutic interventions that harness the immune system to fight cancer cell growth[155]. Immunotherapies can therefore fall into two vast families:

-Immunotherapies which foster a specific anti-tumour immune response (e.g chimeric antigen receptor T-cells)

-Immunotherapies which strengthen the anti-tumour immune response (e.g checkpoint blockade therapy)

Examples of immunotherapy that foster the anti-tumour immune response.

Chimeric antigen receptor (CAR) T-cell therapy involves the *ex vivo* modification of autologous T cells from cancer patients to express a CAR, and the reinfusion of these modified T cells into the patient. The CAR extracellular domain is composed of the variable region of a monoclonal antibodies specific to a TAA, while the intracellular portion is composed of CD3ζ and co-stimulatory molecules. There are a few advantages in using an antibody-based receptor. Firstly, the antigen recognition is not restricted to MHC presentation, making the T cell able to recognise cancer cells through a cellular marker, potentially overriding tolerance. Secondly, this also means that the CAR construct can be transduced into T cells from different patients, as the recognition will be MHC-independent. Finally, the affinity of an antibody is higher than the respective TCR for its MHC-peptide complex target, which promotes strong and persistent T cell activation[156].

One major example of CAR T cells therapy is the CAR targeting CD19 receptor, expressed on B cells, which are expanded in B cell malignancies. This has resulted in impressive results in patients with B-cell acute lymphoblastic leukaemia and large B-cell lymphoma[157,158]. Despite these amazing results in haematological malignancies, CAR T cells have shown limited efficacy against solid tumours. This is because solid tumours have more heterogeneous cell types than blood malignancies. In addition, the CAR T cells must be able to penetrate and function in the immunosuppressive TME[159]. Furthermore, important adverse effects such as cytokine release syndrome (CRS) have been described. CRS are characterised by the systemic release of inflammatory cytokines leading to fever,

hypotension and sometimes affects neurological functions[160]. Finally, because CAR T cells involve personalised medicine, the cost per patient is extremely high with an estimated cost for a single round of anti-CD19 CAR T cells being US $^{+}$475,000[161].

Other than CAR T cells, research have developed protocol to harvest patient's TiLs, and reinvigorate them *ex vivo* and re-injecting them into the patients. Alternatively, blood lymphocytes have also been taken and reengineered to express TCR specific to a TAA. However, these 2 methods involve a higher level of personalised medicine than CAR T cells. Indeed, engineered TCR must be designed with a high compatibility to the patient MHC, while TiLs are dependent of the state of each patient's tumour (i.e hot or cold tumours). Furthermore, one main limitation is the persistence of these cells *in vivo*. Despites millions of cells being injected, their survival after injection is very limited and protocol of expansion are being adapted to inject phenotypes with stem cell properties[159].

Examples of immunotherapy that strengthen the anti-tumour immune response.

One main example of immunotherapy that strengthen the anti-tumour immune response is checkpoint blockade therapy. Unlike CAR T cells which have solely been approved in haematologic malignancies, checkpoint blockade therapy has been approved, alone or in combination with chemotherapy, as standard of care for many solid malignancies[162]. Checkpoint blockade therapy comprises of monoclonal antibodies. These antibodies are referred as checkpoint inhibitors (CPIs) as they inhibit the interaction between immune checkpoint molecules expressed on effector immune cells and the co-ligands upregulated by the tumour cells or immunosuppressive immune cells (such as the interaction between PD1 and PD-L1). Hence, it will prevent the inhibition of effector T cell functions and promote anti-tumour T cell efficacy.

There are 3 major targets of CPIs: PD1, PD-L1 and CTLA-4[108]. Treatment with CPIs has promoted durable tumour regression in advanced cancer patients. However, as single

therapy these antibodies were effective in only a small portion of patients, hence, the use of combination of CPIs. The strongest results so far have been observed in advanced melanoma with the combination of ipilimumab and nivolumab, an anti-CTLA-4 and anti-PD1, respectively. While the 5-year survival rate of advanced melanoma is of 10% without CPIs[163], in the CheckMate 067 trial, overall survival from the combination of Nivolumab and ipilimumab treatments has remained above 50% at 5 years follow-up[164]. Such combinations have shown promising results in other cancers such as NSCLC and metastatic colorectal cancer among others[165]. So far, one CPI against CTLA-4, three CPIs targeting PD1, and three CPIs targeting PD-L1 have been approved in the U.S for a wide range of cancers, and similar approval are occurring in many countries[165].

One main drawback of CPI therapies has been the generation of immune-related adverse events (IRAEs). Indeed, CPI effects will be systemic, not only at the tumour sites. Checkpoint molecules have major physiological roles in controlling the immune response. Hence, their blockade will impair self-tolerance but also lead to poor resolution of immune response, causing healthy tissue damages[166]. Importantly, although the combination of several CPIs is significantly better than the monotherapy, it will lead to further increased toxicity. Furthermore, the response rate is still low in many cancer types such as advanced renal cell carcinoma with a high proportion of patients not responding to the therapy[167]. Therefore, the combination of CPIs with other immunotherapy treatments is of interest and is currently explored to achieve better anti-tumour response whilst limiting toxicity. In parallel, several investigations are currently working on targeting other immune checkpoint molecules, such as Tim3[168].

Multiple immunotherapies can also target the systemic or TME-infiltrated immunosuppressive cells such as MDSCs[169]. Apart from chemotherapy, MDSC depletion can be mediated by the tyrosine kinase inhibitor Sunitinib via the blockage of VEGF and

c-kit signalling[170]. Alternatively, some investigations have explored strategies to induce MDSC differentiation into more mature cells. MDSCs can be differentiated into antigen presenting precursor cells with the use of all-trans retinoic acid[171]. Another way to target MDSCs is to affect their suppressive mechanisms. STAT3 inhibitors was able to decrease PD-L1 and indoleamine 2,3-dioxygenase (IDO) expression in liver MDSCs leading to enhance CAR T cell activity in MC38 tumour models[172]. Targeting the expression and function of ROS and Arginase 1 with nitroaspirin[173] and phosphodiesterase-5 inhibitor[174] respectively have also been explored in murine tumour models in order to decrease MDSC suppressive effects. Moreover, nitroaspirin in combination with vaccination in a murine colon carcinoma model showed an expansion of tumour specific $CD8^+$ T cells and an increase in mouse survival[173].

Collectively, immunotherapies that aim at strengthening the anti-tumour immune response achieve their best efficacy in combination with other therapies. Ultimately, the anti-tumour response and particularly $CD8^+$T cells are essential to achieve therapeutic efficacy. Indeed, without TiLs, which is the case in cold tumours, CPIs display very limited effects[175]. The development of more immunotherapies that foster the anti-tumour immune response, and ideally applicable to many cancer types, is therefore of first importance.

1.2.2.2 Therapeutic cancer vaccines

The concept of vaccination involves the notion of prevention against the development of diseases, by inducing an immunological memory specific to an infectious agent. In the context of cancer, cancer vaccines are designed to be used as treatments that trigger anti-tumour immunity. In principle, a patient with an established cancer diagnosis will be vaccinated against TAAs in the aim to create a T cell response specific to the tumour [176]. The generation of cytotoxic $CD8^+$ T cells will promote cancer cell killing. The killing of tumour cells will reveal and spread more TAAs, feeding the CIC. Hence, according to the

concept of antigen spreading, vaccination could promote the generation of several immune responses to fight the heterogeneity of tumours[177,178]. Interestingly, there are evidence from murine models that the generation of tumour-specific $CD8^+$ T-cells with vaccination have the potential to increase the response rate to CPI[179–181].

Therapeutic vaccination has been explored many times in the past without success. Those years of research highlighted the importance of the platform of vaccination used. Indeed, the vaccine platform will define the strength and type of immune responses raised[182]. For cancer, a strong $CD8^+$ T cell response is preferred, particularly due to their direct cytotoxicity to tumour cells. Hence, different vaccine platforms have been developed including autologous cell vaccine such as DCs loaded with antigens or tumour lysate, DNA or RNA-based, synthetic long peptides-based, and viral vectors-based vaccines[176,183]. However, only one therapeutic cancer vaccine has been approved so far which is Sipuleucel-T, a DC-based autologous cell vaccine against prostate cancer. With Sipuleucel-T, the peripheral blood mononuclear cells (PBMCs) from the patients were stimulated with GM-CSF to activate DCs and incubated with the antigen of interest which consisted of a prostate cancer antigen, prostatic acid phosphatase (PAP). The PBMCs/DCs were then transferred back to the patient and promoted the generation of anti-PAP T cells. However, since approval, this vaccine has only promoted an extra 4.1 month of median survival compared to the placebo group in castration resistant prostate cancer patients[184].

The limitation of the Sipuleucel-T platform is the lack of generation of $CD8^+$ T cells. Most vaccine platforms have first been designed against infectious diseases where the presence of antibody responses is tested as a marker of sufficient memory. However, neutralising antibodies are insufficient to control cancer cell growth. One platform that has shown great promise in generating cell-based immunity and particularly $CD8^+$ T cells are viral vector-based vaccines[185].

1.2.2.3 Viral vector vaccines

Viral vector-based vaccines have first been designed and tested against infectious diseases where T cell immunity is of importance for disease protection. Although replication deficient, viral vectors are naturally immunogenic and mimic an infection[186]. Indeed, they release pathogen associated molecular patterns (PAMPs) which, such as DAMPs, will promote the recruitment of APCs at the infection site and stimulate their activation. Because they mimic an infection, viral vectors lead to the generation of intra-cellular antigens which are loaded on MHCI, privileging a $CD8^+$ T cell based immune response. The precise mechanism by which viral vectors promote $CD8^+$ T cell activation has not been completely understood yet[187]. Most likely, recruited DCs uptake cell debris from dying viral vector-infected cells and present them onto MHCI[188]. Interestingly, DCs can also uptake already formed MHCI/epitope complex at the surface of infected cells through a process designated as cross-dressing[189]. This will lead to the priming of specific $CD8^+$ T cells. Other than the type of immunity they induce, viral vectors are interesting platforms because they are highly adaptable. In fact, their genome can be engineered to express antigens of interest, including TAAs[186].

Many different viral vectors have been evaluated for their efficacy as vaccines inducing cell-based immunity, in both infectious disease and in cancer settings. One major family of viral vectors evaluated has been adenoviruses, which showed promise in inducing $CD8^+$T cell immunity. However, their use as vaccines is compromised as a large proportion of the human population can have neutralising antibodies against the platforms due to previous adenoviral infections[190]. Alternatively, poxviruses such as Vaccinia virus and Modified vaccinia Ankara (MVA) have been tested. Although, MVA has shown limited efficacy to generate an immune response, MVA displayed important boosting capacities [190,191].

Especially, a vaccination strategy based on a chimpanzee adenovirus ChAdOx1 as a prime and MVA as a boost has shown great efficacy in inducing a $CD8^+$ T cell response[179].

ChAdOx1/MVA heterologous prime/boost

Replication incompetent adenoviruses based on human serotype 5 (hAd) have been shown to be efficient agents for priming an immune response. However, hAd has shown limited efficacy as a potential vaccine due to the presence of neutralising antibodies against these vectors, hence requiring the need for another type of viral vectors[192]. Interestingly, simian adenoviruses have been a promising tool with low seroprevalence in human[193] and an ability in inducing cellular immunity[194]. ChAdOx1 was isolated from Y25 of type E chimpanzee adenoviruses, and depleted for E1 and E3, preventing viral replication as well as providing an extra 8kb for the transcript inserts. ChAdOx1 was tested as a potential vaccine and showed higher magnitude of $CD8^+$ T cells than human adenoviruses. This platform is particularly interesting as there is a lower seroprevalence of neutralising antibodies against this virus compared to human adenoviruses and even other chimpanzee adenoviruses [195].

Replication-deficient MVA was first licensed as a third-generation vaccine against smallpox. Once the modification of MVA genome became possible, the possibility to use MVA as a vaccine platform was explored[196]. Interestingly, this viral vector has shown great efficacy when used as a boost[190]. The combination of Chad63, a chimpanzee adenovirus, and MVA encoding the liver stage malaria antigen ME-TRAP, displayed an increase magnitude of $CD8^+$ T cells and enhance disease protection compared to homologous combination. MVA boost also promoted the polyfunctionality of the expanded $CD8^+$ T cells overtime[197].

The use of ChAdOx1 as a prime and MVA as a boost was first explored against infectious disease, such as Middle East respiratory syndrome coronavirus (MERS-CoV)[198],

HBV[199] and Influenza[200]. This strategy has proven a greater efficacy in inducing polyfunctional $CD8^+$T cells in humans compared to the viral vector alone or in homologous combinations (i.e., same viral platform used as prime and boost). The rationale to use heterologous strategies is to prevent immunity against the viral vector itself which can occur due to the presence of anti-vector neutralizing antibodies. Hence, by using different prime/boost vectors, the neutralisation of the boost is prevented[201].

This strategy has also been tested in prostate cancer mouse models as cancer vaccines against six transmembrane epithelial antigen of the prostate 1 (STEAP1). This platform was shown to display high magnitude of $CD8^+$ T cells specific to STEAP1. However, the T cell response did not translate into a significant tumour control in transplantable or spontaneous tumour models of prostate cancer. The combination of anti-PD1 with this vaccination regimen improved the survival of the mice with 80% of tumour free mice after the combination of treatment[181]. Furthermore, the use of the same ChAdOx1/MVA platform encoding 5T4 prostate antigen in a Phase I clinical trial in early-stage prostate cancer patients has shown an excellent safety profile, and specific T cell responses against 5T4 were detected in patient's blood[202].

More recently, murine studies showed good promise against MAGE-type antigens. The ChAdOx1/MVA platform encoding MAGE-A3 and New York oesophageal squamous cell carcinoma 1 (NYESO-1), 2 MAGE-type antigens, showed high $CD8^+$ T cell responses. When assessing therapeutic efficacy in murine tumour models, ChAdOx1/MVA encoding the surrogate of MAGE-type antigen P1A, improved tumour control of P1A expressing tumour models. This control was correlated to the magnitude of the P1A specific $CD8^+$ T cells. Moreover, when the vaccine was combined with anti-PD1, the control of tumour growth and mouse survival were significantly increased compared to the vaccine alone, albeit half of the mice in the combination group not being able to resolve the tumours[179].

These results highlighted one major limitation for cancer vaccines: the immunosuppressive TME. Cancer vaccine-induced immune response need to be sustained and supported in a challenging environment to achieve cancer cell killing. Hence, the combination of different types of immunotherapies is essential to get an efficient anti-cancer strategy[155].

To further improve chimpanzee adenoviruse and MVA vector vaccines, molecular adjuvant sequences have been used. These molecular adjuvants are usually linked to the antigen of interest sequence[203]. One particularly efficient molecular adjuvant is the MHCII Ii chain, which has been seen to improve the magnitude and duration of antigen specific $CD4^+$ and $CD8^+$ T cell responses induced following vaccination with Chad63 and MVA against ME-TRAP[204]. Additionally, this study conducted by Benedict R. Halbroth *et al.* showed that a truncated Ii sequence corresponding to the N-terminal transmembrane domain was more efficient than the full-length sequence at enhancing $CD8^+$ T cell responses. However, the mechanism behind the effect of the transmembrane domain of Ii on CD8 responses remain unclear. Indeed, Benedict R. Halbroth *et al.* showed that Ii adjuvant effect on CD8 response was linked to antigen multimerisation. Multimerisation is known to promote antigen stabilisation thereby promoting better cross presentation of the antigen of interest in APCs[204]. Interestingly, another study by Ilaria Esposito *et al.* showed that the adjuvant effect of li in Chad63 in human against HCV antigen was due to a small region just after the transmembrane domain. This domain was able to promote protein ubiquitination and proteosome degradation of the peptide of interest, which in turn improved MHCI-peptide complex formation[205]. The two studies generated their mutant differently but also explored two different peptides which could explain the discrepancy between the different mechanisms found. Additionally, it is not excluded that Ii acts on different aspect of the antigen processing process to improve CD8 responses, with preferential mechanisms being influenced by the antigen linked to Ii. Importantly,

ChAdOx1-Ii-P1A using the transmembrane domain of Ii has been shown to enhance $CD8^+$ T-cell response magnitude and anti-tumour activity compared to ChAdOx1-P1A in murine tumour models[179].

1.2.2.4 Combination therapies with immunomodulatory agents

Our understanding of the tumour environment and suppressive mechanisms have given rise to numerous therapies modulating this environment to fight cancer progression. However, each strategy has been designed to target one particular aspect of the TME. As previously discussed, the TME is heterogeneous in terms of its cell composition and immunosuppressive and growth mechanisms. Therefore, it is necessary to combine therapies for the development of effective strategies against cancer. Particularly, the combinations of immunotherapies and chemotherapies has recently been investigated in order to create, support and sustain the anti-tumour responses[206]. For example, the combination of anti-PD1 with vaccination has shown enhanced tumour control compared to the single treatments in murine models[179,181]. The combination of chemotherapy and cancer peptide vaccines has also been explored, showing improved tumour control in HPV murine tumour models[150] and improved survival in cervical cancer patients[207]. Similarly, the combination of CAR T cells with an RNA based cancer vaccine improved the cytolytic activity and expansion of the CAR T cells improving their efficacy against solid tumours[208]. CAR T cells have been combined with chemotherapy which also showed great promise in amplifying CAR T cell efficacy[209]. Moreover, pembrolizumab in combination with CarboTaxol is now the standard of care (SoC) for NSCLC patients[210]. Collectively, combination of two treatments have shown promising efficacy, but still needs improvement. Hence, the further addition of other therapies with complimentary roles could supplement these combinations. In fact, anti-cancer strategies need to target the

multi-dimensional aspects of cancer. As such, the strategies for treating cancer need to be as smart and relentless as the tumour growth is fast and aggressive.

Importantly, when combining immunomodulatory agents, the therapeutic window for every single one of the treatments will be of major importance to achieve the best synergistic effects. One main example was the loss of synergy between anti-PD1 and cancer vaccines when the anti-PD1 was given prior to vaccination in TC-1 tumour model[211]. The synergistic effects between paclitaxel or cyclophosphamide and a GM-CSF expressing whole cell vaccine made from irradiated GM-CSF-expressing mammary tumour cell lines, were dependent of the sequence of administration. Indeed, improved tumour control was observed only when paclitaxel or cyclophosphamide was given one day prior to the vaccine, but not seven days later. In contrast, doxorubicin synergised with the same whole cell vaccine when given 7 days later [212]. Similarly, adoptive immunotherapy given 24h after cyclophosphamide showed maximum anti-tumour activity in DBA/2 mice, whereas adoptive cells transferred 3 days after treatment displayed reduce anti-tumour activity[213]. As previously discussed, chemotherapy immunomodulatory effects are dependent on the type of chemotherapy but also on the dose and frequency of treatments[137]. Therefore, the sequence of administration of chemotherapy and immunotherapies such as anti-PD1 and vaccines, must be built by taking into consideration the mechanism of each drug and the timing of their impact on the immune system. Only a full comprehension of these immunomodulatory drug's optimal therapeutic window will give birth to efficient synergy and anti-cancer strategies.

1.3 Thesis Aims

The central paradigm of this project was to test a combination of three different types of treatments: 1) chemotherapy, composed of an alkylating agent Carboplatin and a taxane Paclitaxel, 2) the CPI anti-PD1 and 3) the viral vector vaccines ChAdOx1/MVA.

The specific aims of this thesis were:

- To test the efficacy of a triple combination of treatment based on chemotherapy (Carboplatin+Paclitaxel, referred as CarboTaxol), anti-PD1, and viral vector vaccine ChAdOx1/MVA.
- To investigate the mechanism behind the synergy of these three treatments.
- To understand the mechanism through which CarboTaxol improves ChAdOx1/MVA vaccine immunogenicity.
- To determine the importance of the therapeutic window for chemotherapy relative to the vaccine.
- To explore the importance of the therapeutic window for anti-PD1 relative to the vaccine.

Chapter II: Materials and methods

2.1 Materials

2.1.1 Reagents and kits

Table 1. List of reagents and kits

Reagent	Supplier	Catalogue No.
ACK (Ammonium-Chloride-Potassium) lysing buffer	Gibco™, ThermoFisher Scientific	A10492-01
Anti-Mouse CD16/CD32 (Mouse BD Fc Block)	BD Biosciences	553142
Anti-Mouse CD28 (37.51 clone)	Tonbo Biosciences	70-0281-U100
Anti-mouse CD3ε (clone 145-2C11)	Biolegend	100339
Brefeldin A	Abcam	ab193369
CD8a+ T Cell Isolation Kit, mouse	MACS Miltenyi Biotec	130-104-075
CellTrace™ Violet Cell Proliferation Kit	Thermo Fisher Scientific	C34557
Collagenase type I	Gibco™, Thermo Fisher Scientific	17100017
Cytofix/Cytoperm™ solution	BD Biosciences	554722
Desoxyribonuclease I (DNase I)	Roche	10-104-159-001
eBioscience™ Foxp3 / Transcription Factor Staining Buffer Set	Invitrogen, Thermofisher Scientific	00-5523-00
EDTA, 0.5M solution	VWR	E522-100ML
ELISA MAX™ Deluxe Set Mouse IL-12/IL23 (p40)	Biolegend	431604
ELISA MAX™ Deluxe Set Mouse IFN-α	Biolegend	447904
ELISA MAX™ Standard Set Mouse IL-1β	Biolegend	432601
Isoflurane	Zoetis, IsoFlo®	50019100
Mouse rIL3	Tonbo	1-8031-U002

Myeloid-Derived Suppressor Cell Isolation Kit, mouse	MACS Miltenyi Biotec	130-094-538
Sodium Chloride 0.9%	Sigma Aldricth	S8776-100ml
Trypsin-EDTA (0.25%)	Gibco, Life Tech	25200-056
Tween-20	Sigma Aldritch	P-7949

2.1.2 Buffers and media

Table 2. ACK lysis buffer for mouse blood (10X, ph7.3)

Reagent	Concentration	Supplier
ddH2O	-	-
NH4Cl	0.15mM	Sigma Aldrich
KHCO3	1mM	VWR
Tetrasodium EDTA	0.1mM	Flourochem

Table 3. Tumour dissociation buffer

Reagent	Concentration	Supplier
RPMI 1640 medium	-	Gibco™, ThermoFisher Scientific
DNase I	20ug/ml	Roche
Collagenase type I	175U/ml	VWR

Table 4. Complete RPMI

Reagent	Concentration	Supplier
RPMI 1640 medium	-	-
Penicillin/Streptomycin(100X)	1%	Gibco™, ThermoFisher Scientific
L-Glutamine (100X)	1%	Gibco™, ThermoFisher Scientific
Foetal Bovine Serum (FBS)	10%	Labtech

Table 5. 15V4T3 culture media (complete IMDM)

Reagent	Concentration	Supplier
Iscove's Modified Dulbecco's Medium (IMDM)	-	-
Penicillin/Streptomycin(100X)	1%	Gibco™, ThermoFisher Scientific
L-Glutamine (100X)	1%	Gibco™, ThermoFisher Scientific
Foetal Bovine Serum (FBS)	10%	Labtech

Table 6. T cell media for co-culture

Reagent	Concentration	Supplier
RPMI 1640 medium	-	-
Penicillin/Streptomycin(100X)	1%	Gibco™, ThermoFisher Scientific
L-Glutamine (100X)	1%	Gibco™, ThermoFisher Scientific
Foetal Bovine Serum (FBS)	10%	Labtech
Sodium Pyruvate (100mM)	1%	Cytiva, HyClone Labs
MEM non-essential AA	1%	Gibco, Life Tech
1M Hepes Buffer	1%	Gibco, Life Tech
2-mercaptoethanol (1000X)	0.1%	Gibco, Life Tech

Table 7. FACS buffer

Reagent	Concentration	Supplier
PBS	-	Gibco™, ThermoFisher Scientific
FBS	2%	Labtech
EDTA	2mM	VWR

Table 8. MACS buffer

Reagent	Concentration	Supplier
PBS	-	Gibco™, ThermoFisher Scientific
BSA	0.5%	Sigma Aldritch
EDTA	2mM	VWR

2.1.3 Cell lines

Table 9. Cell lines

Cell line	Supplier
15V4T3	Provided by Prof. Benoit Van Den Eynde's Lab, Ludwig Institute for Cancer Research, Brussels branch
TC-1	Provided by Dr Andrei Ramirez-Valdez, NIH

2.1.4 Vaccines

Table 10. Viral vector vaccines

Viral vector	Insert
ChAdOx1	mIi-P1A GFP DPY E6-E7
MVA	tpA-P1A -P1A DPY E6-E7

2.1.5 Therapeutic monoclonal antibodies

Table 11. Monoclonal antibodies

Monoclonal antibody's target	Clone	Supplier
PD1	RMPI-14	BioXcell
GR1	RB6-8C5	BioXcell

Ly6G	1A8	BioXcell
IL12/23(p40)	C17.8	BioXcell
Rat IgG2a isotype control (for anti-PD1, Ly6G and IL12(p40) antibodies)	2A3	BioXcell
Rat IgG2b isotype control (for anti-GR1 antibody)	LTF-2	BioXcell

2.1.6 Chemotherapies

Table 12. chemotherapies

Chemotherapy	Supplier
Carboplatin	Accord
Paclitaxel	Accord

2.1.7 Mice

The studies performed for this thesis were carried out in accordance with the terms of the UK Animals Act Project License (PPL) (PPB050649E).

Table 13. Mouse strains

Strain	Supplier	Age for studies
DBA/2	Envigo,UK	8-11 weeks old
C57BL/6	Envigo,UK	8-11 weeks old

2.1.8 Peptides

Peptides for P1A and E6/ E7 proteins used for T-cell stimulations were synthesised by peptides and elephant. For the P1A protein, 54 15-mer peptides overlapping each over by 10 amino acids and covering the entire length of the protein were used. For the E6, the

25-mer CKQQLLRREVYDFAFRDLCIVYRDG was used while for the E7 the 19-mer GQAEPDRAHYNIVTFCCKCD was used. Individual peptides were initially dissolved in DMSO then P1A peptides were pooled; and E6 was pooled with E7 for stimulation. Details of the peptide sequences contained in each of the P1A pools can be found in the appendix.

2.1.9 Flow cytometry antibodies

Table 14. Cytokine panel

Antigen	Fluorophore	Clone	dilution	Supplier
CD4	BV421	GK1.5	1:200	Biolegend
CD8a	BUV395	53-6.7	1:200	BD Horizon
IFNγ	APC	XMG1.2	1:200	Biolegend
TNFα	FITC	MP6-XT22	1:250	Biolegend
IL2	PE	JES6-5H4	1:200	Biolegend
Live/Dead Aqua	NA	NA	1:400	Thermo Scientific

Table 15. General panel

Antigen	Fluorophore	Clone	dilution	Supplier
CD45	FITC	30-F11	1:200	Biolegend
CD4	Alexa-Fluor 700	GK1.5	1:200	Biolegend
CD8a	BV605	53-6.7	1:200	Biolegend
PD1	PE	29F.1A12	1:200	Biolegend
CD19	BV650	6D5	1:200	Biolegend
GR1	BV421	RB6-8C5	1:200	Biolegend
CD11b	APC	M1/70	1:200	Biolegend
CD11c	PE-dazzle 594	N418	1:100	Biolegend
Ly6G	PE-cy7	1A8	1:200	Biolegend
Ly6C	APC-Cy7	HK1.4	1:200	Biolegend
Live/Dead Aqua	NA	NA	1:400	Thermo Scientific

Table 16. T cell panel for Harvest

Antigen	Fluorophore	Clone	dilution	Supplier
CD38	Alexa-Fluor 700	90	1:200	ebioscience
CD4	FITC	GK1.5	1:200	Biolegend
CD8a	BUV395	53-6.7	1:200	BD Horizon
CD69 (or Tetramer)	PE	H1.2F3	1:250	Biolegend
TCF1	Alexa-Fluor 647	C63D9	1:1000	Cell Signaling technology
CD44	BUV805	IM7	1:200	Biolegend
CD62L	BV650	MEL-14	1:200	Biolegend
PD1	BV421	29F.1A12	1:200	Biolegend
CD25	BV605	PC61	1:200	Biolegend
Foxp3	PE efluor 610	61-5773-82	1:300	Biolegend
NKP46	PE-cy7	29A1.4	1:100	Biolegend
CD3	APC-Cy7	17A2	1:200	Biolegend
Live/Dead Aqua	NA	NA	1:400	Thermo Scientific

Table 17. T cell exhaustion panel and tetramer for late Harvest

Antigen	Fluorophore	Clone	dilution	Supplier
CD38	Alexa-Fluor 700	90	1:200	ebioscience
CD4	BV605	GK1.5	1:200	Biolegend
CD8a	FITC	53-6.7	1:200	Biolegend
Tetramer	PE	NA	1:250	NA
Lag3	BV650	C9B7/W	1:100	Biolegend
Tim3	BV421	RMT3-23	1:200	Biolegend
CD3	APC	17A2	1:200	Biolegend
PD1	PE-cy7	29F.1A12	1:200	Biolegend
CD44	APC-Cy7	IM7	1:200	Biolegend
Live/Dead Aqua	NA	NA	1:400	Thermo Scientific

Table 18. Myeloid cell panel for Harvest

Antigen	Fluorophore	Clone	dilution	Supplier
CD45	BUV805	30-F11	1:200	Biolegend
F4/80	BV421	BM8	1:50	Biolegend
MHCII	BUV395	2G9	1:200	BD Horizon
CD11b	FITC	M1/70	1:200	NA
Ly6G	PE-cy7	1A8	1:200	Biolegend
Ly6C	APC-cy7	HK1.4	1:200	Biolegend
CCR2	APC	SA2O3G11	1:150	Biolegend
CD38	AX700	90	1:200	Biolegend
CD11c	PE-dazzle	N418	1:100	Biolegend
CD14	BV605	SA14-2	1:250	Biolegend
iNos	PE	CXNFT	1:100	eBioscience
CD206	BV605	C068C2	1:100	Biolegend
Live/Dead Aqua	NA	NA	1:400	Thermo Scientific

Table 19. Dendritic cell panel for Harvest

Antigen	Fluorophore	Clone	dilution	Supplier
CD45	BUV805	30-F11	1:200	Biolegend
F4/80	BV650	BM8	1:50	Biolegend
MHCII	BUV395	2G9	1:200	BD Horizon
CD11b	FITC	M1/70	1:200	NA
Ly6G	PE-cy7	1A8	1:200	Biolegend
CD86	APC-cy7	GL-1	1:200	Biolegend
CD64	APC	x54-5/7.1	1:150	Biolegend
CD172a	AX700	P84	1:200	Biolegend
CD11c	PE-dazzle	N418	1:100	Biolegend
CCR2	BV605	SA2O3G11	1:250	Biolegend
XCR1	PE	ZET	1:100	eBioscience
CD80	BV421	16-10A1	1:100	Biolegend
Live/Dead Aqua	NA	NA	1:400	Thermo Scientific

Table 20. IL12/23(p40) panel

Antigen	Fluorophore	Clone	dilution	Supplier
CD45	BUV805	30-F11	1:200	Biolegend
IL12/23(p40)	APC	C15.6	1:100	Biolegend
Ly6G	PE	1A8	1:200	Biolegend
CD19	BV650	6D5	1:200	Biolegend
F4/80	BV421	BM8	1:50	Biolegend
CD11b	FITC	M1/70	1:200	Biolegend
CD11c	PE-dazzle 594	N418	1:100	Biolegend
Ly6C	PE-Cy7	HK1.4	1:200	Biolegend
Live/Dead Aqua	NA	NA	1:400	Thermo Scientific

2.1.10 Tetramer

H-2L^{d}/P1A$_{35-43}$- LPYLGWLVF multimer was provided by Prof Benoit Van Den Eynde's Lab, Ludwig Institute for Cancer Research, Brussels branch.

2.1.11 Instruments and software

Table 21. Instruments

Instrument	Supplier
BD Fortessa flow cytometer	BD Biosciences
SH800z FACS sorter	Sony

gentleMACS dissociator	Miltenyi Biotec, Surrey, UK
CLARIOstar PLUS	BMG Labtech
Cell Counter	Biorad

Table 22. Software

Software	Supplier
FlowJo version 10	Tree Star, Ashland, OR, UDA
GraphPad Prism version 8	GraphPad software, CA, USA
gentleMACS dissociator	Miltenyi Biotec, Surrey, UK
Reader Control, MARS (CLARIOstar)	BMG Labtech

2.2 Methods

2.2.1 ChAdOx1 and MVA viral vectors

ChAdOx1 and MVA viral vectors were produced by the Viral Vector Core Facility, University of Oxford, UK. Insert sequences for the viral vectors were cloned by Dr Carol Leung and Dr Emily Pollock. In this study, ChAdOx1 encoding for the P1A antigen was also expressing the transmembrane domain of the murine MHC-class II invariant chain (mIi also refers as Ii) fused to the N-terminus domain of P1A. Unless specified, the MVA vector encoding P1A was also encoding for the signal peptide from the transmembrane domain of the murine tissue plasminogen activator (tpA) which was fused to P1A N-terminus. For the E6/E7 vaccines, only the 2 unmodified E6-E7 coding sequences were inserted.

2.2.2 Cell culture

All cell cultures were maintained in an incubator set at 37°C, 5% CO2.

15V4T3

15V4T3 were thawed in IMDM complete media supplemented with 25 U/ml of mouse recombinant IL3 to help their recovery after cryostorage. Subsequently, 15V4T3 were cultured in complete IMDM and passaged every 2 to 3 days before they reach 90% confluency. Briefly, 15V4T3 cells were diluted in pre-warmed complete IMDM medium to the desired splitting ratio and transferred to fresh tissue culture flasks.

TC-1

TC-1 cells were thawed and culture in complete RPMI. They were passaged every 2 to 3 days before they reach 90% confluency. TC-1 cells are adherent cells and were passaged by first removing the old media. Then cells were washed with PBS to remove residual dead

cells and cell culture medium. TC-1 cells were incubated for less than 5 min with trypsin-EDTA (0.05%) at 37^{o}C to detach cells from the surface of the tissue culture flask. Trypsinisation was stopped by the addition of cell culture medium, and detached cells were then diluted in new pre-warmed medium at the desired density and seeded into a new fresh tissue culture flask.

2.2.3 Collection of tissues

Tissues were kept on ice throughout their processing. Buffers used for processing were kept at a temperature of 4 °C unless mentioned otherwise. Centrifugation steps were also performed at 4 °C.

2.2.3.1 Blood

Blood was collected from mice via a tail vein bleed. Mice were first warmed in a heat box for 10 minutes at 38°C to promote vasodilation. Blood was withdrawn by making a small incision in the lateral vein of the mouse tail using a scalpel blade. Blood was then collected into 1.5ml Eppendorf tubes containing 200µl of 12.5mM EDTA in PBS to inhibit coagulation. Between 70 to 150µl of blood per mouse was collected. No more than 10% of a mouse's total blood volume was collected at any one time and no more than 15% of total blood volume was collected within a month as stipulated in the terms of the PPL. If plasma was needed, tubes were centrifuged at 500g for 2min, and plasma collected and frozen down at -20°C before the following steps. Then, red blood cells were lysed by incubating samples in the ACK buffer specified in table 2 for use with mouse blood. Two cycles of ACK lysis were performed in order to get purified Peripheral Blood Mononuclear Cells (PBMCs) and to maximise their viability. 1ml of ACK lysis buffer was added to the collected blood samples for the first step and samples were incubated with ACK buffer for 10 minutes at room temperature (RT). The blood samples were then washed with cold PBS,

centrifuged at 500g resuspended for 5 min. The supernatants were removed through aspiration to avoid any cell loss after this first step. For the second cycle, another ml of ACK buffer was added to the samples for 5min at RT. Blood samples were then washed twice more with cold PBS, supernatants decanted, before being resuspended in complete RPMI medium prior to downstream analysis.

For serum collection, blood was collected into special serum collection tubes (BD Microtainer™ tubes). The blood was incubated for 30min in these tubes, then spun at 10000g for 5min. Once isolated, serum was frozen at -20°C for future ELISAs.

2.2.3.2 Spleens

Mice were euthanised and spleens were harvested by surgical excision on their left flank. Spleens were weighted and transferred into Eppendorf tubes, containing cold RPMI. Each spleen was mashed through a 70 μm cell strainer placed on 50 ml falcon tube. The strainer was rinsed with 3 or 10 ml of cold RPMI or PBS respectively depending on downstream experiments (i.e ELISA or not). The volume of RPMI or PBS-containing the dissociated spleen was passed through the strainer again. The tubes were then centrifuge for 5min at 500g and the supernatants were either decanted (PBS, 10ml) or froze down (RPMI, 3 ml) for subsequent ELISA analysis(-20°C). The samples were lysed with 1ml of ACK lysis buffer for 5min at RT and then diluted with PBS to stop the lysis. Cells were then pass through a 70μm cell strainer into a new falcon tube, and centrifuge for 5min at 500g. The loose pellet was resuspended in complete RPMI and strained in a 70um strainer into a new falcon tube before counting.

2.2.3.3 Bone marrows

Bones (femur + tibia) were harvested and cleaned before being placed in RPMI-containing Eppendorf tubes. The bones extremities were cut and placed into 0.5ml PCR

tubes, perforated at the bottom with the use of a 30G needle. The PCR tubes were placed in 1.5ml Eppendorf tubes and centrifuged at 11000g for 20 seconds. 1ml of PBS was then added to the 1.5ml Eppendorf tubes, containing bone marrow cells. The cell suspensions were gently resuspended, strained through a 70μm strainer into a 50ml falcon tubes, topped with 10ml of PBS and centrifuged 5min at 500g. Finally, the cells were resuspended in 1ml of R10 and, if necessary, strained again in a new 50ml tube through a 70μm strainer, before counting.

2.2.3.4 Tumours

Tumours were weighted and collected into RPMI 1640 medium in 1.5ml Eppendorf tubes. Tumours were then transferred into gentleMACS C-tubes containing 4ml of tumour dissociation buffer. To obtain single cell suspensions, tumours were dissociated using programme m_impTumor_01 of the gentle MACS dissociator instrument and incubated for 15 minutes in tumour dissociation buffer at 37°C and 5% CO2. Following incubation, cell suspensions were centrifuged at 500g for 5 min and supernatants were harvested and froze down for future ELISA assays (-20°C). Tumour cells were then resuspended with 15-20ml of PBS and passed through 70μm cell strainers and centrifuged at 500g for 5min. Cell suspensions were then resuspended in 1ml of R10 and strained through filtered 5ml FACS tube before cell counting. Cell count was always performed manually for tumour samples.

2.2.3.5 Lymph Nodes

Popliteal Lymph nodes (pLN) were collected by surgical excision and transferred into 1.5ml Eppendorf tubes. Lymph nodes were gently mashed between 2 microscope glass slides onto a petri dish and collected into 5 ml of PBS. The cell suspension was then stained through a 70um strainer, topped with 5ml of cold PBS and centrifuged for 5 min at 500g. Supernatant was then aspirated. Cells were finally resuspended into 1ml of R10 for counting.

2.2.4 ELISAs

ELISAs were performed following manufacturer's protocol (Biolegend). Briefly, one day prior to running the ELISA, 96-wells Nunc™ MaxiSorp™ ELISA plates were coated with 100µl of the capture antibody solution per well, sealed and incubated overnight at 4°C. The next day, plates were washed 4 times with at least 300µl of wash buffer per well and residual buffer were discarded by firmly tapping plate upside down on absorbent paper. All subsequent washes were performed similarly. To block non-specific binding and reduce background, 200µl of assay diluent was plated into each well and plates were incubated at RT for 1 hour and placed on a plate shaker at 400 rpm. Then, plates were washed 4 times with wash buffer. 50 µl/well of standard dilutions and samples were added to the appropriate wells. Of note, spleen, and tumour supernatants and plasma-EDTA from tissue collection were not further diluted. Serum was diluted 1:3 in assay diluent. Samples were incubated at RT for 2 hours with shaking. Plates were washed and samples were incubated with 100µl of detection antibody solution (diluted in assay diluent) for 1 hour at RT with shaking. Plates were once again washed 4 times and 100µl of diluted Avidin-HRP solution was added to each well for 30 minutes. For the final wash, plates were washed 5 times. Then 100µL of TMB substrate solution were added as quick as possible into each well and incubated in the dark for 15 to 30 minutes the colour develops. Finally, 100µl of stop solution was added to each well to stop the reaction. Absorbance was read with the CLARIOstar at 450 nm within 15 minutes.

2.2.5 Co-culture

2.2.5.1 Isolation of $Ly6G^+$ cells

All centrifugation steps were performed at 4°C, 300g for 7min for $CD11b^+Ly6G^+$ cell extraction. The samples were kept cold throughout the extraction and the incubation steps were carried out at 4°C.

Spleens from tumour bearing DBA/2 mice (size range between 300 to 500 mm^3), were collected and processed following protocol mentioned in 2.3.2. Once the splenocyte suspension was counted, $CD11b^+Ly6G^+$ cells were extracted by magnetic selection with the Myeloid-Derived Suppressor Cell Isolation Kit, from Miltenyi Biotec. Briefly, splenocytes were washed with 10ml of MACS buffer centrifuged and the pellet was resuspended in 350µl of MACS buffer and 50µl of Fc block reagent per 10^8 cells and incubated for 10min. Following incubation, an additional 100µl of anti-ly6G-biotin was directly added to the mix and incubated for an extra 10 min. Cells were washed with 10ml of MACS buffer and then resuspended in 800µl of MACS buffer and 200µl of anti-biotin microbeads. Samples were incubated in that mix for 15min. Following this incubation step, cells were washed with 15ml of buffer, and resuspended in at least 1ml of MACS buffer for separation in LS column. Column was place on magnetic field and washed once with 3ml of MACS buffer and cells were passed through the column. Column was then washed 3 times with 3ml of MACS buffer. Following the washing step, the column was removed from the magnetic field and flush with 5 ml of MACS buffer into a 30ml white cap tubes. The fraction of cells collected were the $CD11b^+$ $GR1^{hi}$ $Ly6G^+$ cells. However, for DBA/2 mice the purity was usually below 70% and this fraction contained many dead cells and debris. Therefore, the fraction of $Ly6G^+$ cells were then sorted to achieve a higher purity of 98 % or above. The cells were counted, centrifuged, and resuspended in 500ul of PBS containing Live/Dead (aqua), anti-mouse CD11b(APC, biolegend), Ly6G (PE, biolegend).

Cells were incubated for 20min and washed once with 5ml of FACS buffer. The pellet was resuspended in 2ml of FACS buffer and $Ly6G^+$ cells were sorted on the Sony SH800z FACS sorter. Following sort, cells were counted cells, and viability was first assessed using the trypan blue exclusion method. Furthermore, the viability was confirmed by flow cytometry together with the purity of the sorted fraction using BD Fortessa flow cytometer. $CD11b^+Ly6G^+$ cells were then washed in 5ml of T cell media, resuspended at the right concentrations to achieved different T cell to $CD11b^+Ly6G^+$ cell ratios. 100µl of the different concentrations of $CD11b^+Ly6G^+$ were plated into a round-bottom 96-well plate coated with anti-CD3 antibody. Plate was coated with 100µl of 1µg/ml of anti-CD3 and incubated for 2h at 37°C. Directly prior to plating $CD11b^+Ly6G^+$ cells, plate was washed twice with 200µl of RT PBS and lastly, once with 200µl T cell media also at RT.

2.2.5.2 $CD8^+$ T cell isolation

Spleens from naïve mice were collected and $CD8^+$ T cell were isolated using negative selection, CD8a+ T Cell Isolation Kit from Miltenyi Biotec. Briefly, splenocytes were obtained following the protocol presented in section 2.3.2, counted, and resuspended in 40µl of MACS buffer and 10 µl of biotin-antibody cocktail per 10^7 cells. The cell suspension was then incubated for 5 minutes at 4°C. Following incubation, 30 µL of MACS buffer per 10^7 total cells was added together with 20 µL of anti-biotin MicroBeads and incubated for 10 minutes at 4°C. A LS column was placed on a magnetic field and rinse with 3ml of MACS buffer. The cell suspension was applied onto the column and the enriched $CD8^+$ T cell fraction was collected from the flow through in a 30ml white cap tube. The column was washed once with 3ml of MACS buffer and the flow through with $CD8^+$ T cells was collected. $CD8^+$ T cells were then counted prior to CellTrace staining.

2.2.5.3 CellTrace Violet staining and $CD8^+$ T cell culture with $CD11b^+Ly6G^+$ cells

Following $CD8^+$ T cell isolation, cells were centrifuged in cold PBS and resuspended in PBS at RT with a concentration range of 10 to $20x10^6$ cells/ml. 1µl of CellTrace Violet stock solution (in DMSO) was added to each ml of cell suspension for a final working solution of 5µM. Cells were incubated for 20 min at RT, protected from light. Then, to remove any free dye remaining in the solution, five times of the original staining volume of T cell media (pre-warmed) was added to the cells and incubated for 5 min at RT. The cells were centrifuged for 5min at 500g and resuspended in fresh pre-warmed T cell media. $1x10^5$ $CD8^+$ T cells were plated in the 96-well round-bottom plate containing $CD11b^+$ Ly6G+. Finally, anti-CD28 was added at a final concentration of 1µg/ml into the plate. 72h later, $CD8^+$ T cells were stained with Live/Dead (aqua) and anti-CD8 (PE, biolegend) and proliferation was assessed.

2.2.6 In vivo mouse studies

2.2.6.1 Vaccination

C57BL/6 and DBA/2 mice were vaccinated with ChAdOx1 and MVA viral vectors encoding either E6/E7 or P1A antigens. Vaccinations were performed under inhalational anaesthesia, using isoflurane as the anaesthetic agent. Vaccines were administrated via intramuscular injection (i.m.) into the right thigh at either a high or low dose regime. The high dose comprised of 10^8 (high) infectious units (IU) of ChAdOx1 virus and 10^7 (high) plaque forming units (PFU) of MVA virus. The low dose comprised of 10^7 IU of ChAdOx1 and 10^6 PFU of MVA in a total volume of 50µl per animal. Vaccines were diluted in sterile PBS for injections. The interval of time between prime and boost differed and were as indicated in treatment schemes. To control for the viral vector itself, ChAdOx1 and MVA expressing DPY, an irrelevant human protein, were used.

2.2.6.2 Monoclonal antibody treatments

CPI

Mice were treated with anti-PD1 monoclonal antibody or the relevant isotype control via intraperitoneal (i.p) injections. Anti-PD1 was and diluted in cold PBS, prepared immediately and kept on ice prior to the injection.100µg of antibody was administrated in 100µl per mouse, at a frequency of 1 injection every third day for a total of 3 to 4 injections. Different timings were tested, relative to the vaccine administration time point, and are indicated in the relevant schemes.

Anti-GR1 and anti-Ly6G

To assess the importance of $CD11b^{+}Ly6G^{+}$ depletion in the synergy observed between vaccine and CarboTaxol, anti-GR1 or anti-Ly6G treatment or the relevant isotype control were used. If one injection schedule was performed, antibodies were administered at a dose of 400ug. In the case where 5 injections were carried out twice weekly, a dose of 200µg per mouse in 100µl total volume was used. The vehicle used for all injections was sterile cold PBS. Antibodies solutions were prepared immediately prior to use and kept on ice until administration.

Anti-IL12/23(p40)

To assess the effect of IL12/23(p40) on TCF1 expression, mice were treated with anti-IL12/23(p40) monoclonal antibody or the relevant isotype control via intraperitoneal (i.p) injections. Anti-IL12/23(p40) was diluted in cold PBS, and prepared immediately and kept on ice prior to the injection. 400µg of antibody was administrated in 100µl per mouse, followed by a dose of 200µg administered in 100µl the next day.

2.2.6.3 Chemotherapy treatment

Mice with an average weight of 20g were administered with Carboplatin and paclitaxel diluted in sterile sodium chloride via i.p injections. Carboplatin was given in 1 dose of 40mg/kg per mouse in 200µl total volume and paclitaxel was given in 2 doses of 20mg/kg per mouse in 200µl total volume. The first dose of paclitaxel was given the same day of the carboplatin administration, and the second dose was given 24h later.

2.2.6.4 Tumour implantation and tumour measurement

Mice were injected subcutaneously (s.c.) in the right flank with $1x10^6$ 15V4T3 cells or $1x10^5$ TC-1 cells suspended in 100ul of cell culture medium without added supplements. Prior to injection, cells were washed with minimal culture medium to remove traces of FCS present the in the complete growth medium. Briefly, cells were harvested from their culture flasks as a single cell suspension, transferred to a 50ml Falcon tube and spun at 400g for 5 mins to obtain a cell pellet. Then, the culture medium was aspirated off and the cell pellet resuspended in 45ml of minimal culture medium. A total of three washes were carried out. After the third wash, cells were manually counted using a haemocytometer, the degree of viability assessed using the trypan blue exclusion method and then resuspended at the required concentration for implantation.

After implantation, mice were monitored for tumour growth. Upon the development of palpable tumours, measurements of tumour length and width were carried out 2-3 times per week using digital callipers. The volume of tumour masses (V) was calculated according to the formula: $V = ((\text{length (mm)} \times \text{width}^2 \text{ (mm)}) \times 0.52)$. On average, tumour studies were started when tumour size reached 50 mm^3. Mice were sacrificed via cervical dislocation when tumour size reached a maximum volume of 900mm^3or when the width or length reached 15mm.

2.2.7 Staining for flow cytometry

2.2.7.1 Peptide stimulation

PBMCs, splenocytes or tumour cells were cultured in complete RPMI media (table 4) and stimulated with αCD28 (2µg/ml) and DNAse I (20µg/ml) and P1A peptide pool or E6/E7 pool (4mg/ml) at 37°C 5% CO2 for 5 hours, with the addition of Brefeldin A (5µg/ml) after 1 hour to promote intracellular cytokine accumulation.

2.2.7.2 Intracellular staining

Samples were kept cold on ice during processing and all incubations and centrifugations were performed at 4°C. Centrifugation steps were performed at 500g.

Cell surface marker staining was performed either in 96-well plate or FACS tubes. After a first washing step with 200µl or 3 ml for respectively 96-well plate or tubes, a blocking step using 50µl Fc block, anti-mouse CD16/CD32 antibody was performed. Then, to assess surface markers, cells were stained with 50µl of a mix of viability dye and specific fluorophore-conjugated antibodies diluted in PBS for 15 to 20 minutes at 4°C. After surface staining, cells were washed twice with 200µl PBS (or once with 3ml for tubes). To assess the presence of cytokine production or cytoplasmic markers in T cells, the cells were fixed and permeabilized by incubation in 100µl of CytoFix/CytoPerm buffer for 20 minutes, washed twice with 1X Perm/Wash buffer and stained specific antibodies in 1X Perm/Wash buffer for 20 minutes. After staining, cells were washed twice more and then resuspended in 120ul of 1X Perm/Wash buffer. Alternatively, to assess the presence of nuclear markers, such as Foxp3 or TCF1, cells were fixed with eBioscience™ Foxp3 / Transcription Factor Staining Buffer Set for 35min at 4°C. After fixation and permeabilization, samples were washed twice with 1X Perm/wash buffer. For the staining of nuclear, and if included in the panel, cytoplasmic markers, antibodies were diluted in 1X perm/wash and samples were

incubated with 50ul of the master mix overnight (12 to 16h). The next day, samples were washed twice in 200µl and resuspended in 120 to 140ul of 1XPerm/wash buffer. Details on antibodies and dilutions used can be found in the materials and reagents section. Samples were acquired on a BD Fortessa cytometer and data were analysed using FlowJo software. Of note, for experiment using the in vivo anti-GR1 antibody, cells were stained intracellularly for the GR1,Ly6C and Ly6G marker as the epitope for these markers were masked by the rat anti-GR1 antibody.

2.2.7.3 Tetramer staining

If tetramer staining was performed, the samples were first washed with 200µl (96-well plate) or 3ml (tube) of cold PBS and then incubated with Fc receptors blocked with CD16/CD32 antibody (5µg/ml) and PE-conjugated H-2L^{d}/P1A$_{35\text{-}43}$-specific multimer diluted in cold PBS, 50ul per wells, for 35 minutes at 4°C. Following multimer staining, samples were washed once with 3ml or, for plate, 3 times with 200µl of PBS and then stained for cell surface and intracellular markers.

2.2.8 Flow cytometry panel gating strategy

2.2.8.1 Intracellular cytokine panel

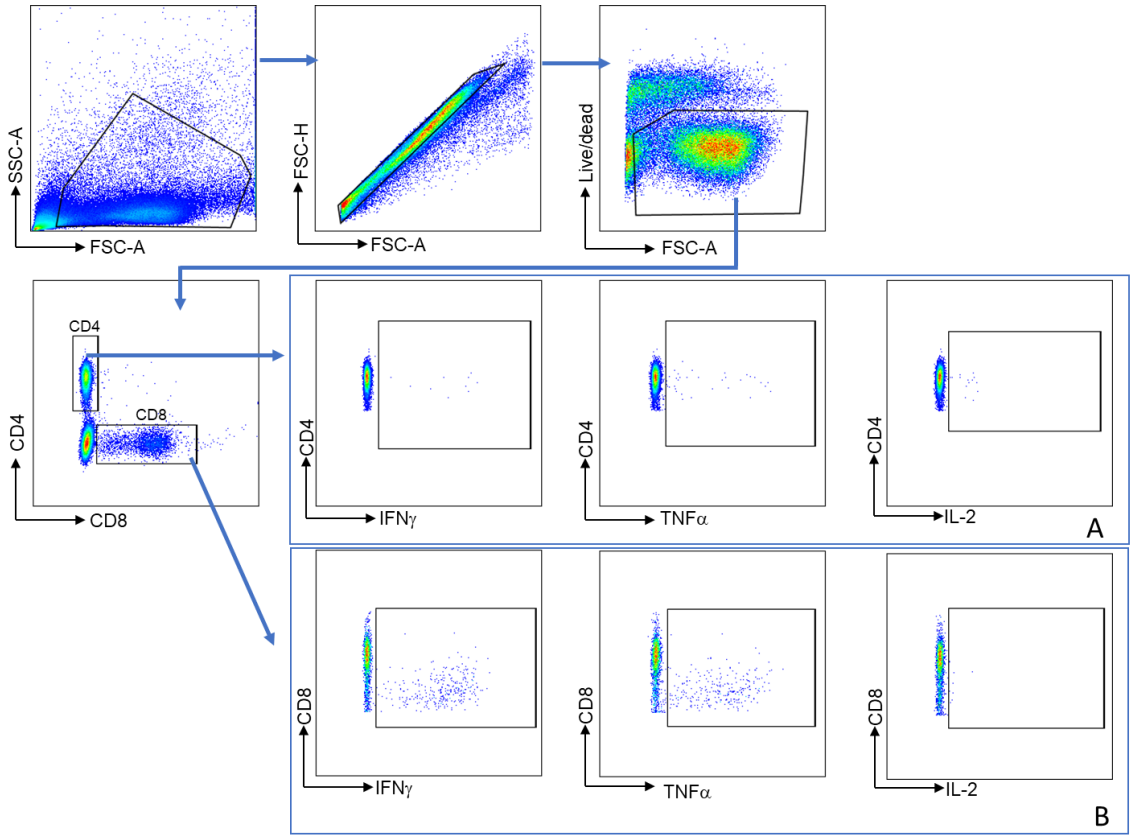


Figure 2.1 Gating strategy for intracellular cytokine staining by flow cytometry. Cells were first gated based on FSC-A and SSC-A properties to exclude debris. Single cells were then gated to exclude doublets and aggregates based on a FSC-H vs FSC-A plot. Live single cells were then gated based on staining with a LIVE/DEAD Aqua marker. $CD8^+$ and $CD4^+$ cells were then discriminated via a CD8 vs CD4 plot. Antigen-specific T-cells responding to antigenic stimulation were then identified by gating on $IFN\gamma^+$, $TNF\alpha^+$, $IL2^+$ events in the $CD4^+$ (B) $CD8^+$ (A) populations. The gates for the cytokine positive cells were set based on the staining signal observed in unstimulated cells taken from unvaccinated control animals. This gating strategy was made from blood samples.

2.2.8.2 General phenotyping panel

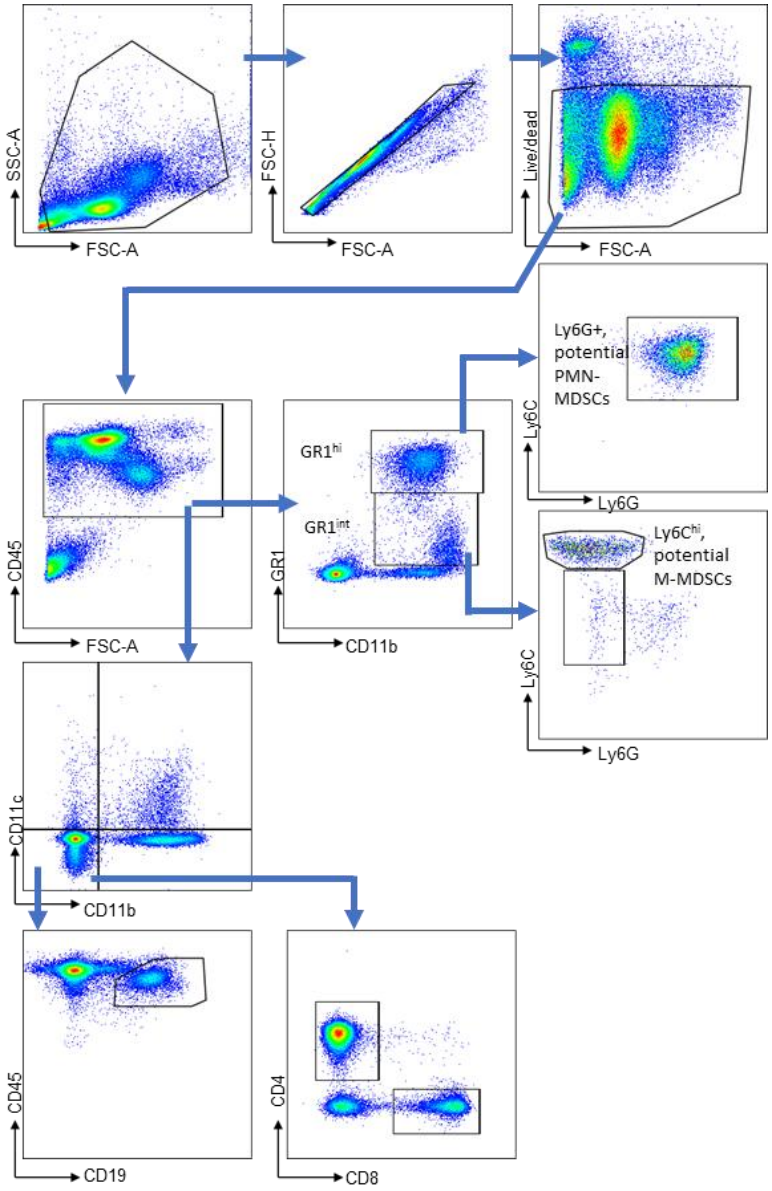


Figure 2.2 Gating strategy for general phenotyping panel. Cells were first gated based on FSC-A and SSC-A properties to exclude debris. Single cells were then gated to exclude doublets and aggregates based on a FSC-H vs FSC-A plot. Live single cells were then gated based on staining with a LIVE/DEAD Aqua marker. $CD45^+$ leucocytes were then gated. Within the leucocyte population, $CD11b^+$, $GR1^+$ cells were discriminated. Within $Gr1^{hi}$ cells, the Ly6G+ positive were determined and within the $GR1^{int}$, the $Ly6C^{hi}$ and ^{int} were defined. $CD19^+$, $CD8^+$ and $CD4^+$ cells were then discriminated within the CD11b-CD11c- cells. This gating strategy is based on blood samples.

2.2.8.3 T cell phenotyping for harvest panel

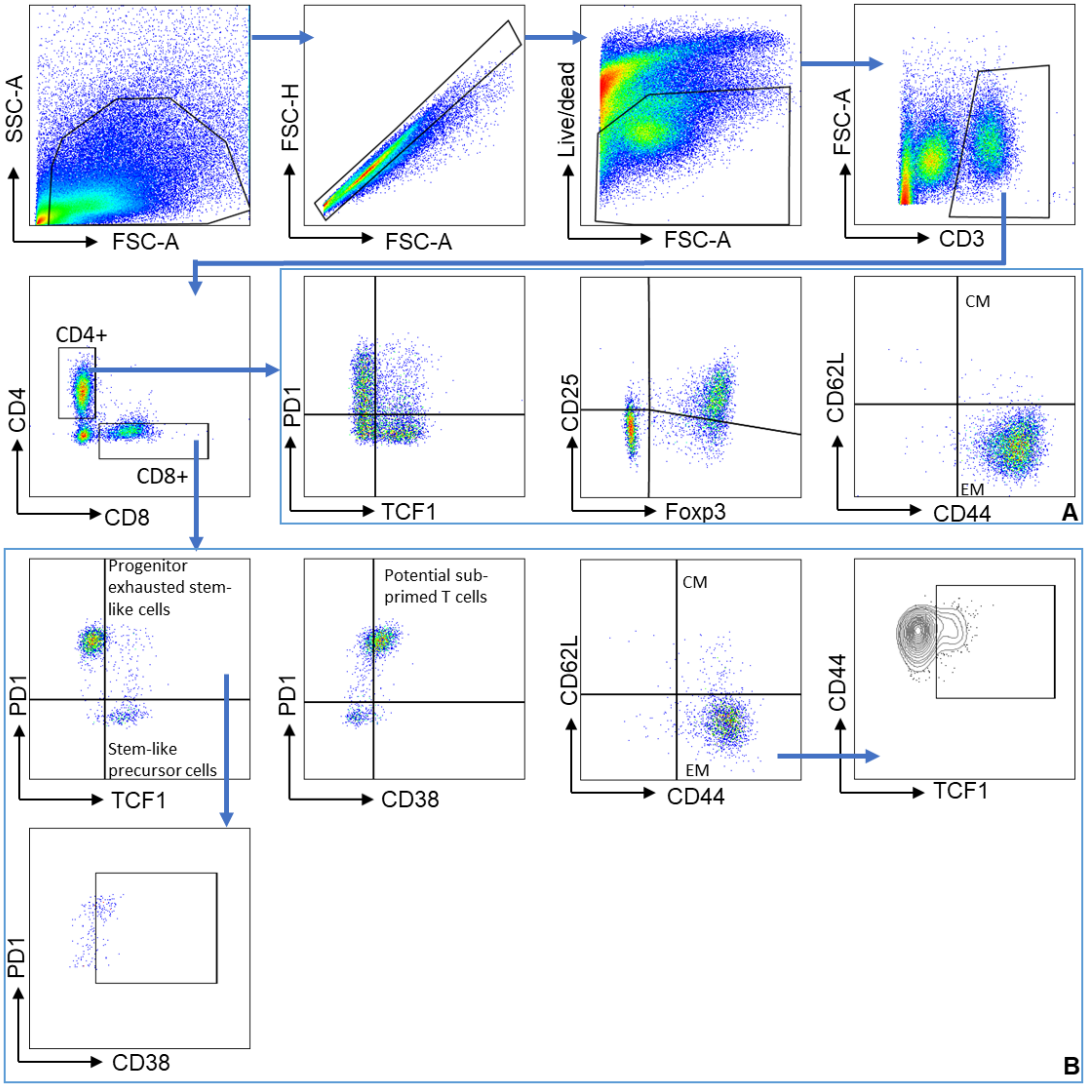


Figure 2.3 Gating strategy for T cell phenotyping panel. Cells were first gated based on FSC-A and SSC-A properties to exclude debris. Single cells were then gated to exclude doublets and aggregates based on a FSC-H vs FSC-A plot. Live single cells were then gated based on staining with a LIVE/DEAD Aqua marker. $CD3^+$ cells were gated. Within this lymphocyte population, $CD8^+$ and $CD4^+$ cells were then discriminated, and populations gated in $CD4^+$ T cells are shown in (A) and in $CD8^+$ T cells are shown in (B). TCF1+PD1+ and $TCF1^+PD1^-$, CM and EM were gated in both $CD4^+$ and $CD8^+$ T cells. Treg (Foxp3, CD25+) were gated in $CD4^+$ T cells. The $CD38^+PD1^+$, potential sub-primed T cells were discriminated in the $CD8^+$ population, such as the $TCF1^+PD1^+$ $CD38^+$ T cells. In $CD8^+$ T cells the TCF1 expression in EM $CD44^+$ cells was confirmed too. This gating strategy was made from tumour samples.

2.2.8.4 T cell exhaustion and tetramer panel for late harvest panel

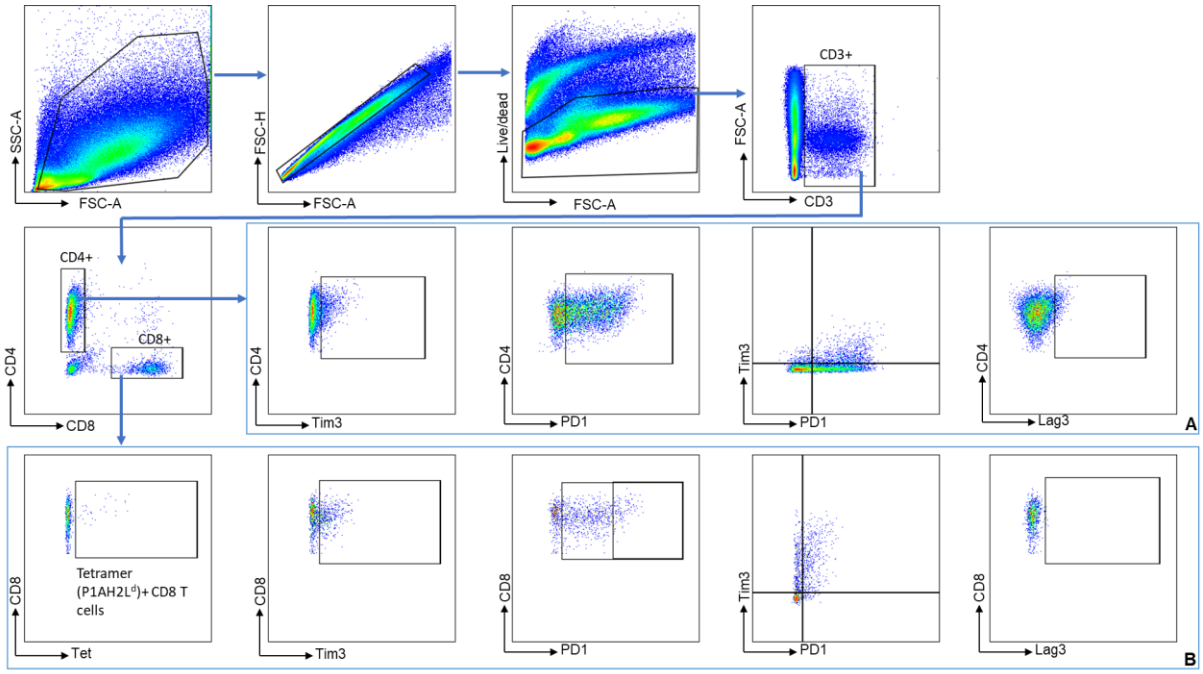


Figure 2.4 Gating strategy for T cell exhaustion and tetramer panel. Cells were first gated based on FSC-A and SSC-A properties to exclude debris. Single cells were then gated to exclude doublets and aggregates based on a FSC-H vs FSC-A plot. Live single cells were then gated based on staining with a LIVE/DEAD Aqua marker. CD3^{+} cells were then gated. Within this lymphocyte population, CD8^{+} and CD4^{+} cells were discriminated via a CD8 vs CD4 plot. Exhaustion markers TIM3, PD1 and LAG3 were evaluated in CD4^{+} T cells (A) and in CD8^{+} T cells (B). The Tetramer^{+} T cells were defined in CD8^{+} T cells. This gating strategy was made from tumour samples.

2.2.8.5 Myeloid cell panel: gating MDSCs without GR1 marker

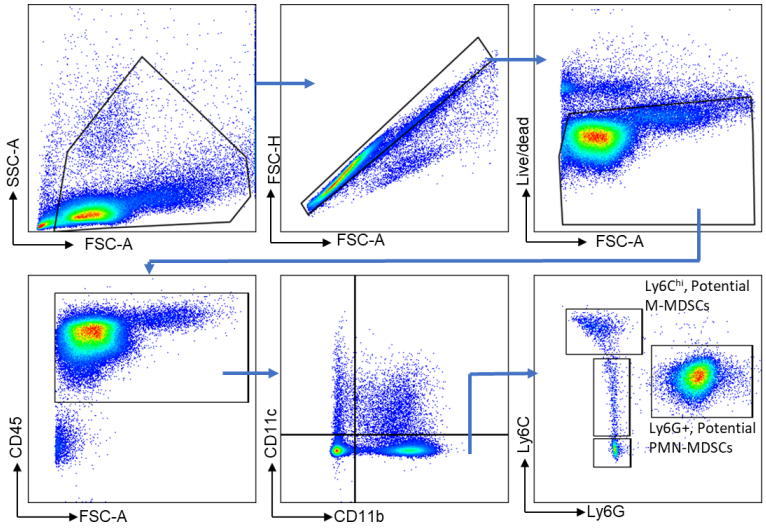


Figure 2.5 Gating strategy for potential MDSCs with the Myeloid cell panel. Cells were first gated based on FSC-A and SSC-A properties to exclude debris. Single cells were then gated to exclude doublets and aggregates based on a FSC-H vs FSC-A plot. Live single cells were then gated based on staining with a LIVE/DEAD Aqua marker. CD45^{+} leucocytes were then gated. Within the leucocyte population, CD11b^{+}, CD11c- cells were gated. Within CD11b^{+} CD11c- cells, the Ly6G^{+} cells (potential PMN-MDSCs) were discriminated against the Ly6C populations among which Ly6C^{hi} (potential M-MDSCs) and ^{int} were defined. This gating strategy is based on splenocyte samples.

2.2.8.6 DC phenotyping panel

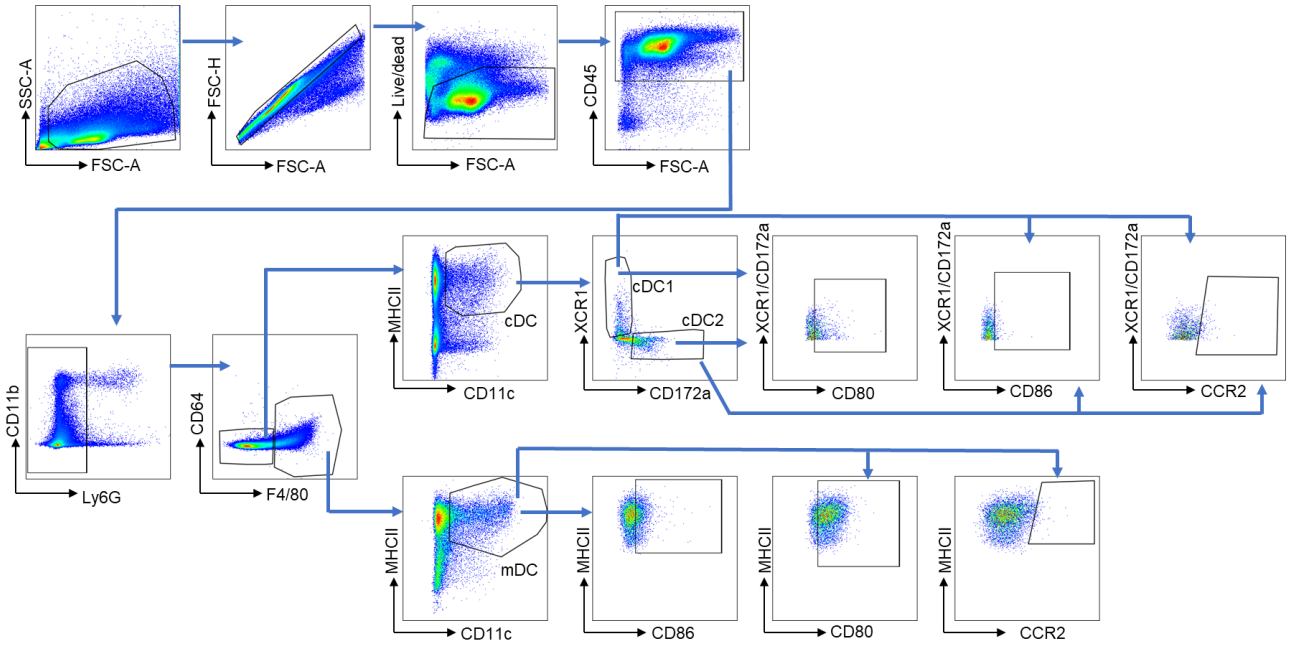


Figure 2.6 Gating strategy for DC phenotyping staining. Cells were first gated based on FSC-A and SSC-A properties to exclude debris. Single cells were then gated to exclude doublets and aggregates based on a FSC-H vs FSC-A plot. Live single cells were then gated based on staining with a LIVE/DEAD Aqua marker. $CD45^+$ leucocytes were then gated. Within the leucocyte population, Ly6G- cells were gated. Within this population, $F4/80^+$ and F4/80- cells were discriminated. Within the F4/80- population, cDC (conventional)were determined based on CD11c and MHCII expression. Within cDCs the cDC1 were distinguished from cDC2 based on XCR1 and CD172a expression respectively. Activation markers expression were evaluated in these 2 subsets. Within the $F4/80^+$ population, mDC (monocytic) were determined based on their expression of MHCII and CD11c. Within the mDC population, activation was also evaluated based on the expression of CD80 and CD86 and CCR2. This gating strategy is based on splenocyte samples.

2.2.8.7 IL12/23(p40) panel

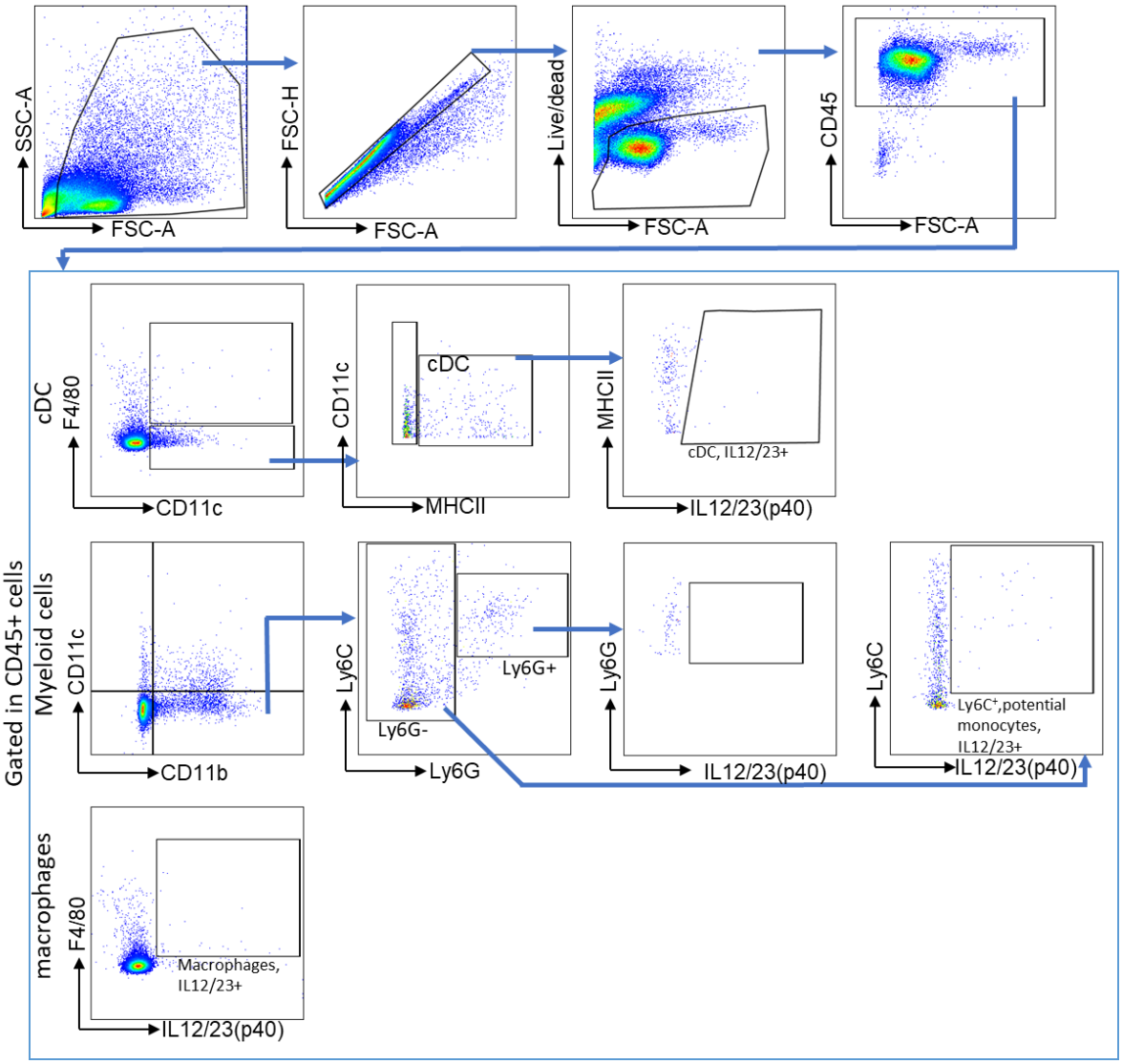


Figure 2.7 Gating strategy for IL12/23(p40) expression in different innate cells. Cells were first gated based on FSC-A and SSC-A properties to exclude debris. Single cells were then gated to exclude doublets and aggregates based on a FSC-H vs FSC-A plot. Live single cells were then gated based on staining with a LIVE/DEAD Aqua marker. $CD45^+$ leucocytes were then gated. Within the leucocyte population, myeloid cells cDCs, and macrophages were determined. cDC were defined as F4/80- CD11c+, MHCII+. Within this population IL12/23(p40) production was evaluated by intracellular staining. The production of IL12/23(p40) was also determined within $CD11b^+$ CD11c- $Ly6G^+$ and $CD11b^+$ CD11c- $Ly6C^+$. Finally, IL12/23(p40) production was assessed in macrophages via a $F4/80^+$ vs $IL12/23^+$ plot. This gating strategy is based on blood samples.

2.2.9 Statistical analysis

2.2.9.1 Mouse studies data

Statistical analyses were performed using GraphPad Prism software. To determine significance between immunogenicity responses comparing multiple groups, a Kruskal-Wallis test with a Dunn's post hoc analysis for multiple comparisons was performed. Alternatively, when mouse number was above 15 mice per group, an ordinary one-way ANOVA was performed followed by Tukey's post hoc to determine significance between groups. In murine tumour studies, a two-way ANOVA followed by Tukey's post hoc test was used to determine statistically significant differences between different groups in term of tumour growth. Survival curves for tumour studies were created using the Kaplan-Meier method and statistical significance in survival between different groups of mice was determined using the log-rank (Mantel-Cox) test. All P values < 0.05 were considered statistically significant.

2.2.9.2 Human RNA-seq data

Single-cell RNA-seq data of PBMCs from ovarian cancer were downloaded from GEO (GSE164378- phs002862.v1.p1) based on prior published study from Min *et al.* The downstream method was performed by Ashwin Jainarayanan: The raw counts matrix was loaded into the Seurat package and combined with the metadata available. The Seurat function PercentageFeatureSet was used to calculate the mitochondrial QC metrics. Further, cells with mitochondrial counts below 5% and unique feature counts between a user set range of 200 and 2500 were filtered for downstream analysis. The data was then log normalized with a scale factor of 10000 and the features that exhibit high cell-to-cell variation were identified. We then performed PCA on the scaled data and cells were clustered using the Louvain algorithm. A UMAP embedding was used to visualize the cell clusters and broad cell types were annotated. The CD3E positive T cells from Seurat object

was further subset into CD8 and CD4 for downstream analysis. The expression of *TCF7* and *PDCD1* were investigated in these broad cell types across baseline and chemo treated patients. The CD8 object were re-clustered and visualized with a UMAP embedding. Differential expression of *TCF7* and *PDCD1* across baseline and chemo treated patients was investigated among the resulting cell types and visualized with a violin plot. Expression of genes were computed using one-sided Wilcoxon rank-sum test. The subsequent analysis was performed by me with the help of Dr Vineethkrishna Chandrasekar. Graph representing the proportion of the population of interest were made using Prism 8.0 software (GraphPad) and, after confirming the normality with a Shapiro-Wilk test, paired t test was performed to compare baseline and post chemotherapy proportions.

Chapter III: ChAdOx1/MVA vaccines synergise with CarboTaxol and anti-PD1 for enhanced immunogenicity, tumour control and survival.

3.1 Introduction

Spontaneous anti-tumour immune responses are usually weak or lacking in many cancer patients. Therefore, developing immunotherapies to tackle this problem has been a major focus in cancer research. Therapeutic cancer vaccines are designed to induce a strong and specific immune response against antigens expressed by cancer cells, making them one of the most promising immunotherapies[176] ,[214] . Unfortunately, cancer vaccines' success in clinical trials has been underwhelming, bringing to light several challenges that must be addressed.

One challenge is the need to find immunogenic targets expressed by cancer cells. Indeed, an ideal tumour antigen should be unique to cancer cells and different enough from healthy tissues to stimulate a sufficiently robust and specific response against the tumour cells only. It would also need to be widely expressed by most cancer cells, so the anti-cancer response is efficient in fighting the whole tumour as well as potential metastases. An ideal tumour antigen would finally need to be expressed across patients to avoid the need for personalised medicine which can be extremely ressource-intensive[215]. Ultimately, an antigen which comprises these 3 characteristics has not been found yet. Therefore, to compensate for the lack of perfect targets, novel and innovative vaccine platforms and combination strategies are needed to trigger a specific and robust anti-tumour immune response.

The type of the induced immune response is key for cancer vaccine efficacy. Cytotoxic $CD8^+$ T cells are of particular importance for the anti-tumour immune response. Through the production of cytotoxic molecules, such as granzyme B, perforin, and type I cytokines, $CD8^+$ T cells directly kill their target cells, and have been defined as the "most powerful effectors in the anticancer response" [50]. Indeed, the magnitude of the $CD8^+$ T

cell response specific to TAAs has been shown to correlate with tumour rejections in animal models[179,216]. The vaccine platform chosen is therefore of major importance as it will define the nature of the induced immune response[176]. Interestingly, viral vector-based vaccines have the potential to induce tumour-specific $CD8^+$ T cells as they mimic an infection, triggering MHCI antigen-presentation as well as the right cytokine environment. In 2021, McAuliffe *et al.*, showed that ChAdOx1 and MVA, two viral vector-based vaccines tested in a prime/boost regimen, were able to induce specific cytotoxic $CD8^+$ T cells against P1A, a surrogate for MAGE-type antigen in mice. The P1A protein has similar expression profile compared to human MAGE antigens and has been shown to be naturally expressed in some tumour models in the DBA/2 strain. In that strain, the P1A antigen was naturally slightly immunogenic but the magnitude of the responses were too low to translate into tumour control (low magnitude of P1A specific T cells observed in the TME of non-treated tumour bearing mice, not the blood and spleen). Interestingly, the P1A-specific $CD8^+$ T cell response induced by the vaccine regimen correlated with better tumour control and better survival[179]. Overall, the magnitude of the immune responses observed against P1A are rather small compared to immunogenic antigens such as viral antigens (i.e E6-E7, shown later in this chapter). Therefore, some non-responders were observed in these mouse tumour studies. These data highlighted the need to further improve our vaccine platform and especially underline another challenge for cancer vaccine efficiency to overcome: tumour immunosuppression.

Despite inducing a strong and specific anti-tumour CD8 response, cancer vaccines efficacy can be counteracted by tumour immunosuppression. More precisely, there are various mechanisms of exhaustion and immune evasion that co-exist in the TME and will counteract an efficient recognition and killing of cancer cells [50]. In fact, in 2000,

the evasion of immune response was defined as a hallmark of cancer progression[3]. To name a few of these mechanisms, cancer cells can express high level of immune-checkpoint ligands (i.e., PD-L1), downregulate MHCI, and recruit immunosuppressive cells such as MDSCs[217]. Therefore, in parallel to inducing an immune response against tumour cells it is also important to sustain it, by preventing exhaustion and combatting immune-evasion mechanisms. Hence, effectively treating tumour seems to require multi-dimensional strategies, emphasizing the need of combination therapies to trigger not only a specific but also a sustained anti-tumour immune response.

Anti-PD1 or anti-PD-L1 therapies have shown promising efficacy in cancer patients[218]. In fact, in many cancer types, PD-L1 has been shown to be highly upregulated which usually correlates with poor clinical outcome[219]. These antibodies prevent the interaction of PD1 with its ligand PD-L1, expressed on T cells and cancer cells respectively. In the absence of the blocking antibody, the interaction of PD1 and PD-L1 may trigger T cell anergy and prevent T cell effector function, hence preventing an effective response against cancer cells[220]. Furthermore, in a randomised phase II clinical trial, in non-small-cell lung cancer patients, the progression free survival was improved in the pembrolizumab (anti-PD1) with chemotherapy (carboplatin+paclitaxel) cohort compared to the chemotherapy alone[221]. Interestingly, combining the ChAdOx1/MVA-P1A vaccine with anti-PD1 has shown very promising synergistic effects in mouse studies, the combination being more efficient in controlling tumour growth than the vaccine alone[5].

Chemotherapy has long been known for its cytotoxic effects against cancer cells. However, recent studies have been focusing on the effects of chemotherapy on the immune system and brought to light the potential of combining immunotherapies with chemotherapies[206]. In a 2016 study, Welters *et al.*, combined Carboplatin and Paclitaxel

(CarboTaxol) with a long peptide vaccine (E6-E7) against HPV-16 tumour model in C57BL/6 mice. Interestingly, they showed that chemotherapy depleted $CD11b^{+}GR1^{hi}$ cells which they defined as PMN-MDSCs[150]. They concluded that vaccination with their vaccine platform during myeloid depletion by chemotherapy improved tumour control and $CD8^{+}$ T cell responses [150]. Several other studies have investigated the impact of different chemotherapies such as gemcitabine, cyclophosphamide, or 5-Fluoro-Uracil on the immune system[222]. In a dose dependent manner, cyclophosphamide can trigger effector function of $CD8^{+}$ T cells and decrease regulatory T cell (Treg) functions[223]. Gemcitabine and 5-Fluoro-Uracil have been shown to deplete MDSCs[222]. Given the immune-modulatory effects of chemotherapy and the promising effect of combining it with anti-PD1, we sought to test our cancer vaccines in a triple combination with both chemotherapy and anti-PD1.

In order to test the triple combination therapy, we used two different models. First, the ChAdOx1/MVA-P1A vaccines were tested in DBA/2 mice bearing 15V4T3 tumour, a mastocytoma model which naturally expresses the P1A antigen. Given that our vaccine platform was aimed to be tested in lung cancer patients, CarboTaxol chemotherapies were chosen as they are the standard of care for many of these patients. Anti-PD1 regimen was added to the vaccine and chemotherapy treated mice. In parallel, we further investigated this triple combination of treatments in another model. For this purpose, we used C57BL-6 mice bearing TC-1 tumours which express the E6/E7 antigens. We vaccinated them with ChAdOx1/MVA encoding the E6 and E7 viral antigens from oncogenic HPV. These vaccines were combined with CarboTaxol and anti-PD1. To investigate the anti-tumour efficacy of these treatments, we evaluated the tumour control by measuring the tumour size of these 2 subcutaneous models. We also evaluated the survival of the mice by defining a humane endpoint corresponding to a tumour size of a maximum 12mm in diameter. The

$CD8^+$ T cell response was evaluated after peptide stimulation by assessing the production of type I cytokines: IFNγ, TNFα and IL2. Lastly, we evaluated the immune composition of the TME, spleen and blood 5 days post boost which corresponded to a time point where tumour size start to decrease in responders.

3.2 Chapter aims

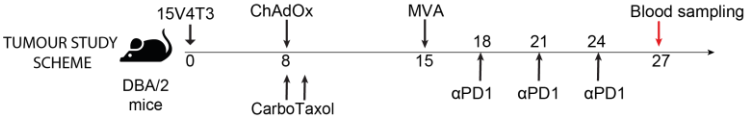
- To evaluate whether a synergy of treatments exists between chemotherapy, anti-PD1 and ChAdOx1/MVA vaccines designed against P1A antigen, in 15V4T3 tumour model. This synergy is evaluated in terms of tumour growth control, survival of the mice and vaccine immunogenicity.
- To explore the phenotype of $CD8^+$T cells in the TME, spleen and blood after chemotherapy and anti-PD1 treatment.
- To further evaluate the same combinations of treatments in the TC-1 tumour-bearing BL/6 mouse model with ChAdO/MVA vaccines designed against E6/E7 antigens.

3.3 Improving ChAdOx1/MVA efficacy against 15V4T3 syngeneic tumour model in DBA/2 mice

3.3.1 15V4T3 tumour model: Experimental design

To evaluate the therapeutic efficacy of a triple combination of treatments in a tumour model, DBA/2 mice were subcutaneously (s.c) implanted with $1x10^6$ 15V4T3 cells. Treatments were started when at least 95% of the mice were bearing tumours (day 8 or 10 post tumour implantation) (fig 3.1 A). The mice were vaccinated with ChAdOx1-Ii-P1A and MVA-tpA-P1A one week apart. Vaccination was also combined with CarboTaxol and

A



B

Days of treatments / Groups	8	9	17	18	21	24
Control	ChAdOx-DPY+ Nacl	Nacl	MVA-DPY	Isotype control	Isotype control	Isotype control
Chemo only	Carboplatin+Paclitaxel	Paclitaxel	PBS	Isotype control	Isotype control	Isotype control
αPD1 only	ChAdOx-DPY+ Nacl	Nacl	PBS	αPD1	αPD1	αPD1
Vaccine only	ChAdOx-li-P1A+Nacl	Nacl	MVA-tpA-P1A	Isotype control	Isotype control	Isotype control
Vaccine+chemo	ChAdOx-li-P1A+ Carboplatin+Paclitaxel	Paclitaxel	MVA-tpA-P1A	Isotype control	Isotype control	Isotype control
Vaccine+αPD1	ChAdOx-li-P1A+Nacl	Nacl	MVA-tpA-P1A	αPD1	αPD1	αPD1
Chemo+αPD1	Carboplatin+Paclitaxel	Paclitaxel	PBS	αPD1	αPD1	αPD1
Vaccine+αPD1+Chemo	ChAdOx-li-P1A+ Carboplatin+Paclitaxel	Paclitaxel	MVA-tpA-P1A	αPD1	αPD1	αPD1

C

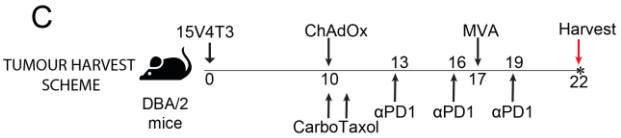


Figure 3.1 Timeline of tumour study and harvest and treatment regimens of each group tested. *(*A) DBA/2 mice were implanted with $1x10^6$ 15V4T3 cells via s.c injections to initiate tumour growth. 8 days after tumour implantation, mice were vaccinated via intramuscular injection (i.m) with 10^7 IU of ChAdOx1 (referred as ChAdOx)-li-P1A or ChAdOx1-DPY or PBS sham and treated with carboplatin (40mg/kg) and paclitaxel (20mg/kg) and 24h later with paclitaxel (20mg/kg) via intraperitoneal injections (i.p). The mice were then vaccinated with 10^6 PFU of MVA-tpA-P1A or MVA-DPY or PBS sham and treated with 100μg of immune checkpoint inhibitor anti-PD1 (αPD1 in scheme and graphs) every third day for 3 i.p injections. Mice were randomised into 8 different groups (6 to 8 mice per groups) based on tumour volume (as measured on day 6) and injected with the treatments indicated in table (B). To evaluate the TME mice were treated according to scheme (C), treatments started from day 10 post tumour implantation to allow the tumours to grow bigger. Also, for the harvest scheme the anit-PD1 was given from day 13 every third day, so the harvest can be performed on day 5 post boost, which is a time after which some tumours may be lost in the responders.

anti-PD1, referred to as the triple combination. The appropriate matched single-treatment or double-treatment control groups were also included in the study (fig 3.1 B).

3.3.2 Tumour growth and mouse survival evaluation

Tumour measurements were performed every 2-3 days. We observed a significant improvement in tumour control in mice that have received the vaccine in the triple combination group compared to vaccine alone, vaccine+CarboTaxol or vaccine+anti-PD1 (fig 3.2 A). Indeed, with the triple combination of treatments, six mice out of eight showed a complete tumour regression at day 45 post tumour implantation (fig 3.2 B). At this time point, the survival of the mice was of 75% in the triple combination group, while only 20% of the mice survived in the vaccine alone group (fig 3.3). At day 91 post tumour implantation, 40% of the mice were still tumour free, whilst none of the mice in the vaccine alone group survived after day 70 (fig 3.3). Interestingly the double treatment groups, vaccine+chemo and vaccine+anti-PD1, also showed a significant improvement in terms of tumour control compared to the vaccine alone. Indeed, as shown in figure 3.2 B, two mice out of seven were tumour free in the vaccine+chemo group and one out of seven in the vaccine+anti-PD1 group, whilst in the vaccine alone group no mice showed complete tumour regression. Although the vaccine+chemo and vaccine+anti-PD1 groups showed a significant improvement in terms of tumour control, it did not in terms of survival. We could also observe an improved survival in the vaccine+chemo group, although it did not reach significance (fig 3.3). Altogether, these data suggest that the combination of two or three treatments is beneficial for the vaccine efficacy in improving tumour control and survival.

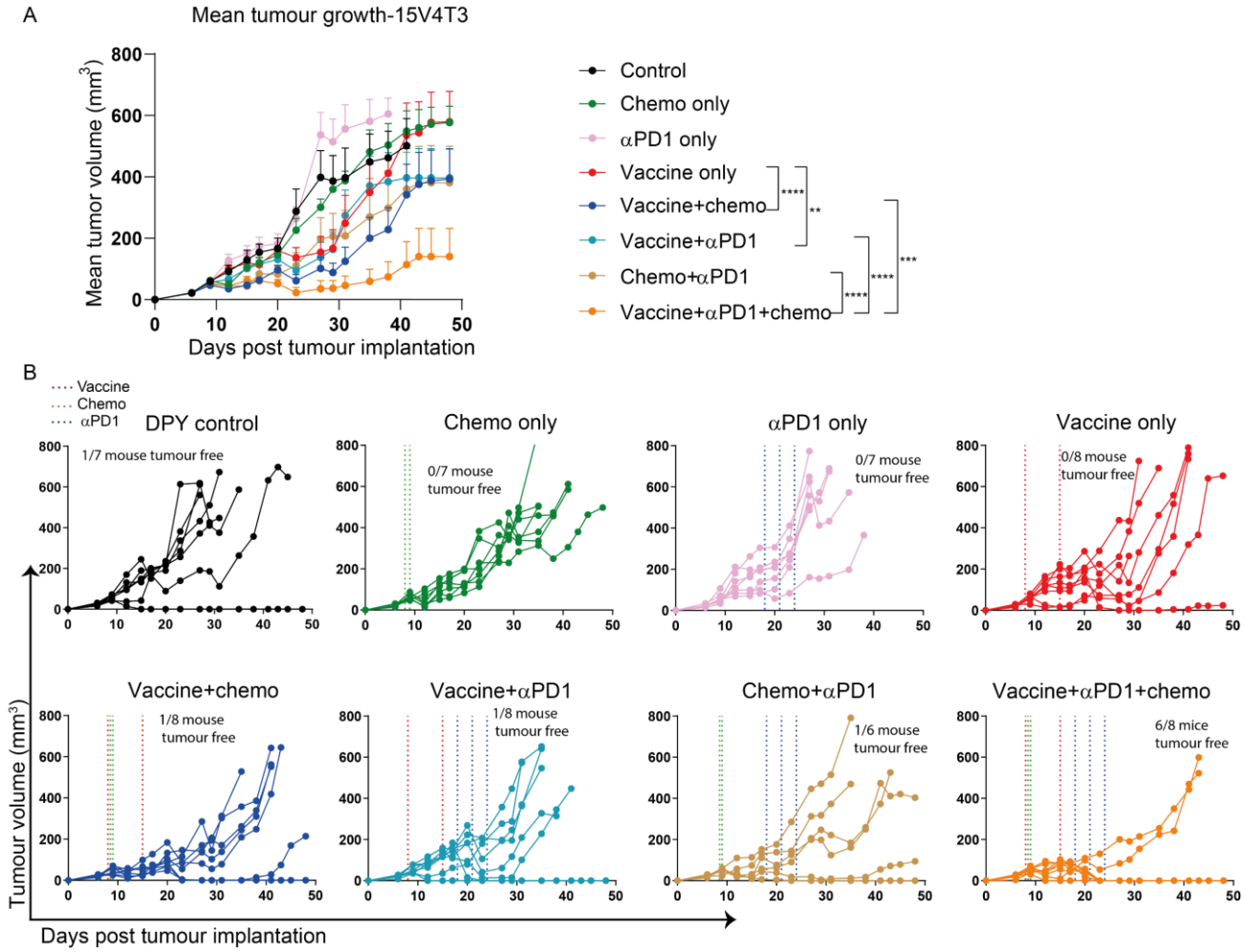


Figure 3.2 Tumour growth control efficacy of ChAdOx1/MVA-P1A vaccination in combination with chemotherapy and anti-PD1 treatments. DBA/2 mice were implanted with $1x10^6$ 15V4T3 cells via s.c. injection to initiate tumour growth. 8 days after tumour implantation, mice were treated according to the schedules described in figure 3.1. Tumour growth was followed for 50 days and mice were culled when tumour size reached human endpoint. Mean tumour growth (A), and individual tumour growth curves from each group are shown (B). Tumour growth data in (A) are presented as mean tumour volume (mm^3) ± SEM. Each group contained 6 to 8 mice, with data representative of at least 3 independent experiments. Statistically significant differences in tumour volume between groups were determined by a two-way ANOVA followed by Tukey's post hoc test **, $p \leq 0.01$ ***, $p \leq 0.001$ ****, $p \leq 0.0001$.

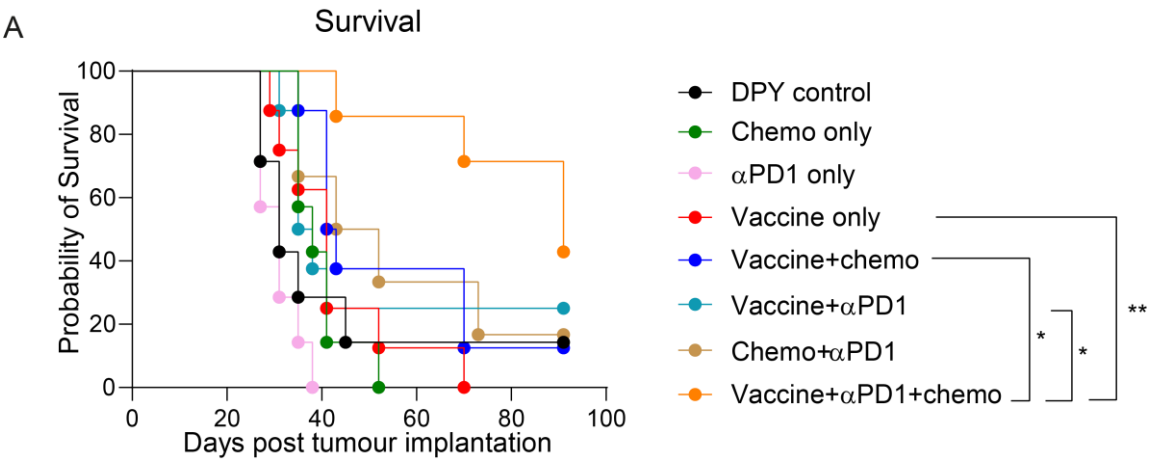


Figure 3.3 Survival of mice vaccinated with ChAdOx1/MVA-P1A in combination with chemotherapy and anti-PD1 treatments. DBA/2 mice were implanted with $1x10^6$ 15V4T3 cells via s.c. injection to initiate tumour growth. 8 days after tumour implantation, mice were treated according to the schedules described in figure 3.1. Mouse survival was monitored for 91 days, Survival curves for each group are shown. Statistical differences in survival data were determined by a Log Rank test. *, $p \leq 0.05$, **, $p \leq 0.01$

3.3.3 Evaluation of ChAdOx1/MVA-P1A immunogenicity and its modulation by the combination of treatments

ChAdOx1/MVA-P1A vaccines have previously been shown to induce a good CD8 response against the P1A antigen in tumour studies[179]. To address the impact of the combination of treatments on the proportion of the P1A specific-$CD8^+$ T cells, blood sampling was performed at day 5 and at day 12 post boost. Total PBMCs were stimulated with overlapping peptides of the P1A protein for 5h and the levels of intracellular type I cytokines were evaluated.

At day 12 post boost (day 27 post tumour implantation), the proportion of overall $CD8^+$ T cells in the blood is similar between the vaccinated and non-vaccinated groups (fig 3.4 A). Interestingly, we were able to see an increased levels of $IFN\gamma^+$, $TNF\alpha^+$ and $IL2^+$ $CD8^+$ T cells with vaccine+chemo and the triple combination group compared to the vaccine alone group (fig 3.4 B, C, D). Importantly, the triple combination showed the highest increased magnitude (2.5 % $IFN\gamma^+$ $CD8^+$ cells in the triple combination vs 0.6% in the vaccine alone). Furthermore, it is important to highlight the effect CarboTaxol on vaccine immunogenicity. Indeed, while the vaccine+anti-PD1 do not show a higher magnitude of the P1A specific immune response compared to the vaccine alone, the vaccine+CarboTaxol and triple combination groups displayed a better immunogenicity (fig 3.4 B, E). Of note, the $IFN\gamma^+$ CD8 + parameter is the clearer readout for the magnitude of the anti-P1A $CD8^+$ T cell response. - the IL2 level was low and the TNFα response showed higher background than the IFNγ response. Furthermore, IFNγ has been shown to be the major Th1 and cytotoxic effector cytokine for cell-mediated immunity[224]. Hence, although all these type 1 cytokines were evaluated, we will focus here on evaluating the IFNγ response to address vaccine and combination of treatments efficacy. Furthermore, as previously described by McAuliffe et al. in 2021, the level of CD8+ IFNγ+ T cells strongly negatively correlates

with the tumour size, with higher magnitude of specific T cells correlating with smaller tumours (fig 3.4 E)

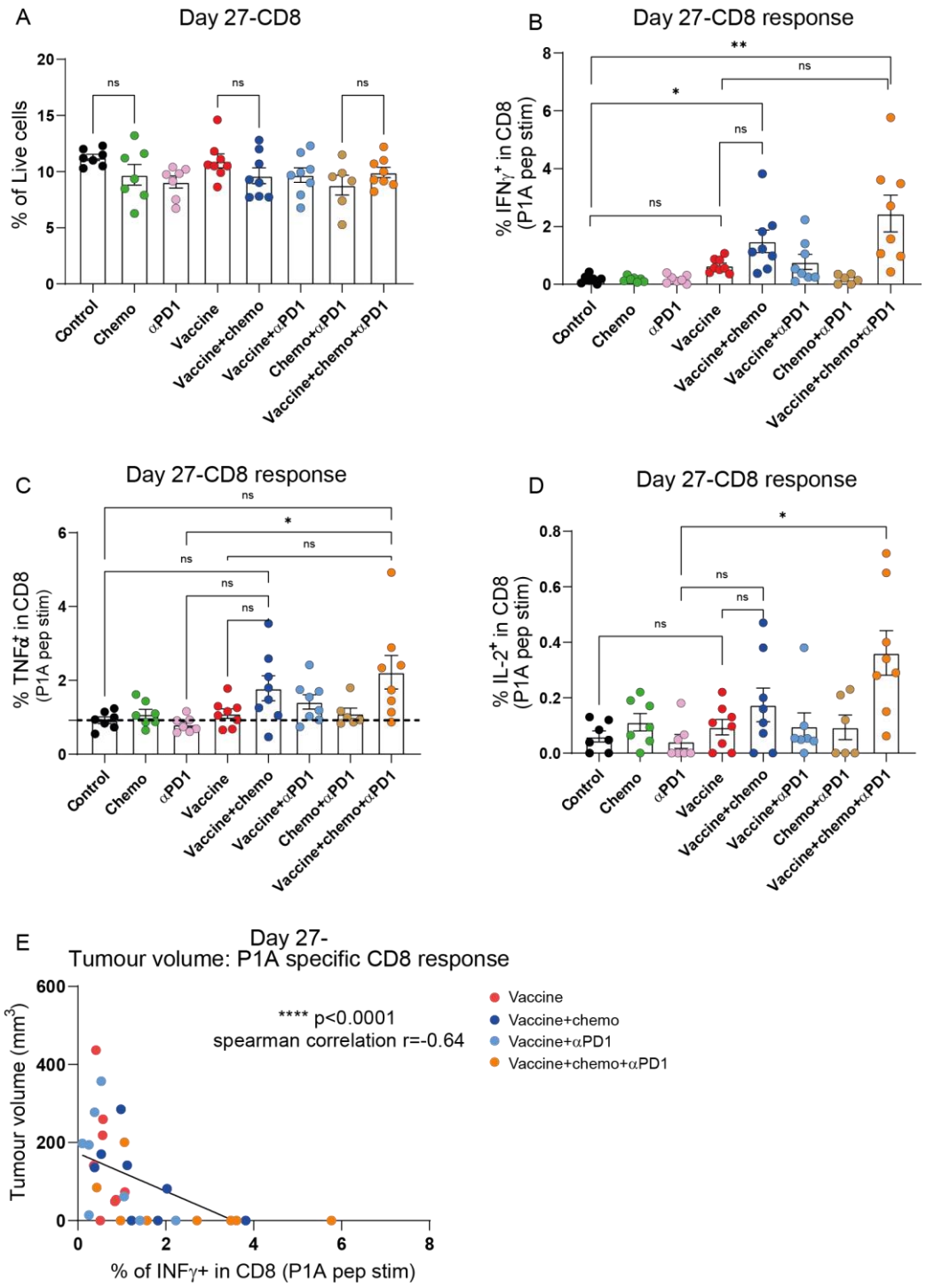


Figure 3.4 P1A-specific CD8⁺ T-cell responses 12 days post ChAdOx1/MVA P1A vaccination. DBA/2 mice were implanted with 1x10^6 15V4T3 cells via s.c. injection to initiate tumour growth. 8 days after tumour implantation, mice were vaccinated according to the schedules described in 3.1. To determine the magnitude of vaccine induced P1A-specific CD8⁺ cell responses in 15V4T3 tumour-bearing mice, mice were bled 12 days after MVA-tpa-P1A boost. PBMCs were stimulated ex vivo with 4µg/ml of P1A peptides and the percentage of cytokine-producing P1A-specific CD8⁺ cells in the blood was determined by flow cytometry. (A) Proportion of CD8⁺ cells in the blood. (B) Average of IFNγ⁺CD8⁺ response is shown. (C) Average of TNFα⁺CD8⁺ response is shown. (D) Average of IL2⁺CD8⁺ response is shown. Data are representative of at least 3 independent experiments and shown as the mean± SEM response of each group. Each symbol represents an individual mouse, with 6 to 8 mice per group. Statistically significant differences between groups were determined by a Kruskal-Wallis test with Dunn's multiple comparisons test. ns for non-significant, *, p ≤ 0.05,**,p ≤ 0.01 ***, p ≤ 0.001 ****, p ≤ 0.0001. Tumour size on day 27 after implantation was correlated with the magnitude of IFNγ producing P1A-specific CD8⁺ T-cells in the blood evaluated 27 days after implantation (E). Significance was determined by a Spearman Rank correlation test.

We then evaluated the magnitude of the IFNγ$^+$CD8$^+$ response in the TME at day 5 post boost, before complete tumour regression was observed in responders (fig 3.5 C, tumour harvest scheme). In parallel, we also investigated the systemic (blood and spleen) CD8$^+$ T cell response against P1A. The magnitude of IFNγ$^+$ CD8$^+$ T cells was elevated to a similar extent in the vaccine+chemo and the vaccine+chemo+anti-PD1 groups compared to the vaccine alone group in the spleen (fig 3.5 A, B). Similarly, in the blood, we observed around 4.5% and 4.4% of IFNγ$^+$ CD8$^+$ cells in the triple combination and vaccine+chemo groups respectively and only 1.8% of IFNγ$^+$ CD8$^+$ cells in the vaccine group in the blood (fig 3.5 C). Interestingly, the trend observed in the blood and spleen concerning the magnitude of the CD8 response was similar in the TME (fig 3.5 D): the increased magnitude of the P1A specific CD8 response was observed in the groups treated with chemotherapy+vaccine, regardless of anti-PD1 treatment (fig 3.5 D). This indicates a potential role of chemotherapy in augmenting the vaccine CD8$^+$ T-cell response. Finally, we also investigated the induction of the P1A specific CD8$^+$ T-cells by performing staining with an MHC-class I tetramer bound to a 9-mer peptide LPYLGWLVF corresponding to amino acids 35 to 43 of the P1A protein. This is the established immunogenic CD8 epitope derived from the P1A protein[225]. In the spleen and blood, we observed a similar increased proportion of H2L^d P1A+ cells in CD8$^+$ T cells in the vaccine+chemo and triple combination groups compared to the vaccine alone, confirming the effect of chemo on the magnitude of P1A-specific cells (fig 3.5 E, F). The tetramer analysis could not be performed on tumour cells due to the limited number of cells retrieved from tumours from mice with positive response to treatment (mainly in vaccine+chemo and triple combination group) and priority was given to the P1A stimulation and IFNγ production evaluation.

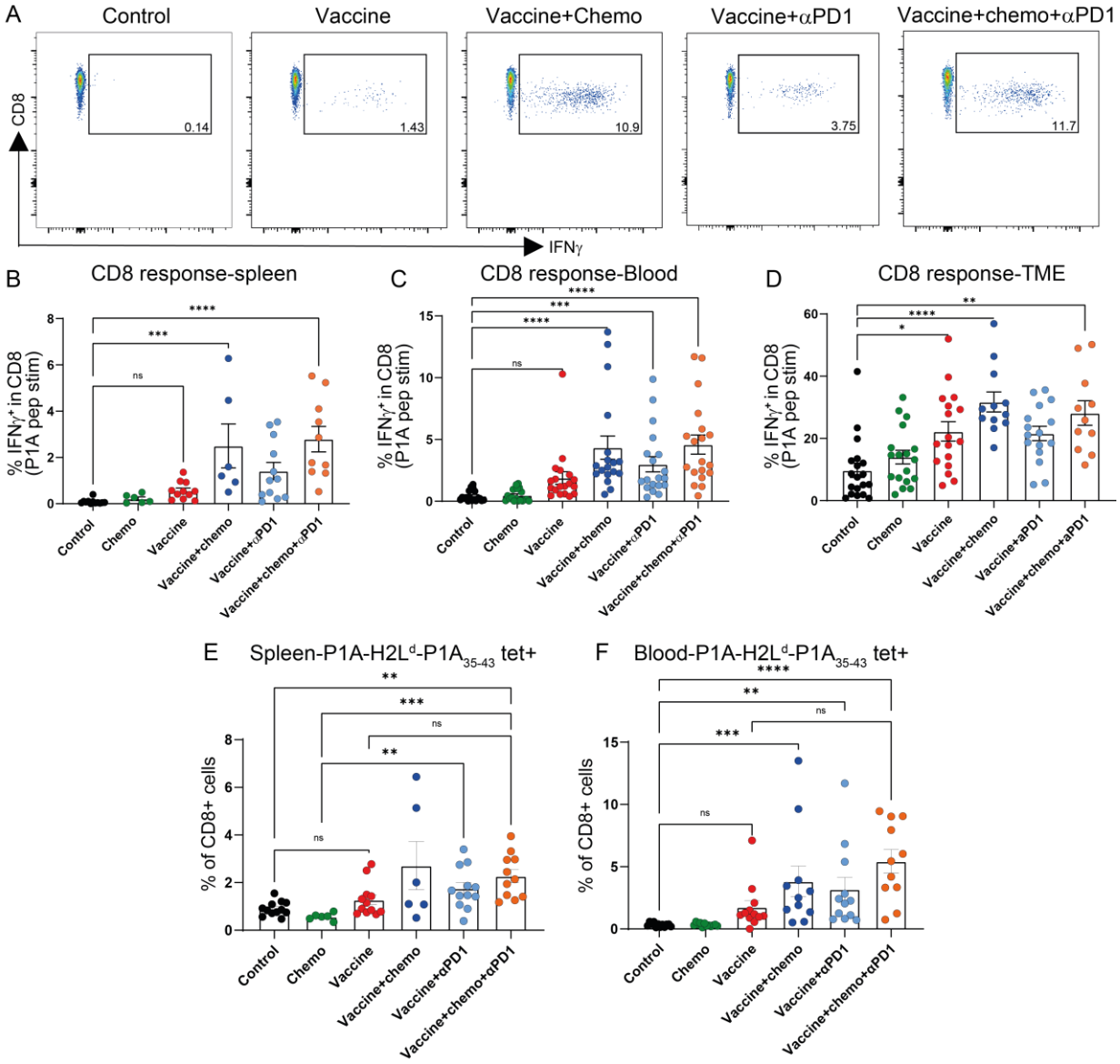


Figure 3.5 P1A-specific CD8⁺ T-cell responses 5 days post ChAdOx1/MVA P1A vaccination. DBA/2 mice were implanted with 1x10^6 15V4T3 cells via s.c. injection to initiate tumour growth. 10 days after tumour implantation, mice were vaccinated according to the schedules described in figure 3.1. To determine the magnitude of vaccine induced P1A-specific CD8⁺ T-cell responses in 15V4T3 tumour-bearing mice, mice were bled 5 days after MVA-tpa-P1A boost, and tumour and spleens were harvested. Cells were stimulated ex vivo with 4µg/ml of P1A peptides and the percentage of cytokine-producing P1A-specific CD8⁺ T-cells in the blood, spleen and TME was then determined by flow cytometry. Representative gating of IFNγ⁺ CD8⁺ T-cells in response to stimulation with P1A peptides in the TME of different groups are shown (A). The average IFNγ⁺CD8⁺ response in spleen, blood and tumour is shown in respectively B, C and D. To confirm the specificity of the CD8⁺ response we stained total PBMCs (E) and splenocytes (F) with H2L^d tetramer presenting peptide 35-43 of the P1A protein. Data are pooled from 3 independent experiments and shown as the mean ± SEM response of each group. Each symbol represents an individual mouse, with 6 to 19 mice per group. Statistically significant differences between groups were determined by a Kruskal-Wallis test with Dunn's multiple comparisons test, *, p ≤ 0.05, **,p ≤ 0.01, ***, p ≤ 0.001, ****, p ≤ 0.0001.

Although viral vector-based vaccines are utilised to trigger a $CD8^+$ T cell response as they mimic viral infection, we were also interested in the P1A specific CD4 response. We therefore evaluated the IFNγ levels after P1A peptide stimulation in $CD4^+$T cells, in the spleen, blood and TME at day 5 post boost. We did not observe any systemic CD4 response triggered by the vaccine. Indeed, the percentages of $IFN\gamma^+$ $CD4^+$in the blood were below 0.2 % on average and no improvement was observed between the control groups and the vaccinated groups nor between the vaccine alone group and the vaccine+chemo and triple combination groups (fig 3.6 A). In the spleen, the level of $IFN\gamma^+$ $CD4^+$T cells were also very low (< 0.15 % average) but the vaccine+chemo and the triple combination groups showed a significant increase compared to the control group (fig 3.6 B). Finally, our vaccine induced a significant P1A specific $CD4^+$response in the TME, which seems further improved with the addition of CarboTaxol (not significant) (fig 3.6 C).

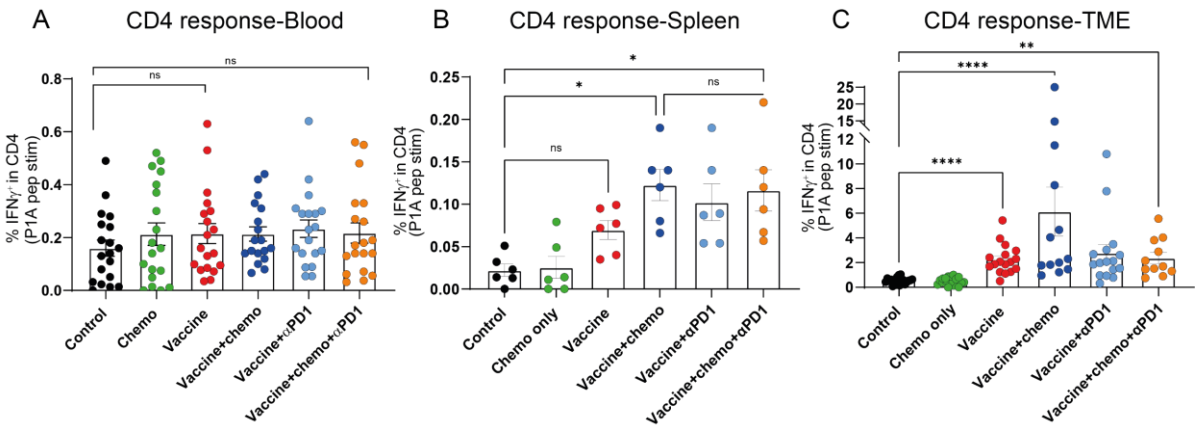


Figure 3.6 P1A-specific $CD4^+$ T-cell responses 5 days post ChAdOx1/MVA P1A vaccination. DBA/2 mice were implanted with $1x10^6$ 15V4T3 cells via s.c. injection to initiate tumour growth. 10 days after tumour implantation, mice were vaccinated according to the schedules described in figure 3.1. To determine the magnitude of vaccine induced P1A-specific $CD4^+$ T-cell responses in 15V4T3 tumour-bearing mice, mice were bled 5 days after MVA-tpa-P1A boost, and tumour and spleens were harvested. PBMCs were stimulated ex vivo with 4µg/ml of P1A peptide pools and the percentage of cytokine-producing P1A-specific $CD4^+$ T-cells in the blood was then determined by flow cytometry. Representative gating of $IFN\gamma^+$ $CD4^+$ T-cells in response to stimulation with P1A peptides in the different groups are shown in blood (A), spleen (B) and TME (C). The data are pooled from 3 independent experiments and shown as the mean± SEM response of each group. Each symbol represents an individual mouse, with 6 to 19 mice per group. Statistically significant differences between groups were determined by a Kruskal-Wallis test with Dunn's multiple comparisons test, *, $p \leq 0.05$, **, $p \leq 0.01$, ***, $p \leq 0.001$ ****, $p \leq 0.0001$.

Taken together these data suggest that the chemotherapy can increase the systemic immune response triggered by vaccination which correlate with an increase magnitude of P1A specific $CD8^+$ T cells in the TME. Combining anti-PD1 treatment with vaccine+chemotherapy seems to help further sustain on the long term the immune response, as both tumour control and survival were improved. Furthermore, on day 12 post boost (fig 3.4), the overall magnitude of the $IFN\gamma^+$ $CD8^+$ T cell response dropped compared to day 5 post boost (fig 3.5), but less so in the triple combination group compared to the vaccine+chemo group (see Appendix figure 1 for evolution over time). Indeed, the P1A specific immune response dropped from 5% on average to 1.8% in the vaccine+chemo group while in the triple combination the response was still 2.5% at day 12 post boost. This further supports the hypothesis of the beneficial effect offered by anti-PD1 to aid sustaining the P1A specific immune response. These data indicate the importance of the phenotype and fitness of the $CD8^+$ T cells in controlling tumour growth, not only the magnitude. Therefore, in the next section, we investigated the lymphocyte composition of the TME, spleen and blood at day 5 after the triple combination of treatments (scheme fig 3.1 C).

3.4 Impact of the triple combination of treatments on the TME, spleen and blood

3.4.1 Evaluation of the TME infiltrated CD8$^+$ T cells

In light of the observed improvement in both tumour control but particularly the anti-tumour immune response when chemotherapy and anti-PD1 are combined with ChAdOx1/MVA P1A vaccination, we further investigated the impact of the triple combination on the phenotype of the Tumour infiltrated T lymphocytes (TiLs), and particularly CD8$^+$ T cells at 5 days post-boost. Moreover, we sought to address whether CarboTaxol also impacts CD8$^+$ T cell phenotype to promote a higher vaccine-induced immune response and a better tumour control.

Using flow cytometry analysis, we examined the innate and adaptive immune populations. As previously published by McAuliffe *et al* in 2021, we observed an increased proportion of CD3+ CD8$^+$ T-cells in the TME in all the vaccinated groups (fig 3.7 A, B), confirming that our vaccine platform has the potential to turn "cold" tumours "hot". However, no difference of CD8 infiltration was noticed with the addition of further treatments to the vaccine. Within the CD8$^+$ T cell populations, we did notice an expansion of effector memory CD8$^+$ T cells in mice from vaccinated groups, which were not further expanded by the addition of chemotherapy (fig 3.7 C). Interestingly, we noticed an expansion of TCF1$^+$ PD1$^+$ activated stem-like T cells as well as an expansion of the CD8$^+$ TCF1$^+$ PD1$^-$ progenitor stem-like cells in the triple combination, which are less exhausted T cells, with higher proliferation potential (fig 3.7 D, E). This phenotype was not significantly increased in the vaccine+chemo group compared to the vaccine alone or control groups.

However, we observed a high magnitude of the PD1$^+$ TCF1$^-$ populations in CD8$^+$ T cells in all the groups (fig 3.7 F). PD1 expression alone can be both an indicator of

exhaustion and T cell activation so in a subsequent experiment we also explored the double positive $CD8^+$ Tim3+ $PD1^+$ cells as well as the MFI of these markers in this populations. The proportion of $CD8^+$ T cells expressing both $TIM3^+$ and $PD1^+$ was high in all the groups, with no major differences observed between groups (fig 3.7 G), The MFI of PD1 but not Tim3 (fig 3.7 I) was significantly reduced in the double treated groups as well as the triple combination group and reduced but not significantly in the vaccine alone group compared to the control group (fig 3.7 H).

Overall, we observed that the triple combination of treatments displayed slightly higher $TCF1^+$ $PD1^-$ and $TCF1^+$ $PD1^+$ $CD8^+$ T cells. However, we did not see any major changes induced by chemotherapy on the TiLs at 5 days post boost. Therefore, we decided to explore the systemic impact of chemotherapy and triple combination by evaluating T cell phenotypes in the blood and spleen at 5 days post boost.

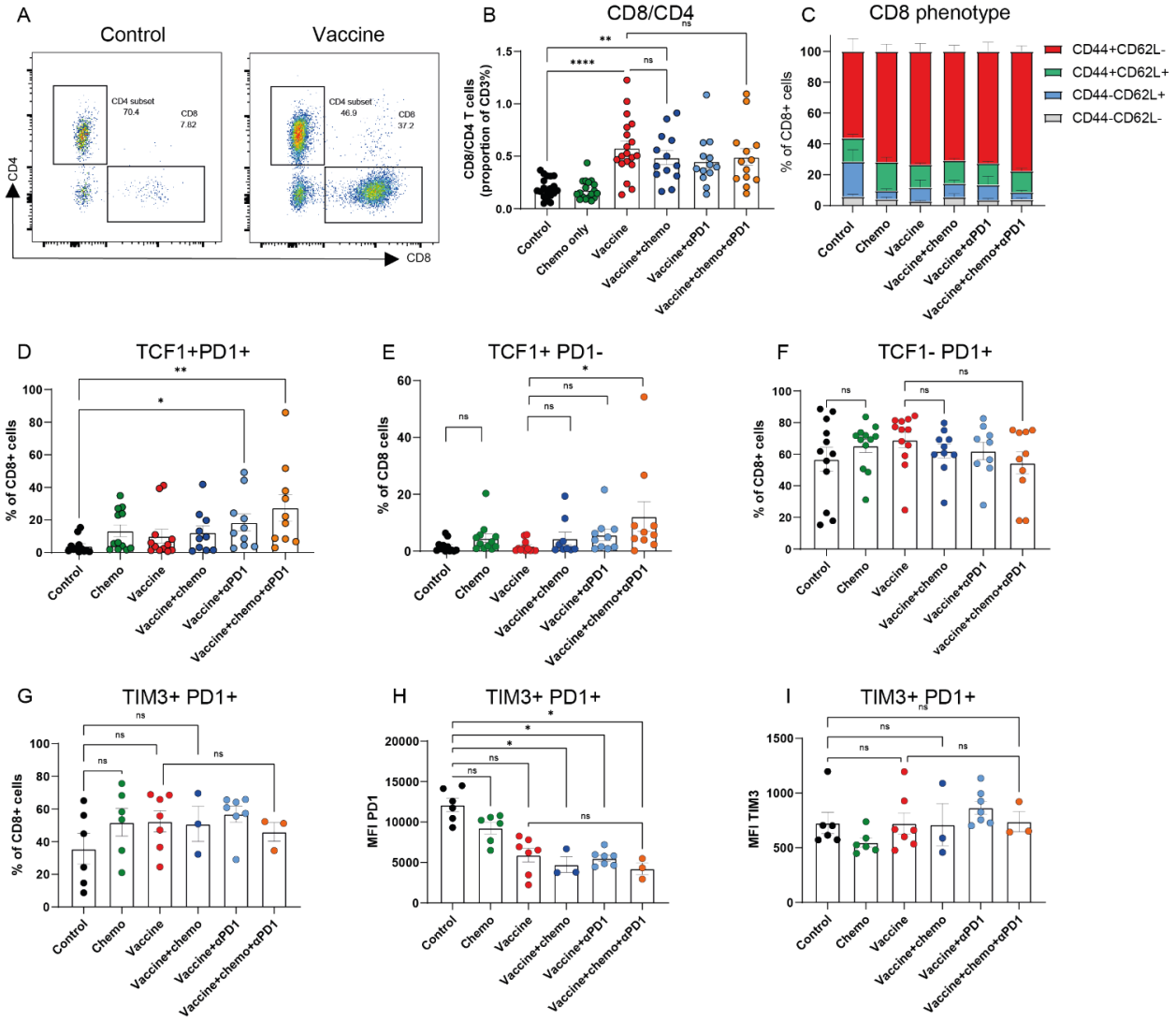


Figure 3.7 T cell infiltration and CD8⁺ T cell phenotype in the TME of 15V4T3 tumour bearing mice. DBA/2 mice were implanted with 1x10^6 15V4T3 cells via s.c. injection to initiate tumour growth. 10 days after tumour implantation, mice were vaccinated according to the schedules described in figure 3.1 C. To determine the TME immune profile, tumours were harvested on day 5 post boost and cells were stained and analysed by flow cytometry. Gating of CD4⁺ and CD8⁺ (A), CD8 to CD4 ratio is shown in (B). CD8⁺ T cell activation status was investigated (C). CD8⁺ T cell stemness status is shown in (D) and (E). CD8⁺ T cell PD1 expression is shown in (F). The data are pooled from 2 independent experiments and mean± SEM for each group is shown. The double positive TIM3⁺PD1⁺ CD8⁺ T cell proportion is shown in (G) and the MFI of PD1(H) and TIM3 (I) were calculated in the double positive population. For G, H, and I, data shown are from one experiment. Each symbol represents an individual mouse. Statistically significant differences between groups were determined by a Kruskal-Wallis test with Dunn's multiple comparisons test,*, p ≤ 0.05, **, p ≤ 0.01, ***, p ≤ 0.001 ****, p ≤ 0.0001.

3.4.2 Investigation of long-term impact on systemic CD8$^+$T cells

Similarly to what was observed in the TME, we observed a trend toward an increased number of effector memory (CD44$^+$CD62L$^-$) T cells within the CD8$^+$ T cell population in the blood and spleen of vaccinated groups compared to non-vaccinated groups. The increase in effector memory cells were significant between the vaccine+chemo or the triple combination group compared to the control group in the blood (fig 3.8 C). In the spleen, the number of effector CD8$^+$ T cells in the triple combination but not the vaccine+chemo group was significantly different compared to the control (fig 3.8 A). Interestingly, the total number of H2L^d-P1A specific CD8$^+$ T cells displaying an effector phenotype seemed to increase in the combination groups compared to the vaccine alone in both spleen and blood (fig 3.8 B,D). We also investigated the presence of TCF1$^+$PD1$^+$ CD8$^+$ T stem-like cells (fig 3.9 A,B). The stem-like phenotype of these cells was not significantly impacted in the system although the combination group displayed slightly higher level of TCF1$^+$PD1$^+$ T cells in the blood, similarly to the TME (fig 3.9 B). Concerning the P1A specific TCF1$^+$ PD1$^+$ CD8$^+$ T cells, no significant differences were observed between vaccine alone and the combination groups (fig 3.9 C,D). Interestingly, we noticed increased numbers of TCF1$^-$ PD1$^+$ P1A specific CD8$^+$ T cells in the double-treatment groups compared to the vaccine alone (fig 3.9 E,F). Altogether this supports the importance of combining the vaccine with other treatments as it improves T cell activation, with higher level of effector memory cells compared to vaccine alone. However, no chemotherapy-related effects, which could explain the increased immune response magnitude, were observed concerning the CD8 phenotype.

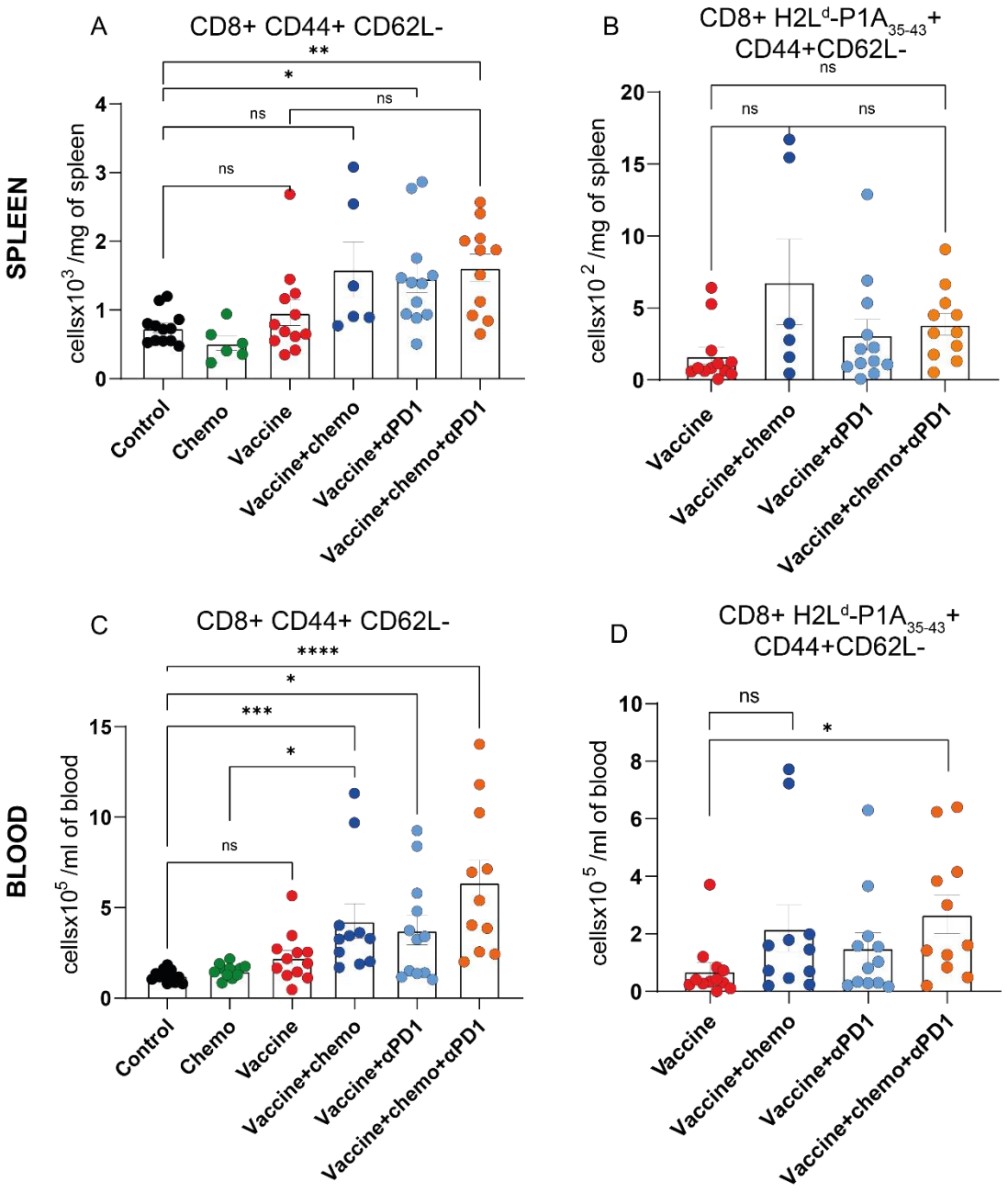


Figure 3.8 CD8⁺ T cell activation phenotype in the spleen and blood of 15V4T3 tumour bearing mice. 10 to 12 days after 15V4T3 tumour implantation, DBA/2 mice were vaccinated and treated according to the schedules described in figure 3.1 C. To determine the systemic immune profile, spleen and blood were harvested on day 5 post boost and cells were stained and analysed by flow cytometry. Numbers of effector (CD44+ CD62L-) $CD8^+$ T cells are shown in the spleen (A) and in the blood (C). $CD8^+$ T cells were also stained with $H2L^d$ tetramer presenting the P1A peptide (amino acids 35 to 43) and number of $tetramer^+$ $CD8^+$ T cells are shown in the spleen (B) and in the blood (D) (cell numbers). The data are pooled from 2 independent experiments and mean for each group are shown (n= 6 to 12 mice per group). Each symbol represents an individual mouse. Statistically significant differences between groups were determined by a Kruskal-Wallis test with Dunn's multiple comparisons test,*, $p \leq 0.05$, **, $p \leq 0.01$, ***, $p \leq 0.001$ ****, $p \leq 0.0001$.

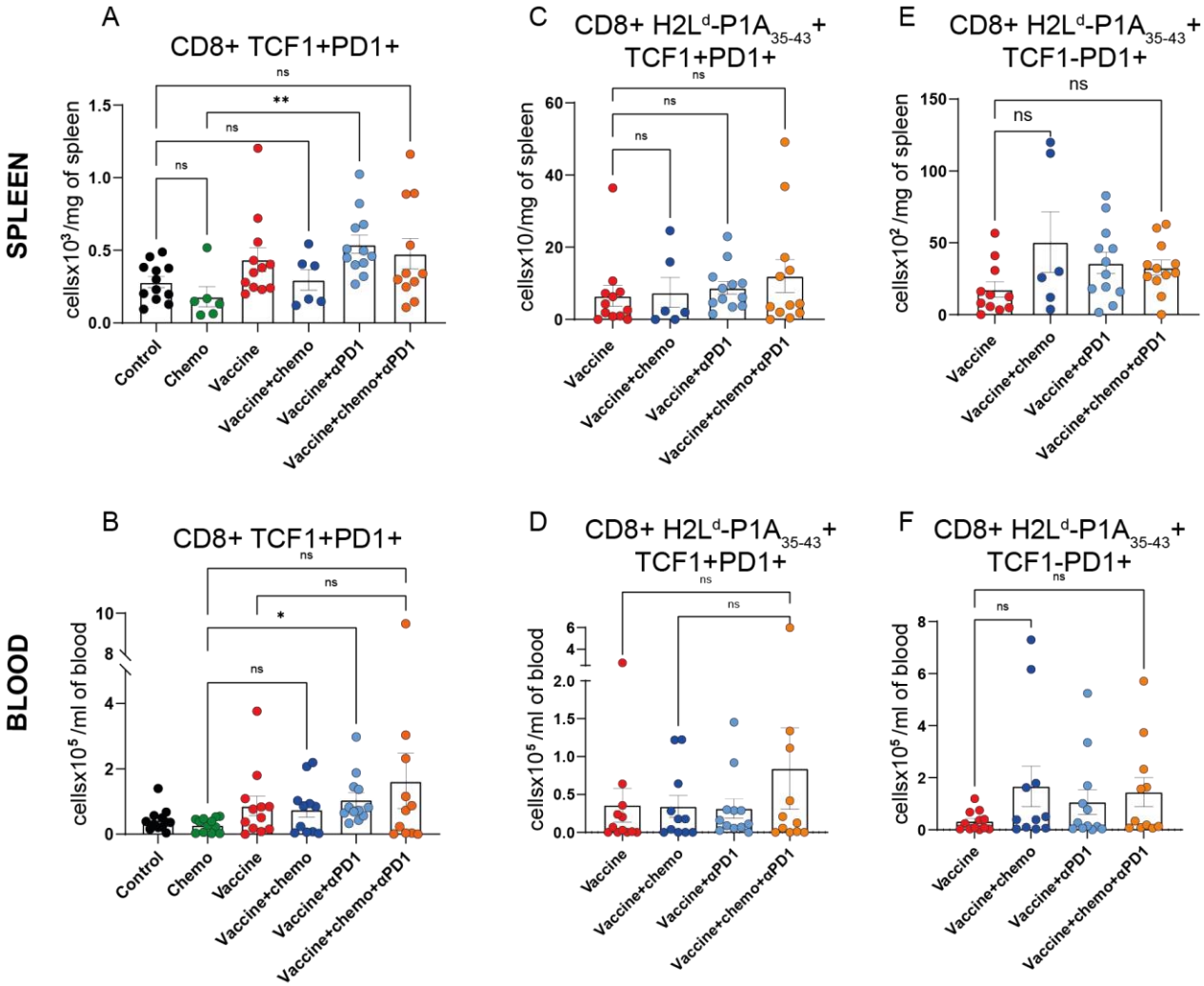


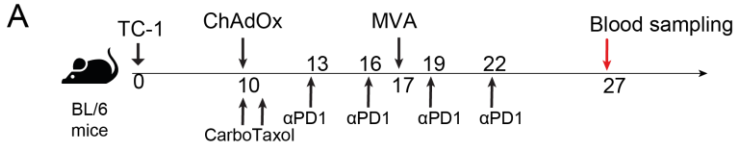
Figure 3.9 Stemness status of total and P1A-specific CD8⁺ T cell in the spleen and blood of 15V4T3 tumour bearing mice. To determine the systemic immune profile of 15V4T3 implanted DBA/2 mice after treatments (figure 3.1.C), spleen and blood were harvested on day 5 post boost and cells were stained and analysed by flow cytometry. Numbers of total pre-exhausted stem-like CD8⁺ T cells are shown in the spleen (A) and blood (B). Numbers of TCF1⁺ PD1⁺ P1A specific CD8⁺ T cells are shown in the spleen (C) and blood (D). Numbers of P1A specific CD8⁺T cells PD1⁺ TCF1- are shown in (E) for the spleen and (F) for the blood. The data are pooled from 2 independent experiments and mean for each group are shown (n= 6 to 12 mice per group). Each symbol represents an individual mouse. Statistically significant differences between groups were determined by a Kruskal-Wallis test with Dunn's multiple comparisons test,*, $p \leq 0.05$, **, $p \leq 0.01$.

3.5 Improving ChAdOx1/MVA-E6-E7 mediated tumour control and immunogenicity against TC-1 syngeneic tumour model in C57BL/6 mice

3.5.1 TC-1 tumour model: experimental design

We were also interested in investigating whether this protocol of three combined treatments could be applied to another model. To this end, C57BL-6 mice were implanted with TC-1 cells expressing the E6 and the E7 tumour antigens. The mice were vaccinated with ChAdOx1/MVA platform encoding E6 and E7 antigens. CarboTaxol was given together with the prime vaccination, and the anti-PD1 treatment was given starting 2 days post-prime every third day for a total of three injections (fig 3.10 A).

A



B

Days of treatment / Groups	10	11	13	16	17	19	22
Control	ChAdOx-DPY+ Nacl	Nacl	Isotype control	Isotype control	MVA-DPY	Isotype control	Isotype control
Chemo only	Carboplatin+Paclitaxel	Paclitaxel	Isotype control	Isotype control	PBS	Isotype control	Isotype control
αPD1 only	PBS+Nacl	Nacl	αPD1	αPD1	PBS	αPD1	αPD1
Vaccine only	ChAdOx-E6/E7+ Nacl	Nacl	Isotype control	Isotype control	MVA-E6/E7	Isotype control	Isotype control
Vaccine+chemo	ChAdOx-E6/E7+ Carboplatin+Paclitaxel	Paclitaxel	Isotype control	Isotype control	MVA-E6/E7	Isotype control	Isotype control
Vaccine+αPD1	ChAdOx-E6/E7+ Nacl	Nacl	αPD1	αPD1	MVA-E6/E7	αPD1	αPD1
Chemo+αPD1	PBS+ Carboplatin+Paclitaxel	Paclitaxel	αPD1	αPD1	PBS	αPD1	αPD1
Vaccine+chemo+αPD1	ChAdOx-E6/E7+ Carboplatin+Paclitaxel	Paclitaxel	αPD1	αPD1	MVA-E6/E7	αPD1	αPD1

Figure 3.10 Timeline of tumour study and treatment regimens of each group tested in C57BL/6 mice. C57BL/6 mice were implanted with $1x10^5$ TC-1 cells via s.c injections to initiate tumour growth. 10 days after tumour implantation, mice were vaccinated via i.m with 10^7 IU of ChAdOx1-E6/E7 or ChAdOx1-DPY or PBS sham and treated with carboplatin(40mg/kg) and paclitaxel (20mg/kg) and 24h later with paclitaxel (20mg/kg) via i.p. The mice were then vaccinated with 10^6 PFU of MVA-E6/E7 or MVA-DPY or PBS sham and treated with 100μg of immune checkpoint inhibitor anti-PD1 every third day for 4 i.p injections. Mice were randomised into 8 different groups based on tumour volume (as measured on day 10) and injected with the treatments indicated in table B.

3.5.2 TC-1 tumour growth evaluation and mouse survival

The tumour control with vaccine+chemo was significantly better than the vaccine alone, as was the triple combination group compared with the vaccine alone. This data displays similar trend than what was observed in the DBA/2 model. However, the triple combination group was not significantly improved compared to the vaccine+chemo group, although a slightly better tumour control was observed (fig 3.11 A). In this model, the role of CarboTaxol seems essential in improving tumour control while the addition of anti-PD1

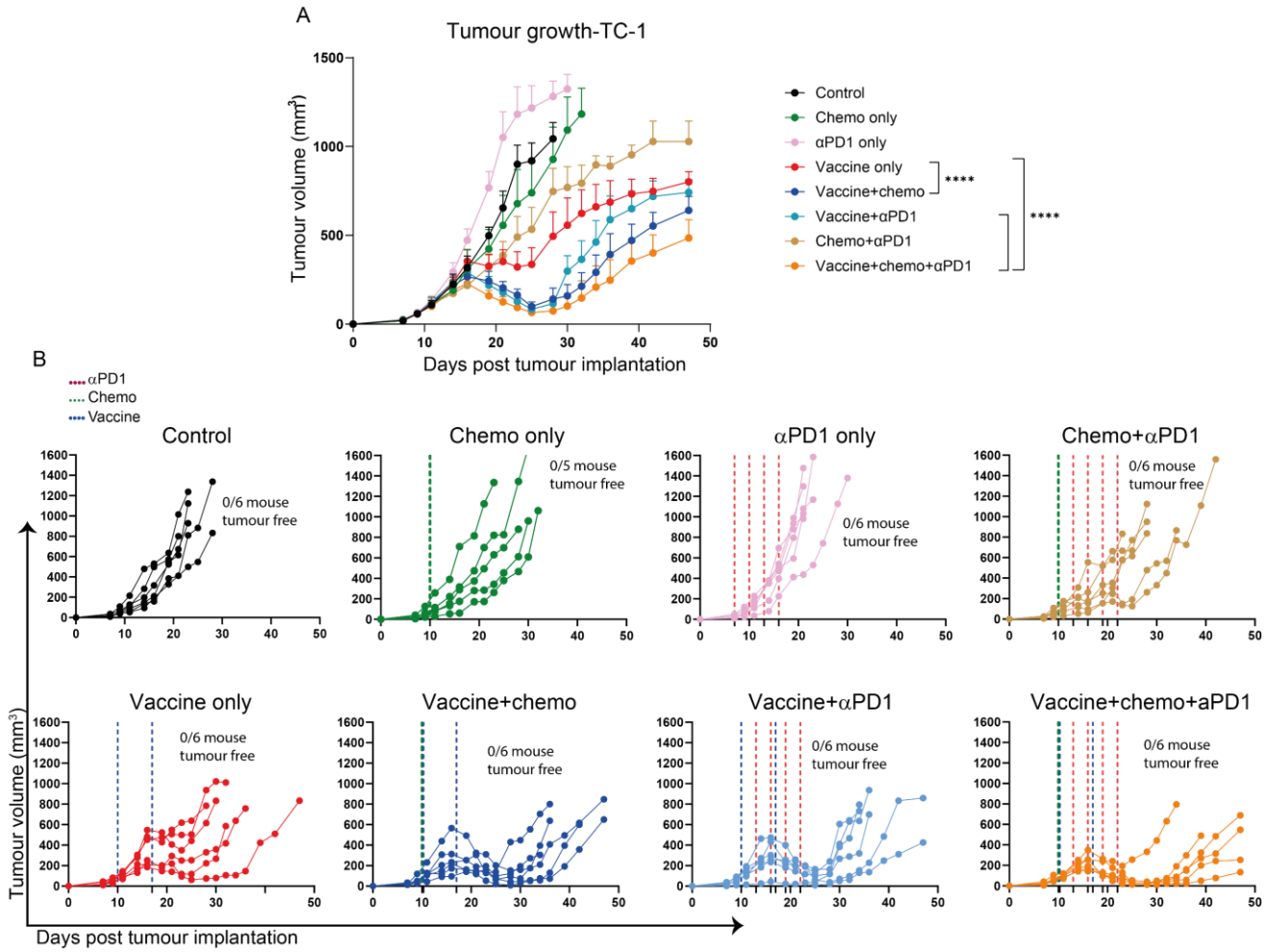


Figure 3.11 Tumour growth control efficacy of ChAdOx1/MVA-E6/E7 vaccination in combination with chemotherapy and anti-PD1 treatments. C57BL/6 mice were implanted with 1x10^5 TC-1 cells via s.c. injection to initiate tumour growth. 10 days after tumour implantation, mice were treated according to the schedules described in figure 3.10 Tumour growth was followed for 50 days and mice were culled when tumour size reached human endpoint. Mean tumour growth (A), and individual tumour growth curves from each group are shown (B). Tumour growth data in (A) are presented as mean tumour volume (mm^3) ± SEM. Each group contained 6 mice, with data representative of 2 independent experiments. Statistically significant differences in tumour volume between groups were determined by a two-way ANOVA followed by Tukey's post hoc test, ****, $p \leq 0.0001$.

to the vaccine combined with chemotherapy showed only a mild benefit in terms of tumour control compared to the vaccine+chemo regimen. Of note, this model is known to be aggressive, and complete tumour regression was not observed in mice from any group (fig 3.11 B). Moreover, the vaccine+chemo group also showed a better survival, although not significant compared to the vaccine alone. Similarly, to what we observed in DBA/2 mice, the triple combination group showed significantly improved survival of the mice compared to the vaccine alone (fig 3.12). However, in term of tumour control, the double combination group with vaccne+chemo seems to show the best synergy with no significant improvement with the triple combination. So, in this model caution has to be taken in regard of the triple

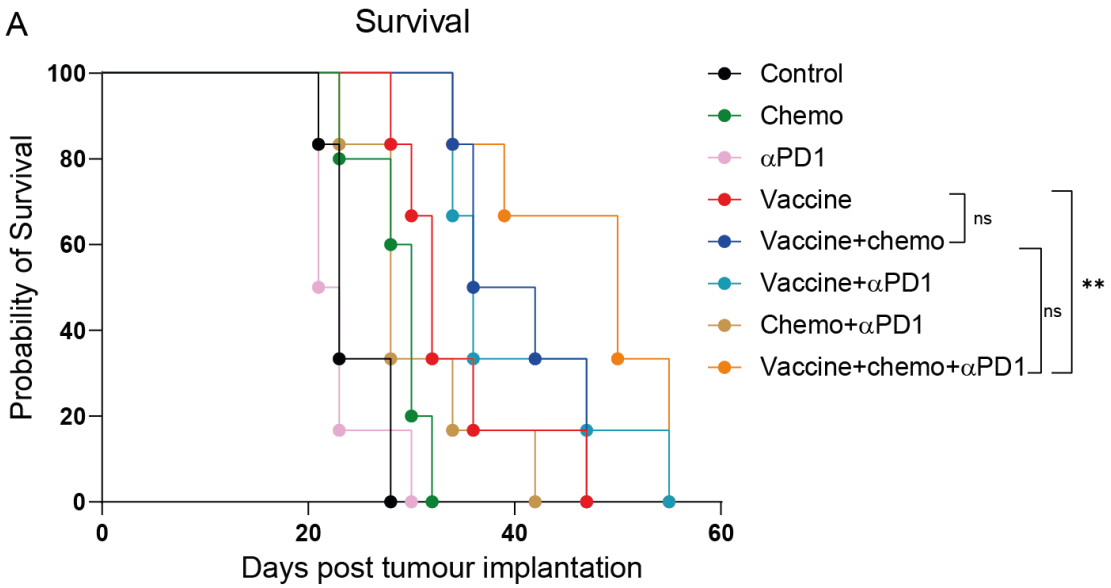


Figure 3.12 Survival of mice vaccinated with ChAdOx1/MVA-E6/E7 in combination with chemotherapy and anti-PD1 treatments. C57BL/6 mice were implanted with $1x10^5$ TC-1 cells via s.c. injection to initiate tumour growth. 10 days after tumour implantation, mice were treated according to the schedules described in figure 3.10 Mouse survival was monitored for 58 days, Survival curves for each group are shown. Statistical differences in survival data were determined by a Log Rank test. **, $p \leq 0.01$

combination, as a double treatment regimen could be sufficient.

3.5.3 ChAdOx1/MVA-E6-E7 immunogenicity and modulation by CarboTaxol

Finally, we investigated the immunogenicity of the vaccine, alone or combined with the different treatments, against the E6 and E7 antigens. 10 days post boost, total PBMCs were stimulated with E6 and E7 peptides. Although the vaccine alone was able to induce an average of 20% of E6/E7- specific IFNγ^+ and TNFα^+ cells and 3% of IL2$^+$ out of total CD8$^+$ T cells, the vaccine together with CarboTaxol or together with CarboTaxol+anti-PD1 did not show a significant increase compared to the vaccine alone (fig 3.13 A, B, C). Interestingly, the proportion of overall CD8$^+$ T cells was increased in the vaccinated group when chemotherapy was also added (fig 3.13 D). Therefore, the vaccine+chemo and triple combination groups also showed expansion of IFNγ^+ CD8$^+$ cells in the blood at day 10 post boost, although this was not significant compared to the vaccine alone (fig 3.13 E). Finally, we noticed that the magnitude of the E6-E7 CD8$^+$ T cell response correlated significantly with the tumour control, with the highest IFNγ^+CD8$^+$T cell proportion corresponding to smaller tumour volumes at day 27 post tumour implantation (fig 3.13 F). These data lend further strength to the observation of significant synergistic effects of CarboTaxol combined with therapeutic ChAdOx1/MVA vaccination.

Altogether these data support the improved efficacy of a triple combination of treatments consisting of CarboTaxol chemotherapy, therapeutic ChAdOx1/MVA vaccination and anti-PD1 immune checkpoint blockade (ICB) against different cancer types and tumour antigens. They also highlight an interesting and specific role for the importance of chemotherapy in improving cancer vaccine efficacy.

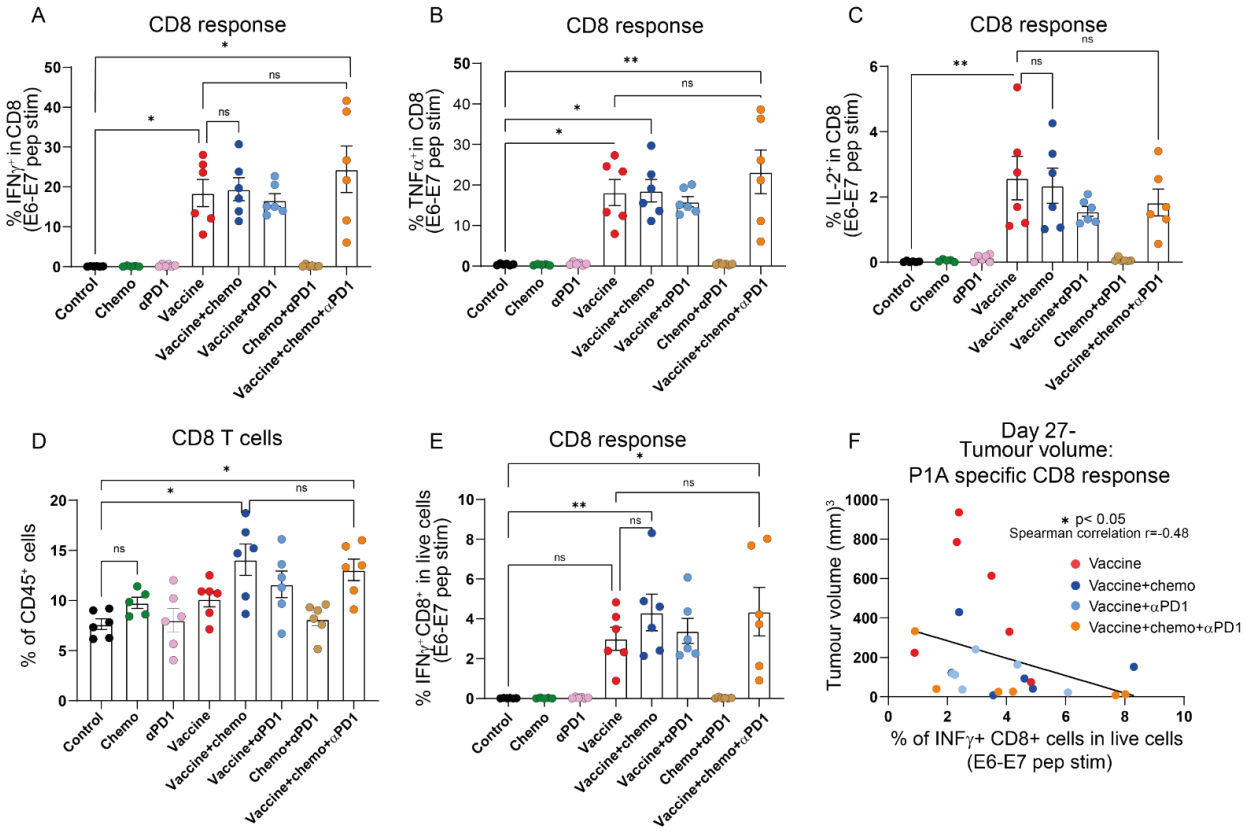


Figure 3.13 P1A-specific CD8⁺ T-cell responses 10 days post ChAdOx1/MVA-E6/E7 vaccination. BL/6 mice were implanted with 1x10^5 TC-1 cells via s.c. injection to initiate tumour growth. 10 days after tumour implantation, mice were vaccinated according to the schedules described in figure 3.10. To determine the magnitude of vaccine induced E6/E7-specific CD8⁺ cell responses in TC-1 tumour-bearing mice, mice were bled 10 days after MVA-E6/E7 boost. PBMCs were stimulated ex vivo with 4μg/ml of E6/E7 peptide pool and the percentage of cytokine-producing E6/E7-specific CD8⁺ cells in the blood was then determined by flow cytometry. (A) Average of IFNγ⁺CD8⁺ response is shown. (B) Average of TNFα⁺CD8⁺ response is shown. (C) Average of IL2+CD8⁺ response is shown. (D) Average of CD8⁺ T cells in the blood out of total PBMCs. (E) Average of IFNγ⁺ CD8⁺ out of total PBMCs is shown. Data representative of 1 experiment and shown as the mean± SEM response of each group. Each symbol represents an individual mouse, with 6 mice per group. Statistically significant differences between groups were determined by a Kruskal-Wallis test with Dunn's multiple comparisons test. *, p ≤ 0.05,**,p ≤ 0.01. Tumour size on day 28 after implantation was correlated with the magnitude of IFNγ producing E6-E7-specific CD8⁺ T-cells in the blood measured 27 days after implantation (F). Significance was determined by a Spearman Rank correlation test.

3.6 Discussion

3.6.1 Synergy of a novel combination therapy

For the first time a combination of CarboTaxol, anti-PD1, and a ChAdOx1/MVA heterologous prime-boost vaccine was tested in both, TC-1 tumour model in C57BL/6 mice (targeting E6/E7 antigens) and in 15V4T3 tumour model in DBA/2 mice (targeting the P1A antigen). In both models, we were able to show that this triple combination significantly improved the tumour control compared to the vaccine alone, the vaccine+anti-PD1 and the vaccine+chemo (for the DBA/2 model only) groups (fig 3.2, 3.11). Moreover, the survival of the mice receiving the triple combination was significantly higher than the vaccine alone in both models (fig 3.3, fig 3.12). Therefore, this protocol is not restricted to one tumour antigen nor to a certain tumour type. In the DBA/2 tumour model, 75% of the mice achieved complete remission with the triple combination regimen (fig 3.3 B). In C57BL/6 as well as in DBA/2 mice the tumour control correlated with the magnitude of the specific CD8 responses (against P1A or against E6/E7 antigens, fig 3.4 B and fig 3.13 F). At day 5 post boost, in the blood, spleen and TME, the P1A specific CD8 response was increased to a similar extent in both, vaccine+chemo and triple combination groups compared to the vaccine group (fig 3.5). These results highlighted the important synergistic effects of the combination of the vaccine with chemotherapy in increasing the magnitude of specific CD8 responses. Indeed, the addition of anti-PD1 was not essential for an increased immunogenicity at day 5 post boost. At day 12 post-boost, in the blood, we again observed an increased magnitude of the P1A and the E6-E7 CD8 responses in the vaccine+chemo and triple combination groups (fig 3.4, fig 3.13). In DBA/2, we also observed a slight increase in immunogenicity in the triple combination group compared to the vaccine+chemo (fig 3.4 B, C, D). This data highlighted the role of anti-PD1 in sustaining the vaccine-induced immune response and thereby supporting the anti-tumour response

efficacy for longer (fig 3.4, Appendix figure 1). But this support was less evident in the TC-1 model, which shows more resistance to anti-PD1 treatment[218].

To further understand the synergy of treatment observed, the next question we addressed was whether the phenotype of $CD8^+$T cells was impacted by the triple combination. Particularly, we hypothesise that CarboTaxol might increase the magnitude of the P1A specific response by impacting the fitness of the $CD8^+$ T cells.

3.6.2 Impact of the triple combination therapy on $CD8^+$ T cell phenotypes

Interestingly, CarboTaxol has been mostly studied for its effect on depleting granulocytic myeloid cells with immunosuppressive properties (PMN-MDSCs) in mice and patients with HPV16+ cervical cancer[207] . Only a few studies have reported a direct effect of CarboTaxol on $CD8^+$ T cells. In NSCLC patients and metastatic melanoma, CarboTaxol was shown to induce proliferation of effector $CD8^+$ T cells[146,147]. In ovarian cancer patients, CarboTaxol showed an expansion of central memory $CD8^+$ T cells, and better functionality of the $CD8^+$ T cells from CarboTaxol-treated patients [145]. Remarkably, previous studies showed that cyclophosphamide promotes effector function in $CD8^+$ T cells, highlighting the potential impact of chemotherapies on lymphocyte phenotype[223].

Firstly, we were interested by the impact of the treatment combinations on the T cell composition in the TME. Overall, the vaccinated groups showed a higher $CD8^+$ T cell proportion in the TME, which correlated with previously reported data (fig 3.7 A, B). Indeed, McAuliffe *et al*. showed that the ChAdOx1/MVA-P1A vaccines were able to change “cold” tumours “hot” and promote a more inflammatory microenvironment[179]. In line with these data, the TME of vaccinated groups displayed higher effector $CD8^+$ T cells than the PBS group. However, the addition of chemotherapy with the vaccine did not further increase the proportion of effector $CD8^+$ T cells (fig 3.7 C). In parallel, we

investigated the proportion of $TCF1^{+}PD1^{+}$ and $TCF1^{+}$ $PD1^{-}$ in $CD8^{+}$ T cells. TCF1 is a transcription factor that defines a stem-like phenotype, with $TCF1^{+}$ cells having a higher proliferation and self-renewal potential[59,60]. The presence of $CD8^{+}$ $TCF1^{+}$ $PD1^{+}$T cells has been correlated with better tumour control and survival outcome in both mice and patients[226]. Interestingly, the triple combination group showed an increased proportion of $TCF1^{+}PD1^{+}$ $CD8^{+}$ T cells and $TCF1^{+}$ $PD1^{-}$ $CD8^{+}$ T cells (fig 3.7 D, E), indicating that this synergy of treatment sustains the fitness of $CD8^{+}$ T cells in the TME. Therefore, $TCF1^{+}$ $PD1^{+}$ $CD8^{+}$ T cell infiltration could correlate with a better tumour control in our model too. Finally, a substantial proportion of $TCF1^{-}$ $PD1^{+}$ $CD8^{+}$ T cells as well as $TIM3^{+}PD1^{+}$ $CD8^{+}$ cells were observed in all groups (fig 3.7 F, G). Interestingly we noticed a reduction of the MFI of PD1 in the vaccinated groups, which was significant in the vaccine+chemo, the vaccine+anti-PD1 and the triple combination (fig 3.7 H). This possibly indicates a decrease in the exhaustion profile of the vaccinated groups, which was further reduced by the addition of chemotherapy and anti-PD1. Hence the triple combination displays less exhausted and higher stem-like T cell proportion in the TME which highlights the benefit of this combination in inducing not only specific but also effective T cells. However, chemotherapy per se did not induce reduction of $CD8^{+}$ T cell exhaustion nor displayed higher proportion of stem-like cells which could have explained the increased proportion of P1A specific $CD8^{+}$ T cell in the TME of vaccine+chemo treated mice.

An impact of CarboTaxol on the systemic phenotype of lymphocytes could also explain the higher magnitude of the P1A-specific CD8 responses. Especially, we observed a higher magnitude of the P1A-specific $CD8^{+}$T cells in the spleen and blood, which supports the idea that chemotherapy displays systemic effect (fig 3.5 B, C, E, F). Interestingly the double combination groups and the triple combination group showed slightly higher P1A-specific $CD8^{+}$ T cells with an effector memory and terminally differentiated $TCF1^{-}PD1^{+}$ phenotype

compared to the vaccine alone (fig 3.8 and fig 3.9). Effector memory T cells are highly cytotoxic T cells, hence being more efficient in killing cancer cells [50 227]. However, to support this pool of cytotoxic T cells, $TCF1^+$ stem-like cells might be crucial [228,229]. The triple combination showed the highest proportion of total and P1A-specific $TCF1^+PD1^+$ $CD8^+$ T cells, in the blood. However, this increase was not significant compared to the vaccine alone group and was not observed in the double combination groups. The pool of $TCF1^+PD1^+$ $CD8^+$T cells has been shown to be expanded in draining lymph nodes (dLN), found close to the tumour site, and feed directly the pool of terminally differentiated cytotoxic T cells[229]. Future work will involve investigating the presence of this pool of progenitor exhausted stem-like cells in dLN. Altogether these data highlight a potential role of $TCF1^+PD1^+$ T cells in the efficacy of the triple combination group. However, these data did not reveal any effect of CarboTaxol per se on $CD8^+$ T cell phenotypes in the system nor the TME.

Another important factor to consider when investigating chemotherapy effects would be the time point post treatment (day 12 post CarboTaxol might not be optimal). We can hypothesise that chemotherapy has an impact closer to the time of treatment injection. Welters *et al.* in 2016, showed that priming of $CD8^+$ T cells during MDSC depletion by chemotherapy was inducing a better tumour control than the vaccine alone[150]. Indeed, it is possible that CarboTaxol supports the generation of the P1A specific T cells by influencing their phenotype during priming or their priming environment, hence acting as an adjuvant. For instance, an early depletion of MDSCs, which have systemic immunosuppressive mechanisms[105], could explain the generation of a higher magnitude of the vaccine-induced immune response. Therefore, assessing CarboTaxol's impact on immune cells at early time-points post-treatment seems of importance to determine its mechanism of action.

Chapter IV: Effects of CarboTaxol on the immune system and tumour microenvironment

4.1 Introduction

For many years chemotherapy has been used as the standard of care for many cancer patients to reduce tumour progression. These cytotoxic drugs, such as CarboTaxol, induce the death of highly proliferative cells. Hence, cancer cells are particularly sensitive to chemotherapy but so are rapidly dividing healthy cells. Chemotherapy's impact on healthy cells often leads to strong adverse side effects in cancer patients. Intriguingly, the last decade of research has revealed some beneficial effects of chemotherapy on the immune system and its ability to stimulate anti-tumour immune responses[129,130]. It is important to note that the potential immune modulating effect of chemotherapies is class and dose dependent[130]. It is therefore important to understand the mechanism of action of these different cytotoxic drugs in order to target their use rationally, especially now that they are often used alongside with immunotherapies. Hence, being able to define the best dose and class of chemotherapy in combinational therapies will be essential to generate the best synergistic effects[206,207].

Among the different chemotherapy drugs that have been studied, two main types of effects of chemotherapy on the immune system have been characterised: tumour-cell dependent or independent[129]. The tumour-cell dependent effect is more commonly known as immunogenic cell death (ICD). First, immunogenic tumour-cell death leads to release of DAMPs and extracellular tumour-specific antigens, inducing dendritic cell activation. Dendritic cells, once recruited and activated, will then trigger T cell activation and infiltration into the tumour site[129,136]. Although Carboplatin alone has not been shown to induce ICD, a few alkylating chemotherapy drugs, such as cyclophosphamide, can induce ICD[136]. However, not all chemotherapy-effects are tumour-cell intrinsic. Chemotherapy can also have a direct impact on $CD8^+$ and $CD4^+$T cell phenotype[147]. A study in NSCLC patients showed that CarboTaxol can induce effector $CD8^+$ and $CD4^+$T cells[146]. Another

study in epithelial ovarian cancer patients undergoing CarboTaxol revealed the expansion of central memory $CD8^+$ T cells, which have a better potential for anti-viral responses after chemotherapy [145]. CarboTaxol has also been shown to deplete MDSC cells. Furthermore, combining vaccination with CarboTaxol-mediated MDSCs depletion has been demonstrated to improve vaccine efficacy by enhancing tumour control in TC-1 mouse tumour model [222]. Altogether, these recent findings support the use of chemotherapy as an immune-modulatory treatment and highlight the potential of using it in combinational therapy regimes.

MDSCs are a subset of immunosuppressive cells known to be expanded and recruited by the TME[230]. In many cancer types, the presence of these cells has been correlated with poor disease prognosis. It is widely accepted that two subsets of MDSCs exist: PMN- and M-MDSCs. PMN-MDSCs are granulocytic cells that are $CD11b^+$, $Ly6G^+$ and express high level of GR1 ($CD11b^+$ $GR1^{hi}$ $Ly6G^+$). As neutrophils express the same markers, functional assays assessing PMN-MDSC suppressive capabilities are necessary to confirm suppressive functions and fully define them[106]. M-MDSCs are monocytic cells which are defined as $CD11b^+$ $GR1^{lo}$ $Ly6C^{hi}$. They resemble inflammatory monocytes which can also express high level of Ly6C ($Ly6C^{hi}$). Interestingly, $Ly6C^{hi}$ monocytes in the TME mostly display immunosuppressive functions, and hence can be considered as M-MDSCs [106]. However, systemic M-MDSCs require functional assays to fully define them. Depending on the cancer type, either or both MDSC subsets can be expanded upon tumorigenesis. Moreover, different MDSC subsets can present different mechanisms of immunosuppression[231]. M-MDSCs have been shown to upregulate NO expression whilst PMN-MDSCs have been shown to preferentially increase the production of ROS. Both molecules have been shown to impair the activation and effector functions of $CD4^+$and $CD8^+$ T cells [231,232]. Other strategies than chemotherapy have been explored to target

MDSCs at different levels [233]. Interestingly targeting MDSCs recruitment and trafficking has been shown to improve adoptive T cell transfer and anti-PD1 immunotherapy in murine models[234–236].

As previously mentioned, effector $CD8^+$ T cells are of major importance for anti-tumour immunity as they possess cytotoxic function to directly kill cancer cells. However, one major challenge for effective immunotherapy in cancer patients is to sustain an efficient anti-tumour $CD8^+$ response once generated, $CD8^+$ T cells can become exhausted following prolonged activity and antigenic stimulation [50]. $CD8^+$ T cell exhaustion is characterised by the loss of cytotoxic effector function of these anti-tumour cells, which ultimately leads to the loss of immune-mediated disease control. Very interestingly, some phenotypes of $CD8^+$ T cells have been associated with prolonged anti-tumour responses. One of them is the stem-like $CD8^+$ T cells which are defined as $CD8^+$ $TCF1^+$ $PD1^+$ T cells. TCF1 is a transcription factor which is expressed downstream of the WNT/β-Catenin canonical pathway[60]. TCF1 has long been associated with the regulation of T cell development and T-cell fate[237,238]. More recently, studies have shown the importance of TCF1 expression in tumour T cells for the generation of an effective and sustained anti-tumour T cell response[226]. TCF1 expression is associated with the induction of $CD8^+$ T cell stemness and T cell subsets with highly proliferative capacity. Recent evidence has correlated TCF1 expression with success of anti-tumour immunotherapies. Indeed, TCF1 expression in $CD8^+$ T cells has been related to a better clinical response to checkpoint inhibitor in cancer patients[226]. Only very few drugs have been shown to induce TCF1 expression such as PI3 kinase inhibitor[239]. While chemotherapy has been shown to induce effector T cells[146], the induction and expression of TCF1 through chemotherapy in anti-tumour T cells has not been studied.

Ideally, in combinatorial therapy, a synergy of treatments is observed when the effect of the combination is greater than the sum of their separate effects [130 240]. In our studies, we observed that one dose of CarboTaxol, given together with a prime vaccination, was sufficient to synergise with our vaccine platform for a better immunogenicity, tumour control and survival. This synergy was even further improved by the addition of anti-PD1. In this chapter, we focus on the mechanism of action of CarboTaxol to determine why it synergises with ChAdOx1/MVA vaccination when given at the same time point of ChAdOx1. As reported in Chapter III, we did not observe any major changes in the TME, nor the spleen and blood, at day 12 post chemotherapy treatment. Therefore, in this chapter, we investigated the short-term effects of CarboTaxol, at 4 days post treatment. We observed some major changes in the immune landscape early after CarboTaxol administration. We further explored whether CarboTaxol impact on immune phenotypes was tumour-cell independent. To do so, we investigated the effects of this chemotherapy in tumour free mice where we confirmed its potential adjuvant role. When combining several therapies with immune modulatory capacities, the relative timing of each treatment is of major importance. So, in parallel, we assessed the importance of the timing of chemotherapy administration relative to the vaccination. This chapter highlights the immediate effects of CarboTaxol on the immune system and its long-lasting effects on ChAdOx1/MVA-induced immune response.

4.2 Chapter Aims

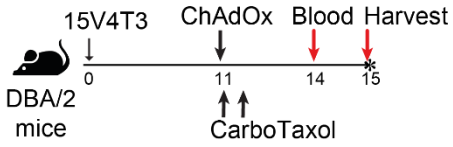
- To investigate the effect of CarboTaxol on the MDSCs in tumour bearing mice and the importance of MDSC depletion.
- To investigate the effect of CarboTaxol on T cells in a tumour and tumour free environment.
- To explore the impact of CarboTaxol on ChAdOx1/MVA immunogenicity independent of its effect on tumour cells.
- Ultimately, to elucidate how CarboTaxol improves vaccine immunogenicity.

4.2 CarboTaxol has early effects on the systemic and tumour-infiltrated innate immune cells in tumour bearing mice

4.2.1 Chemotherapy has short-term impact on myeloid cells

The impact of CarboTaxol on myeloid cells has been previously shown in mice and in cancer patients. In mice treated with CarboTaxol, the effects were observed 72h after the first dose of carboplatin and paclitaxel[150]. We therefore decided to explore the short-term effect of CarboTaxol on the immune system in the 15V4T3 tumour model. DBA/2 mice were implanted with 15V4T3. At day 11 post tumour implantation, mice were randomised into 4 different groups (fig 4.1,B). The mice were vaccinated with ChAdOx1-Ii-P1A and given carboplatin and paclitaxel on the same day. The next day another injection of paclitaxel was given to the corresponding treatment groups. Blood was sampled on day 14 (3 days after the first chemotherapy injections); spleen, bone marrow (BM) and tumour were harvested on day 15 (4 days after the first chemotherapy injections).

A



B

Groups \ Days of treatments	11	12
Control	ChAdOx-DPY+ Nacl	Nacl
Chemo only	Carboplatin+Paclitaxel	Paclitaxel
Vaccine only	ChAdOx-Ii-P1A+Nacl	Nacl
Vaccine+chemo	ChAdOx-Ii-P1A+ Carboplatin+Paclitaxel	Paclitaxel

Figure 4.1 Timeline of tumour harvest and treatment regimens of every group tested. (A) DBA/2 mice were implanted with $1x10^6$ 15V4T3 cells via s.c injections to initiate tumour growth. 11 days after tumour implantation, mice were vaccinated via i.m with 10^7 IU of ChAdOx1-Ii-P1A or PBS sham and treated with carboplatin(40mg/kg) and paclitaxel (20mg/kg) and 24h later with paclitaxel (20mg/kg) via i.p. Mice were randomised into 4 different groups (7 to 8 mice per groups) based on tumour volume (as measured on day 11) and injected with the treatments indicated in table B. At day 3 post prime and first chemotherapy injections, the blood were harvested, at day 4 post prime and first chemotherapy injections, spleen, BM and tumour of each mouse were harvested (A).

MDSCs were then profiled using flow cytometry. We assessed the $CD11b^{+}$ $GR1^{hi}$ $Ly6G^{+}$ (PMN-MDSCs) and $CD11b^{+}$ $GR1^{int}$ $Ly6C^{hi}$ (M-MDSC). In figure 4.2, we observed that the chemo only and the vaccine+chemo group displayed a depletion of the $GR1^{hi}$ cells, composed at 99% of $Ly6G^{+}$ $Ly6C^{int}$ cells (referred as $Ly6G^{+}$, potential PMN-MDSCs). However, the depletion was less clear when observing $CD11b^{+}$ $GR1^{int}$ cells.

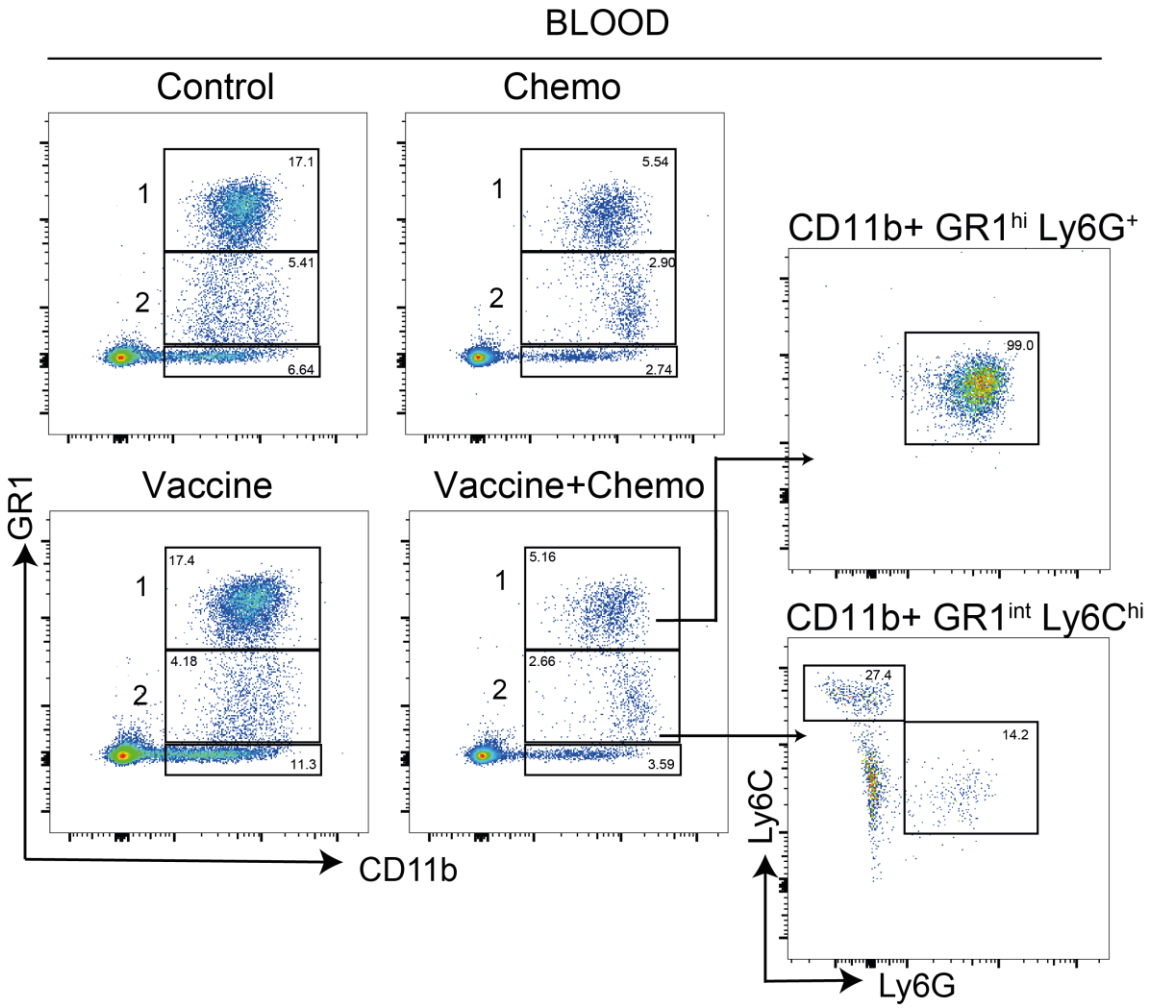


Figure 4.2 Myeloid cells gating strategy in blood of 15V4T3 DBA/2 tumour bearing mice. To determine the myeloid cells profile of 15V4T3 implanted DBA/2 mice after treatments, we stained different organs and used the same gating strategy to explore potential MDSCs. Here the gating strategy showed is from the blood of tumour bearing DBA/2 mice 4 days post chemotherapy. Differences between the different treatment groups are shown. Cells were stained with CD11b and GR1 markers as this were first defined markers for granulocytic or monocytic myeloid cells. To further define the GR1 high (hi) and intermediate (int) population, cells were stained with Ly6G and Ly6C markers.

To precisely discriminate M-MDSCs, the Ly6C and Ly6G markers are needed. Indeed, as shown in figure 4.2, the GR1^{int} population is composed of different sub-populations, among which we can observe the Ly6C^{hi} Ly6G- cells (referred as Ly6C^{hi}, potential M-MDSCs). Therefore, staining presented later in this chapter will always assess the Ly6G and Ly6C markers as they allow the precise gating of the potential M-MDSCs population, sometimes without the use of GR1 marker (see materials and methods for gating strategy).

The statistical differences between the groups in term of potential PMN-MDSCs (fig 2.3 A,B) were also evaluated. In figure 4.2, we observed a significant depletion of CD11b^{+} GR1^{hi} Ly6G^{+} cells in the blood of the chemotherapy-treated group in terms of proportion and cell numbers (fig 4.3 A and B). Although this depletion was not complete, these cells were reduced by more than half in the groups treated with the CarboTaxol compared to the non-treated ones. Having observed this, we then looked more closely at the potential M-

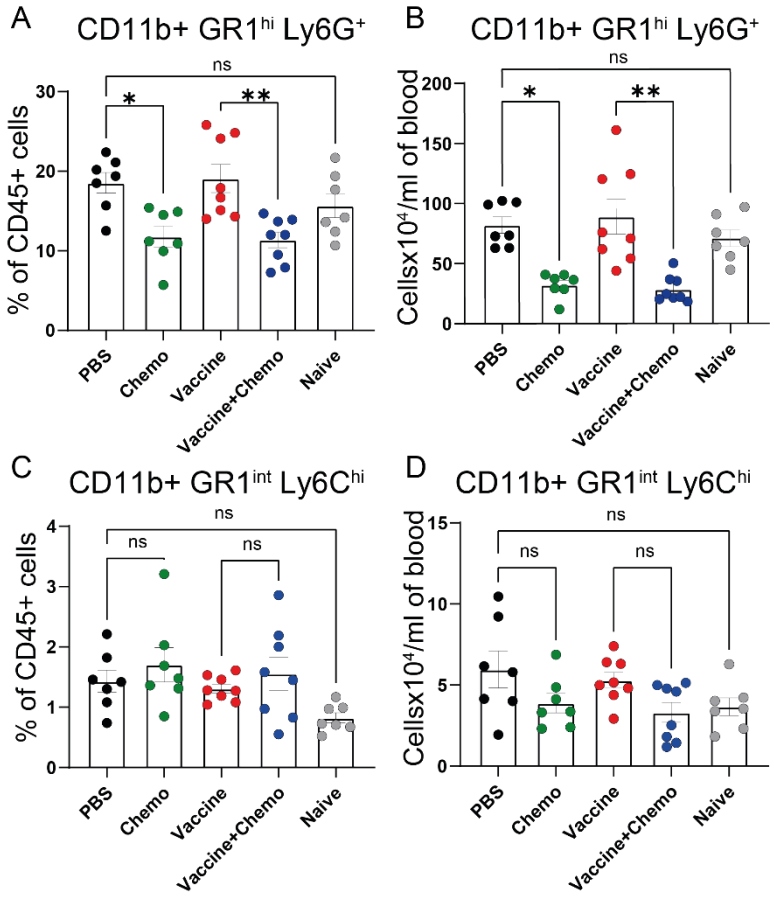


Figure 4.3 Myeloid cells in blood of 15V4T3 DBA/2 tumour bearing mice. DBA,2 mice were implanted with 1x10^{6} 15V4T3 cells. 11 days after tumour implantation, mice were vaccinated via i.m with 10^{7} IU of ChAdOx1-Ii-P1A or PBS sham and treated with CarboTaxol via i.p. (figure 4.1). A tumour free mice group was also included in this study and PBS sham injected at the same time of the start of the treatment for the tumour bearing mice. At day 3, blood was harvested, and cells were stained and analysed by flow cytometry. Percentages and numbers of CD11b^{+} GR1^{hi} Ly6G^{+} are shown in (A) and (B). Percentages and numbers of CD11b^{+}GR1^{int} Ly6C^{hi} cells are shown in (C) and (D). The data are representative of 2 independent experiments and mean ± SEM for each group are shown. Each symbol represents an individual mouse (n=7 to 8 mice per group). Statistically significant differences between groups were determined by a Kruskal-Wallis test with Dunn's multiple comparisons test,*, p ≤ 0.05, **, p ≤ 0.01.

MDSCs. We did not observe a significant decrease of $CD11b^{+}$ $GR1^{int}$ $Ly6C^{hi}$ with chemotherapy in the blood (fig 4.3 C and D). Finally, MDSCs have been shown to be expanded in tumour bearing mice[106], we therefore also compared tumour bearing mice with tumour free mice (naïve) at this time point. Interestingly, in the 15V4T3 DBA/2 model, there was no significant myeloid cell expansion in tumour-bearing compared to tumour free mice (PBS vs naïve group fig 4.3).

The effect of CarboTaxol on $CD11b^{+}$ $GR1^{hi}$ $Ly6G^{+}$ and $CD11b^{+}$ $GR1^{int}$ $Ly6C^{hi}$ was also explored in the spleen, the BM and the TME. At day 4 after the first CarboTaxol injections, we observed a significant depletion of the $CD11b^{+}$ $GR1^{hi}$ $Ly6G^{+}$ cells in the BM (fig 4.4 A), spleen (fig 4.4 B), and TME (fig 4.4 C) compared to non-chemo treated groups. However, the numbers of $CD11b^{+}$ $GR1^{int}$ $Ly6C^{hi}$ potential M-MDSCs were not significantly different in the chemotherapy-treated groups, in any of the organs tested, compared to the PBS and vaccine alone groups (fig 4.4 D, E, F).

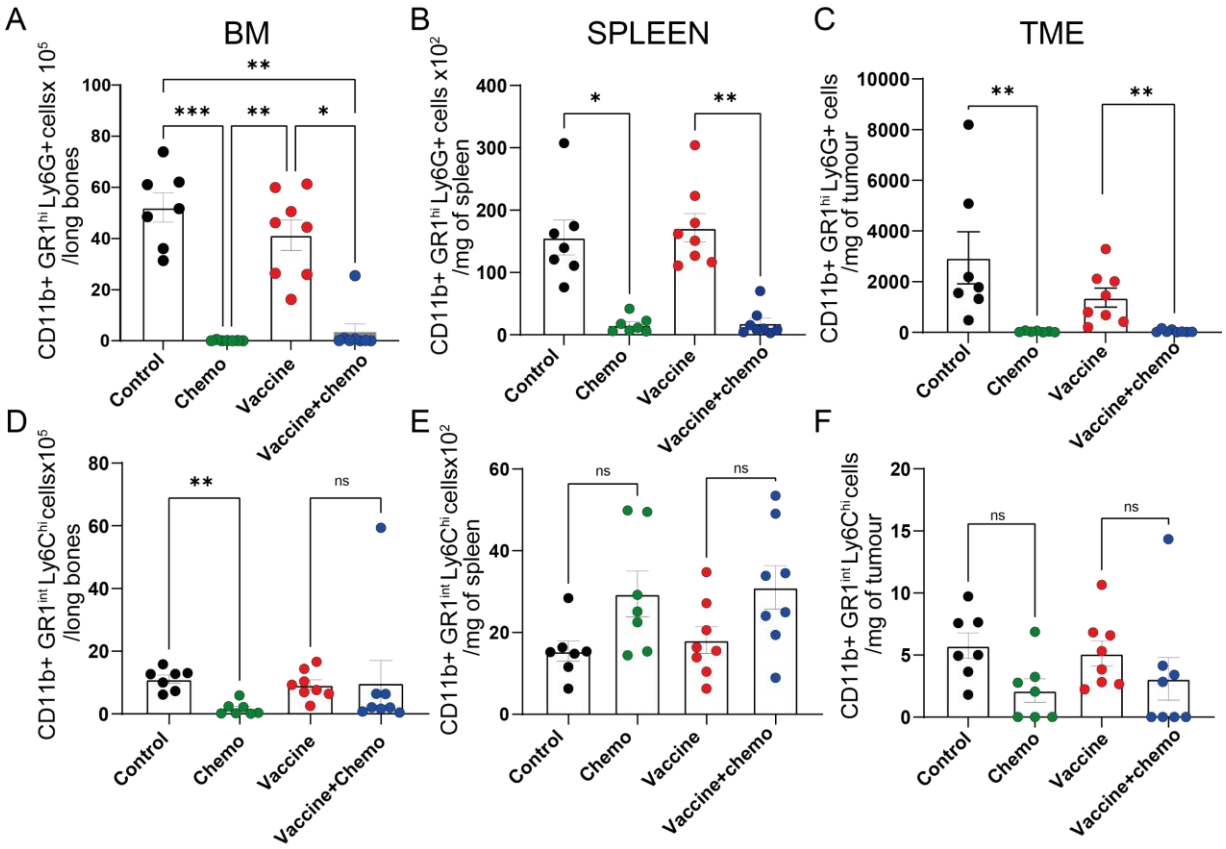


Figure 4.4 Myeloid cells in BM, spleen and tumour of 15V4T3 DBA/2 tumour bearing mice. DBA/2 mice were implanted with $1x10^6$ 15V4T3 cells. 11 days after tumour implantation, mice were vaccinated via i.m with 10^7 IU of ChAdOx1-Ii-P1A or PBS sham and treated with carboplatin(40mg/kg) and paclitaxel (20mg/kg) and 24h later with paclitaxel (20mg/kg) via i.p. At day 4 post treatment, spleen, bone marrow (BM) and Tumours were harvested and stained with CD11b, GR1 and Ly6G and Ly6C markers to assess potential MDSCs populations. The numbers $CD11b^+GR1^{hi}$ Ly6G+ cells are shown in the BM (A), spleen (B) and TME (C). The numbers of $CD11b^+$ $GR1^{int}$ $Ly6C^{hi}$ are shown in the BM (D), spleen (E) and TME (F). The data are representative of 2 independent experiments and mean ± SEM for each group are shown. Each symbol represents an individual mouse (n=7 to 8 mice per group). Statistically significant differences between groups were determined by a Kruskal-Wallis test with Dunn's multiple comparisons test,*, $p \leq 0.05$, **, $p \leq 0.01$, ***, $p \leq 0.001$ ****, $p \leq 0.0001$.

In chapter III, CarboTaxol treatment was evaluated in the TC-1 model in combination with ChAdOx1/MVA expressing E6/E7. The combination was more efficient in terms of tumour control and immunogenicity than the vaccine alone. Therefore, we also investigated the potential MDSCs in the blood, 4 days after treatment (fig 4.5 A) in the TC-1 model. We observed that the proportion and numbers $CD11b^{+}$ $GR1^{hi}$ $Ly6G^{+}$ cells were also significantly reduced in the chemotherapy treated groups compared to the chemotherapy non-treated groups (fig 4.5 B).

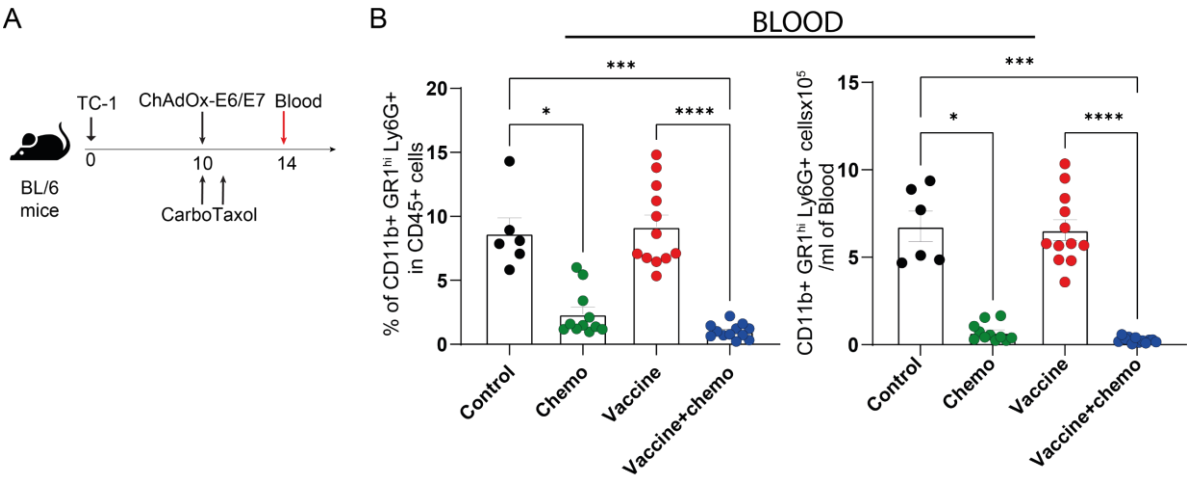


Figure 4.5 CD11b+GR1^{hi}Ly6G+ in blood of TC-1 C57BL/6 tumour bearing mice. C57BL/6 mice were implanted with 1x10^5 TC-1 cells via s.c injections to initiate tumour growth. 10 days after tumour implantation, mice were vaccinated via i.m with 10^7 IU of ChAdOx1-E6/E7 or ChAdOx1-DPY and treated with carboplatin(40mg/kg) and paclitaxel (20mg/kg) and 24h later with paclitaxel (20mg/kg) via i.p (A). At day 4 post treatments, blood was harvested, and cells were stained and analysed by flow cytometry. Percentages and numbers of $CD11b^{+}$ $GR1^{hi}$ $Ly6G^{+}$ are shown in (B). The data are representative of 2 independent experiments and mean ± SEM for each group are shown. Each symbol represents an individual mouse (n=6 to 12 mice per group). Statistically significant differences between groups were determined by a Kruskal-Wallis test with Dunn's multiple comparisons test, *, $p \leq 0.05$, **, $p \leq 0.01$, ***, $p \leq 0.001$ ****, $p \leq 0.0001$.

Very importantly, in order to define cells as PMN- or M-MDSCs, functional assays evaluating their suppressive abilities on the proliferation of $CD8^+$ or $CD4^+$T cells are necessary. Because CarboTaxol induces the depletion of only potential PMN-MDSCs, we focused on investigating the immunosuppressive abilities of $CD11b^+Ly6G^+$ cells. $Ly6G^+$ cells from spleen of 15V4T3 tumour bearing DBA/2 mice were sorted, their viability and purity were also assessed. With purity above 95%, $CD11b^+$ $Ly6G^+$ cells (fig 4.6 C) were then co-cultured with $CD8^+$ T cells from spleens of naïve DBA/2 mice. $CD8^+$ T cells were stimulated for 3 days with CD3 and CD28 and their proliferation was evaluated by flow cytometry. In this model, we observed that the $CD11b^+Ly6G^+$ cells were able to supress the proliferation of $CD8^+$ T cells in a ratio-dependent manner (fig 4.6 A). Indeed, we observed a decrease in proliferation of 25 % at 1:3 CD8: MDSC and over 30% at 1:4 CD8: MDSC ratio. Interestingly, the suppression was also observed with a 1:2 CD8: MDSC ratio but was not significant. CD8: MDSC ratio of 1:1 was not sufficient to induce a suppression (fig 4.6 B).

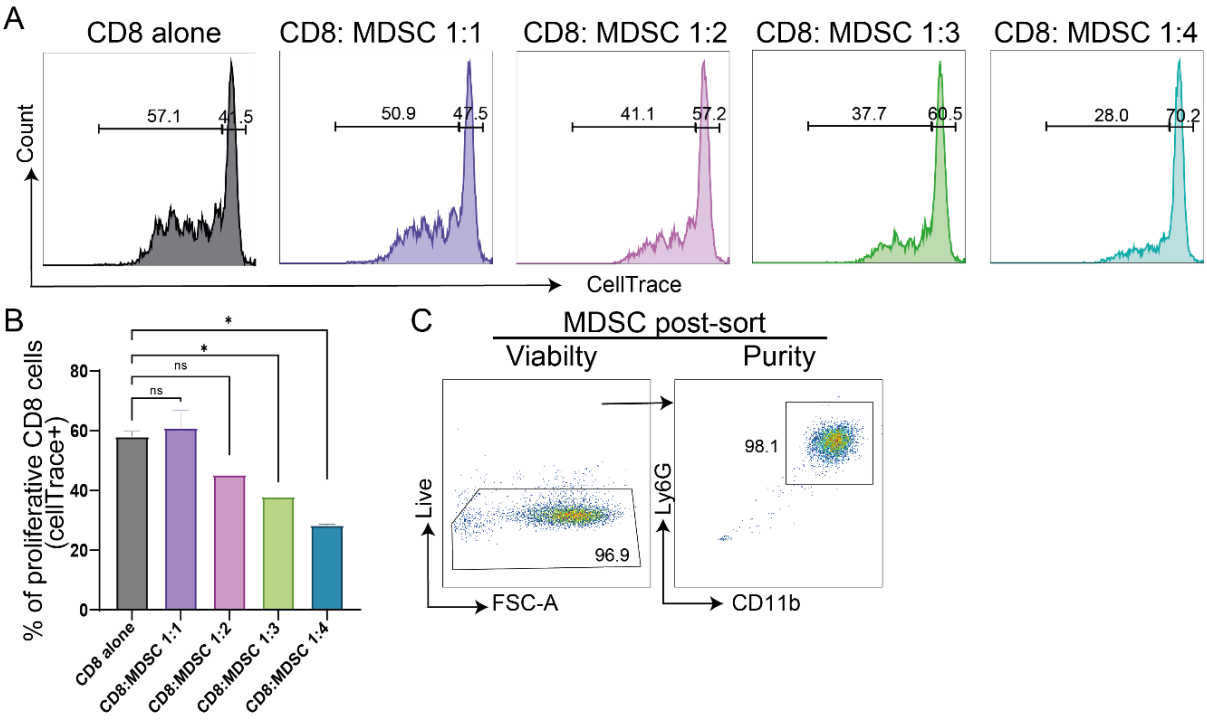


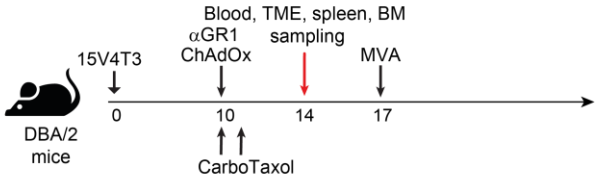
Figure 4.6 CD11b+Ly6G+ cell immunosuppressive functions on CD8⁺ T cell proliferation. DBA,2 mice were implanted with 1x10^6 15V4T3 cells. When tumour reach 300 to 400 mm^3, spleens were harvested and processed to extract by magnetic selection Ly6G$^+$ cells. The fraction of Ly6G$^+$ cells were then sorted to achieve a higher purity of 98 % or above. CD8$^+$T cells from naïve mice were sorted with magnetic selection. The CD8$^+$ T cells were stained with CellTrace violet. MDSCs and CD8$^+$ T cells were co-culture at different ratio and proliferation of CD8$^+$ T cells was assessed 72h later. The CD8$^+$ T cells were stimulated with coated CD3 (1μg/ml) and soluble CD28 (1μg/ml). Gating of proliferative and non-proliferative CD8$^+$ T cells at 72h is shown in (A) and mean percentage of proliferative cells at different ratio are shown in (B). The viability and purity of the CD11b$^+$ Ly6G$^+$ cells post-sort are shown in (C) The data are pooled from 2 independent. Statistically significant differences between groups were determined by a Kruskal-Wallis test with Dunn's multiple comparisons test,*, $p \leq 0.05$.

To summarise, CarboTaxol induces CD11b$^+$GR1^{hi}Ly6G+ cell depletion in tumour bearing mice 3- and 4-days post treatment both in the TME and systemically (blood, spleen, and BM). We were able to show that these CD11b$^+$GR1^{hi}Ly6G+ cells displayed suppressive activities against CD8$^+$ T cell by decreasing their proliferation. It is important to note that the ratio of cells needed for this suppressive function was quite high (1:3 minimum). Also, in the 15V4T3 model we did not observe an expansion of these cells compared to tumour free mice, which is an important characteristic of MDSCs in cancer. Therefore, in our model, it is possible that there is a non-negligible proportion of non-suppressive granulocytes/neutrophils within the CD11b$^+$Ly6G$^+$ population.

4.2.2 In vivo depletion of PMN-MDSCs using in vivo anti-GR1 antibody does not improve tumour control nor vaccine immunogenicity

The next question to address was whether the depletion of PMN-MDSCs is responsible for the synergistic effect observed when vaccine and CarboTaxol are combined. Indeed, the short-term systemic and tumoral depletion of MDSCs could promote a better priming environment for the $CD8^+$ T cells. To answer this important question, DBA/2 mice were implanted with 15V4T3, and mice were vaccinated with the ChAdOx1-Ii-P1A 10 days post tumour implantation. Together with the prime vaccination, the mice received anti-GR1 antibody, in one i.p injection, which have been published to deplete GR1+ cells[241]. This combination was compared with vaccine+CarboTaxol regimen. A week later, the mice were boosted with MVA-tpA-P1A (fig 4.7 A and B). Tumours were measured throughout the study and survival was assessed.

A



B

Days of treatment / Groups	10	10	11	17
Control	Isotype control	ChAdOx-DPY	Nacl	MVA-DPY
Chemo only	–	PBS+ Carboplatin+Paclitaxel	Paclitaxel	PBS
αGR1 only	αGR1	PBS	–	PBS
Vaccine only	Isotype control	ChAdOx-li-P1A	–	MVA-tpa-P1A
Vaccine+chemo	–	ChAdOx-li-P1A+ Carboplatin+Paclitaxel	Paclitaxel	MVA-tpa-P1A
Vaccine+αGR1	αGR1	ChAdOx-li-P1A	–	MVA-tpa-P1A

Figure 4.7 Timeline of tumour harvest and treatment regimens of every group tested. *(*A) DBA/2 mice were implanted with $1x10^6$ 15V4T3 cells via s.c injections to initiate tumour growth. 10 days after tumour implantation, mice were vaccinated via i.m with 10^7 IU of ChAdOx1-Ii-P1A or PBS sham and treated with anti-GR1 antibody injected i.p (400µg) or with carboplatin(40mg/kg) and paclitaxel (20mg/kg) and 24h later with paclitaxel (20mg/kg) via i.p. 7 days after the prime, mice were boosted with 10^6 PFU of MVA-tpA-P1A. Mice were randomised into 6 different groups (6 to 7 mice per groups) based on tumour volume (as measured on day 10) and injected with the treatments indicated in table (B). At day 4 post prime and first chemotherapy injections, the blood, TME, spleen and BM were harvested(A). Tumour growth was monitored throughout the experiment.

The combination of anti-GR1 with the vaccine did not show any improvement in terms of tumour growth and survival compared to the vaccine alone (fig 4.8 A and B). As previously shown, the vaccine+chemo group significantly improved tumour control (fig 4.8 A) and displayed a better survival compared to the vaccine alone group (fig 4.8 B). We confirmed that the anti-GR1 antibody was able to deplete $CD11b^{+}$ ly6G+ cells in the blood (fig 4.8 C), spleen (fig 4.8 D) and TME (fig 4.8 E) of tumour bearing mice. However, we could not see a significant depletion of the $CD11b^{+}Ly6G^{+}$ by this antibody in the BM (F). Importantly, cautions are to be taken when interpreting these data, as this dose and frequency of $CD11b^{+}$ $Ly6G^{+}$ after anti-GR1 was evaluated only once in spleen, TME and BM (n= 4 for αGR1, fig 4.8 D,E,F).

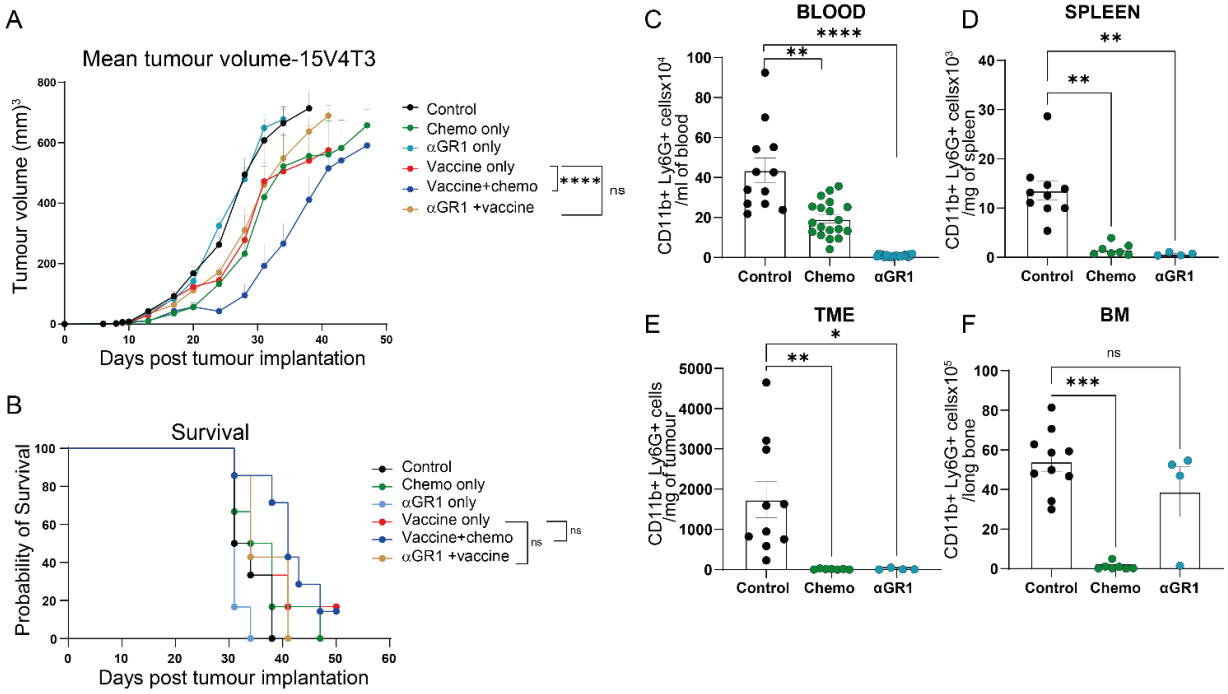
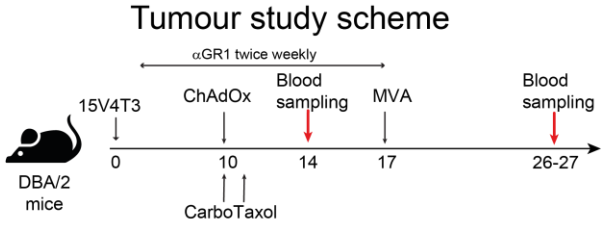


Figure 4.8 One injection of anti-GR1 combined with ChAdOx1/MVA-P1A in tumour bearing DBA/2 mice. DBA/2 mice were implanted with $1x10^{6}$ 15V4T3 cells via s.c injections to initiate tumour growth. Tumour growth is shown in (A) and mouse survival is shown in (B). To confirm the efficacy of anti-GR1, the blood spleen,BM and TME were analysed for PMN-MDSCs and the numbers of CD11b+Ly6G+ cells are shown in (C),(D),(E),(F). Tumour growth data are from one experiment and are presented as mean tumour volume (mm3) ± SEM. Stastical differences were evaluated using two-way ANOVA followed by Tukey's post hoc test. Statistical differences in survival data were determined by a Log Rank test. For (C)-(E) Mean ± SEM is shown and each symbol represents an individual mouse and data are pooled from different groups (n= 4 to 19 mice per groups). Statistically significant differences between groups were determined by a Kruskal-Wallis test with Dunn's multiple comparisons test,*, $p \leq 0.05$, **, $p \leq 0.01$, ***, $p \leq 0.001$ ****, $p \leq 0.0001$.

Given the ineffectiveness of one injection of anti-GR1 in improving survival or delaying tumour growth, we then increased the number of anti-GR1 injections, in order to start the depletion earlier and possibly further block $CD11b^{+}Ly6G^{+}$ recruitment in spleen, TME and blood. Therefore, DBA/2 mice were implanted with 15V4T3, and received anti-GR1 antibody twice weekly by i.p injection from day 3 post tumour implantation. Mice were vaccinated with the ChAdOx1-Ii-P1A on day 10. The vaccine+anti-GR1 treatment efficacy was compared with the vaccine combined with CarboTaxol. Mice were boosted 7 days later with MVA-tpA-P1A (fig 4.9 A,B). Tumour growth and survival were monitored

A



B

Days of treatment / Groups	3	7	10	10	11	14	17
Control	Isotype control	Isotype control	Isotype control	ChAdOx-DPY	Nacl	Isotype control	MVA-DPY
Chemo only	—	—	—	PBS+ Carboplatin+Paclitaxel	Paclitaxel	—	PBS
αGR1 only	αGR1	αGR1	αGR1	PBS	—	αGR1	PBS
Vaccine only	Isotype control	Isotype control	Isotype control	ChAdOx-Ii-P1A	—	Isotype control	MVA-tpa-P1A
Vaccine+chemo	—	—	—	ChAdOx-Ii-P1A+ Carboplatin+Paclitaxel	Paclitaxel	—	MVA-tpa-P1A
Vaccine+αGR1	αGR1	αGR1	αGR1	ChAdOx-Ii-P1A	—	αGR1	MVA-tpa-P1A

C

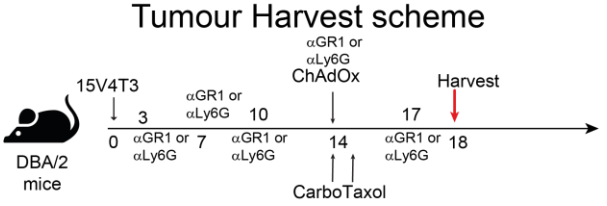


Figure 4.9 Timeline of tumour harvest and treatment regimens of every group tested. *(*A) DBA/2 mice were implanted with $1x10^{6}$ 15V4T3 cells via s.c injections to initiate tumour growth. Mice were treated with anti-GR1 antibody injected i.p from day 3, then twice a week (200μg). 10 days after tumour implantation, mice were vaccinated via i.m with 10^{7} IU of ChAdOx1-Ii-P1A or PBS sham and treated with carboplatin(40mg/kg) and paclitaxel (20mg/kg) and 24h later with paclitaxel (20mg/kg) via i.p. 7 days after the prime, mice were boosted with 10^{6} PFU of MVA-tpA-P1A. At day 14 and day 26 to 27, the blood, was harvested. Mice were randomised into 6 different groups (6 to 7 mice per groups) based on tumour volume (as measured on day 10) and injected with the treatments indicated in table (B). Tumour growth was monitored throughout the experiment. In (C), tumour harvest scheme is presented where DBA/2 were treated similarly to (A) with the vaccination starting on day 14 to allow for bigger tumour size for the harvest. In parallel of testing anti-GR1 some mice were treated with anti-Ly6G injected i.p from day 3 (200μg).

throughout the experiment. We also investigated the impact of anti-GR1 on the immunogenicity of the vaccine and compare it with the effect of the chemotherapy on immunogenicity. In parallel, anti-GR1 efficacy in depleting $CD11b^{+}Ly6G^{+}$ was assessed (fig 4.9 C).

The anti-GR1 and vaccine combination did not display better tumour control nor a better survival compared to the vaccine alone group (fig 4.10 A,B). Once again CarboTaxol significantly improved the tumour control of the vaccine, and a significantly better survival was observed compared to the vaccine alone group (fig 4.10 B). Moreover, the anti-GR1 antibody was not able to recapitulate the chemotherapy effect on the vaccine immunogenicity. Indeed, we did not see any significant differences in terms of $IFN\gamma^{+}CD8^{+}$

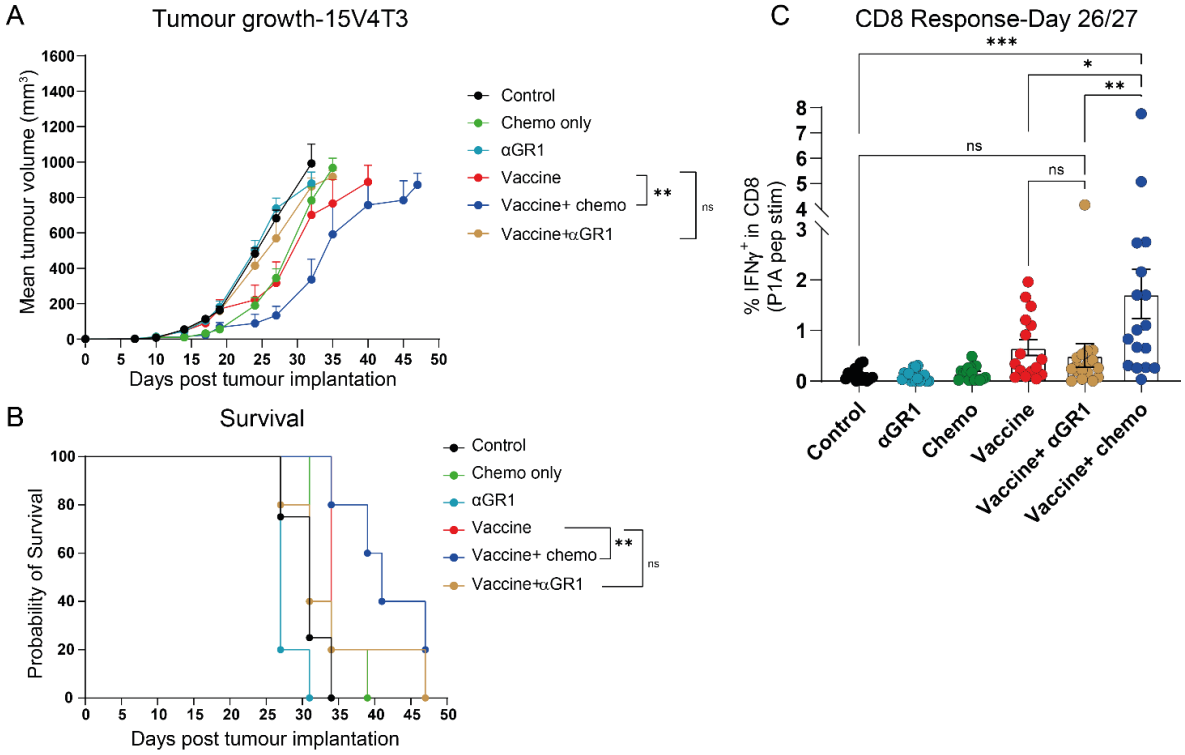


Figure 4.10. Combination of ChAdOx1/MVA-P1A with anti-GR1 injections in tumour bearing DBA/2 mice. DBA/2 mice were implanted with $1x10^{6}$ 15V4T3 cells via s.c injections to initiate tumour growth. Mice were treated as shown in figure 4.9 (A). Tumour growth is shown in (A) and mouse survival is shown in (B). Tumour growth data are from one experiment and are presented as mean tumour volume (mm3) ± SEM. Statistically significant differences between groups were determined by two-way ANOVA followed by Tukey's post hoc test for tumour growth data and statistical differences in survival data were determined by a Log Rank test. Blood from mice treated with the schedules represented in figures 4.7 and 4.9 was harvested and PBMCS were stimulated with P1A peptides for 5h. The proportion of P1A specific $CD8^{+}$ T cells is shown in (C). Mean± SEM is shown and each symbol represents an individual mouse and data are pooled from 3 independent experiments (n= 16 to 17 mice per groups). Statistically significant differences between groups were determined by a an ordinary one-way ANOVA comparisons test, *, $p \leq 0.05$, **, $p \leq 0.01$, ***, $p \leq 0.001$.

T cell proportions between the vaccine group and the vaccine+anti-GR1 group (fig 4.10 C).

We verified that the depletion by the anti-GR1 in the spleen, blood and TME were still efficient with this new schedule. We also compared this antibody with anti-Ly6G antibody, potentially more specific for $CD11b^{+}Ly6G^{+}$ cell depletion. The anti-Gr1 antibody demonstrated good depletion of $CD11b^{+}$ $Ly6G^{+}$ cells in the blood and TME of tumour bearing mice (fig 4.11 A, C). Surprisingly, at this frequency, anti-GR1 seemed to induce some cytotoxicity in the spleen, as enlarged spleens and no depletion of $CD11b^{+}Ly6G^{+}$ were observed (fig 4.11 B). However, we did not assess again the BM with this new schedule, and this will need to be evaluated to see the impact of this new schedule on MDSCs generation. The anti-Ly6G efficacy in depleting the $CD11b^{+}$ $Ly6G^{+}$ in the blood and in the TME was not as efficacious as the anti-GR1 antibody or the chemotherapy. Although we observed a depletion in the spleen with anti-Ly6G, it was not significant nor as efficient as the chemotherapy (fig 4.11 B). Therefore, anti-Ly6G antibody was not a

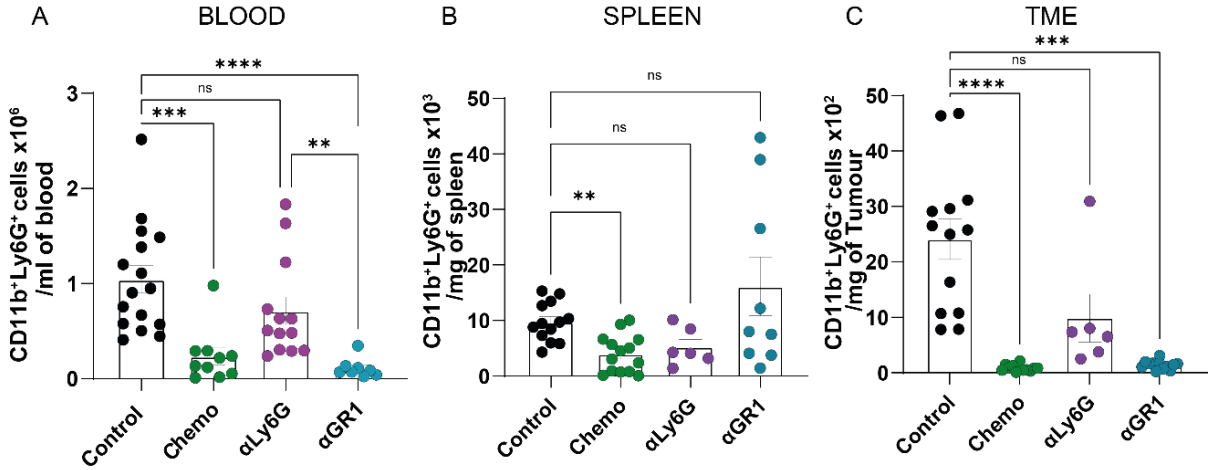


Figure 4.11 CD11b+Ly6G+ depletion after sequential injections of anti-GR1. DBA/2 mice were implanted with $1x10^6$ 15V4T3 cells via s.c injections to initiate tumour growth. Mice were then treated as shown in figure 4.9 (B). To confirm the efficacy of anti-GR1, the blood, spleen and TME were analysed for PMN-MDSCs depletion and the numbers of CD11b+Ly6G+ cells are shown in (A) for the blood, (B) for the spleen, (C) for the TME. Each symbol represents an individual mouse and data are pooled from at least 2 independent experiments except for the anti-Ly6G group where only one experiment was performed to analyse spleen and tumours (n= 6 to 16 mice per groups). Mean ± SEM is shown.Statistically significant differences between groups were determined by a Kruskal-Wallis test with Dunn's multiple comparisons test, **, $p \leq 0.01$, ***, $p \leq 0.001$ ****, $p \leq 0.0001$.

better choice to understand the importance of the $CD11b^{+}Ly6G^{+}$ depletion in improving vaccine efficacy.

To conclude, the use of monoclonal antibodies against either GR1 or Ly6G could not completely deplete PMN-MDSC in the system, in contrast to CarboTaxol. However, one dose of anti-GR1 seemed to be the best schedule to mimic CarboTaxol-mediated MDSC depletion. Nevertheless, this schedule could not improve vaccine induced tumour control nor improve vaccine immunogenicity. Likely, the $CD11b^{+}Ly6G^{+}$ depletion is not the main mechanism by which chemotherapy improves vaccine-mediated tumour control and vaccine immunogenicity. Therefore, we then investigated the effect of CarboTaxol on $CD8^{+}$ T cells. Indeed, an impact on the phenotype of $CD8^{+}$ T cells during priming might promote a better vaccine-induced response.

4.3 CarboTaxol impacts CD8$^+$ and CD4$^+$T cells in tumour bearing and tumour free mice

4.3.1 TCF1 expressing CD8$^+$ and CD4$^+$T cells are increased after CarboTaxol treatment in tumour bearing mice

We next investigated the impact of CarboTaxol on T cells. Indeed, CD8$^+$ T cells are the main effectors seen in the ChAdOx1/MVA vaccine-induced response. Hence, observing their phenotype during priming could give us insight into the mechanism of how CarboTaxol improves vaccine efficacy. The CD4$^+$T cell phenotype was also evaluated as these cells have major importance in providing help and survival signals during CD8$^+$ T cell activation. Indeed, activated CD4$^+$T cells have been shown to promote DC activation, which ultimately can promote CD8$^+$ T cell priming. DBA/2 mice were implanted with 15V4T3, vaccinated with ChAdOx1-Ii-P1A and treated with CarboTaxol 14 days post tumour-implantation (fig 4.12 A). Four days post treatment, blood, spleen, TME were harvested, and T cell phenotype was analysed by flow cytometry.

After chemotherapy, we observed an increase of TCF1+ cells and MFI in CD8$^+$ T cells. The level of expression seem significantly increased in the spleen of CarboTaxol-treated mice compared to untreated as shown in figure 3.1.1 B. Indeed 95% of CD8$^+$ T cells in the spleen and blood were expressing TCF1 after CarboTaxol (fig 4.12 C,D), compared to only 40/50% in the control and vaccine alone groups. In the TME, there was also an increased proportion of CD8$^+$ T cells expressing TCF1, 5-10% in non-treated compared to 25% of CD8$^+$ T cells in chemotherapy-treated groups (fig 4.12 E). The CD8$^+$TCF1$^+$PD1$^-$ cell numbers followed the same trend. Indeed, tumour bearing mice treated with chemotherapy or chemotherapy+vaccine showed major expansion of the CD8$^+$ TCF1$^+$ PD1$^-$ T cells in the spleen, blood and TME. This is promising as CD8$^+$TCF1$^+$PD1- cell have been shown to have a higher proliferation and differentiation potential[242].

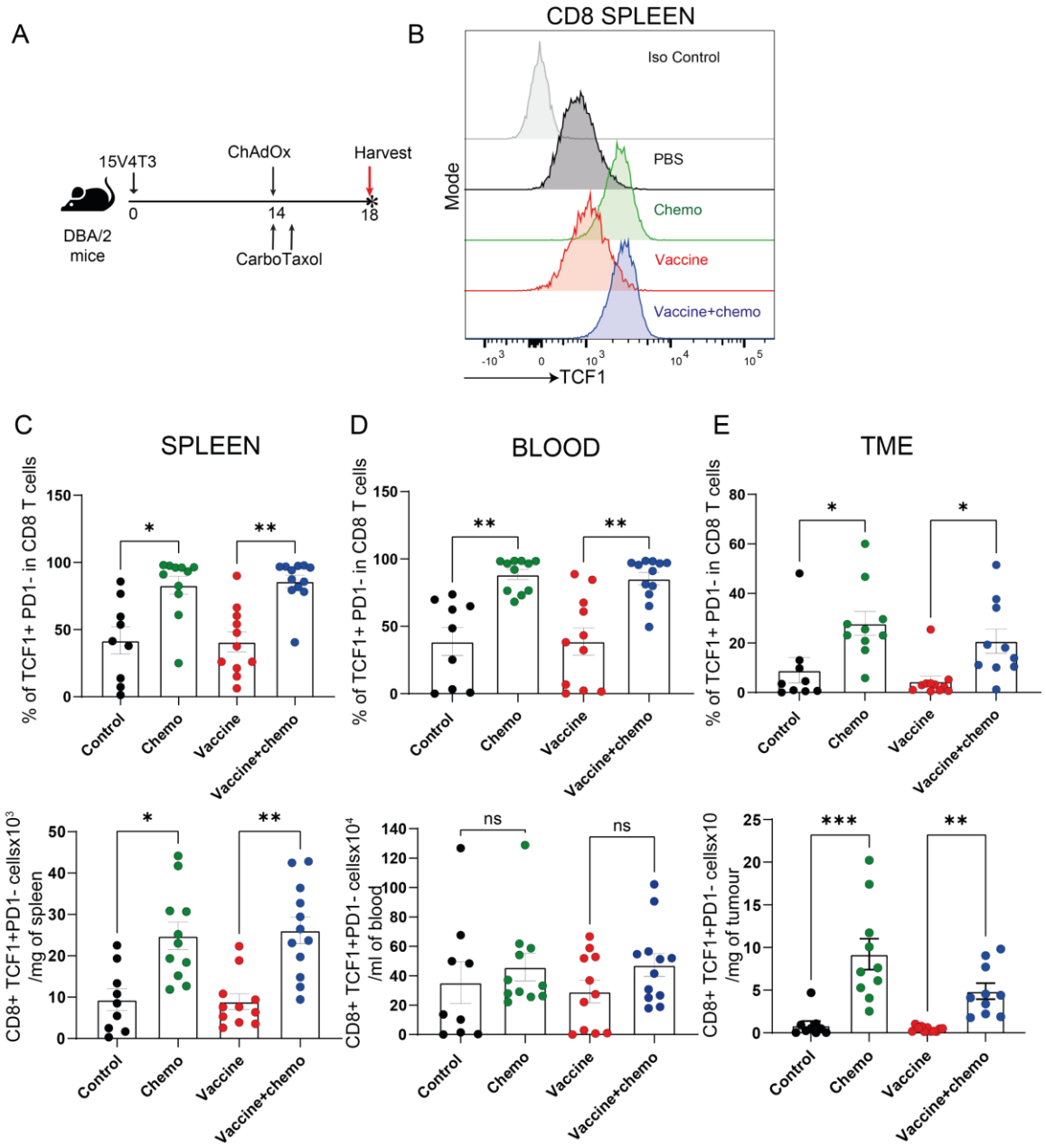


Figure 4.12 CarboTaxol impacts CD8⁺ T cell phenotype in the blood, spleen and TME of 15V4T3 DBA/2 tumour bearing mice. (A) DBA/2 mice were implanted with 1x10^6 15V4T3 cells. 14 days after tumour implantation, mice were vaccinated via i.m with 10^7 IU of ChAdOx1-Ii-P1A or PBS sham and treated with carboplatin(40mg/kg) and paclitaxel (20mg/kg) and 24h later with paclitaxel (20mg/kg) via i.p injections. At day 4 post treatment, spleen, blood and tumours were harvested and CD8⁺ T cell phenotype was investigated by flow cytometry. The level of TCF1 expression in CD8⁺ T cells in the spleen of the different indicated groups is shown in (B). The proportions and numbers of CD8⁺ TCF1⁺ T cells are shown in the spleen (C), blood (D) and TME (E). The data are representative of 3 independent experiments and mean± SEM for each group are shown. Each symbol represents an individual mouse (n=9 to 12 mice per group). Statistically significant differences between groups were determined by a Kruskal-Wallis test with Dunn's multiple comparisons test,*, $p \leq 0.05$, **, $p \leq 0.01$, ***, $p \leq 0.001$.

When looking at the double positive $CD8^+TCF1^+PD1^+$ T cells, which have been defined as pre-exhausted- cells or progenitor exhausted- stem-like cells in the literature[243,244], we also observed an expansion in terms of proportion of $TCF1^+$ $PD1^+$ cells in $CD8^+$ T cells in the spleen, blood and TME after chemotherapy (fig 4.13). Very few $CD8^+$ T cells were double positive for TCF1 and PD1 in the spleen (less than 2%) (fig 4.13 A) and in the blood (less than 1%) (fig 4.13 B). Hence, in terms of cell numbers we only observed a non-significant increase of $TCF1^+$ $PD1^+$ $CD8^+$ T cell in the spleen and blood (fig 4.13 A,B). Interestingly this population was largely present in the TME and significantly increased in terms of proportion and cell numbers (fig 4.13 C). In the TME, the proportion of $TCF1^+$ $PD1^+$ cells in $CD8^+$ T cells was significantly increased from 10 to 25/30% in the chemotherapy-treated group compared to PBS or vaccine groups. This might indicate that the stemness phenotype is improved with chemotherapy systemically which might lead to more $TCF1^+$ $PD1^-$ $CD8^+$ cells, precursor for pre-exhausted stem-like $TCF1^+$ $PD1^+$ $CD8^+$T cells in the TME.

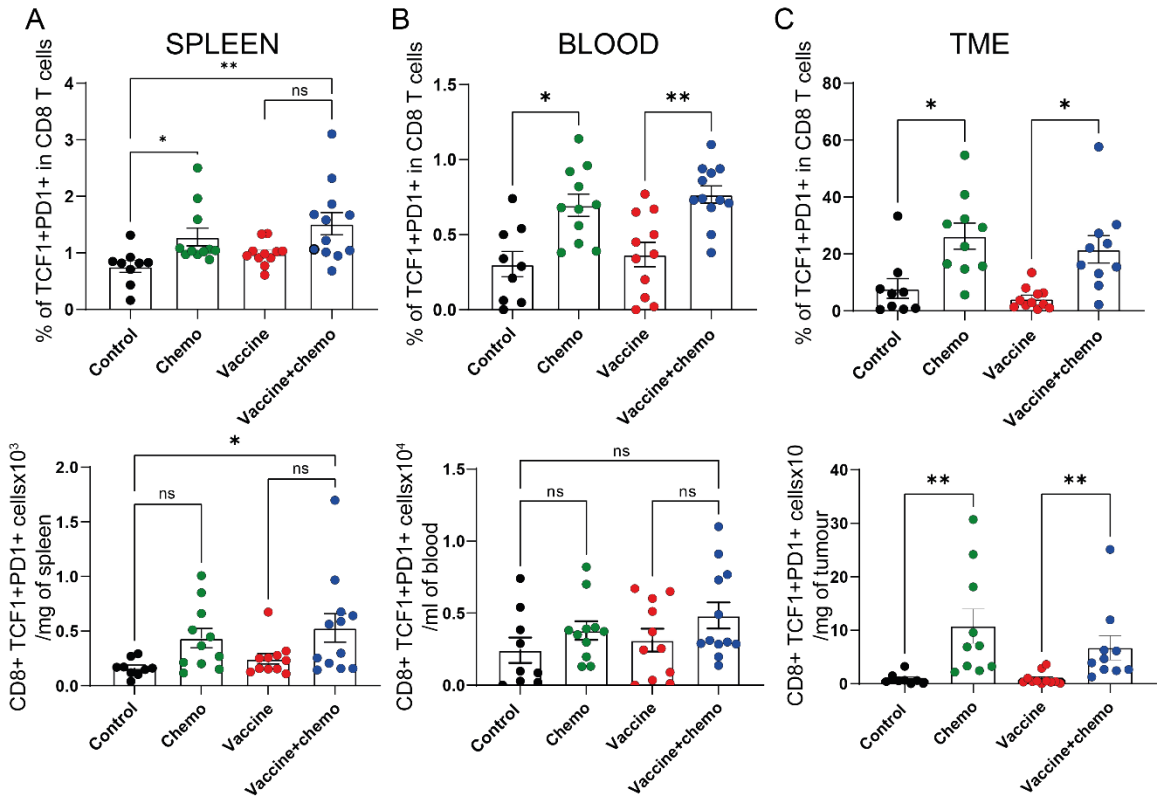


Figure 4.13 CarboTaxol impacts stem-like progenitor-exhausted CD8⁺ T cell phenotype in the TME of 15V4T3 DBA/2 tumour bearing mice. DBA/2 mice were implanted with $1x10^6$ 15V4T3 cells. 14 days after tumour implantation, mice were vaccinated via i.m with 10^7 IU of ChAdOx1-li-P1A or PBS sham and treated with carboplatin(40mg/kg) and paclitaxel (20mg/kg) and 24h later with paclitaxel (20mg/kg) via i.p. At day 4 post treatment, spleen, blood and tumours were harvested and CD8⁺ T cell phenotype was investigated by flow cytometry. The TCF1⁺ as well as PD1⁺ expression in CD8⁺ T cells is shown in term of proportions and numbers in the spleen (A), blood (B) and TME (C). The data are representative of 3 independent experiments and mean ± SEM for each group are shown. Each symbol represents an individual mouse (n=9 to 12 mice per group). Statistically significant differences between groups were determined by a Kruskal-Wallis test with Dunn's multiple comparisons test,*, $p \leq 0.05$, **, $p \leq 0.01$.

At the same time point, we assessed the $TCF1^+$ levels in $CD4^+$T cells and observed a similar tendancy than in $CD8^+$ T cells, although the magnitude of differences between chemotherapy and non-chemo treated group were less than for the $CD8^+$ T cells. The role of TCF1 expression in $CD4^+$T cells in the context of cancer has not been investigated. However, evidence has shown that TCF1 can promote the differentiation of Tfh, Th2 and stem-like Th17 cell with the potential to further differentiate into Th1 cells in infectious and autoimmune models[245,246]. The proportion of $TCF1^+PD1^-$ cells in systemic $CD4^+$T cells was increased after CarboTaxol (fig 4.14 B,C). In the spleen, the increased in TCF1 expressing cells in $CD4^+$T cells was clear between chemotherapy-treated and non-treated groups (fig 4.14 A) and this difference was also observed in terms of cell number (fig 4.14 B). Interestingly, we observed the same trend in the TME, with significantly higher level of TCF1 in $CD4^+$T cells as well as increased number of $CD4^+TCF1^+PD1^-$ T cells after CarboTaxol (fig 4.14 D). As shown in figure 4.15, the $CD4^+$T cells expressing both TCF1 and PD1 were also increased in terms of proportion and cell numbers in the TME (fig 4.15 C). However, we did not observe a significant expansion of the $TCF1^+$ $PD1^+$ $CD4^+$population in the blood (fig 4.15 A) and spleen (fig 4.15 B). Of note, $TCF1^+PD1^+$ $CD4^+$T cell population was almost non-existent in the system, representing less than 5% of the total $CD4^+$T cells. This data could indicate that the expansion of $TCF1^+PD1^+$ $CD8^+$ and $CD4^+$T cells in the TME might be due to the expansion of $TCF1^+$ $PD1^-$ $CD8^+$ and $CD4^+$T cells in the system, spleen and blood. The $TCF1^+PD1^-$ cells will migrate to the TME where they could become pre-exhausted stem-like cells, double positive for TCF1 and PD1.

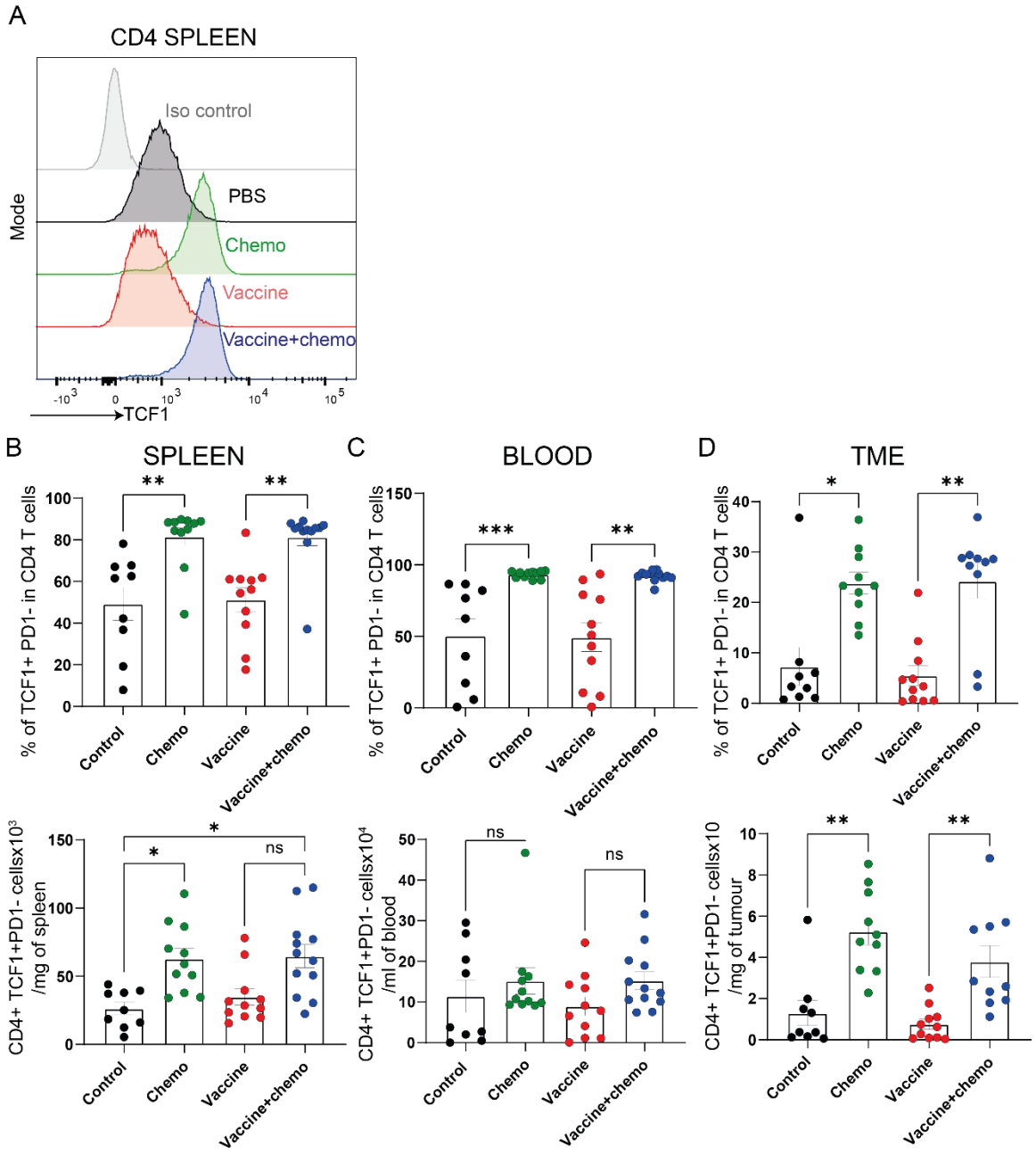


Figure 4.14 CarboTaxol impacts CD4⁺ T cell phenotype in the blood, spleen and TME of 15V4T3 DBA/2 tumour bearing mice. DBA/2 mice were implanted with 1x10^6 15V4T3 cells. 14 days after tumour implantation, mice were vaccinated via i.m with 10^7 IU of ChAdOx1-Ii-P1A or PBS sham and treated with carboplatin(40mg/kg) and paclitaxel (20mg/kg) and 24h later with paclitaxel (20mg/kg) via i.p. At day 4 post treatment, spleen, blood and tumours were harvested and CD4⁺ T cell phenotype was investigated by flow cytometry. The level of TCF1 expression in CD4⁺ T cells in the spleen of the different indicated groups is shown in (A). The proportions and numbers of CD4⁺ TCF1⁺ T cells are shown in the spleen (B), blood (C) and TME (D). The data are representative of 3 independent experiments and mean ± SEM for each group are shown. Each symbol represents an individual mouse (n=9 to 12 mice per group). Statistically significant differences between groups were determined by a Kruskal-Wallis test with Dunn's multiple comparisons test,*, p ≤ 0.05, **, p ≤ 0.01.

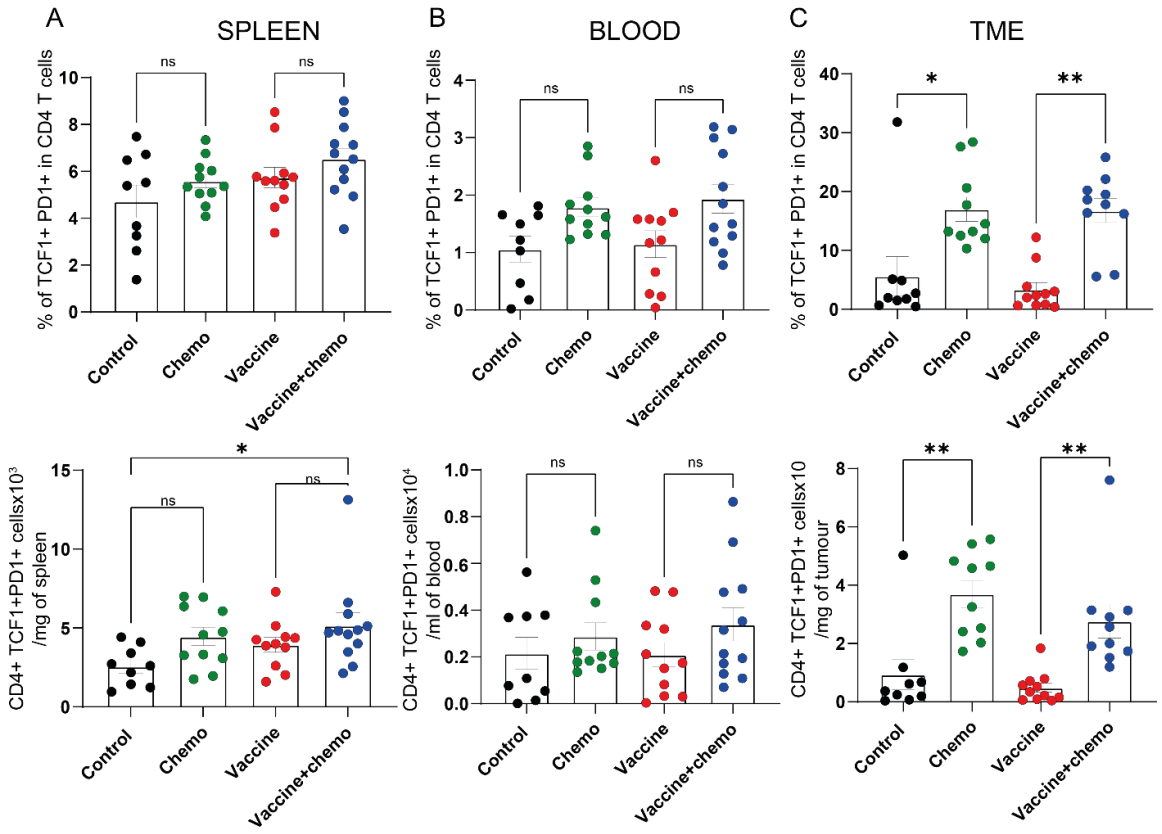


Figure 4.15 CarboTaxol impacts TCF1⁺PD1⁺CD4⁺ T cell phenotype in the TME of 15V4T3 DBA/2 tumour bearing mice. DBA/2 mice were implanted with 1x10^6 15V4T3 cells. 14 days after tumour implantation, mice were vaccinated via i.m with 10^7 IU of ChAdOx1-li-P1A or PBS sham and treated with carboplatin(40mg/kg) and paclitaxel (20mg/kg) and 24h later with paclitaxel (20mg/kg) via i.p. At Day 4 post treatment, spleen, blood and Tumours were harvested and CD4⁺ T cell phenotype was investigated by flow cytometry. The TCF1⁺ as well as PD1⁺ expression in CD4⁺ T cells is shown in term of proportions and numbers in the spleen (A), blood (B) and TME (C). The data are representative of 3 independent experiments and mean± SEM for each group are shown. Each symbol represents an individual mouse (n=9 to 12 mice per group). Statistically significant differences between groups were determined by a Kruskal-Wallis test with Dunn's multiple comparisons test,*, $p \leq 0.05$, **, $p \leq 0.01$.

TCF1 has been shown to promote MPEC T cells [238] [247]. Hence, after observing this increased $TCF1^+$ expression in T cells after chemotherapy, we were interested to explore whether $CD8^+$ and $CD4^+$T cells were of a central memory or effector memory phenotype. $CD4^+$ and $CD8^+$ T cells were assessed for expression of CD44 and CD62L. As shown in figure 4.16 A, central memory cells were defined as $CD44^+CD62L^+$ while effector memory cells were defined as $CD44^+$ $CD62L^-$. We did not observed an increase in central memory $CD4^+$and $CD8^+$ T cells in the spleen (fig 4.16 B,F) nor the blood. In the TME, we observed a trend toward increased central memory $CD8^+$ T cells where the significance was reached only in the control vs chemotherapy alone group (fig 4.16 D,H). A slight increase in effector memory $CD8^+$ and $CD4^+$T cells (fig 4.16 E,I) was observed after chemotherapy treatment. However, the differences observed were not significant between the controls and chemotherapy-treated groups.

Altogether, this phenotypic analysis performed here by flow cytometry highlights an effect of CarboTaxol on the expansion in $TCF1^+$ $CD8^+$ and $CD4^+$T cells, with higher numbers of lymphocytes expressing TCF1 in the spleen, blood and TME were observed. However, only a corresponding mild effect on central memory and effector memory cells in tumour bearing mice was observed.

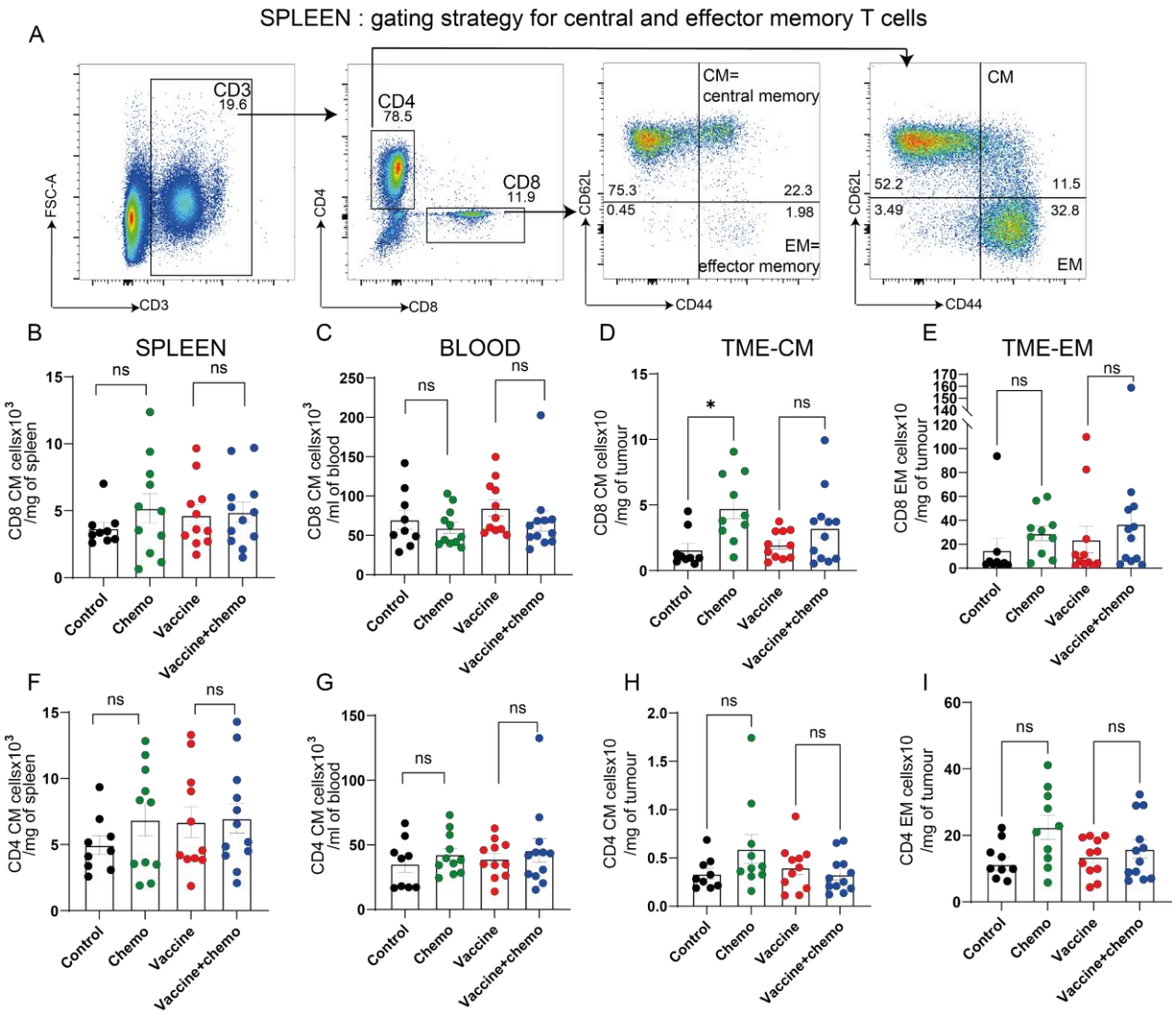


Figure 4.16 CarboTaxol impact on central memory and effector memory CD8⁺ an CD4⁺ T cells of 15V4T3 DBA/2 tumour bearing mice. DBA/2 mice were implanted with 1x10^6 15V4T3 cells. 14 days after tumour implantation, mice were vaccinated via i.m with 10^7 IU of ChAdOx1-Ii-P1A or PBS sham and treated with carboplatin(40mg/kg) and paclitaxel (20mg/kg) and 24h later with paclitaxel (20mg/kg) via i.p. At day 4 post treatment, spleen, blood and tumours were harvested and CD44 and CD62L expression were assessed in CD8⁺ and CD4⁺ T cell by flow cytometry. The gating strategy defining central memory cells (CD44⁺, CD62L⁺: CM) and effector memory cells (CD44⁺, CD62L-: EM) in T cells is shown in (A). The numbers of CM CD8⁺ T cells are shown in the spleen (B), blood (C) and TME (D).The numbers of EM CD8⁺ T cells in the TME are shown in (E). The numbers of CM CD4⁺ T cells are shown in the spleen (F), blood (G) and TME (H). The number of EM CD4⁺ T cells in the TME are shown in (I). The data are representative of 3 independent experiments and mean ± SEM for each group are shown. Each symbol represents an individual mouse (n=9 to 12 mice per group). Statistically significant differences between groups were determined by a Kruskal-Wallis test with Dunn's multiple comparisons test.

4.3.2 CaboTaxol-treated tumour free mice show an expansion of $CD8^+$ and $CD4^+TCF1^+$ cells

The observed effects of CarboTaxol on TCF1 expression in tumour bearing mice raise the question as to whether this expansion of $TCF1^+$ T cells was a direct effect of the chemotherapy on T cells or if it was an indirect effect, through the cytotoxic effect of the chemotherapy on tumour cells. Indeed, chemotherapy has previously been shown to induce ICD which results in a better priming of T cells. To unravel tumour-independent effects, we tested our vaccination and chemotherapy combination in tumour free mice. DBA/2 mice were vaccinated with ChAdOx1-P1A and treated with the same dose of CarboTaxol used in tumour bearing mice. At day 4 post treatment, the blood, spleen and BM were harvested and stained for TCF1 expression (fig 4.17 A,B). Very interestingly, $TCF1^+$ $CD8^+$ T cells were expanded after chemotherapy in tumour free mice, to the same extent as in tumour bearing mice. Indeed, we observed more than 90% of $CD8^+$ T cells being $TCF1^+$ after chemotherapy in the blood (fig 4.17 E) and spleen (fig 4.17 B,C). In both organs the cell number of $TCF1^+$ $PD1^-$ $CD8^+$ T cells were significantly higher than the control groups. Very interestingly, we also observed an expansion of $TCF1^+$ $PD1^-$ $CD8^+$ T cells in the bone marrow after chemotherapy, significantly higher than the PBS control group or the vaccine group (fig 4.17 D). In the BM, almost 20% of $CD8^+$ T cells were $TCF1^+$ after chemotherapy which represents more than double the proportion of $TCF1^+CD8^+$ T cells in the control or vaccine only group.

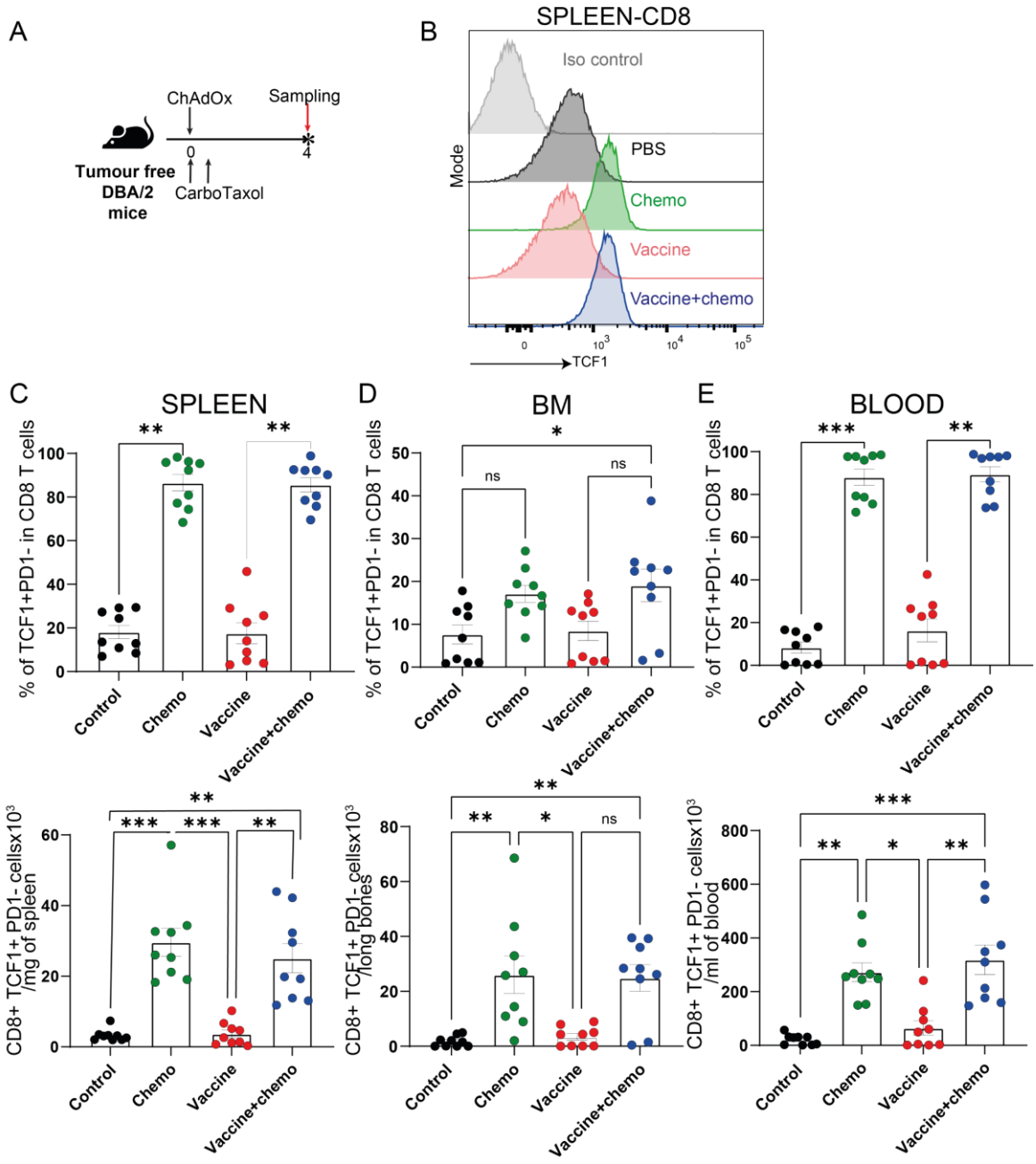


Figure 4.17 CarboTaxol impacts CD8⁺ T cell phenotype in the blood, spleen and TME of tumour free DBA/2 mice. (A) DBA,2 mice were vaccinated via i.m with 10^7 IU of ChAdOx1-li-P1A or PBS sham and treated with carboplatin(40mg/kg) and paclitaxel (20mg/kg) and 24h later with paclitaxel (20mg/kg) via i.p. At Day 4 post treatment, spleen, blood and BM were harvested and CD8⁺ T cell phenotype was investigated by flow cytometry. The TCF1 level of expression in CD8⁺ T cells in the spleen of the different indicated groups is shown in (B). The proportions and numbers of CD8⁺ TCF1⁺ T cells are shown in the spleen (C), BM (D) and blood (E). The data are pooled from 2 independent experiments and mean± SEM for each group are shown. Each symbol represents an individual mouse (n=9 mice per group). Statistically significant differences between groups were determined by a Kruskal-Wallis test with Dunn's multiple comparisons test,*, $p \leq 0.05$, **, $p \leq 0.01$, ***, $p \leq 0.001$
.

Moreover, the same trend was observed in CD4⁺T cells in spleen (fig 4.18 A,B) and blood (fig 4.18 E), where both proportions and numbers of TCF1⁺ CD4⁺T cells were

increased in the chemotherapy treated groups. In the BM there was a significant increase in terms of cell numbers after CarboTaxol, and only a slight increase in TCF1^{+} CD4^{+}T cells after CarboTaxol+vaccine combination which did not reach significance (fig 4.18 C).

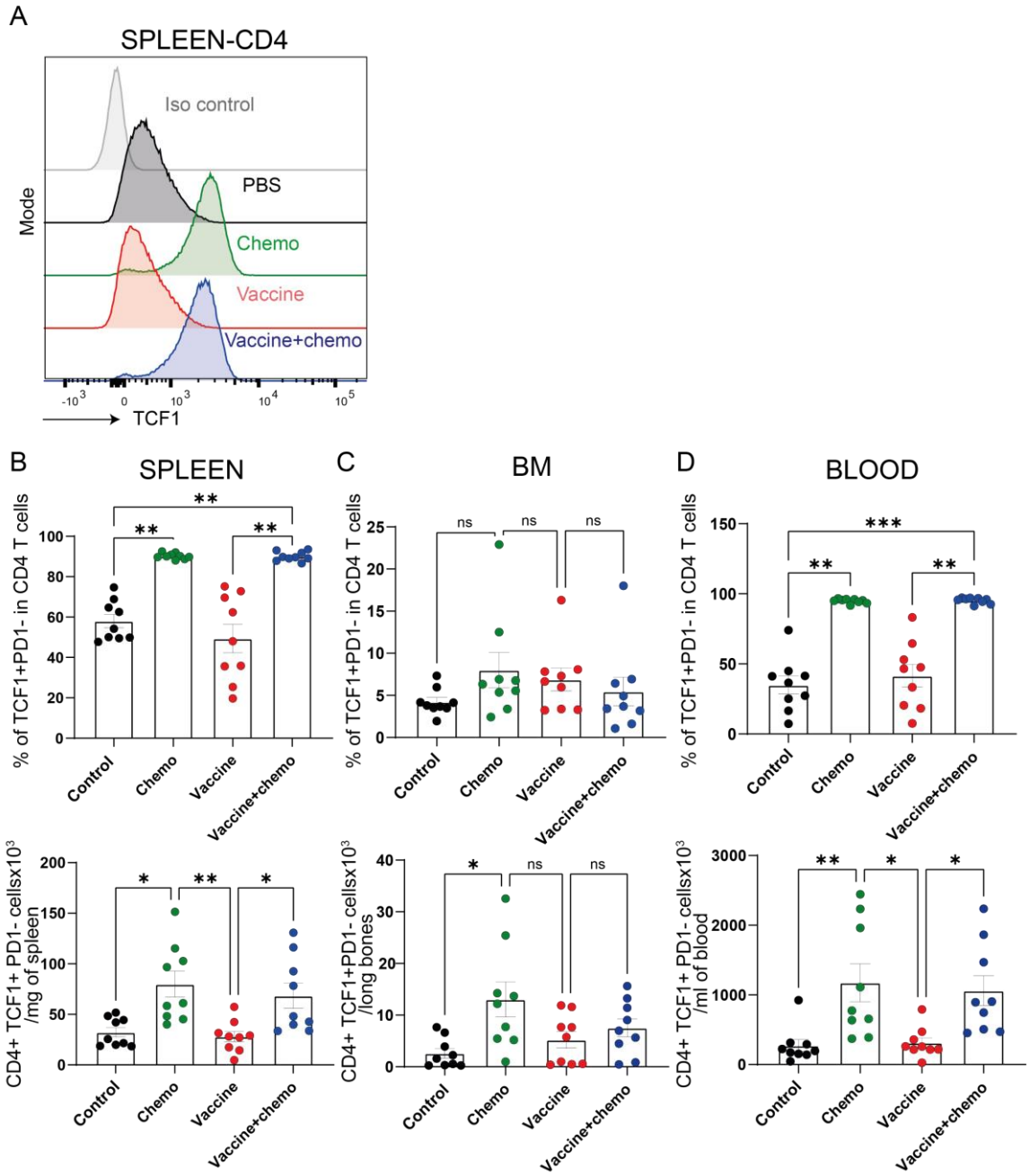


Figure 4.18 CarboTaxol impacts CD4^{+} T cell phenotype in the blood, spleen and TME of tumour free DBA/2 mice. DBA,2 mice were vaccinated via i.m with 10^{7} IU of ChAdOx1-li-P1A or PBS sham and treated with carboplatin (40mg/kg) and paclitaxel (20mg/kg) and 24h later with paclitaxel (20mg/kg) via i.p. At day 4 post treatment, spleen, blood and BM were harvested and CD4^{+} T cell phenotype was investigated by flow cytometry. The TCF1 expression level in CD4^{+} T cells in the spleen of the different indicated groups is shown in (A). The proportions and numbers of CD4^{+} TCF1^{+} T cells are shown in the spleen (B), BM (C) and blood (D). The data are pooled from 2 independent experiments and mean ± SEM for each group are shown. Each symbol represents an individual mouse (n=9 mice per group). Statistically significant differences between groups were determined by a Kruskal-Wallis test with Dunn's multiple comparisons test,*, $p \leq 0.05$, **, $p \leq 0.01$, ***, $p \leq 0.001$.

We also investigated the memory phenotype of $CD4^+$and $CD8^+$ T cells 4 days post-treatment in tumour free mice, just like in tumour bearing mice. Using the same flow cytometry strategy, we assessed CD44 and CD62L expression (fig 4.19 A). Very interestingly, central memory $CD4^+$and $CD8^+$ T cells were significantly increased after chemotherapy compared to vaccine only or control groups. This phenotype was significant in the BM (fig 4.19 C), and the spleen for the control vs chemotherapy alone groups (fig 4.19 B). These data confirmed tumour-independent effects of CarboTaxol on TCF1 and memory phenotype in $CD8^+$ and $CD4^+$T cells.

We can conclude that chemotherapy has a tumour-independent impact on $CD8^+$ and $CD4^+$T cells. Indeed, $CD8^+$ and $CD4^+$T cells expressing TCF1 are surprisingly expanded

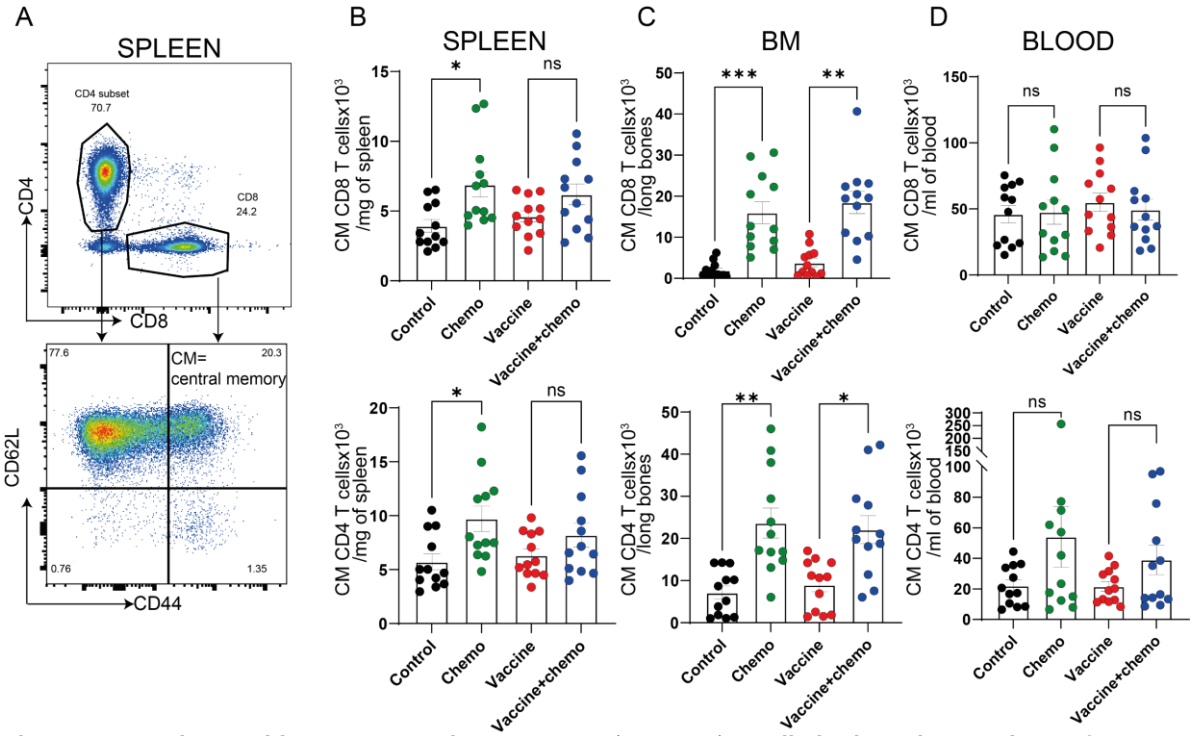


Figure 4.19 CarboTaxol impacts central memory $CD8^+$ an $CD4^+$ T cells in the spleen and BM of tumour free DBA/2 mice. DBA,2 mice were vaccinated via i.m with 10^7 IU of ChAdOx1-Ii-P1A or PBS sham and treated with carboplatin (40mg/kg) and paclitaxel (20mg/kg) and 24h later with paclitaxel (20mg/kg) via i.p. At day 4 post treatment, spleen, blood and BM were harvested and CD44 and CD62L expression were assessed in $CD8^+$ and $CD4^+$ T cell by flow cytometry. The gating strategy defining central memory cells ($CD44^+$, $CD62L^+$: CM)) in T cells is shown in (A). The numbers of CM $CD8^+$ and $CD4^+$ T cells are shown in the spleen (B), blood (C) and TME (D). The data are representative of 3 independent experiments and mean ± SEM for each group are shown. Each symbol represents an individual mouse (n=12 mice per group). Statistically significant differences between groups were determined by a Kruskal-Wallis test with Dunn's multiple comparisons test,*, $p \leq 0.05$, **, $p \leq 0.01$, ***, $p \leq 0.001$.

after chemotherapy in tumour free mice as well as in tumour bearing mice. In tumour free mice, this seems to correlate with an expansion of central memory $CD8^+$ and $CD4^+$T cells.

4.4 Potential link between TCF1 expression in $CD8^+$ T cells and $CD11b^+Ly6G^+$ cell depletion after CarboTaxol treatment

4.4.1 A strong correlation exists between TCF1 expression in $CD8^+$ T cells and $CD11b^+Ly6G^+$ cell depletion

In parallel with the increase of $TCF1^+$ cells in tumour free mice, we investigated the myeloid cell subsets. We were interested to investigate $CD11b^+Ly6G^+$ cells, which would mostly be neutrophils in tumour free mice. At day 4 post treatment (fig 4.20 A), we observed a depletion of these $CD11b^+$ $Ly6G^+$ cells in the spleen, blood and BM (fig 4.20 B). This was significant compared to the control groups in all the tissues tested. However, functional assays assessing the effect of $Ly6G^+$ cells from tumour free mice on T cells will have to be performed to differentiate them from PMN-MDSCs.

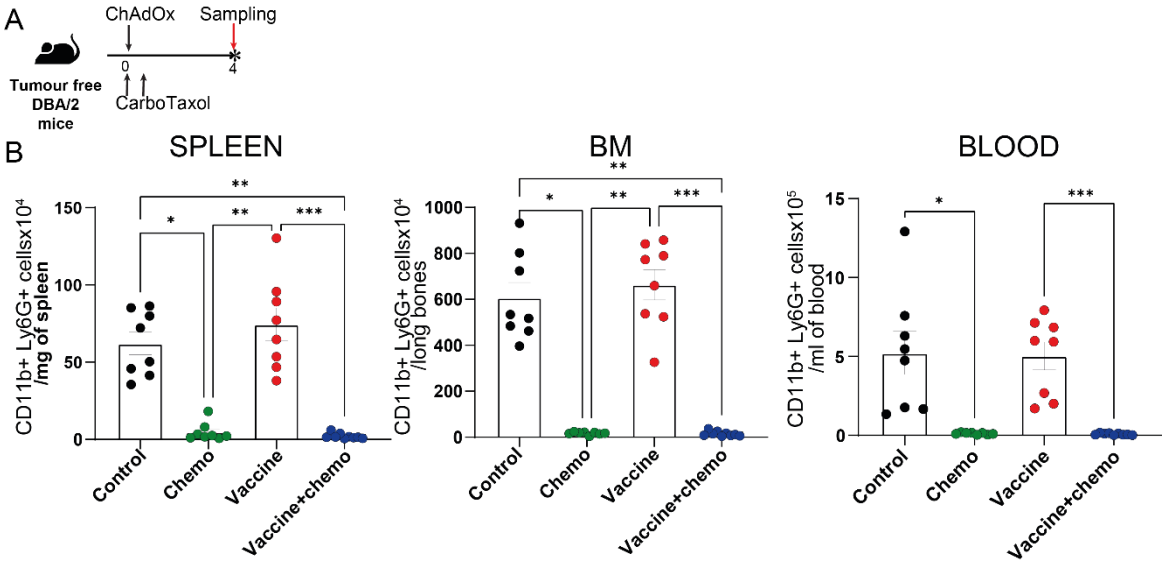


Figure 4.20 Myeloid cells in spleen, BM, and blood after CarboTaxol treatment of tumour free DBA/2 mice. DBA,2 mice were vaccinated via i.m with 10^7 IU of ChAdOx1-li-P1A or PBS sham and treated with carboplatin(40mg/kg) and paclitaxel (20mg/kg) and 24h later with paclitaxel (20mg/kg) via i.p. At day 4 post treatment, spleen BM and blood were harvested and stained with CD11b, Ly6G markers to assess potential neutrophil population. The same gating strategy for the $Ly6G^+$ population than for tumour bearing was used for these experiments. Numbers of $CD11b^+$ $Ly6G^+$, potential neutrophils, cells are shown in the spleen (A), BM (B) and blood (C). Data are representative of 2 independent experiments and mean ± SEM for each group are shown. Each symbol represents an individual mouse (n= 8 mice per group). Statistically significant differences between groups were determined by a Kruskal-Wallis test with Dunn's multiple comparisons test,*, $p \leq 0.05$, **, $p \leq 0.01$, ***, $p \leq 0.001$.

CarboTaxol promote an increase in TCF1 expressing $CD8^+$ and $CD4^+$T cells which occurs at the same point of $Ly6G^+$ cells depletion in both tumour free and tumour bearing mice. Hence, we were interested in evaluating the correlation between these two populations. Splenocytes, PBMCs, BM cells and TME cells were evaluated by flow cytometry on day 4 post-chemotherapy (fig 4.21 A). In tumour bearing mice, we observed a strong negative correlation in the blood and the TME between the proportion of $CD11b^+$ $Ly6G^+$ and $TCF1^+$ $PD1^-$ cells in $CD8^+$T cells with a spearman coefficient of respectively r=-0.62 and r=-0.67 (fig 4.21 B,D) - the lower the proportion of $CD11b^+Ly6G^+$ cells, the higher the proportion of $CD8^+$ T cells expressing TCF1+. Interestingly, while this correlation was linear in the blood, we observed a threshold of 1% of $CD11b^+Ly6G^+$ cells below which the TCF1 expressing cells in $CD8^+$ T cells were expanded in the majority of the mice, in the TME (fig 4.21 B). In the TME, we consistently observed the same correlation between the proportion of double positive $TCF1^+$ $PD1^+$ cells in $CD8^+$ T cells and the proportion of $CD11b^+Ly6G^+$ cells (fig 4.21 C). In the spleen of tumour bearing mice, the correlation was more variable. But regardless of this variability, the negative correlation between the proportion of $CD11b^+Ly6G^+$ cells and $TCF1^+$ expression in $CD8^+$ T cells in the spleen was significant (fig 4.21 E). This data might indicate that the depletion of $CD11b^+Ly6G^+$ cells in blood, TME, BM and spleen could be linked to TCF1 expression in $CD8^+$ T cells in tumour bearing mice.

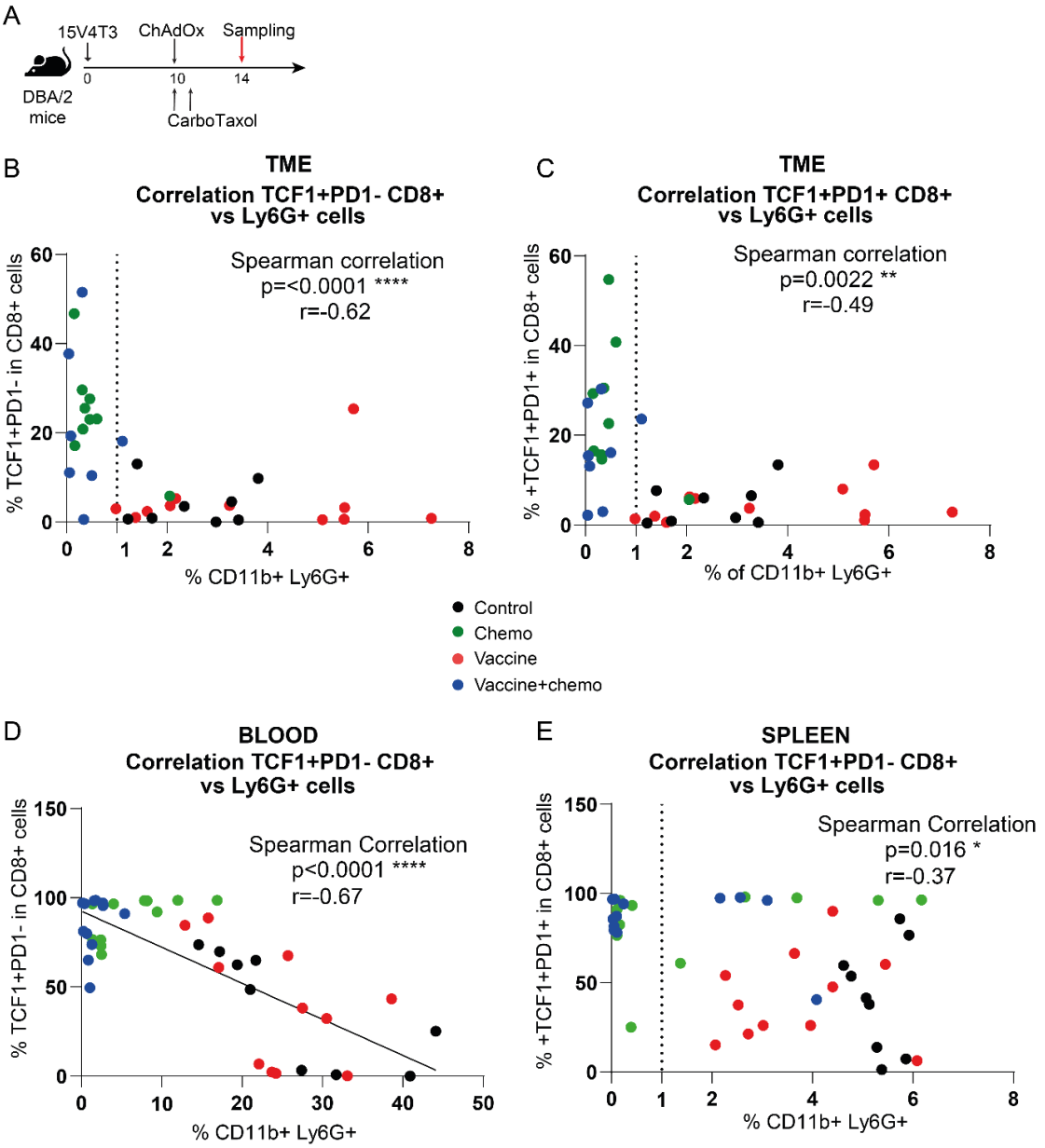


Figure 4.21 Correlation between CD11b+Ly6G+ cells proportion and TCF1 expression in CD8⁺ T cells in 15V4T3 tumour model. (A) DBA/2 mice were implanted with $1x10^6$ 15V4T3 cells. 10 days after tumour implantation, mice were vaccinated via i.m with 10^7 IU of ChAdOx1-Ii-P1A or PBS sham and treated with carboplatin(40mg/kg) and paclitaxel (20mg/kg) and 24h later with paclitaxel (20mg/kg) via i.p. At Day 4 post treatment, spleen, tumour and blood were harvested and stained to assess the proportion of CD11b+ Ly6G+ cells as well as the TCF1 expression in CD8⁺ T cells. The correlation between these 2 variables is shown in the TME (B), the blood (D) and the spleen (E). In the TME, the correlation between the proportion of CD11b+Ly6G+ cells and the double expression of TCF1 and PD1 in CD8⁺ T cells is shown in (C). Dash lines represent a potential threshold of level of CD11b+Ly6G+, below which TCF1 expression in CD8⁺ T cell is induced. Data are representative of 3 independent experiments and mean for each group are shown. Each symbol represents an individual mouse (n= 8 to 12 mice per group). Significance was determined by a Spearman Rank correlation test,*, $p \leq 0.05$, **, $p \leq 0.01$, ***, $p \leq 0.001$, ****, $p \leq 0.0001$.

In tumour free mice, we observed the same negative correlation in the spleen, blood, and BM at day 4 post treatment (fig 4.22 A). Interestingly, we noticed a similar threshold as in tumour bearing mice, below which the TCF1 expressing cells in $CD8^+$ T cells were dramatically increased (fig 4.22 A). For the spleen, this threshold was very noticeable, with below 1% of $CD11b^+Ly6G^+$ cells, 100% of the mice had more than 70% $TCF1^+$ expressing $CD8^+$ T cells (fig 4.22 B). For the blood, we noticed that mice having less than 10% of $CD11b^+Ly6G^+$ cells, displayed TCF1 expression in more than 70% of the $CD8^+$ T cells (fig

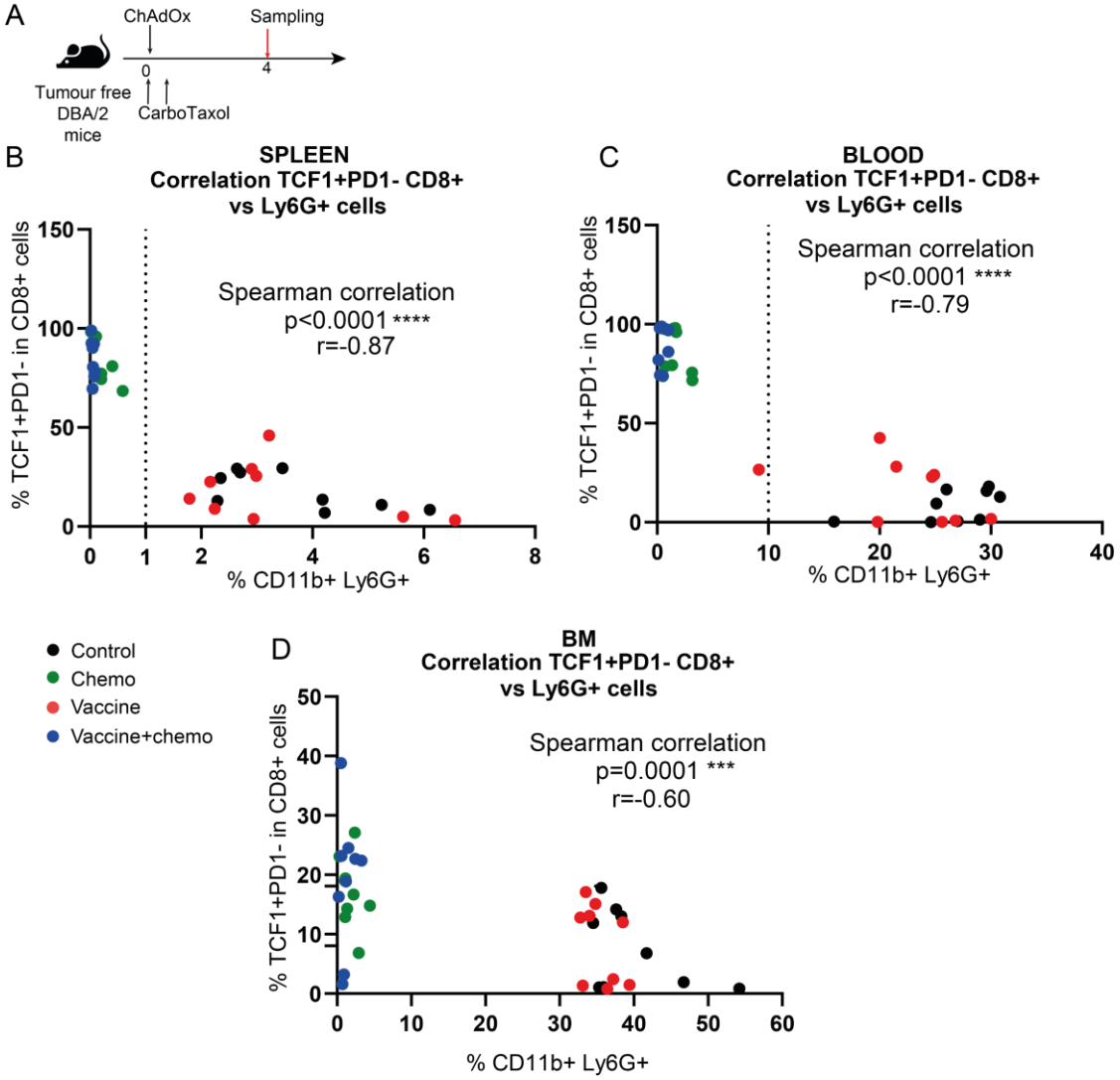


Figure 4.22 Correlation between CD11b+Ly6G+ cells proportion and TCF1 expression in $CD8^+$T cells in tumour free DBA/2 mice. (A) DBA/2 mice were vaccinated via i.m with 10^7 IU of ChAdOx1-Ii-P1A or PBS sham and treated with carboplatin(40mg/kg) and paclitaxel (20mg/kg) and 24h later with paclitaxel (20mg/kg) via i.p. At Day 4 post treatment, spleen, BM and blood were harvested and stained to assess the proportion of CD11b+ Ly6G+ cells as well as the TCF1 expression in $CD8^+$ T cells. The correlation between these 2 variables is shown in the spleen (B), the blood (C) and the BM (D). Dash lines in blood and spleen represent a potential threshold of level of CD11b+Ly6G+, below which TCF1 expression in $CD8^+$ T cell is induced. Data are representative of 3 independent experiments and mean for each group are shown. Each symbol represents an individual mouse (n= 9 mice per group). Significance was determined by a Spearman Rank correlation test,*, $p \leq 0.05$, **, $p \leq 0.01$, ***, $p \leq 0.001$, ****, $p \leq 0.0001$.

4.22 C). In the BM, we could not define a threshold, but the negative correlation was significant between $CD11b^{+}Ly6G^{+}$ cells and $CD8^{+}TCF1^{+}$ cells (fig 4.22 D).

We concluded that the depletion of $CD11b^{+}Ly6G^{+}$ alone could not explain the synergistic effect on vaccine immunogenicity. Could TCF1 expression in T cells be the mechanism through which CarboTaxol improve vaccine immunogenicity? Given the significant correlation between $TCF1^{+}$ cell expansion in $CD8^{+}$ cells and $CD11b^{+}Ly6G^{+}$ cells, is $CD11b^{+}Ly6G^{+}$ cell depletion linked with TCF1 expression?

4.4.2 Anti-GR1 antibody does not induce TCF1.

As previously demonstrated, anti-GR1 antibody did not recapitulate the chemotherapy effect in improving vaccine immunogenicity nor tumour growth control. Anti-GR1 was efficient in depleting the $CD11b^{+}Ly6G^{+}$ cells in the TME and blood, and with one administration, in the spleen too. Therefore, we concluded that in our model the PMN-MDSCs depletion at day 4 post-treatment might not be the main mechanism involved in improving vaccine efficacy.

We demonstrated that the $CD11b^{+}Ly6G^{+}$ depletion was correlated with the increase of $TCF1^{+}$ cells in $CD8^{+}$ T cells after chemotherapy. To verify the potential link between these 2 populations we then investigated whether anti-GR1 displays similar impacts on TCF1 expression. Furthermore, this would exclude TCF1 expression as a potential mechanism for the increase immunogenicity observed in tumour bearing mice after vaccine+chemotherapy.

Blood, spleen and TME of mice treated with 5 injections of anti-GR1 antibody, were analysed for TCF1 expression at day 4 post prime (see the scheme on fig 4.9 C). No significant expansion in terms of number of $TCF1^{+}$ $PD1^{-}$ $CD8^{+}$ T cells were observed after anti-GR1 treatment in the blood (fig 4.23 A) and spleen (fig 4.23 C), and similar results were observed in the TME (fig 4.23 E). No expansion of the numbers of $TCF1^{+}$ $PD1^{+}$ $CD8^{+}$ T cells were observed after anti-GR1 in blood (fig 4.23 B), spleen (fig 4.23 D) and TME (fig 4.23 F). Surprisingly, we did observe a slight increase in the proportion of $CD8^{+}$ T cells expressing TCF1 in the blood after chemotherapy (fig 4.23 A,B), but this was variable and not significantly higher in the chemo only group. Therefore, we concluded that increase of TCF1 expression in $CD8^{+}$ T cells is not directly linked to the absence of $CD11b^{+}Ly6G^{+}$ cell after anti-GR1 antibody treatment.

However, the mechanism through which anti-GR1 and CarboTaxol are depleting $CD11b^+Ly6G^+$ cells are different[248,249]. Therefore, the absence of $CD11b^+Ly6G^+$ cells might not trigger $TCF1^+$ induction in $CD8^+$ T cells. But we cannot exclude that it is rather the process of cell death mediating $CD11b^+Ly6G^+$ depletion by chemotherapy that induces TCF1. Indeed, anti-GR1-mediated $CD11b^+$Ly6G depletion could occur through a different cell death process, and different types of cell death and their resolution can induce different signals, more or less inflammatory[248,250,251]. Moreover, the increase in TCF1 expressing cells could explain why chemotherapy, but not anti-GR1, triggers a better priming of the vaccine which results in a higher immunogenicity and a better tumour control. As TCF1+ cells were also expanded in tumour free mice treated with CarboTaxol, could this chemotherapy improve vaccine immunogenicity in tumour free mice?

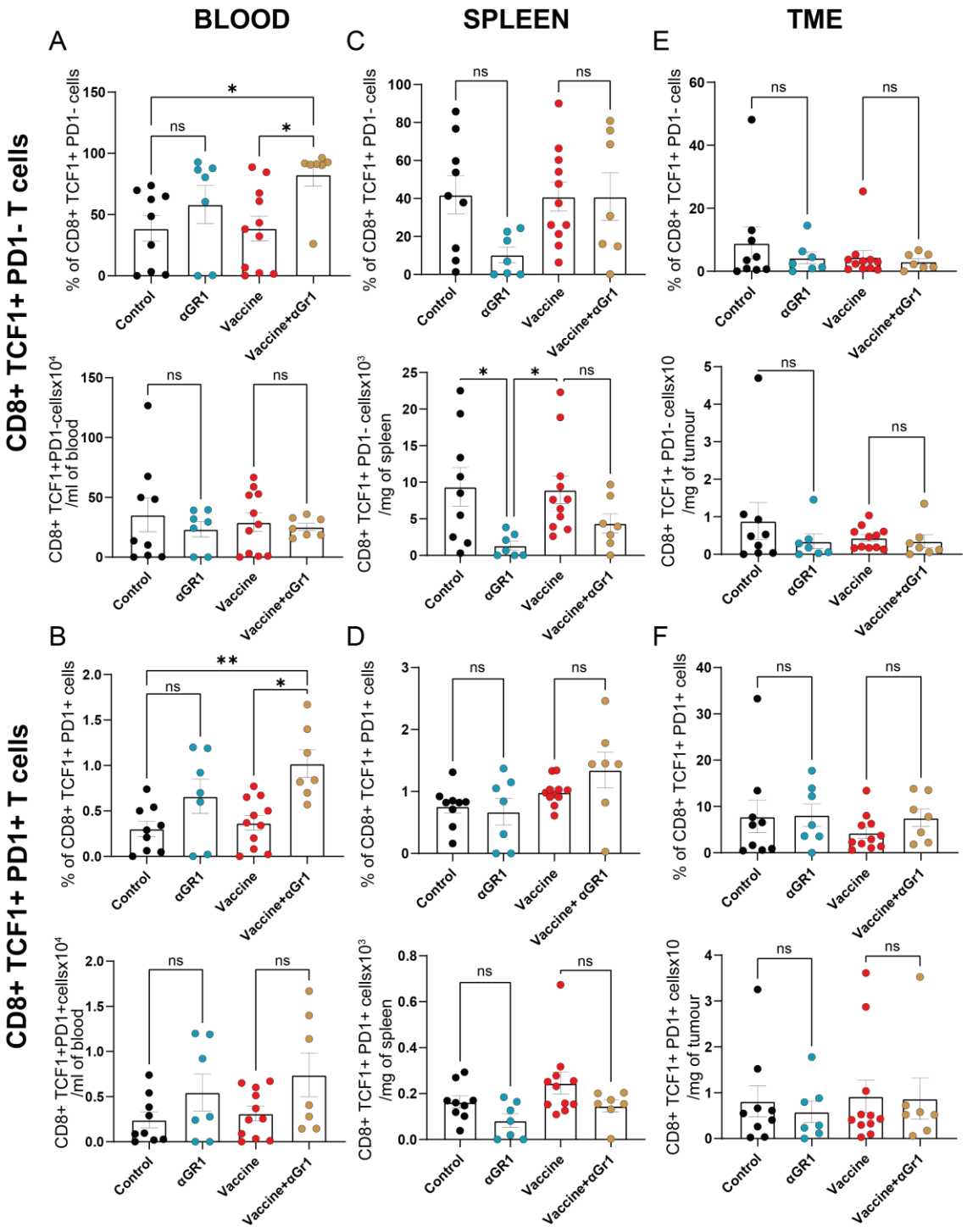


Figure 4.23 Anti-GR1 does not significantly expand TCF1⁺ CD8⁺ T cells in the spleen, blood and TME of 15V4T3 DBA/2 tumour bearing mice. DBA,2 mice were implanted with 1x10^6 15V4T3 cells. 10 days after tumour implantation, mice were vaccinated via i.m with 10^7 IU of ChAdOx1-Ii-P1A or PBS sham. Mice were treated with anti-GR1 antibody injected i.p from day 3, then twice a week (200µg) (see fig 3.10 C for scheme). At day 4 post prime, spleen, blood and tumours were harvested and the TCF1 expression was assessed in CD8⁺ cell by flow cytometry. The numbers and proportions of TCF1⁺PD1- CD8⁺ T cells are shown in the blood (A), spleen (C) and TME (E). The numbers and proportions of TCF1⁺PD1+ CD8⁺ T cells are shown in the blood (B), spleen (D) and TME (F). The data are pooled from 2 independent experiments and mean for each group are shown. Each symbol represents an individual mouse (n=7 to 11 mice per group). Statistically significant differences between groups were determined by a Kruskal-Wallis test with Dunn's multiple comparisons test ,*, p ≤ 0.05, **, p ≤ 0.01,

4.5 CarboTaxol acts as an adjuvant for ChAdOx1/MVA vaccine platform: importance of the timing of treatments

4.5.1 CarboTaxol improves vaccine immunogenicity in tumour free mice

We observed that CarboTaxol induces the expansion of TCF1$^+$ CD8$^+$ and CD4$^+$T cells in tumour free mice, similar to tumour bearing mice. Therefore, we investigated whether CarboTaxol could improve vaccine immunogenicity in tumour free mice too. DBA/2 mice were vaccinated with ChAdOx1/ MVA-P1A, 4 weeks apart at a higher dose than in tumour bearing mice (10^8 IU for ChAdOx1 and 10^7 PFU for MVA). CarboTaxol injections were initiated together with the prime (fig 4.24 A). The P1A-specific CD8$^+$ T cell response was assessed 14 days post prime and 14 days post boost, in the blood. PBMCs were stimulated for 5h with P1A peptides and stained for inflammatory cytokines as previously described.

When vaccine was combined with CarboTaxol, we observed a significant increased magnitude of IFNγ^+ CD8$^+$ T cells specific to P1A after prime and after boost compared to the vaccine alone group (fig 4.24 B). This indicates that CarboTaxol effects on the priming of the vaccine response promote a better generation of P1A specific CD8 T cells in tumour free mice too. Therefore, CarboTaxol seems to act as an adjuvant with our vaccine model. Furthermore, the vaccine+chemo group displayed a better tumour protection than vaccine alone when the mice were challenged with 15V4T3 3 weeks post boost, emphasising the long term effect that one dose of CarboTaxol has on the vaccine immune response (see appendix figure 2).

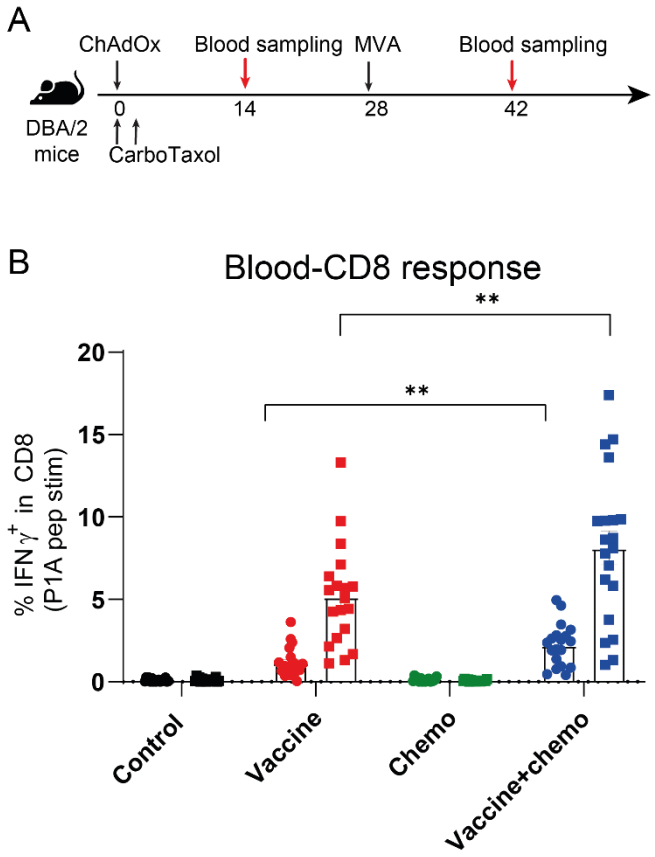


Figure 4.24 Combination of ChAdOx1/MVA-P1A with CarboTaxol in tumour free DBA/2 and C57BL/6 mice. (A) DBA/2 mice were vaccinated via i.m with 10^8 IU of ChAdOx1-Ii-P1A or PBS sham and treated with carboplatin(40mg/kg) and paclitaxel (20mg/kg) and 24h later with paclitaxel (20mg/kg) via i.p 4-weeks later mice received 10^7 PFU of MVA-tpA-P1A. (B) 2 weeks post-prime and 2 weeks post-boost blood was harvested and PBMCS were stimulated with P1A peptides for 5h. The proportion of IFNγ-producing P1A specific $CD8^+$ T cells is shown. Mean ± SEM is shown and each symbol represents an individual mouse and data are pooled from 3 independent experiments (n= 16 to 17 mice per groups). Statistically significant differences between groups were determined by an ordinary one-way ANOVA comparisons test. **, $p \leq 0.01$.

The effects of CarboTaxol on TCF1 expression occurs on day 3 to 5 post injections. Because this occurs early-on post chemotherapy injection and for a short window of time, one important question to be answered is whether the timing of the CarboTaxol injections relative to the injection of the vaccines is important. Indeed, both our tumour free and tumour bearing mice data were investigating CarboTaxol and vaccine given on the same day. Therefore, we next tested different time points of chemotherapy. DBA/2 mice were vaccinated with ChAdOx1/MVA-P1A 4 weeks apart, CarboTaxol treatment was either given 7 days before prime, 14 days post prime, or together with the boost (fig 4.25 A).

The P1A-specific CD8 response post prime and post boost were not improved when chemotherapy was given 7 days prior to the prime or 14 days post-prime compared to the vaccine alone. Very interestingly, CarboTaxol given together with the MVA-tpA-P1A

boost vaccine showed a significantly higher magnitude of the IFNγ$^+$CD8$^+$ T cells post boost compared to the vaccine alone (fig 4.25 B). Hence, CarboTaxol can augment the magnitude of the P1A-specific immune response only when given together with the ChAdOx1-Ii-P1A prime or with MVA-tpA-P1A boost.

These data further support the importance of the short-term effect of CarboTaxol on the immune system. Indeed, the expansion of TCF1 either alone or together with CD11b$^+$Ly6G$^+$ cell depletion might be of importance in CarboTaxol adjuvant role.

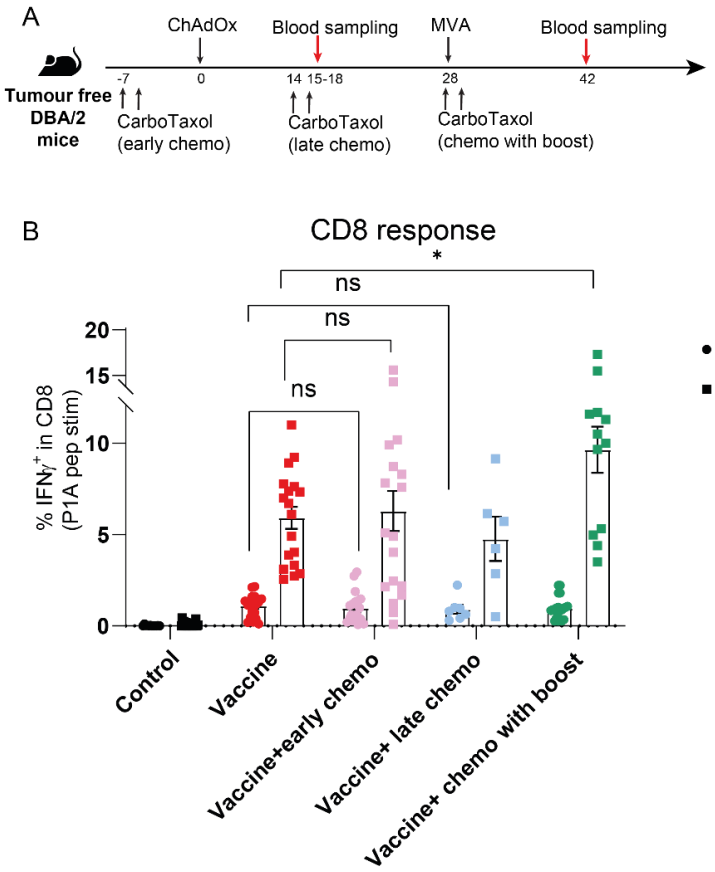


Figure 4.25 The timing of CarboTaxol treatment is of major importance to improve the priming and boosting of the ChAdOx1/MVA-P1A vaccines. (A) DBA/2 mice were vaccinated via i.m with 10^8 IU of ChAdOx1-Ii-P1A or PBS sham. 4-weeks later the mice received 10^7 PFU of MVA-tpA-P1A. Mice were treated with carboplatin(40mg/kg) and paclitaxel (20mg/kg) and 24h later with paclitaxel (20mg/kg) via i.p injections given 7 days before the prime, 14 days after the prime and together with the boost. (B) 15 to 18 days post-prime and 2 weeks post-boost, blood was harvested and PBMCs were stimulated with P1A peptides for 5h. The mean proportion of IFNγ-producing P1A specific CD8$^+$ T cells is shown. Mean ± SEM are shown and each symbol Each symbol represents an individual mouse and data are pooled from at least 2 independent experiments except the vaccine+late chemo group which was performed only once (n= 6 to 18 mice per groups). Statistically significant differences between groups were determined by a Kruskal-Wallis test with Dunn's multiple comparisons test. *, $p \leq 0.05$.

4.5.2 CarboTaxol induces activation of cDC2 but not cDC1

Given the observed adjuvant effect of CarboTaxol, we were interested in looking at CarboTaxol impact on DCs. Classically DCs are the major cell type involved in T cell priming[35]. DCs can present intracellular but also extracellular antigens to $CD8^+$ T cells via MHCI through a process called antigen cross presentation. In brief, through cross-presentation DCs are able to engulf cellular debris of dying/dead cells, and present antigen-derived epitopes to T cells not only on MHC-II (natural endosomal pathway) but also on MHC-I (cytoplasmic pathway)[36–38]. Therefore, it was of particular interest to explore the dendritic cell phenotypes after chemotherapy (see material and methods for gating strategy). Tumour free and tumour bearing mice were treated with CarboTaxol together with ChAdOx1-Ii-P1A. At day 4 post treatment, we harvested the spleen and bone marrow of tumour free mice and the spleen of tumour bearing mice (fig 4.26 A,E). No significant differences in number were seen between mDC, cDC1 and cDC2 in the spleen and BM of tumour free mice (fig 4.26 B,C,D) nor in the spleen of tumour bearing mice (fig 4.26 F,G,H) between chemotherapy-treated and non-treated groups.

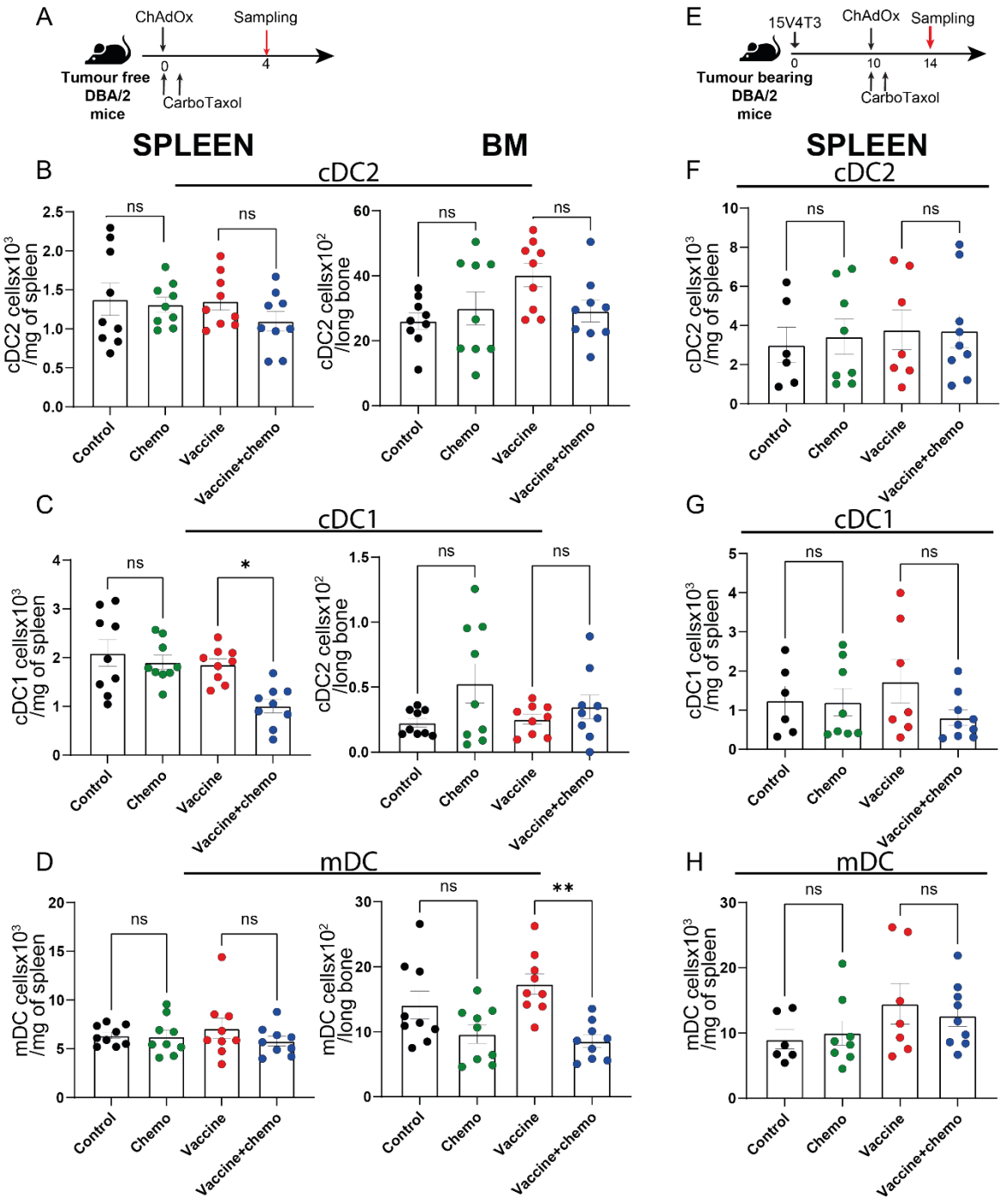


Figure 4.26 Dendritic cell populations in tumour free and tumour bearing mice after CarboTaxol. DBA/2 mice tumour free (A) or tumour bearing (14 days post implantation) (E) were vaccinated via i.m with 10^7 IU of ChAdOx1-li-P1A or PBS sham and treated with carboplatin(40mg/kg) and paclitaxel (20mg/kg) and 24h later with paclitaxel (20mg/kg) via i.p. At day 4 post chemotherapy, spleen and BM were harvested. Cells were stained and analysed by flow cytometry. Monocytic DC (mDC, defined as $CD45^+$ Ly6G- $F4/80^+$ $CD11c^+MHC2^+$), conventional DC 1 (cDC1, defined as CD45+ Ly6G- F4/80- $CD11c^+$ $MHC2^+$ $XCR1^+$) and conventional DC2 (cDC2, defined as $CD45^+$ Ly6G- F4/80- $CD11c^+$ $MHC2^+$ $CD172^+$) were evaluated. In tumour free mice, the cell numbers of cDC2 are shown in the spleen and BM in (B), the cell numbers of cDC1 are shown in the spleen and BM in (C) and the cell numbers of mDC are shown in the spleen and BM in (D). In tumour bearing mice, the cell numbers of cDC2 are shown in the spleen in (F). The cell number of cDC1 is shown in the spleen in G) and the cell numbers of mDC are shown in the spleen in (H). Data are pooled from 2 independent experiments and mean for each group are shown. Mean ± SEM are shown and each symbol represents an individual mouse (n= 6 to 9 mice per group). Statistically significant differences between groups were determined by a Kruskal-Wallis test with Dunn's multiple comparisons test,*, $p \leq 0.05$, **, $p \leq 0.01$.

We also assessed the activation status of DCs. The cDC2 subset contained a higher proportion of $CD80^+$ cells after chemotherapy in the spleen and BM of tumour free mice (fig 4.27 A,B). cDC2 $CD80^+$ cells were also expanded in the bone marrow of tumour free mice in terms of cell numbers (fig 4.27 B). cDC1 $CD80^+$ cells were not expanded in the spleen after chemotherapy (fig 4.27 C). Interestingly, cDC1 $CD80^+$ cells were significantly expanded in the BM of tumour free mice (fig 4.27 D). However, the cDC1 cells were present in very small numbers in the BM therefore the cDC1 $CD80^+$ cells represent a very small portion of BM cells. cDC2 $CD80^+$ cells were expanded in the spleen of tumour bearing mice after chemotherapy, although the differences between chemotherapy-treated and -non-treated group were variable and not significant (fig 4.27 E). Similar to tumour free mice, we did not see an expansion of spleen cDC1 $CD80^+$ in tumour bearing mice after CarboTaxol (fig 4.27 F). The BM DCs populations will have to be assessed in tumour bearing mice. The expansion of cDC2 $CD80^+$ cells indicate a better activation of these cDC2 which are known to activate preferentially $CD4^+$T cells and initiate T helper cell differentiation.

Finally, preliminary data at 24h and 48h post ChAdOx1 alone showed an expansion of cDC1 $CD86^+$ cells similar to the ChAdOx1+CarboTaxol group in the spleen of tumour free mice (see appendix figure 2 B,C). Hence, it appears that CarboTaxol does not promote a better priming of $CD8^+$ T cells through the expansion nor through the increase activation of cDC1. However, we cannot exclude a possible role for increased activation of cDC2 in CarboTaxol adjuvant function, as cDC2 promote the functions of CD4 helper cells which, in turn, are known to improve DC activation and maturation, leading to better $CD8^+$ T cell priming[56].

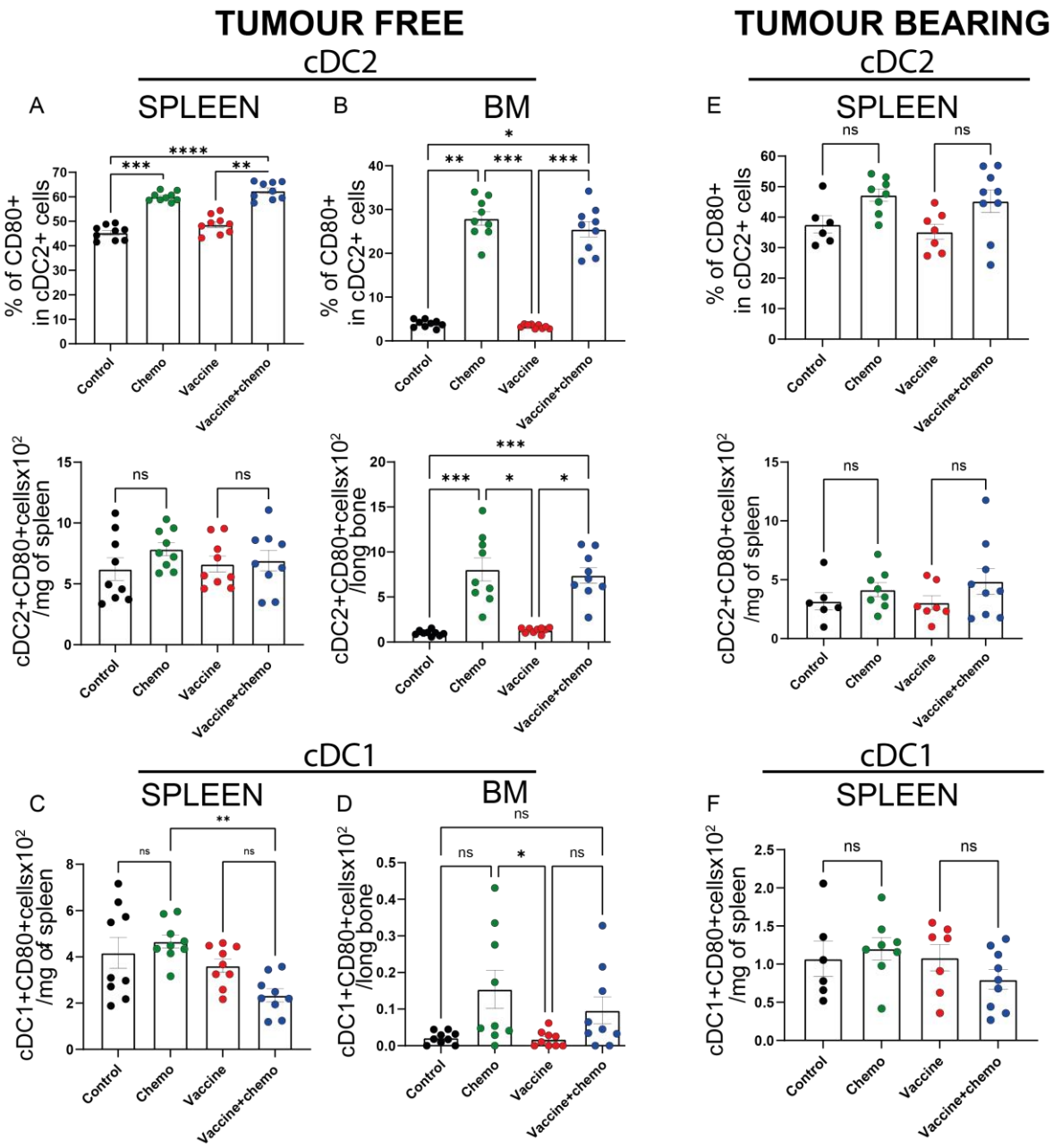


Figure 4.27 cDC phenotype in tumour free and tumour bearing mice after CarboTaxol.
DBA/2 mice tumour free or tumour bearing (14 days post implantation) were vaccinated via i.m with 10^7 IU of ChAdOx1-Ii-P1A or PBS sham and treated with carboplatin(40mg/kg) and paclitaxel (20mg/kg) and 24h later with paclitaxel (20mg/kg) via i.p. At day 4 post chemotherapy, spleen and BM were harvested. Cells were stained and analysed by flow cytometry. cDC (defined as CD45+ Ly6G- F4/80- CD11c+ MHC2+) were evaluated for CD80 expression. The proportion as well as the cell number of cDC2 (cDC CD172+) expressing CD80 is shown in the spleen (A) and BM (B) of tumour free mice. The cell number of cDC1 (cDC XCR1+) expressing CD80 is shown in the spleen (C) and BM (D) of tumour free mice. In tumour bearing mice, the proportion as well as the cell number of cDC2 expressing CD80 (E) is shown in the spleen. The cell number of cDC1 expressing CD80 is shown in the spleen (F). Data are pooled from 2 independent experiments and mean for each group are shown. Each symbol represents an individual mouse (n= 6 to 9 mice per group). Statistically significant differences between groups were determined by a Kruskal-Wallis test with Dunn's multiple comparisons test,*, $p \leq 0.05$, **, $p \leq 0.01$, ***, $p \leq 0.001$, ****, $p \leq 0.0001$.

4.6 Viral vector vaccines induce expansion of CD11b$^+$ Ly6G$^+$ cells

One may ask if the effects of CarboTaxol on CD11b$^+$Ly6G$^+$ in both tumour free and tumour bearing mice might impact the innate immune response to viral vectors. Indeed, it has been shown that the first line of response after viral infection is the recruitment of neutrophils/ granulocytic cells (CD11b$^+$Ly6G+). Several studies investigating viral vector platforms also reported the recruitment of CD11b$^+$Ly6G$^+$ early post infections [252]. To investigate the impact of our viral vector vaccines on the early immune response, we challenged tumour free DBA/2 mice with either ChAdOx1-P1A or MVA-P1A and profiled the innate immune response at 12h, 24h and 48h. ChAdOx1-GFP and PBS groups were

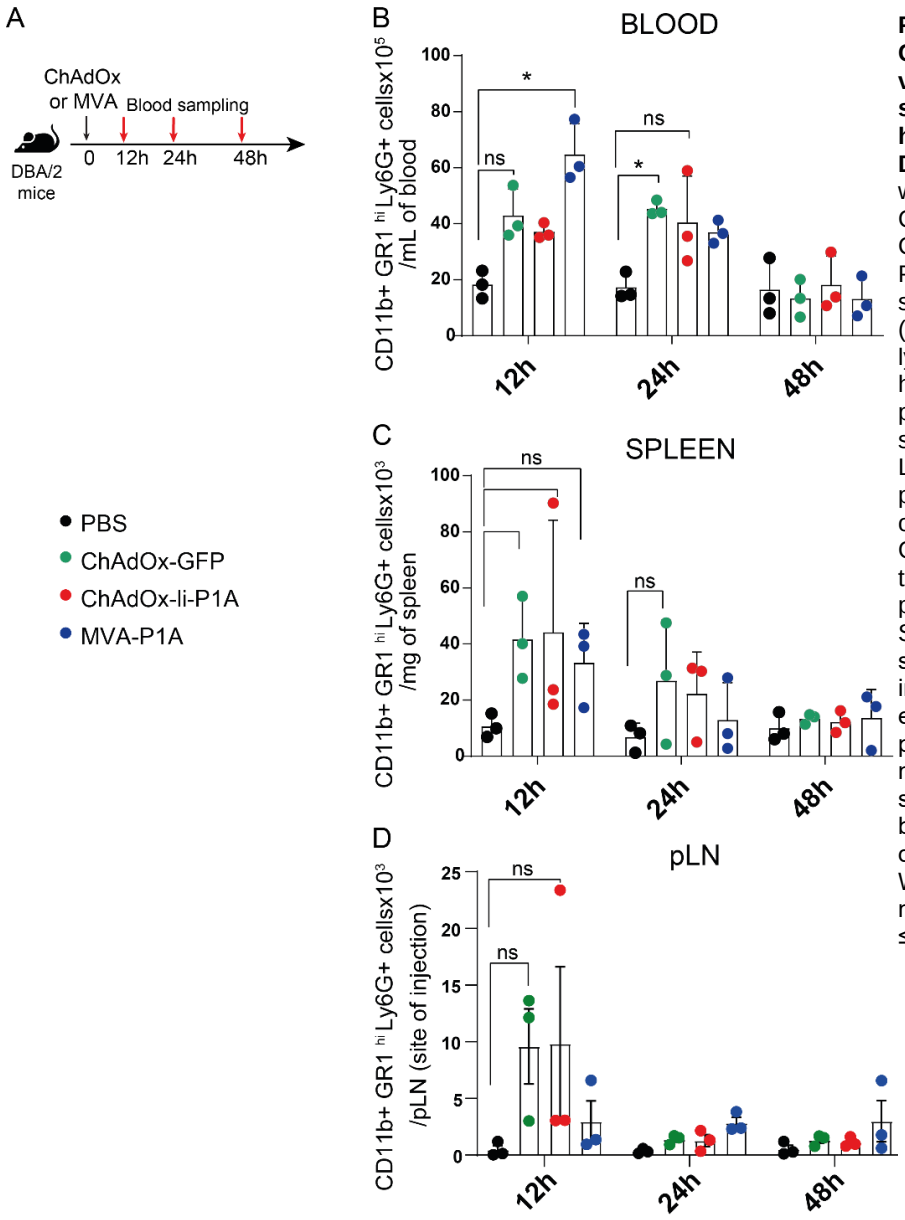


Figure 4.28 Effect of ChAdOx1 and MVA viral vectors on the immune system at 12-, 24- and 28-hours post injection in DBA/2 mice. (A) DBA/2 mice were vaccinated with 10^8 IU of ChAdOx1-li-P1A or ChAdOx1-GFP or with 10^7 PFU of MVA-P1A or PBS sham. Blood, spleen and right (leg of injections) popliteal lymph node (pLN) were harvested 12h, 24h and 48h post injections. Cells were stained for CD11b, GR1, Ly6C and Ly6G to assess the proportions and cell numbers of myeloid cells. CD11b+ GR1^{hi} Ly6G+ cell numbers in the blood (B), spleen (C), and pLN(D) are shown. Mean ± SEM is shown and each symbol represents an individual mouse, only one experiment has been performed in DBA/2 (n= 3 mice per groups). Statistically significant differences between groups were determined by a Kruskal-Wallis test with Dunn's multiple comparisons test. *, p ≤ 0.05.

included to control for the P1A antigen and the viral vector effects respectively (fig4.3.1 A). At 12h and 24 h post infections, we noticed an increased in $CD11b^{+}Ly6G+$, in the blood (fig 4.28 B), spleen (fig 4.28 C) and popliteal lymph nodes (fig 4.28 D, pLN) compared to the PBS group. This effect was due to the viral vectors, both MVA and ChAdOx1, and was antigen-independent as it was observed with ChAdOx expressing-GFP or -P1A. The recruitment of $CD11b^{+}Ly6G^{+}$ was significant 12h post viral vector infections in the blood. Although it was not significant, it was also observed in the spleen and LN. At 24h post infections, the increase in $CD11b^{+}Ly6G^{+}$ was mostly observed in the blood and spleen for all the vectors (fig 4.28 B,C). In the pLNs the level of $CD11b^{+}Ly6G^{+}$ dropped dramatically as early as 24h (fig 4.28 D). These results will have to be repeated due to the low number of mice per group, but the data indicate that our vaccine platform recruits $CD11b^{+}Ly6G^{+}$ cells early-on post infection.

These $CD11b^{+}Ly6G^{+}$ cells have been shown to promote viral-vector-mediated gene transfer by suppressing NK cells direct killing of infected cells[253]. Hence these $Ly6G^{+}$ cells could be important to sustain the duration of antigen expression in infected cell which have been shown to be directly correlated to the induction of $CD8^{+}$T cell responses[254]. Therefore, the next question we addressed was whether the combination of the chemotherapy and the ChAdOx1 prime in tumour free mice depletes these vaccine-recruited granulocytes. Would this depletion abolish the synergistic effect observed? Previously, we observed CarboTaxol depleted $CD11b^{+}$ $Ly6G^{+}$ from 72h (see appendix figure 2 D) when it is given with the prime. Therefore, the vaccine recruited $CD11b^{+}$ $Ly6G^{+}$ cells, which are only expanded during the first 24 hours after vaccination, were not impacted by CarboTaxol given with the prime. To deplete these cells with CarboTaxol, we administrated CarboTaxol 48h prior to the ChAdOx1-P1A (fig 4.29 A). With this new combination schedule, CarboTaxol was also able to deplete the viral vector-recruited granulocytes (fig 4.29 B). However, the

proportion of $CD11b^{+}Ly6G^{+}$ cells after vaccine+chemo was not significantly lower than the PBS group (fig 4.29 B). So, CarboTaxol was able to deplete $CD11b^{+}Ly6G^{+}$ recruited by the vaccine and brought their proportion back to the level observed in PBS control mice. On day 14 post prime, the combination of treatment significantly improved the vaccine immunogenicity such as observed in our previous time point regimen (fig 4.29 C). Importantly, these data indicate that the depletion of $CD11b^{+}$ $Ly6G^{+}$ cells recruited by the vaccine platform is not detrimental for the synergistic effect with chemotherapy.

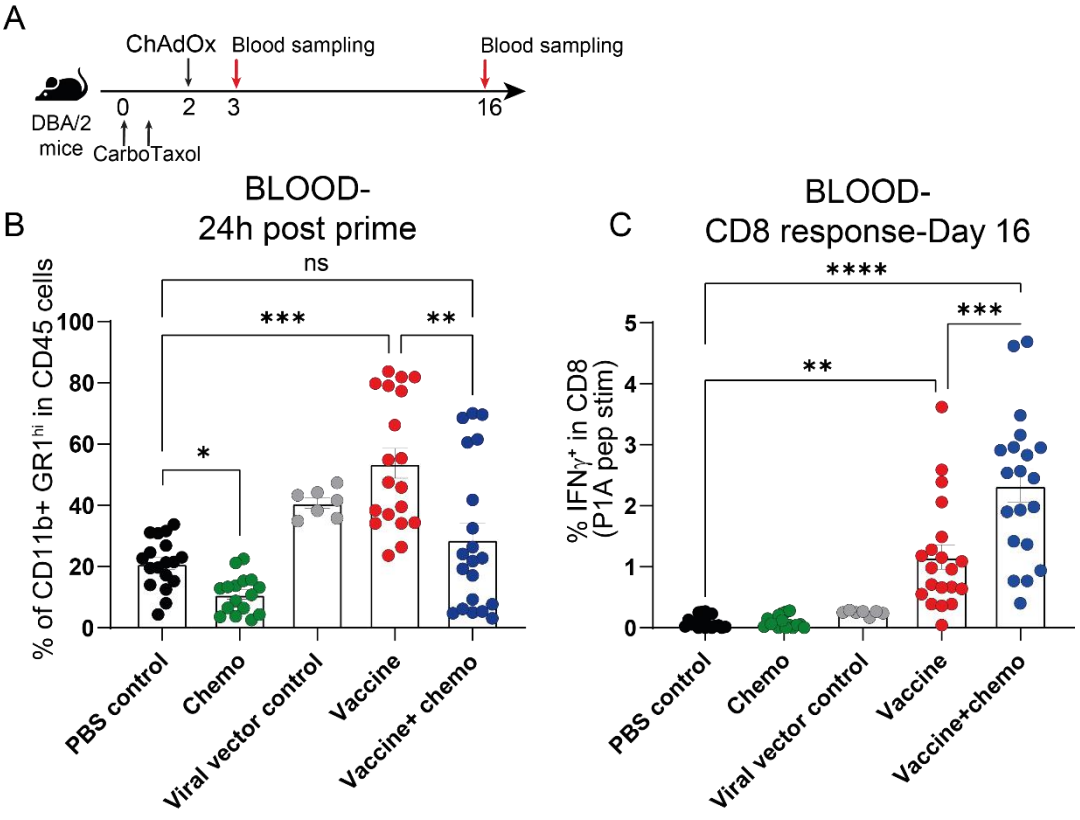


Figure 4.29 Effect of CarboTaxol on viral-vector vaccine granulocytes recruitment in DBA/2 tumour free mice. (A) DBA/2 mice were treated with carboplatin(40mg/kg) and paclitaxel (20mg/kg) and 24h later with paclitaxel (20mg/kg) via i.p injections. 24h later mice were vaccinated with 10^{8} IU of ChAdOx1-li-P1A or ChAdOx1-DPY or PBS sham. Blood was harvested less than 24h later. Cells were stained for CD11b, GR1, Ly6C and Ly6G to assess the proportion of myeloid cells. $CD11b^{+}$ $GR1^{hi}$ $Ly6G^{+}$ cell proportion out of total leucocytes ($CD45^{+}$) in the blood is shown in (B). Statistically significant differences between groups were determined by a Kruskal-Wallis test with Dunn's multiple comparisons test. The P1A-specific $CD8^{+}$ T cell response was assessed 14 days post prime in the blood and is shown in (C). Mean ± SEM is shown and each symbol represents an individual mouse, data are pooled from at least 2 independent experiments (n= 7 to 20 mice per groups). Statistically significant differences between PBS,vaccine and vaccine+chemotherapy (n>15 mice per groups) groups were determined by an Ordinary one-way ANOVA comparisons. *, $p \leq 0.05$. **, $p \leq 0.01$, ***, $p \leq 0.001$,****, $p \leq 0.0001$.

In parallel, we investigated whether CarboTaxol and ChAdOx1/MVA-P1A vaccination could be improved in C57BL/6 mice. In this model, we used a one-week apart strategy between the prime and boost. CarboTaxol was given 48h prior to the prime. Blood sampling was performed 24h post-prime to assess $CD11b^{+}Ly6G^{+}$ cell proportion and 14 days post boost to assess the magnitude of the P1A-specific $CD8^{+}$ T cells (fig 4.30 A). As in DBA/2 mice, the proportion of $CD11b^{+}Ly6G^{+}$ in the vaccine+chemo group was similar to the PBS proportion (fig 4.30 B). 14 days post boost, we observed an increased magnitude of $IFN\gamma^{+}$ $CD8^{+}$ T cells when CarboTaxol was given 48h prior to the prime (fig 4.30 B). Similar to DBA/2 mice, the depletion of $CD11b^{+}Ly6G^{+}$ recruited by the viral vector was not detrimental to the synergistic effect observed (fig 4.30 C,B).

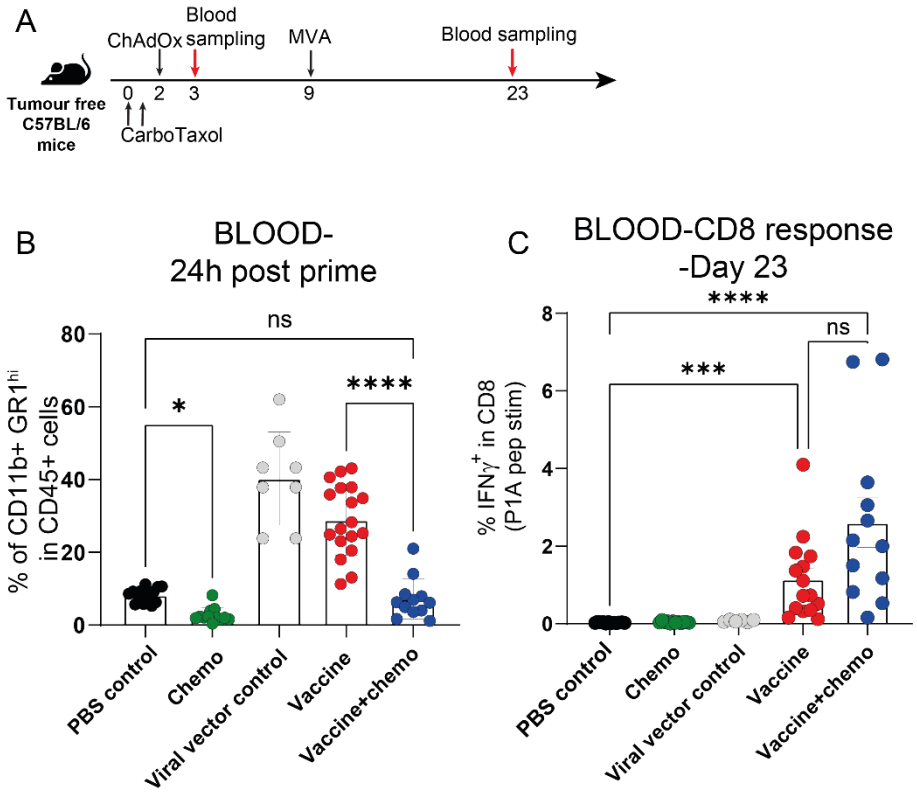


Figure 4.30 Effect of CarboTaxol on viral-vector vaccine granulocytes recruitment and vaccine immunogenicity in C57BL/6 tumour free mice. (A) C57BL/6 mice were treated with carboplatin(40mg/kg) and paclitaxel (20mg/kg) and 24h later with paclitaxel (20mg/kg) via i.p . 24h later, mice were vaccinated via i.m with 10^8 IU of ChAdOx1-Ii-P1A or PBS sham. 1-week later mice received 10^7 PFU of MVA-tpA-P1A. Blood was harvested less than 24h later post ChAdOx1 prime. Cells were stained for CD11b, GR1, Ly6C and Ly6G to assess the proportion of myeloid cells. $CD11b^+$ $GR1^{hi}$ $Ly6G^+$ cell proportion out of total leucocytes ($CD45^+$) in the blood is shown in (B). (C) 2 weeks post-boost, blood was harvested and PBMCS were stimulated with P1A peptides for 5h. The proportion of IFNγ-producing P1A specific $CD8^+$ T cells is shown. Mean± SEM is shown, and each symbol represents an individual mouse and data are pooled from 2 independent experiments (n= 12 to 15 mice per groups). Statistically significant differences between groups were determined by a Kruskal-Wallis test with Dunn's multiple comparisons test. **, p ≤ 0.01, ***, p ≤ 0.001,****, p ≤ 0.0001

To conclude, CarboTaxol acts as an adjuvant and can help the generation of an improved P1A-specific CD8 T cell response in both DBA/2 and BL/6 mice. The adjuvant function is not impacted by the depletion of $CD11b^+Ly6G^+$ cells recruited by viral vector vaccines.

We can now further explore several questions to understand the mechanism for CarboTaxol adjuvant functions: Is there a link between the mechanism of killing the $CD11b^+Ly6G^+$ cells by CarboTaxol and the expansion of $TCF1^+$ T cells? Is there a cause-effect relationship between TCF1 expression and CarboTaxol adjuvant role?

4.7 CarboTaxol impacts on the cytokine environment

4.7.1 CarboTaxol decreases systemic level of IL12/23(p40)

In our model, we observed a strong correlation between the depletion of $CD11b^{+}Ly6G^{+}$ cells and the expansion of $TCF1^{+}$ cells in T cells (fig 4.21 and 4.22). The phagocytosis of apoptotic granulocytes by monocytes and DCs has been shown to promote a decrease in basal inflammation and especially a decrease in IL12/23(p40) [251]. P40 is a subunit shared between IL12 and IL23. Moreover IL12/23(p40) has been shown to inhibit TCF1 expression in a STAT4-dependent manner[227]. Therefore, we aimed to investigate the levels of IL12/IL23(p40) at the same time point (day4) after chemotherapy (fig 4.31 A and D). We were also interested to evaluate levels of IL-1β, given it was defined as a marker for ICD, which can be induced by chemotherapy. Indeed, IL-1β has been shown to be produced by DCs activated through ICD, which ultimately leads to a better CD8 priming. Finally, we evaluated the levels of IFNα to assess systemic inflammatory responses as well as the level in the TME. On day 4 after chemotherapy, the blood was sampled in EDTA tubes, centrifuged and plasma was collected from tumour free mice (fig 4.31 A) or tumour bearing mice (fig 4.31 D). In tumour free mice, we observed a significant decrease in IL-12/23 levels in the blood (fig 4.31 B) and spleen (fig 4.31 C) with the level of p40 being reduced by 50% on average compared to control or vaccine alone groups. At the same time point after chemotherapy (fig 4.31 D), we also observed a significant decrease in IL-12/23(p40) in the spleen (fig 4.31 E) and TME (fig 4.31 F) of tumour bearing mice. This decrease in IL12/23(p40) at the same time as granulocytes depletion is in line with the literature and supports the hypothesis of a potential link between TCF1 expression in T cells and $CD11b^{+}Ly6G^{+}$ depletion[251].

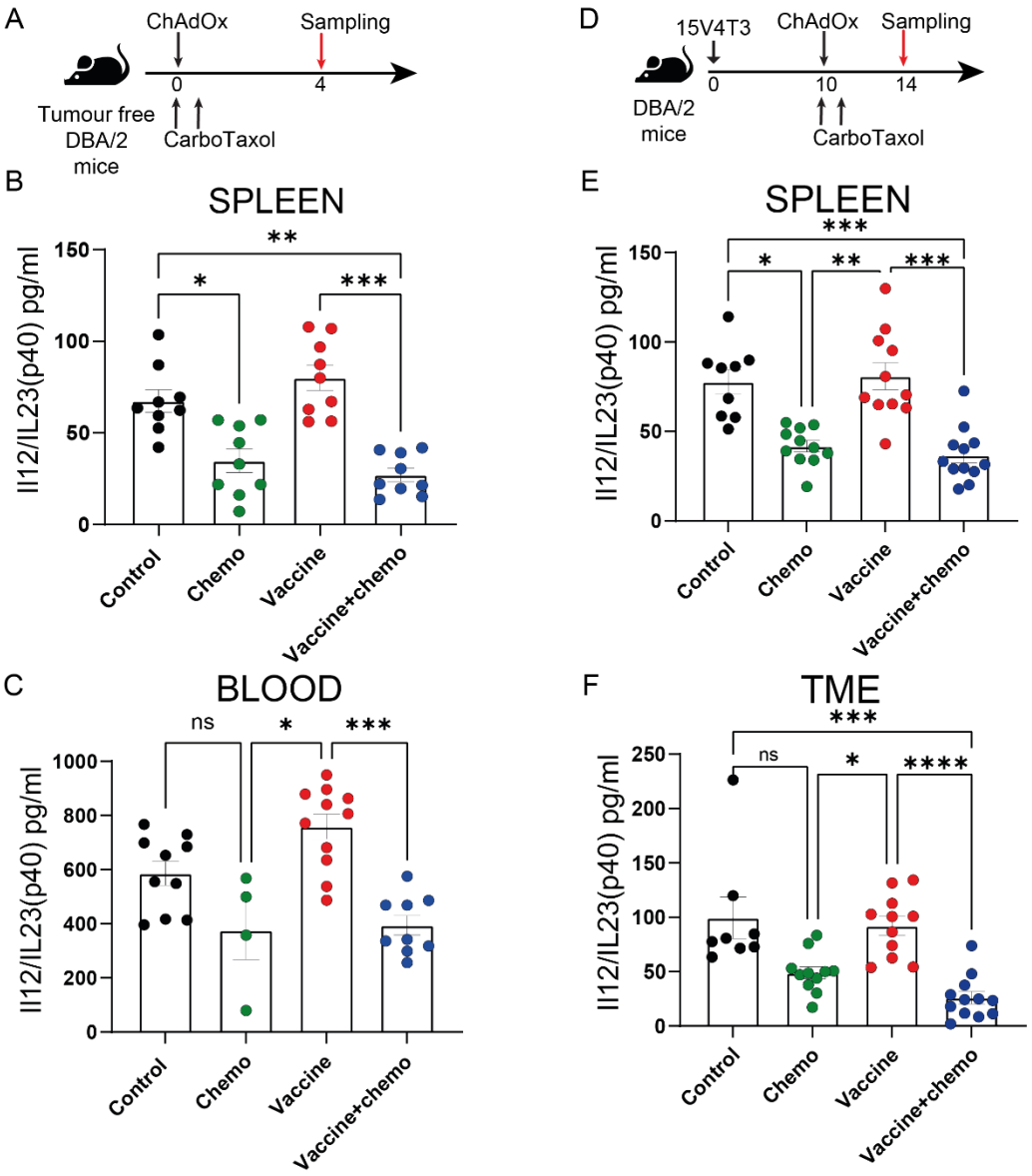


Figure 4.31 IL12/23(p40) levels after CarboTaxol in tumour free and tumour bearing DBA/2 mice. Scheme for tumour free (A) and tumour bearing (D) are presented. DBA/2 mice were vaccinated via i.m with 10^7 IU of ChAdOx1-Ii-P1A or PBS sham and treated with carboplatin(40mg/kg) and paclitaxel (20mg/kg) and 24h later with paclitaxel (20mg/kg) via i.p. At day 4 post chemotherapy, spleen, blood serum for tumour free mice and tumours for tumour bearing mice were harvested. Spleen and tumour processing supernatants (media of the 1st step of tissue processing) were collected. Quantification of the IL12/23(p40) subunit was performed by ELISA. The level of cytokine is presented in the spleen (B) and blood (C) of tumour free mice and in the spleen (E) and TME (F) of tumour bearing mice. Data are representative of 3 independent experiments and mean ± SEM for each group are shown. Each symbol represents an individual mouse (n= 8 to 12 mice per group). Statistically significant differences between groups were determined by a Kruskal-Wallis test with Dunn's multiple comparisons test,*, $p \leq 0.05$, **, $p \leq 0.01$, ***, $p \leq 0.001$, ****, $p \leq 0.0001$.

The detection of IL-1β was variable and not detectable in some samples in the spleen (fig 4.32 A,B) and TME (fig 4.32 C). Overall IL-1β levels were not changed after chemotherapy compared to the control groups in the spleen of tumour free and tumour bearing mice (fig 4.32 A,B,C**)**. Although IFNα was detectable in all samples, the amount detected were very low (below 15 pg/ml in the spleen). We did not detect any differences in the IFNα levels between chemotherapy-non-treated and - treated groups in the spleen (fig 4.32 D,E). In the TME, we noticed a significant decrease of IFNα (fig 4.32 F). Altogether, the cytokines tested indicate decreased inflammation in the systemic environment in tumour free and tumour bearing mice as well as in the TME after chemotherapy. This was a surprising finding given the potential cytotoxic activity of chemotherapy which could lead to immunogenic and inflammatory cell death. However, these findings are in line with the depletion of neutrophils/MDSCs which has been correlated to less IL12/23(p40) production by phagocytic cells [251].

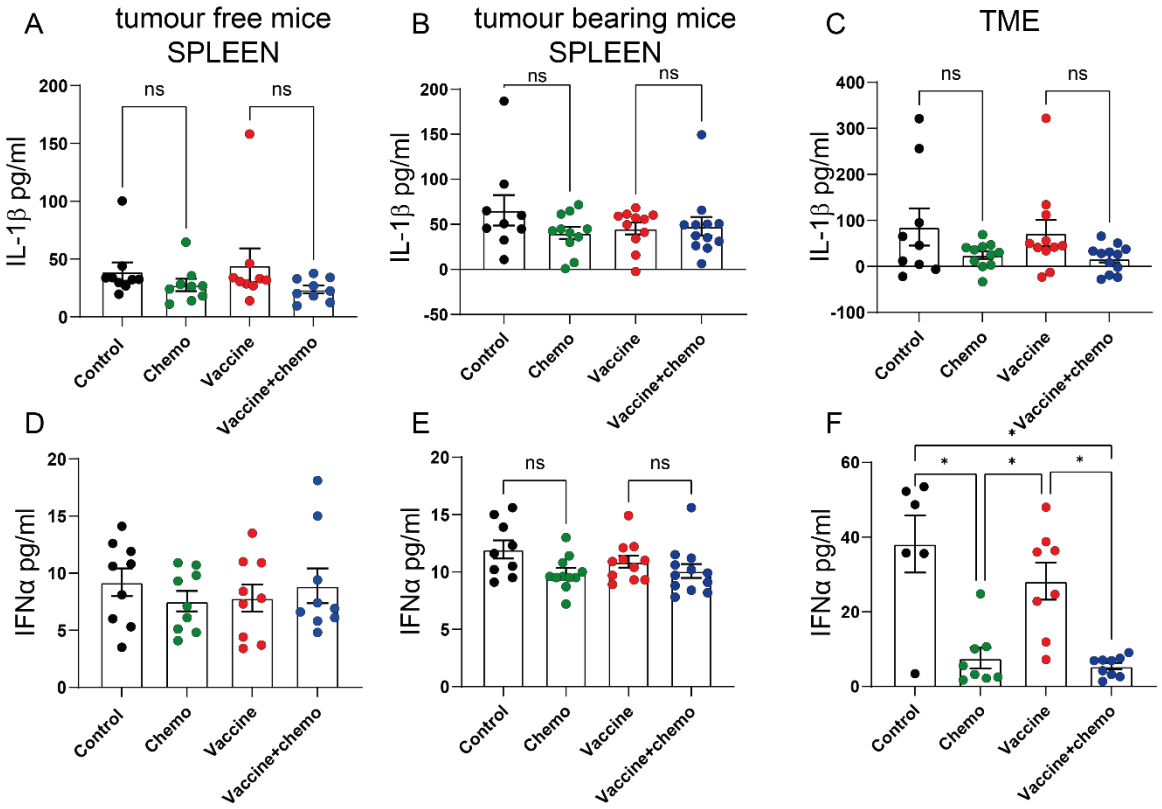


Figure 4.32 IL-1β and IFNα levels after CarboTaxol in tumour free and tumour bearing DBA/2 mice. DBA/2 mice, tumour free or tumour bearing (10 days post implantation) were vaccinated via i.m with 10^7 IU of ChAdOx1-Ii-P1A or PBS sham and treated with carboplatin(40mg/kg) and paclitaxel (20mg/kg) and 24h later with paclitaxel (20mg/kg) via i.p. At day 4 post chemotherapy, spleen and tumours were harvested. Spleen and tumour processing supernatants (media of the 1st step of tissue processing) were collected. Quantification of IL-1β and IFNα levels were performed by ELISA. The level of cytokines are presented in the spleen of tumour free mice(A) and in the spleen of tumour bearing mice (B). The level of cytokines in the TME are presented in (C). Data are representative of 3 independent experiments and mean ± SEM for each group are shown. Each symbol represents an individual mouse (n= 8 to 12 mice per group). Statistically significant differences between groups were determined by a Kruskal-Wallis test with Dunn's multiple comparisons test,*, $p \leq 0.05$, **, $p \leq 0.01$, ***, $p \leq 0.001$, ****, $p \leq 0.0001$.

4.7.2 CarboTaxol-treated groups showed decreased basal IL12/23(p40) production by blood monocytes

We investigated which cells were the potential producers of IL12/IL23(p40) in the blood at day 4 post CarboTaxol. Tumour free mice were treated with chemotherapy and vaccinated on the same day. To control for vaccination, some mice were sham vaccinated with PBS (fig 4.33 A). On day 4 after chemotherapy, PBMCs, left unstimulated to evaluate the basal IL12/23(p40) production, were treated with BrefA and incubated overnight. The cells were then stained intracellularly to evaluate IL12/23(40) production. $Ly6G^+$ cells did not produce high levels of IL12/IL23(p40) and a lot of variation was observed between mice, including some mice with no production of IL12/23(p40) in the PBS and vaccine only groups. However, because chemotherapy depletes these cells the total level of $Ly6G^+$ IL12/23(p40)+ cells were significantly lower in the chemotherapy and vaccine+chemotherapy groups compared to the control groups (fig 4.33 A). Very interestingly, we noticed a decrease in basal IL12/23(p40) expression in potential monocytes ($CD11b^+$ Ly6C+) after chemotherapy (fig 4.33 C). We also assessed the level of the cytokines produced by conventional dendritic cells (cDC) (F4/80- CD11c+ MHCII+). The proportion of IL12/23(p40)-producing cDCs in the blood was very low, representing on average 2% of the CD45+ cells. We did not notice any significant difference in IL12/23(p40) production by cDCs in the blood after chemotherapy compared to the non-treated groups (fig 4.33 D). The IL12/23(p40) production will need to be assessed in the spleen and LNs where there is more DCs and macrophages to evaluate. However, these data support the hypothesis of a decrease in IL12/23(p40) production during $CD11b^+Ly6G^+$ depletion which could potentially be the cause of TCF1 expression in T cells.

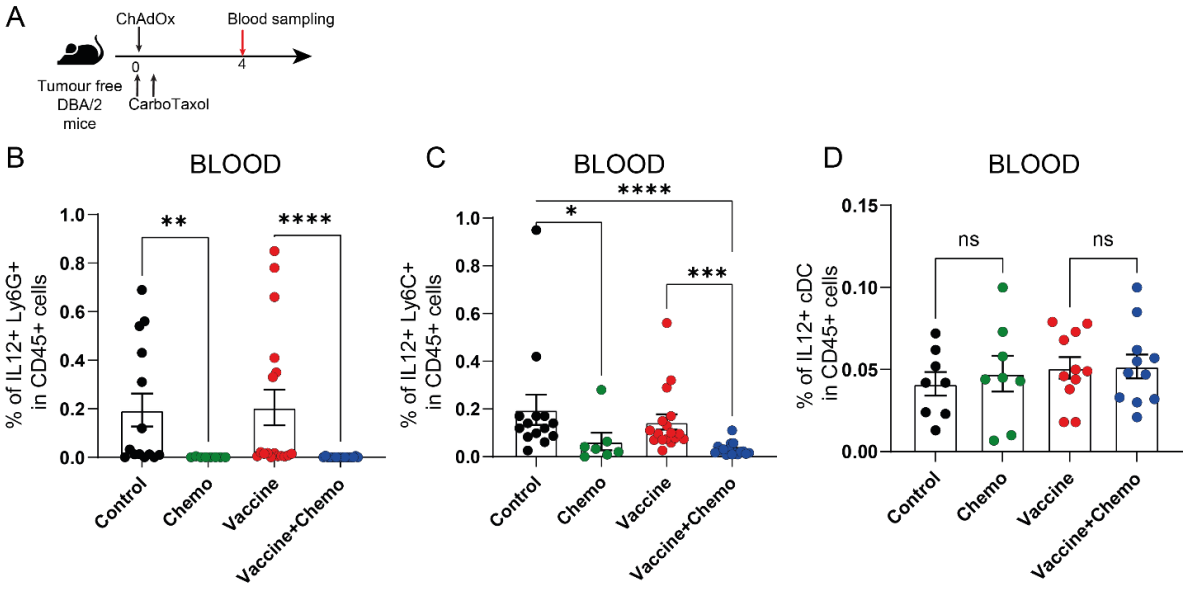


Figure 4.33 IL12/23(p40) basal production in the blood is decreased after CarboTaxol in CD11b+ Ly6C+ and CD11b+Ly6G+ cells in DBA/2 mice. (A) DBA/2 mice tumour free were vaccinated via i.m with 10^7 IU of ChAdOx1-Ii-P1A or PBS sham and treated with carboplatin(40mg/kg) and paclitaxel (20mg/kg) and 24h later with paclitaxel (20mg/kg) via i.p. At day 4 post chemotherapy, blood was harvested. Cells were incubated overnight with BrefA and stained intracellularly to assess the IL12/23(p40) production. The proportion of IL12/23(p40)$^+$ CD11b$^+$ Ly6G$^+$ out of total leucocytes (CD45$^+$) is shown in (B). The proportion of IL12/23(p40)$^+$ CD11b$^+$ Ly6C$^+$ out of total leucocytes is shown in (C). The proportion of cDC (CD45$^+$ Ly6G- F4/80- CD11c$^+$ MHC2$^+$) producing IL12/23(p40) out of total leucocytes is shown in (D). Data are representative of at least 2 independent experiments and mean± SEM for each group are shown. Each symbol represents an individual mouse (n= 6 to 17 mice per group). Statistically significant differences between groups were determined by a Kruskal-Wallis test with Dunn's multiple comparisons test,*, $p \leq 0.05$, **, $p \leq 0.01$, ***, $p \leq 0.001$, ****, $p \leq 0.0001$.

4.7.3 Investigation of IL12/23(p40) impact on TCF1 expression in T cells

So far, we have confirmed that together with $CD11b^{+}Ly6G^{+}$ there is a decrease in IL12/23(p40) levels in the blood, spleen and TME after CarboTaxol. We next asked: is this decrease in the p40 subunit the origin of elevated TCF1 expression that is observed with chemotherapy? To understand the impact of IL12/23(p40) on TCF1 expression, mice were treated with anti-IL12/23(p40) neutralizing antibody given together with the prime. This new regimen was compared with vaccine combined with CarboTaxol (fig 4.34 A).

We validated the efficacy of the dose of antibody used by evaluating the levels of IL12/23(p40) in the blood at day 4 post treatment. The antibody was able to significantly deplete IL12/23(p40) from the blood at day 4 post treatment by more than 50% compared to PBS or vaccine-treated group (fig 4.34 B). However, we did not observe any increase in $TCF1^{+}$ cells in $CD8^{+}$ T cells 4 days post anti-IL12/23(p40) antibody treatment compared to the PBS group (fig 4.34 C). Consistently the CarboTaxol-treated mice displayed an

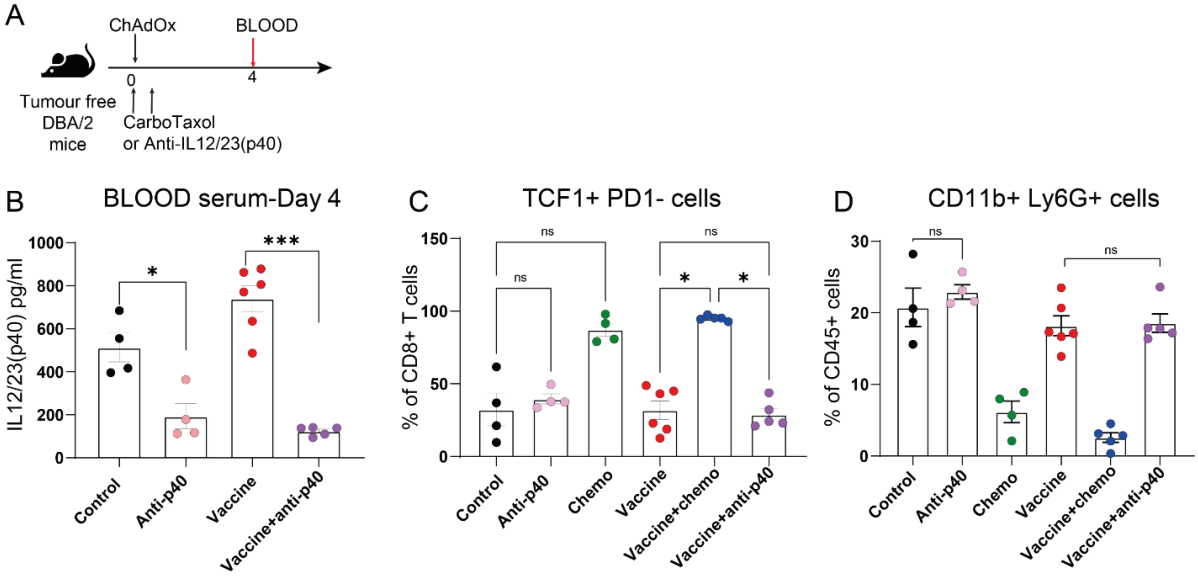


Figure 4.34 Anti-IL12/23(p40) in vivo antibody does not expand $TCF1^{+}$ cells in $CD8^{+}$ T cells. (A) DBA/2 mice tumour free were vaccinated via i.m with 10^{7} IU of ChAdOx1-Ii-P1A or PBS sham and treated with carboplatin(40mg/kg) and paclitaxel (20mg/kg) twice or with anti-IL12/23(p40) (400μg then 200μg) via 2 i.p injections 24h. At day 4 post treatment, blood and serum were harvested. (B) Levels of IL12/23(p40) were evaluated by Elisa. (C) Total PBMCs were stained and analysed by flow cytometry, the proportion of TCD1+ PD1- cells in CD8 T cells is shown. (D) The proportion of $CD11b^{+}$ $Ly6G^{+}$ in $CD45^{+}$ cells is shown. Data represent only 1 independent experiment and mean± SEM for each group is shown. Each symbol represents an individual mouse (n= 4 to 6 mice per group). Statistically significant differences between groups were determined by a Kruskal-Wallis test with Dunn's multiple comparisons test,*, $p \leq 0.05$, **, $p \leq 0.01$, ***, $p \leq 0.001$, ****, $p \leq 0.0001$.

increase in $TCF1^+$ cells in $CD8^+$ T cells (fig 4.34 C). As expected, anti-IL12/23(p40) did not induce a depletion of $CD11b^+Ly6G^+$ cells while CarboTaxol did (fig 4.34 D).

These results were surprising as IL12/23(p40) has been shown to inhibit TCF1 expression in $CD8^+$ T cells[227]. So, when depleting IL12/23(p40) we would have expected an increase in TCF1 expression in $CD8^+$ T cells, which was not the case in our model. However, these results are from one exploratory experiment that will need to be repeated, and further doses and time-points of injections will be evaluated before concluding the absence of the link between IL12/23 decrease and TCF1 expression in $CD8^+$ T cells. Alternatively, these data could indicate that $CD11b^+Ly6G^+$ depletion could induce other signals as part of the resolution of inflammation which could trigger TCF1 expression or promote $CD8^+$ $TCF1^+$ cell expansion.

4.8 Discussion

In this chapter, we focused on understanding the effects of CarboTaxol on the immune system and the mechanism behind which this chemotherapy synergises with therapeutic ChAdOx1/MVA cancer vaccines.

4.8.1 Short-term effects of CarboTaxol

In chapter III, we concluded that CarboTaxol per se does not have major long-term effects (i.e after 12 days in mice) on the immune system in the TME, spleen and blood. However, it is important to note that, in human, most chemotherapies can be eliminated from the system in 24h to 96h[255]. In mice, several studies showed that the half-life of chemotherapy drugs is even shorter[256,257]. Therefore, it was of particular interest to investigate CarboTaxol's short-term effect. Especially, in our regimen, CarboTaxol is given only in one injection together with the prime vaccination. Furthermore, CarboTaxol has previously been published to deplete $CD11b^+$ $GR1^{hi}$ cells (potential PMN-MDSCs) early-on post-injections (72h)[150]. 3- and 4-days post CarboTaxol injections, we noticed a $CD11b^+GR1^{hi}$Ly6G+ cell depletion in tumour bearing mice in the TME and in the system (blood, spleen, and BM) (fig 4.3 and fig 4.4). Surprisingly however our tumour model did not display an expansion of these cells compared to tumour free mice, which is frequently observed with PMN-MDSCs cells in cancer (fig 4.3 A,B)[106]. Interestingly, in our model, $CD11b^+GR1^{hi}$Ly6G+ cells displayed suppressive activities against $CD8^+$ T cells by decreasing their proliferation. The number of $CD11b^+Ly6G^+$ needed to observe a decrease in $CD8^+$T cell proliferation was 3 times the number of $CD8^+$ T cells (fig 4.6). This might be due to the mechanism through which PMN-MDSCs exert their suppressive functions[231]. Indeed, PMN-MDSCs need to be in close contact to induce T cell receptor inactivation through ROS production and thereby decrease $CD8^+$ T cell activation and proliferation. By increasing the density of PMN-MDSCs we may have favoured their suppressive ability

though ROS production. Alternatively, evaluating IFNγ and IL2 production by $CD8^+$ T cells would assess directly their activation which could be more easily dampened by PMN-MDSCs than their proliferation. However, it is also possible that there is a non-negligible proportion of neutrophils within the $CD11b^+Ly6G^+$ population, diluting the immunosuppressive ability of the fraction of PMN-MDSCs contained in that population.

We then wanted to answer if this $CD11b^+Ly6G^+$ depletion was the cause of the synergy observed between ChAdOx/MVA vaccination and CarboTaxol. We depleted the PMN-MDSC using different schedules of anti-GR1 antibody injection. None of the schedules tested was able to improve vaccine induced tumour control, survival (fig 4.8 A,B and fig 4.10 A,B) nor improve vaccine immunogenicity (fig 4.10 C). However, none of the anti-GR1 schedule tested completely recapitulated the $CD11b^+Ly6G^+$ depletion observed after CarboTaxol treatment. Indeed, PMN-MDSCs were not depleted in the BM after anti-GR1 (fig 4.8 F), which has been described in the literature before[249]. Indeed, BM comport stem cells and precursor which are GR1 negative and yet highly proliferative, hence targetable by chemotherapy but not with anti-GR1 antibody. We cannot exclude that the depletion in the BM is important for CarboTaxol and vaccine synergy as $CD8^+$ T cell progenitors as well as mature and memory $CD8^+$ T cells are present in the BM. Hence, the absence of potentially suppressive $CD11b^+Ly6G^+$ cells could impact the phenotype of these BM $CD8^+$ T cells which might eventually be recruited into the system. However, given that the priming and activation of $CD8^+$ T cells happen in secondary lymphoid organs, it is also possible that the depletion in the BM is not of major importance to observe a synergy of treatment. One injection of anti-GR1 was able to deplete $CD11b^+Ly6G^+$ cells in the blood, the spleen and the TME (fig 4.8) but not synergise with ChAdOx1/MVA-P1A. Therefore, we concluded that $CD11b^+Ly6G^+$ depletion is not the entire mechanism by which

chemotherapy improves vaccine-mediated tumour control and vaccine immunogenicity. We then decided to put our focus on T cell phenotype.

When investigating the $CD8^+$ T cell phenotype 4 days after CarboTaxol, we showed that chemotherapy-treated mice have an expansion of $TCF1^+$ $PD1^-$ $CD8^+$ and $CD4^+$T cells in the blood, spleen and TME (fig 4.12 and fig 4.14). This expansion was independent of the chemotherapy effect on tumour cells as we observed this phenotype in tumour free mice (fig 4.17 and fig 4.18) as well as in tumour bearing mice. Interestingly, the $TCF1^+PD1^+$ $CD8^+$ and $CD4^+$T cells were also significantly expanded in the TME (fig 4.14 and fig 4.15). In the system, these cells were present in small numbers and represented less than 1 % of CD8 T cells in the spleen and blood. These data might indicate that chemotherapy promotes the systemic stemness of T lymphocytes which might lead to more precursor stem-like $TCF1^+$ $PD1^-$ $CD8^+$ as well as more progenitor exhausted stem-like $TCF1^+$ $PD1^+$ $CD8^+$T cell infiltration in the TME. These populations have been correlated with better anti-cancer response[226]. Furthermore, the induction of TCF1 in T cells confers them a better proliferative and differentiation potential than TCF1 negative cells[59,60,226]. Therefore, administering vaccine while inducing a higher number of $TCF1^+$ T cells might promote a better priming of T cell response from vaccination.

$TCF1^+$ cell expansion in T cells and $CD11b^+$ $Ly6G^+$ depletion seem linked in tumour free and tumour bearing mice. Indeed, we observed a strong negative correlation between these 2 populations: the lesser the $CD11b^+$ $Ly6G^+$ cell proportion, the more TCF1 expressing cells in $CD8^+$ T cells were observed (fig 4.21 and fig 4.22). Interestingly, the anti-GR1 antibody, which depletes the $CD11b^+$ $Ly6G^+$ cells, did not expand $TCF1^+$ $CD8^+$ nor $TCF1^+PD1^+$ $CD8^+$ T cells (fig 4.23). So, if this population is expanded, it is not due to the absence of $CD11b^+Ly6G^+$ cells. However, we could not exclude that the way

$CD11b^+Ly6G^+$ cells are killed may impact TCF1 expression in T cells or $TCF1^+$ T cell expansion. Indeed, the mechanism of cell death is different between CarboTaxol and anti-GR1. Anti-GR1 induces $CD11b^+Ly6G^+$ cell death through complement-mediated membrane-complex attack which will trigger more inflammatory signals[248,249]. CarboTaxol will induce cell apoptosis due to DNA lesion and cell cycle blockade which will induce a more discrete cell-death of $CD11b^+Ly6G^+$ cells. The difference in the way these 2 drugs deplete $CD11b^+Ly6G^+$ cells might explain the discrepancy in TCF1 expression in $CD8^+$ T cells. Hence, the changes in these 2 population proportions could be linked. More importantly, anti-GR1 does not synergise with the vaccine, hence, the increase of TCF1 expression in $CD8^+$ T cells, observed only after CarboTaxol, could be an explanation for the better induction of the vaccine response which results in a higher immunogenicity and a better tumour control.

We also explored the central memory and effector memory states of $CD8^+$ and $CD4^+$T cells. We only noticed a mild effect of CarboTaxol on central and effector memory cell expansion in the TME of tumour bearing mice (fig 4.16). Interestingly in tumour free mice, chemotherapy induces the expansion of central memory $CD8^+$ and $CD4^+$T cells in the spleen and BM, at day 4 post treatment (fig 4.19). This could indicate that memory $CD8^+$ and $CD4^+$T cells after chemotherapy treatment are more prone to be re-activated and expanded.

4.8.2 CarboTaxol is an adjuvant for viral vector vaccines

Given the effects of CarboTaxol on T cells in tumour free mice, we evaluated the impact of the combination of CarboTaxol with ChAdOx1/MVA on the vaccine-induced T cell response. The magnitude of P1A-specific $CD8^+$ T cells was significantly higher after vaccine combination with CarboTaxol compared to vaccine alone (fig 4.24). Interestingly,

this effect was observed not only post-prime but also post boost, 6 weeks after CarboTaxol injections. This synergy was also observed in C57BL/6 mice (fig 4.30). These data confirm that CarboTaxol promotes a better priming of the T cell response by ChAdOx/MVA vaccination. According to the Oxford languages and google dictionary, an adjuvant is "*a substance that enhances the body's immune response to an antigen".* Therefore, CarboTaxol can be considered as an adjuvant for our vaccine platform. Interestingly, CarboTaxol was able to deplete granulocytes recruited by the viral vector platform itself. However, this was neither detrimental to nor beneficial for the synergistic effect observed (fig 4.29 and fig 4.30). Finally, it is possible that CarboTaxol could have an adjuvant role with other vaccine platforms. Whether this adjuvant effect is limited to viral vector vaccines or can be extended to other vaccine platforms will need to be further explored.

Importantly, CarboTaxol had to be given together with the prime viral vector vaccine (or up to 48h before) to promote a better priming of the CD8 T cells. Indeed, if the ChAdOx1-P1A prime and the chemotherapy were given 7 days apart, the synergistic effect on the P1A-specific immune response was lost. Interestingly, CarboTaxol can also promote a better boosting of the immune response if given together with the boost (fig 4.25). These data highlight the importance of the timing of administration of CarboTaxol, relative to the vaccines timing, to benefit from its adjuvant function. Importantly, these findings are of major importance for future combination of chemotherapies and cancer vaccines in clinical trials, where the timing of administration will have to be planned according to the chemotherapy immunomodulatory action.

Given CarboTaxol's apparent adjuvant role, we investigated DC phenotypes at day 4 post treatment. Indeed, DCs are the main cell type involved in T cell priming and activation. Moreover, cDC1, a subset involves in $CD8^{+}$T cell priming, has been shown to

be activated after chemotherapy through ICD [130 206]. First, in our model, we did not notice any DC subset expansion (fig 4.26) in spleen and BM. However, we noticed an increase in the proportion of $CD80^+$ cells in cDC2 after chemotherapy in the spleen and BM of tumour free mice (fig 4.27 A,B). In terms of cell number, $CD80^+$ cDC2 were only expanded in the BM (fig 4.27 B). $CD80^+$ cDC1 were not expanded in the spleen (fig 4.27 C) and slightly in the BM, where they are present in very low numbers (fig 4.27 D). The spleen of tumour bearing mice was also investigated and although we observed a slight increase of $CD80^+$ cells in cDC2 after CarboTaxol, it was not significant (fig 4.27 E). cDC1 have been shown to be the main actors in $CD8^+$ T cell priming[228] and their expansion could have been a potential mechanism through which CarboTaxol synergises with the vaccine[24,228,258]. However, CarboTaxol seems to decrease systemic inflammation, which correlates with the expansion of cDC2 $CD80^+$ cells but not cDC1. cDC2 have been shown to activate preferentially $CD4^+$T cells and initiate T helper cell differentiation, including Th1[259,260]. Th1 have been shown to promote DC antigen presentation[56]. This could potentially also create a good environment for $CD8^+$ T cell priming. Hence, a role of $CD4^+$T cells in CarboTaxol adjuvant function cannot be excluded. Interestingly, we also observed an expansion of central memory $CD4^+$T cells which could be explained by the increase in cDC2 activation. However, the phenotype of these $CD4^+$T cells will have to be further defined to fully understand the role of cDC2 activation after CarboTaxol.

Although the mechanism through which CarboTaxol exert its adjuvant functions remain unclear, it seems that TCF1 expression or TCF1+ cell expansion is of importance for a better $CD8^+$ T cell priming. The cause-and-effect relationship between TCF1 and the enhanced vaccine-induced immunogenicity will have to be explore by targeting, repressing TCF1 expression. However, as TCF1 is a transcription factor and is complex to target *in vivo*, as it would be required in order to understand its function in the adjuvant effects of

chemotherapy. Indeed, monoclonal antibodies cannot be used to neutralise this factor, and no inhibitors of this transcription factor currently exist. Therefore, *Tcf7* knock out mouse models will be a vital tool to explore if the synergy between CarboTaxol and our vaccines is abolished when TCF1 cannot be induced.

4.8.3 Link between TCF1 expression and $CD11b^+Ly6G^+$ cell depletion

We further explored the potential link between TCF1 expression and $CD11b^+$ $Ly6G^+$ depletion. Indeed, if we could abolish the potential link between these two phenotypes, we could potentially elucidate their importance in CarboTaxol adjuvant effect. We have already concluded that the absence of $CD11b^+Ly6G^+$ cells is not sufficient for expanding TCF1 expressing CD8+ T cells. However, the way chemotherapy is killing $CD11b^+Ly6G^+$ cells might induce a decrease in inflammation. Indeed, it has been previously shown that macrophages/monocytes and DCs decrease their production of IL12/23(p40) when phagocytosing peripheral apoptotic granulocytes[251]. This is part of the mechanisms involved in resolution of inflammation[250]. In parallel, IL12/23(p40) has also been defined as an inhibitor of TCF1 expression through STAT4 induction in $CD8^+$ T cells[227]. Therefore, we hypothesized that IL12/23(p40) could be the link between the two phenotypes observed 4 days post CarboTaxol treatment: with a decrease of IL12/23(p40) due to $CD11b^+Ly6G^+$ cells phagocytosis, TCF1 expression would be induced in T cells and TCF1 expressing cells expanded. Very interestingly, in our model, the levels of IL12/23(p40) post CarboTaxol were significantly decreased compared to the control groups in the blood and spleen of tumour free and tumour bearing mice (fig 4.31). This was also observed in the TME at day 4 post treatment. In the blood, we observed a decrease in IL12/23(40) production by monocytes but not DCs (fig 4.33). However, DCs are rare in blood samples, hence it would be more interesting to evaluate IL12/23(p40) basal

production of DCs in the spleen and LNs. Collectively, these data were consistent with our hypothesis and the literature[251].

Regarding the decreased production of IL12/23(p40) by monocytes as well as the overall depletion of the p40 subunit in the blood, spleen and TME, we then explored if this decrease in p40 was the cause of TCF1 expression in T cells. To do so, we treated DBA/2 mice with anti-IL12/23(p40), an in vivo antibody that neutralises the p40 subunit. We compared it to the effect of CarboTaxol on TCF1 expressing cells. The anti-IL12/23(p40) significantly decreased the levels of p40 in the blood 4 days post treatment as assessed by ELISA (fig 4.34 B). Surprisingly, anti-IL12/23(p40) was not able to increase TCF1 expressing cells in $CD8^+$ T cells (fig 4.34 C). However, only 1 experiment was performed to test this regimen, and future experiments will explore different doses and time point to confirm the effect of IL12/23(p40) on TCF1 expression in our model. Alternatively, future experiments will also investigate mouse recombinant IL12/23(p40) injections together with CarboTaxol to assess if replenishing the levels of IL12/23(p40) could block the expression of TCF1 in $CD8^+$ T cells.

As expected, the anti-IL12/23(p40) antibody did not induce a depletion of $CD11b^+Ly6G^+$ cells together with the depletion of IL12/23(p40) in the system (fig 4.34 D). It is possible that both the $CD11b^+Ly6G^+$ depletion and the decrease in IL12/23(p40) are needed to induce TCF1 in $CD8^+$ T cells. Indeed $CD11b^+Ly6G^+$ cell depletion could induce other signals related to the resolution of inflammation and it is the integration of all these signals, with the decrease of IL12/23(p40), that will trigger TCF1 expression[227,250]. One other signal that has been related to the resolution of inflammation is WNT-3a secretion by macrophages after engulfment of hepatocytes debris. This resulted in the regeneration of hepatocytes[261]. Given that TCF1 expression can be triggered by WNT/β-Catenin

signalling, future experiments will investigate this pathway as a potential link between $CD11b^{+}Ly6G^{+}$ cell depletion and TCF1 expression or TCF1+ T cell expansion.

It is possible that the mechanism of $TCF1^{+}$ cell expansion is not related to IL12/23(p40) nor the $CD11b^{+}Ly6G^{+}$ depletion in our model. Indeed, CarboTaxol could have an impact on TCF1 expression by directly impacting its upstream pathway: the WNT/β-Catenin pathway. TCF4 complexed with β-Catenin has been shown to trigger *TCF7* (TCF1 gene) expression. Moreover, paclitaxel has been correlated with the induction of the β-Catenin pathway in chemotherapy-induced-peripheral-neuropathy[262] and has been shown to induce β-Catenin gene expression as well as regulating its translation[263]. Therefore LF3, an inhibitor of TCF4/β-Catenin complex will be tested together with CarboTaxol to investigate if it can block TCF1 expression in T cells. Another pathway that could be involved in TCF1 expression and $TCF1^{+}$ cell expansion is Notch. Notch1 and Notch3 have a major role in thymic development through the induction of TCF1[264–266]. Similarly, paclitaxel has been shown to induce neuropathic pain that can be prevented in rats with DAPT, a notch inhibitor[267]. Notch inhibitors will also be tested in combination with CarboTaxol to decipher whether the mechanism upstream of TCF1 expression and/or $TCF1^{+}$ cell expansion involves Notch activation.

Chapter V: Translational aspect of the triple combination therapy: emphasis on the importance of timing of treatment

5.1 Introduction

In many cases, fundamental clinical science theories and also new clinical strategies are first evaluated and understood in animal models. However, testing these new clinical strategies in animal models is challenging. One major issue is the complexity in translating the timing, doses but also relative windows of treatments into human patients. Indeed, in mice, it is possible to explore, change and choose the timing of the treatments tested. When it comes to translating these new strategies in patients, there is less flexibility to build clinical protocols, due to ethical and technical regulations. Indeed, for obvious ethical reasons, patients are entitled to the standard of care already in place, which can be challenging to incorporate into the new strategy. Furthermore, when combining and testing immunomodulatory agents, such as with the triple combination tested in this project, changing the timing of one of the treatments could impact the synergistic effects observed. Therefore, it is important to adapt and test the schedules of the triple combination of treatments to a new regimen that are similar to the clinical protocol.

Our vaccines are now in clinical testing in lung cancer patients in the setting of the triple combination of treatments[268]. Vaccines targeting both MAGE-A3 and NYESO-1 will be combined with pembrolizumab (anti-PD1) and CarboTaxol. Pembrolizumab and CarboTaxol treatments are already part of the standard of care (SoC) given to NSCLC patients. More precisely, the standard of care is composed of 6 cycles of CarboTaxol given 3 weeks apart with pembrolizumab starting at the first cycle of CarboTaxol, and also given every 3 weeks. The ChAdOx1/MVA vaccination will be added to this SoC treatment. As an inclusion criterion, patients will have to be tested positive for MAGE-A3, with or without NYESO-1 expression, before they can be vaccinated. Therefore, the standard of care will start prior to vaccination while the patients' entry in the clinical trial will be evaluated. These patients will then receive the ChAdOx1/MVA vaccines expressing

MAGE-A3 and NYESO-1. Yet, as shown in chapter III, anti-PD1 function in the triple combination is to sustain the immune response triggered by vaccination. Hence, giving anti-PD1 prior to the vaccine seems counter-intuitive and will be tested in mice and discussed in this Chapter.

An immune response involves several actors (e.g. cells, receptors, chemokines and cytokines) which are all finely regulated in time and space in order to create an efficient immune response [269]. Immunomodulatory therapies can act on these actors, which act in a define window of time to mount an immune response. This makes the therapeutic window of each therapy particularly important when it comes to create an efficient immune response. In our setting, chemotherapy, anti-PD1 and viral vector-based vaccines synergise together for a better tumour control and vaccine response. Changing the timing of one of the therapies tested could decrease or dampen each therapy's intrinsic effects as well as impacting potential synergistic effects. Indeed, the importance of the relative timing of immunomodulatory therapies has already been highlighted. In 2019, the use of anti-PD1 treatment before vaccination has been shown to induce sub-primed $CD8^+$ T cells in mice[211]. $CD38^+PD1^+$ $CD8^+$ T cells, defined as sub-primed T cells, were more prone to apoptosis and display less activation and central memory and effector memory phenotype. The impact of CD38 expression in $CD8^+$ T is not fully understood but has been previously related to pathological functions in HIV[270] and lupus patients[271]. These cells were the cause of the loss of synergy of treatment between anti-PD1 and the vaccine. Indeed, a synergy between vaccination and anti-PD1 was observed only when the anti-PD1 was given after the vaccination [211].

Similarly, the timing of chemotherapy could potentially impact the synergistic effect observed in cancer patients, as shown in chapter IV, the adjuvant function of

CarboTaxol was observed only when given at the same time point as the prime or the boost vaccination. In parallel, modulating the dose and frequency of chemotherapy has been shown to be efficient in decreasing adverse effects together with inducing potential immunostimulatory effects [137,272].

In the context of an anti-tumour response, the phenotype of $CD8^+$ T cells can directly impact the response to a particular treatment such as CPIs. TCF1 expression in T cells has been correlated with better response to checkpoint blockade[121] and good prognosis in cancer patients[62,273]. In chapter IV, we highlighted that chemotherapy induces TCF1 expression in $CD4^+$and $CD8^+$ T cells as well as triggers an expansion of $CD4^+$and $CD8^+$ $TCF1^+$ T cells in both tumour free and tumour bearing mice. Therefore, we were particularly interested in observing the effect of CarboTaxol on TCF1 expression in immune cells treated with a new schedule of the triple combination where anti-PD1 will be given prior to the vaccine. Lastly, because translating the dose of chemotherapy between mouse studies and human patients is challenging. We were particularly interested to see whether CarboTaxol effect on TCF1 was observable in cancer patients. Moreover, TCF1, encoded by *TCF7*, is highly conserved between species. Similarly, the signalling pathways upstream this transcription factor, such as Notch1 and WNT/b-Catenin pathways[274–276], are also extremely conserved between species. Hence, we studied TCF1 expression in the blood and tumours of ovarian cancer patients after being treated with MTD of Carboplatin and Paclitaxel. To do so, available RNA-seq data from blood at baseline and after the third cycle of CarboTaxol and paclitaxel treatment were evaluated [145].

5.2 Chapter aims

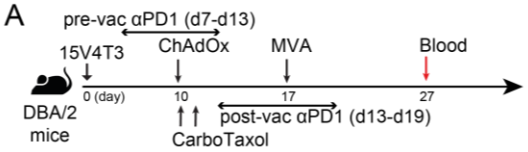
- Investigate a new administration regimen with anti-PD1 prior to vaccination, which corresponds to the schedules that are testing in the clinical trial.
- Investigate the impact of CaboTaxol on this new triple combination schedule, particularly its effect on TCF1 expression in $CD8^+$ T cells.
- Investigate the impact of Carboplatin and Paclitaxel on ovarian cancer patient blood samples.

5.3 Investigating different time points for anti-PD1 treatment

5.3.1 Tumour control and survival upon different time points of anti-PD1 treatment combined with ChAdOx/MVA and CarboTaxol

In this chapter, we aim to mimic the treatment schedule that is testing in the clinical trial NCT04908111. Especially focusing on a new therapeutic window for the anti-PD1 treatment, which will be given prior to the vaccination in cancer patients. Therefore, we treated tumour bearing DBA/2 mice with anti-PD1 prior to the vaccine. Indeed, 2 injections were given prior to the prime, and one after, every third day for a total of 3 i.p injections. This new schedule was compared with a post-prime schedule of anti-PD1 treatment, starting 2 days post-prime (d13) for 3 injections every third day. Mice were vaccinated on

A



B

Days of treatment / Groups	7	10	11	13	16	17	19
Control	Isotype control	Isotype control+ ChAdOx1-DPY	-	Isotype control	-	MVA-DPY	-
Pre-vac αPD1	Anti-PD1	Anti-PD1+PBS	-	Anti-PD1	-	PBS	-
Vaccine	Isotype control	Isotype control ChAdOx1-li-P1A	-	Isotype control	-	MVA-tpA-P1A	-
Vaccine+chemo	-	ChAdOx1-li-P1A+ Carboplatin+paclitaxel	paclitaxel	-	-	MVA-tpA-P1A	-
Vaccine+ pre-vac αPD1	Anti-PD1	Anti-PD1+ ChAdOx1-li-P1A	-	Anti-PD1	-	MVA-tpA-P1A	-
Vaccine+ post-vac αPD1	-	ChAdOx1-li-P1A	-	Anti-PD1	Anti-PD1	MVA-tpA-P1A	Anti-PD1
Triple pre-vac αPD1	Anti-PD1	Anti-PD1+ChAdOx1-li-P1A+Carboplatin+paclitaxel	paclitaxel	Anti-PD1	-	MVA-tpA-P1A	-
Triple post-vac αPD1	-	ChAdOx1-li-P1A+Carboplatin+paclitaxel	paclitaxel	Anti-PD1	Anti-PD1	MVA-tpA-P1A	Anti-PD1

Figure 5.1 Timeline and treatment groups for the evaluation of the pre-vac anti-PD1 new regimen in 15V4T3 tumour model. (A) DBA/2 mice were implanted with $1x10^6$ 15V4T3 cells via s.c injections to initiate tumour growth. 7 days after tumour implantation, some mice were treated with the pre-vac anti-PD1 regimen for 3 i.p injections. 10 days after tumour implantation, mice were vaccinated via i.m with 10^7 IU of ChAdOx1-li-P1A (ChAdOx) or PBS sham and treated with carboplatin(40mg/kg) and paclitaxel (20mg/kg) and 24h later with paclitaxel (20mg/kg) via i.p. The mice were then vaccinated with 10^6 PFU of MVA-tpA-P1A or PBS sham 1 week later. To control the pre-vac anti-PD1 regimen, some mice were treated with 100μg of anti-PD1 every third day for 3 i.p injections, starting on day 13, referred here as post-vac anti-PD1. Mice were randomised into 8 different groups based on tumour volume (as measured on day 10) and injected with the relevant treatments indicated in table B.

day 10 post tumour implantation and treated with CarboTaxol on the same day and 24h later (fig 5.1 A,B). Tumour growth and survival were assessed.

Interestingly, the new schedule of anti-PD1(pre-vac) did not synergise with the vaccine. This group showed similar tumour control (fig 5.2 B,C) and survival (fig 5.3) than the vaccine alone. The anti-PD1 given post-vaccination (post-vac) showed a better tumour control than the vaccine alone (fig 5.2 B, C), indicating its ability to synergise with the vaccine. Very interestingly, both the triple combination groups with anti-PD1 pre-vac

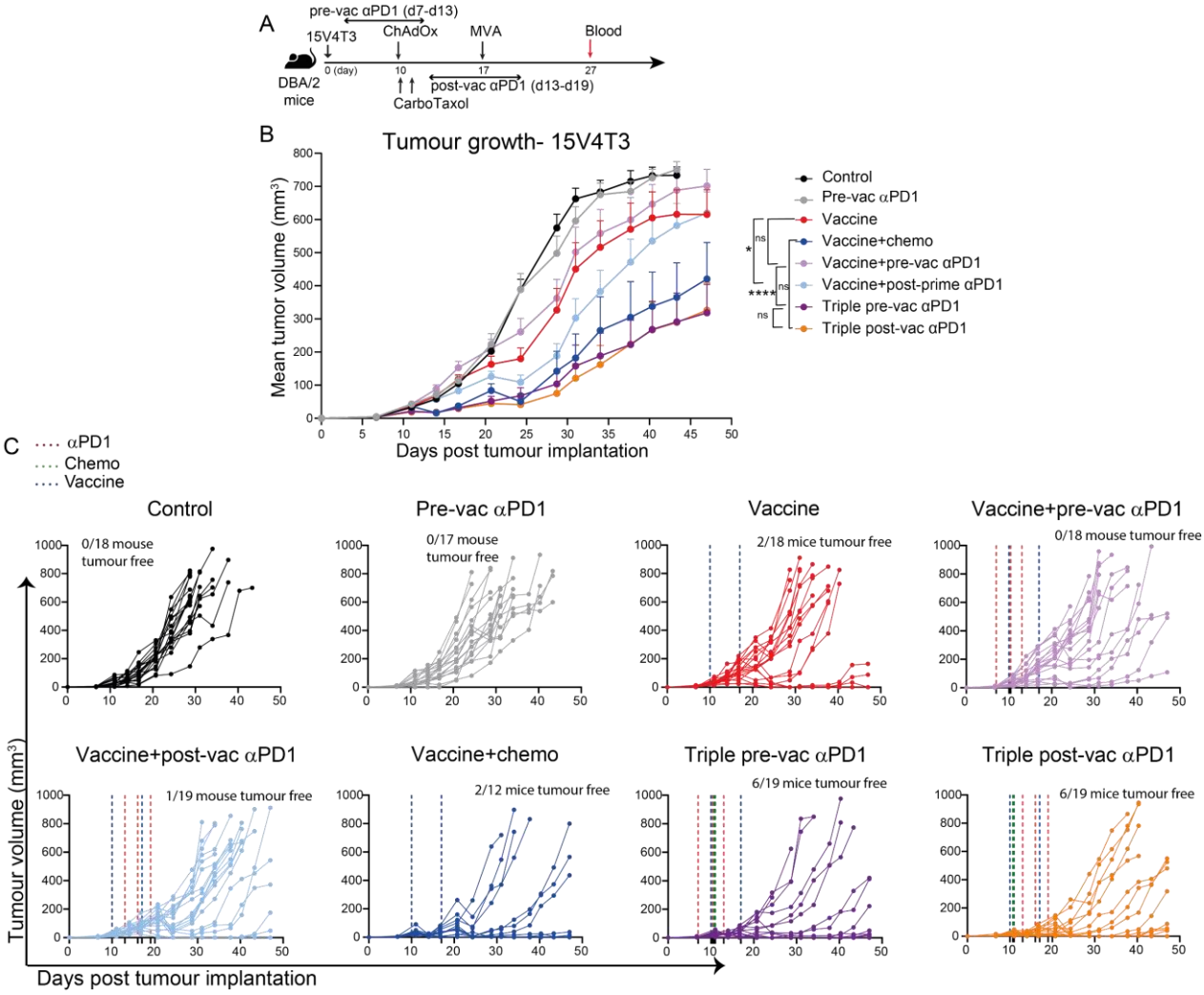


Figure 5.2 The pre-vac anti-PD1 treatment improves tumour growth control only when combined with CarboTaxol+ChAdOx1/MVA-P1A vaccination in 15V4T3 tumour bearing DBA/2 mice.
DBA/2 mice were implanted with $1x10^6$ 15V4T3 cells via s.c injections to initiate tumour growth and treated according to the schedules presented in (A). (B) Mean tumour growth data are pooled from 3 independent experiments and are presented as mean tumour volume (mm3) ± SEM. Individual tumour growth for each group is shown in (C). Each curve represents an individual mouse (n= 18 to 19 mice per groups). Statistically significant differences between groups were determined by a two-way ANOVA followed by Tukey's post hoc test, *, $p \leq 0.05$, ***, $p \leq 0.001$, ****, $p \leq 0.0001$.

showed a similar tumour control than the triple post-vac anti-PD1 (fig 5.2 B,C). Indeed, both groups showed six tumour free mice out of 19 mice while only one mouse out of 19 was tumour free in the vaccine+post-vac anti-PD1 group and no mice was able to clear its tumour in the vaccine+pre-vac anti-PD1 group (fig 5.2 C). Ultimately the vaccine+chemo group displayed a good tumour control, similar to the triple combination groups, which again emphasises the importance of the synergistic effect between the vaccine and chemotherapy in our model. Of note, only 16% of mice clear their tumours in vaccine+chemo group whilst 33% tumour clearance was observed in both triple combination group, potentially pointing the importance of the anti-PD1 addition. Altogether a good synergistic effect in both triple combinations was observed regardless of the timing of anti-PD1, with a major effect due to the addition of CarboTaxol. Therefore, we hypothesize that CarboTaxol rescues the loss of synergy observed in the vaccine+pre-vac anti-PD1, promoting a better tumour control (fig 5.2 B), as good as our original triple combination group. Furthermore, both triple combinations showed similar survival,

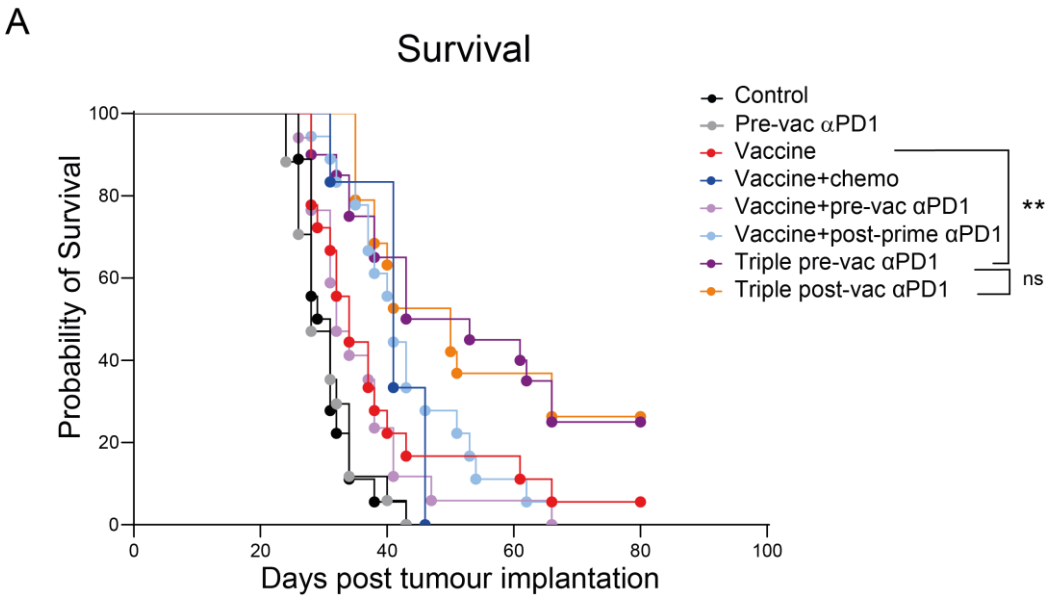


Figure 5.3 The pre-vac anti-PD1 treatment improves mouse survival only when combined with CarboTaxol+ChAdOx1/MVA-P1A vaccination in 15V4T3 tumour bearing DBA/2 mice.
DBA/2 mice were implanted with $1x10^6$ 15V4T3 cells via s.c injections to initiate tumour growth and treated according to the schedules presented in figure 5.1. Percentage of mouse survival in each group is shown in (A). Data are pooled from 3 independent experiments (n= 18 to 19 mice per groups). Statistical differences in mouse survival were determined by a Log Rank test, **, $p \leq 0.01$.

emphasising the fact that CarboTaxol rescues the synergy of the triple combination with pre-vac anti-PD1 (fig 5.3).

5.3.2 Evaluating the impact of anti-PD1 treatment timing on the magnitude of the P1A specific response

We then evaluated the effect of different anti-PD1 administration time points on the magnitude of the immune response against the P1A antigen. PBMCs were harvested 9 to 10 days post boost and stimulated for 5 hours with P1A peptides. The magnitude of the P1A-specific $CD8^+$ T cell response was evaluated in regard of the IFNγ production in response to P1A peptide stimulation. The magnitude of IFNγ-producing $CD8^+$ T cell was similar between vaccine and vaccine given with pre-vac anti-PD1, correlating with what was observed in terms of the tumour control and survival data. As previously observed, the vaccine+post-vac anti-PD1 and vaccine+CarboTaxol displayed higher immunogenicity than the vaccine alone. Interestingly, both triple combinations showed a significantly

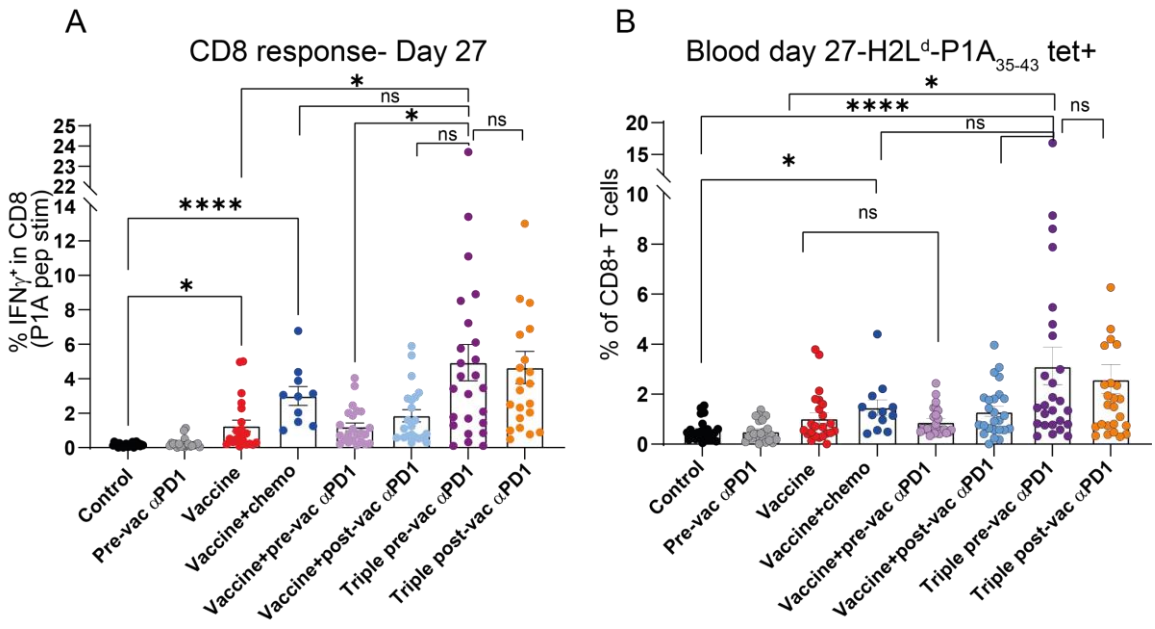


Figure 5.4 The pre-vac anti-PD1 treatment increases P1A-specific $CD8^+$ T cells only when combined with CarboTaxol+ ChAdOx1/MVA-P1A vaccination in 15V4T3 tumour bearing DBA/2 mice. Blood from mice treated with the schedules represented in figure 5.1 was harvested on day 27 post tumour implantation, and total PBMCs were stimulated with P1A peptides for 5h. The levels of IFNγ producing $CD8^+$ T cells were determined. The proportion of P1A specific $CD8^+$ T cells is shown in (A). Alternatively, PBMCs were stained with H2Ld-P1A $_{35-43}$ tetramer. The level of $CD8^+$ tetramer$^+$ T cells are shown in (B). Each symbol represents an individual mouse and the means± SEM are shown. Data are pooled from 3 independent experiments (n= 9 to 24 mice per groups). Statistically significant differences between groups were determined by a Kruskal-Wallis test with Dunn's multiple comparisons test, *, $p \leq 0.05$, **, $p \leq 0.01$, ***, $p \leq 0.001$ ****, $p \leq 0.0001$.

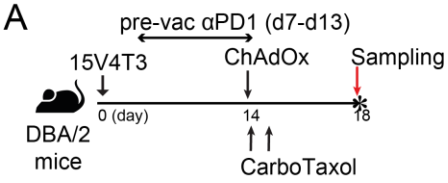
higher magnitude of P1A specific $CD8^+$ T cells compared to the vaccine alone (fig 5.4 A). In parallel, we assessed the binding of tetramer -$H2L^d$-$P1A_{35-43}$ on $CD8^+$ T cells, with $P1A_{35-43}$ being the more immunogenic epitope. In agreement with the peptide stimulation, the 2 triple combination groups showed the highest proportion of $tetramer^+$ $CD8^+$ T cells. Indeed, both showed a similar proportion, with 3% of $tetramer^+$ $CD8^+$ T cells on average, which was significantly higher than the vaccine alone (fig 5.4 B). This is in line with the tumour data and highlights the importance of CarboTaxol in rescuing the loss of synergy between pre-vac anti-PD1+vaccine.

5.4 Impact of CarboTaxol on the triple combination with pre-vac anti-PD1

5.4.1 CarboTaxol induces TCF1 expression in CD8$^+$ T cells regardless of the anti-PD1 treatment timing

TCF1 expression in CD8$^+$ T cells have been shown to promote the efficacy of anti-PD1 therapy [121]. In our model, we showed that CarboTaxol promoted TCF1$^+$ cell increase in CD8$^+$ and CD4$^+$T cells. Therefore, we explored whether CarboTaxol was able to impact TCF1 when anti-PD1 was given early, prior to the vaccine (pre-vac). DBA/2 tumour bearing mice were treated with CarboTaxol and vaccinated on day 14 post tumour implantation. Anti-PD1 therapy started at day 7 post tumour implantation and given 3 times every 3 days (fig 5.5). Tumour, spleen and blood were harvested 4 days post CarboTaxol.

A



B

Days of treatment / Groups	7	10	11	13
Control	Isotype control	Isotype Control+ PBS	-	Isotype control
Pre-vac αPD1	Anti-PD1	Anti-PD1+PBS	-	Anti-PD1
Chemo	-	PBS+ Carboplatin+paclitaxel	paclitaxel	-
Vaccine	Isotype control	Isotype control ChAdOx1-li-P1A	-	Isotype control
Vaccine+chemo	-	ChAdOx1-li-P1A+ Carboplatin+paclitaxel	paclitaxel	-
Vaccine+ pre-vac αPD1	Anti-PD1	Anti-PD1+ ChAdOx1-li-P1A	-	Anti-PD1
Triple pre-vac αPD1	Anti-PD1	Anti-PD1+ChAdOx1-li-P1A+Carboplatin+paclitaxel	paclitaxel	Anti-PD1

Figure 5.5 Timeline and treatment groups for harvest to investigate the pre-vac anti-PD1 new regimen in 15V4T3 tumour model. (A) DBA/2 mice were implanted with 1x10^6 15V4T3 cells via s.c injections to initiate tumour growth. 7 days after tumour implantation, some mice were treated with the pre-vac anti-PD1 regimen for 3 i.p injections. 14 days after tumour implantation, mice were vaccinated via i.m with 10^7 IU of ChAdOx1-Ii-P1A (ChAdOx) or PBS sham and treated with carboplatin(40mg/kg) and paclitaxel (20mg/kg) and 24h later with paclitaxel (20mg/kg) via i.p. On day 18, blood, tumour and spleen were harvested. Mice were randomised into 7 different groups based on tumour volume (as measured on day 10) and injected with the relevant treatments indicated in table B. Control, chemo, vaccine, vaccine+chemo groups were presented in chapter IV, the figures presented below are adapted from chapter IV, showing the new groups which will be discussed in this section.

In the TME, we noticed an increase in $TCF1^+$ cells and MFI in $CD8^+$ T cells in all the groups that received CarboTaxol. Therefore, the proportion of $TCF1^+$ cells in $CD8^+$ T cells as well as the total number of $TCF1^+CD8^+$ T cells were significantly expanded ed with the triple pre-vac anti-PD1 combination compared to the vaccine alone or the vaccine+pre-vac anti-PD1 groups (fig 5.6 A). Regarding the progenitor exhausted stem-like $CD8^+$ T cells, we also noticed a significant increase of this $TCF1^+PD1^+CD8^+$ T cells after chemotherapy in the TME (fig 5.6 B).

In the spleen and blood, we also noticed an increase of these $TCF1^+CD8^+$ T cells as well as the $TCF1^+PD1^+CD8^+$ T cells after chemotherapy (fig 5.7). Especially, pre-vac anti-$PD1^+$ vaccine displayed particularly low number of these two populations. This could potentially indicate that CarboTaxol promote the triple pre-vac anti-PD1 combination efficacy by rescuing these stem-like populations and progenitor exhausted stem-like cells, very important in promoting anti-tumour efficacy.

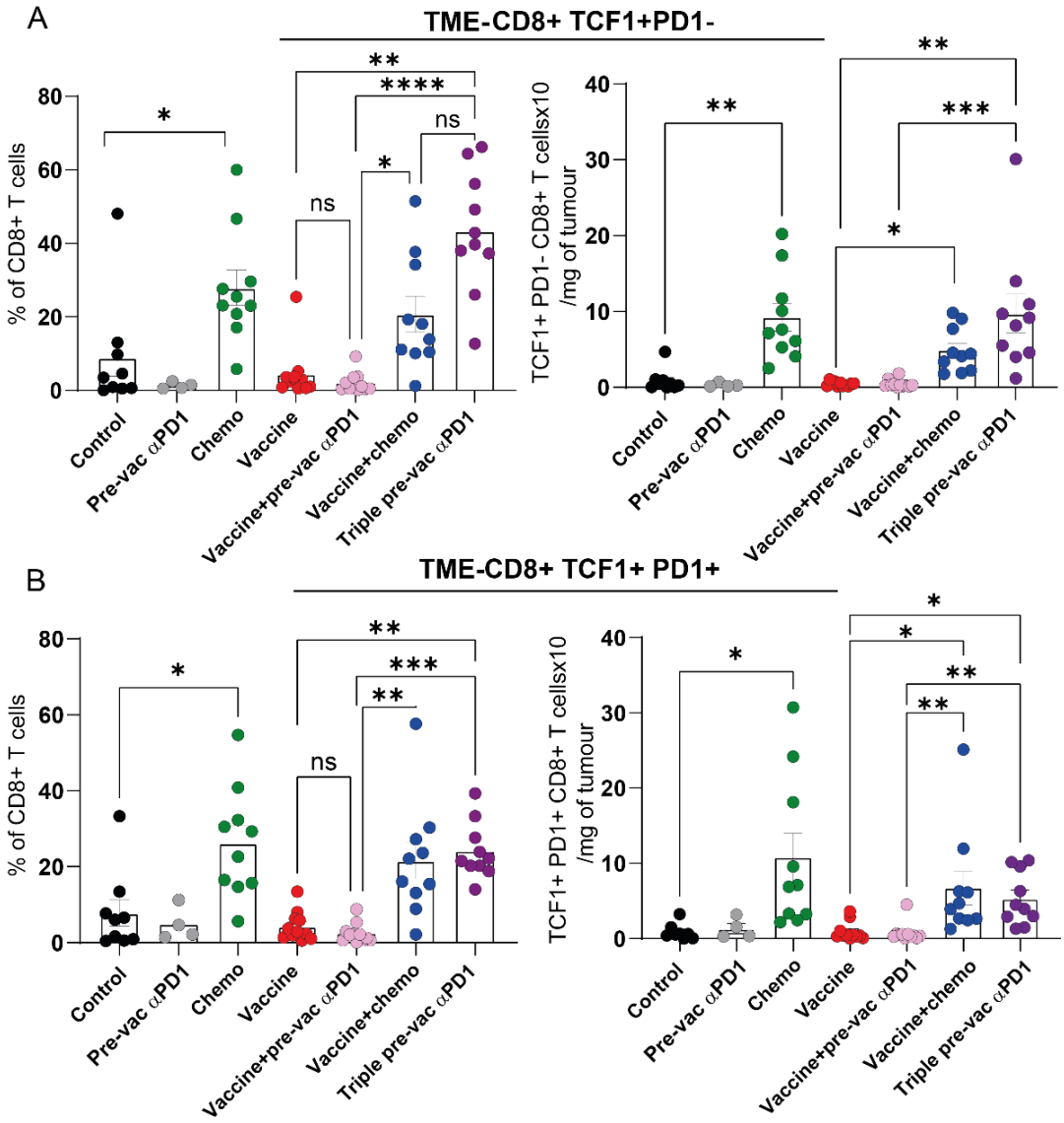


Figure 5.6 TME of mice treated with the triple combination with pre-vac anti-PD1 show expanded TCF1 expressing cells due to the CarboTaxol treatment. DBA/2 mice were implanted with $1x10^6$ 15V4T3 cells via s.c injections to initiate tumour growth. TME from mice treated with the schedules represented in figure 5.5 was harvested on day 18 post tumour implantation. The proportion and cell numbers of $CD8^+$ T cell expressing TCF1 are shown in (A). The proportion and cell numbers of $CD8^+$ T cells expressing both $TCF1^+PD1^+$ are shown in (B). the means± SEM are shown with each symbol representing an individual mouse and data are pooled from at least 2 independent experiments except the pre-vac αPD1 group (n= 4 to 12 mice per groups). Statistically significant differences between groups were determined by a Kruskal-Wallis test with Dunn's multiple comparisons test, **, $p \leq 0.01$, ***, $p \leq 0.001$ ****, $p \leq 0.0001$.

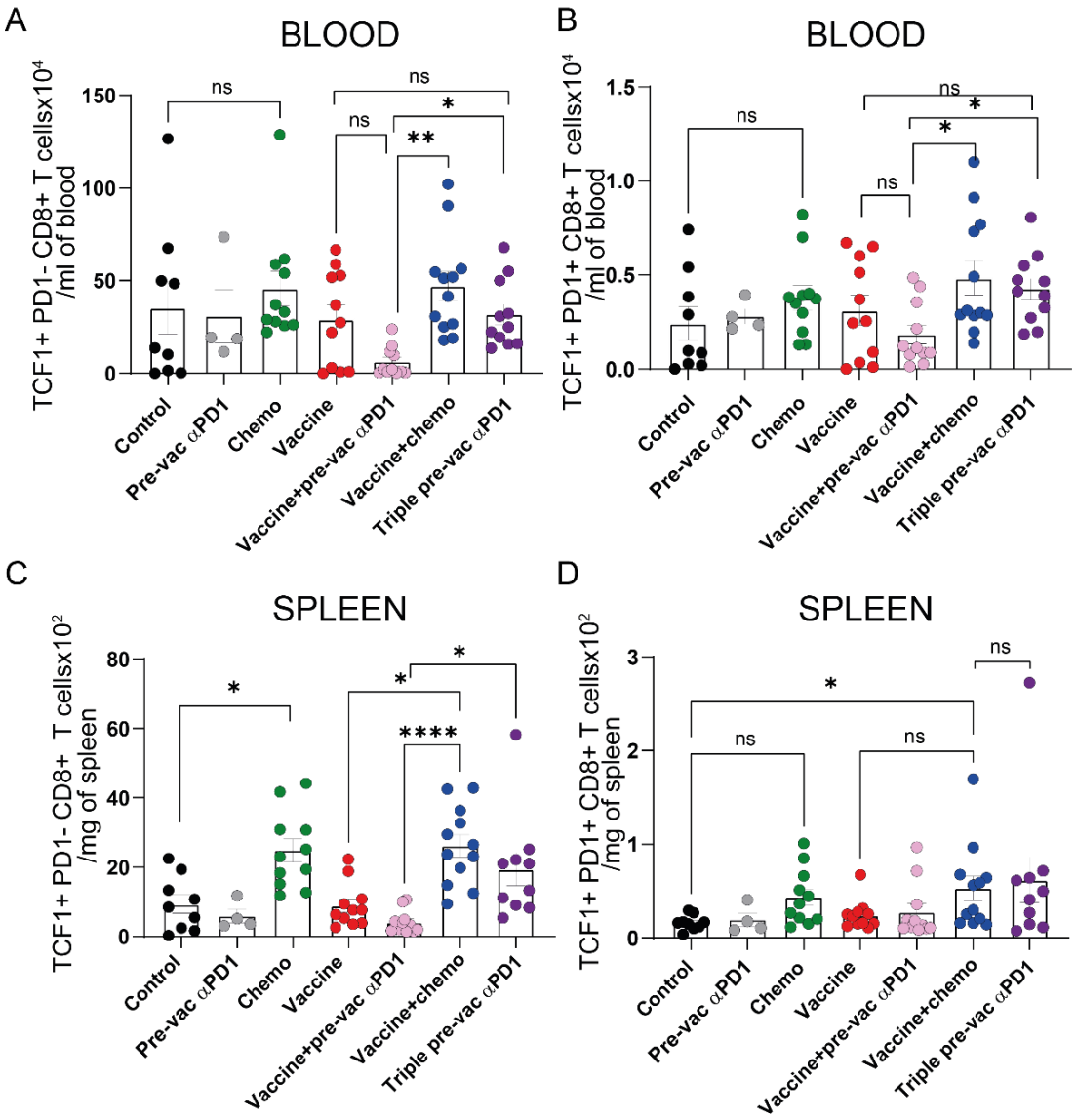


Figure 5.7 Mice treated with the triple combination with pre-vac anti-PD1 display increase of TCF1 expressing cells in the spleen and blood due to the CarboTaxol treatment.
DBA/2 mice were implanted with 1x10^6 15V4T3 cells via s.c injections to initiate tumour growth. Blood and spleen from mice treated with the schedules represented in figure 5.5 were harvested on day 18 post tumour implantation. In the blood, the cell numbers of CD8$^+$ T cell expressing TCF1 are shown in (A) whilst the cell numbers of CD8$^+$T cells double positive for TCF1 and PD1+ are shown in (B). In the spleen, the cell numbers of CD8$^+$ T cells expressing TCF1$^+$ are shown in (C) and expressing both TCF1$^+$PD1$^+$ are shown in (D). The means± SEM are shown with each symbol representing an individual mouse, and data are pooled from at least 2 independent experiments (n= 4 to 12 mice per groups). Statistically significant differences between groups were determined by a Kruskal-Wallis test with Dunn's multiple comparisons test, *, p ≤ 0.05, **, p ≤ 0.01, ****, p ≤ 0.0001.

5.4.2 Evaluation of potentially sub-primed CD8$^+$ T cells

It has previously been published that anti-PD1 prior to vaccination induces the co-expression of CD38$^+$ and PD1$^+$ on T cells[211], which have been defined to be mis-functioning sub-primed T cells. Indeed, CD38$^+$PD1$^+$ were more apoptotic and less prone

to produce IFNγ[211]. Therefore, we analysed the level of $CD38^+PD1^+CD8^+$ T cells in all the groups. Very interestingly, and comparably to what have been published, we observed an expansion of $CD38^+PD1^+$ cells after the pre-vac anti-PD1 regimen alone in the TME (fig 5.8 B). Similarly, when pre-vac anti-PD1 was given in combination with the vaccine, the numbers of $CD38^+PD1^+$ $CD8^+$ T cells were also significantly higher compared to the vaccine alone group in the TME (fig 5.8 B). Surprisingly, CarboTaxol also seemed to promote the expansion of $CD38^+PD1^+$ T cell population in the TME. Indeed, we saw significantly higher numbers of $CD38^+PD1^+CD8^+$ T cells after CarboTaxol and CarboTaxol+vaccine compared to the vaccine alone or control groups (fig 5.8 A, B). We could hypothesise that it is the expression of these 2 markers without TCF1 that promote mis-functioning T cells, leading to the generation of sub-primed $CD8^+$ T cells. Indeed, the absence of synergistic effects were observed in the vaccine+pre-vac anti-PD1 but not the vaccine+chemo. Finally, this expansion occurs only in the TME after pre-vac anti-PD1 or CarboTaxol but was not observed in the spleen (fig 5.8 D). Only one outliner was observed in the vaccine+pre-vac anti-PD1 group in the spleen and the average number of $CD38^+PD1^+$ $CD8^+$ T cells was not significantly higher than the vaccine alone groups (fig 5.8 D).

Very interestingly, when CarboTaxol was combined with pre-vac anti-PD1 and vaccine, the $CD38^+PD1^+CD8^+$ T cells were not expanded (fig 5.8 A,B). Moreover, within the expanded $TCF1^+PD1^+CD8^+$ T cells in the TME due to chemotherapy, the proportion of $CD38^+$ expressing cells was significantly reduced in the triple combination group compared to the vaccine+chemo group (fig 5.8 C). We could hypothesise that it is the combination of CarboTaxol given together with anti-PD1 that stop this expansion of $CD38^+PD1^+$ sub-primed T cells in the TME whilst still inducing stem-like $TCF1^+$ T cells in the TME, blood and spleen. Moreover, the CD38 negative stem-like $TCF1^+PD1^+CD8^+$ T cells might stay

more competent in the TME and promote a better tumour control than $CD38^+$ stem-like $CD8^+$ T cells, observed in the vaccine+CarboTaxol group.

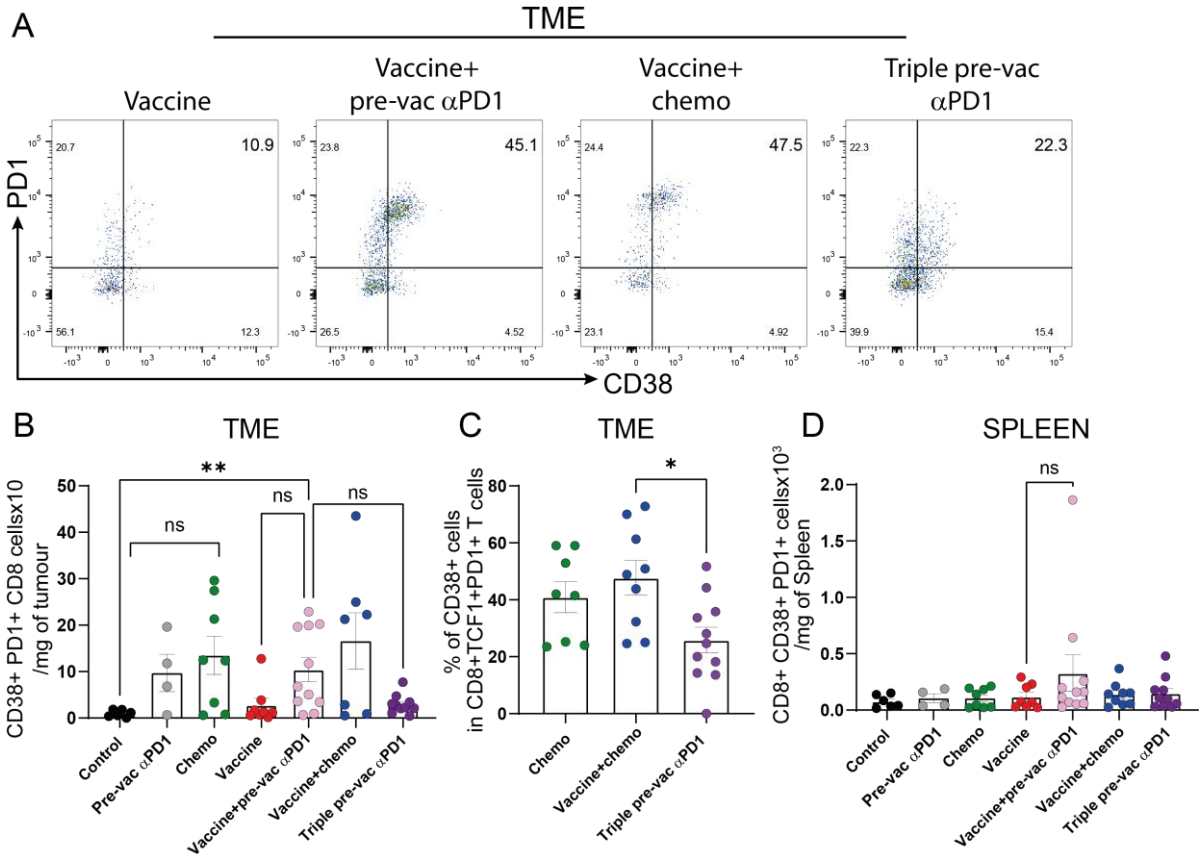


Figure 5.8 Pre-vac anti-PD1 expands $CD38^+PD1^+$ $CD8^+$ T cells in the TME of tumour bearing mice. DBA/2 mice were implanted with $1x10^6$ 15V4T3 cells via s.c injections to initiate tumour growth. TME and spleen from mice treated with the schedules represented in figure 5.5 were harvested on day 18 post tumour implantation. In the TME, the gating strategy of $CD8^+$ T cells double positive for $CD38^+$ and $PD1^+$ and differences between the different vaccinated groups are shown in (A). The cell numbers of $CD38^+PD1^+$ $CD8^+$T cells are shown in (B). The proportion of cells expressing CD38 within the expanded $TCF1^+PD1+$ $CD8^+$T cells in the TME is shown in (C). In the spleen, the cell numbers of $CD38^+PD1^+$ $CD8^+$ T cells are shown in (D). The means± SEM are shown with each symbol representing an individual mouse. Data are pooled from at least 2 independent experiments (n= 4 to 11 mice per groups). Statistically significant differences between groups were determined by a Kruskal-Wallis test with Dunn's multiple comparisons test, *, $p \leq 0.05$, **, $p \leq 0.01$.

5.4.3 Depletion of Ly6G$^+$ CD11b$^+$ cells occurs in the new regimen of triple combination of treatments

The depletion of CD11b$^+$Ly6G$^+$ has been one consistent phenotype observed after CarboTaxol treatment, in both tumour free and tumour bearing mice. This phenotype was observed early on (from day 3 to day 6) post chemotherapy. Therefore, we asked if this depletion was observed when CarboTaxol was combined with vaccine and pre-vac anti-PD1. After 4 days, we harvested blood, tumour and spleen. As previously observed, CarboTaxol induced CD11b$^+$Ly6G$^+$ cell depletion in these 3 organs. This depletion was significant in the triple pre-vac anti-PD1 combination compared to vaccine+pre-Vac or vaccine alone group, in the TME (fig 5.9 A), spleen (fig 5.9 B) and blood (fig 5.9 C). Interestingly, in the TME, we observed a slight increase of CD11b$^+$Ly6G+, potential PMN-MDSCs, after pre-vac anti-PD1 only or vaccine+pre-vac anti-PD1, although it was not significant compared to the control and vaccine alone groups (fig 5.9 A).

We cannot exclude the possibility that CarboTaxol rescues vaccine+pre-vac anti-PD1 synergy due to this PMN-MDSC depletion.

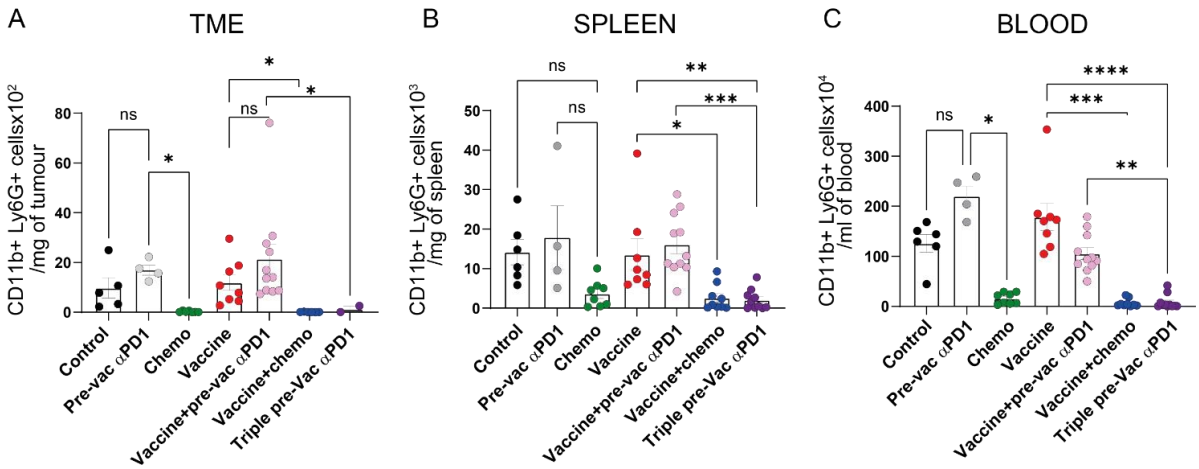


Figure 5.9 CD11b+Ly6G+ cells are depleted in the triple combination with pre-vac anti-PD1.
DBA/2 mice are implanted with 1x10^6 15V4T3 cells via s.c injections to initiate tumour growth. TME, blood and spleen from mice treated with the schedules represented in figure 5.5 were harvested on day 18 post tumour implantation. The numbers of CD11b$^+$Ly6G$^+$ cells in the TME (A), the spleen (B), and blood (C) are shown. The means± SEM are shown with each symbol representing an individual mouse. Data are pooled from at least 2 independent experiments (n= 4 to 12 mice per groups). Statistically significant differences between groups were determined by a Kruskal-Wallis test with Dunn's multiple comparisons test, *, $p \leq 0.05$, **, $p \leq 0.01$, ****, $p \leq 0.0001$.

5.5 *TCF7* expression is increased after 3 cycles of Carboplatin and Paclitaxel in ovarian cancer patients

The translation of doses of chemotherapy from murine models to patients is particularly challenging. Cancer patients are usually treated with the maximum tolerated dose (MTD) given in multiple cycles while, in our mouse model, we used one cycle of CarboTaxol at a dose that could be considered as intermediate. Because chemotherapy effects are dose dependent, we were interested in evaluating whether the effect of CarboTaxol on $TCF1^+$ cells was conserved in patients. We explored this question by using available single cell RNA-sequencing data from epithelial ovarian cancer patient pre- and post- platinum-based chemotherapy. No available data were found in lung cancer patients. In the study "*Improved T-cell Immunity Following Neoadjuvant Chemotherapy in Ovarian Cancer"*, published in 2022, blood of epithelial ovarian cancer patients was investigated at baseline and post 3rd cycle of carboplatin and paclitaxel (fig 5.10 A). With the help of Ashwin Jainarayanan, DPhil student and Dr Vineethkrishna Chandrasekar, who re-analysed the single-cell RNA-sequencing data, we investigated the expression of *TCF7* (TCF1 gene) in T cells. We compared the proportion of $CD8^+$ and $CD4^+$T cells expressing *TCF7* as well as *PDCD1* (PD1 gene). Very interestingly, we observed $CD8^+$ T cell expansion after 3rd cycle of Carboplatin and paclitaxel (C3), although not significant (fig 5.10 B). Furthermore, a significant expansion of $TCF7^+$ $CD8^+$ T cells was observed after C3 compared to baseline (fig 5.10 C). Although a slight increase in $TCF7^+$ $PDCD1^+$ $CD8^+$ T cells was observed, it was not significant (fig 5.10 D). We did not observe CD4 expansion nor increased in $TCF7^+$ and $PDCD1^+$ $CD4^+$T cells (fig 5.10 E,F,G). These data are in line with the phenotype observed in DBA/2 mice after CarboTaxol treatment where the $CD8^+TCF1^+$ T cells were expanded. Finally, the average *TCF7* expression level in $CD8^+$ T cells was significantly higher after C3 than baseline (fig 5.10 H) whilst the level of average *TCF7* expression in $CD4^+$T cells was significantly lower after chemotherapy (fig 5.10 H).

We acknowledged that these data set includes only five patients hence, any conclusion must be taken cautiously. However, it seems that Carboplatin and paclitaxel have an impact on *TCF7* expression in epithelial ovarian cancer patients' $CD8^+$ T cells. Indeed, *TCF7* expression was significantly higher in $CD8^+$ T cells. Moreover, *TCF7* expressing $CD8^+$ T cells were significantly expanded, such as what observed in mice, after platinum-based chemotherapy in epithelial ovarian cancer patients.

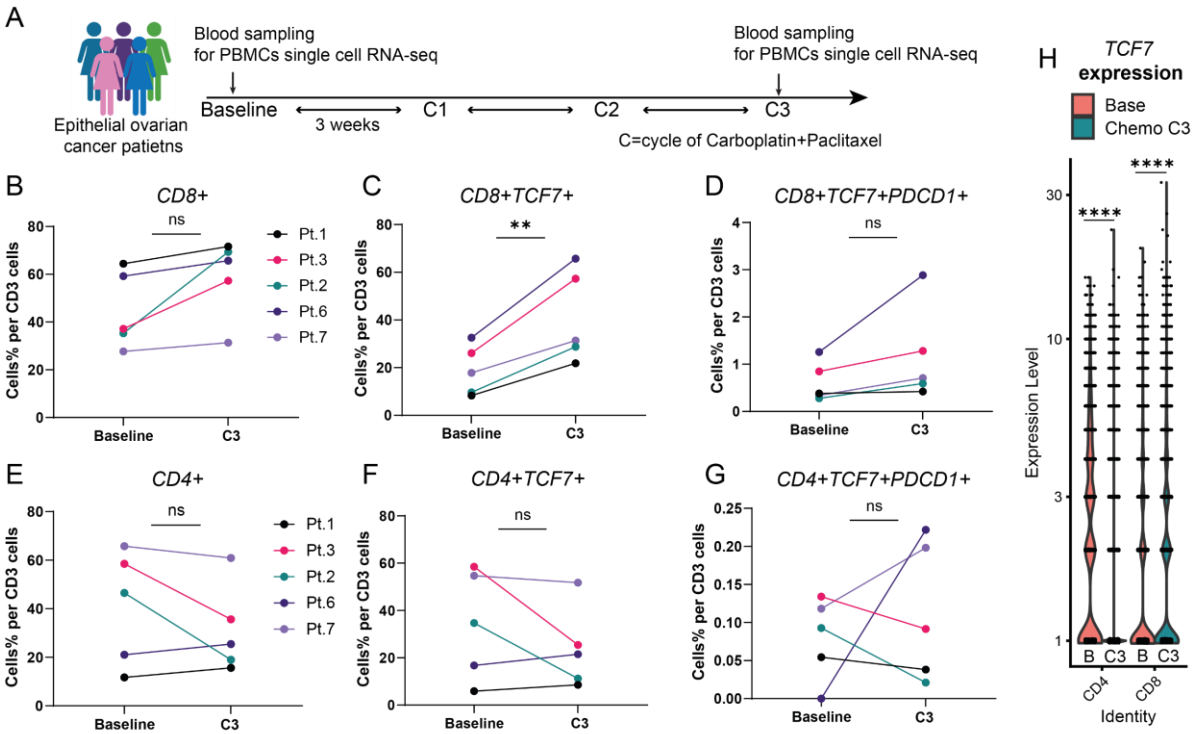


Figure 5.10 Carboplatin and paclitaxel increase TCF1 expression in epithelial ovarian cancer patients. Patients' blood was collected at baseline and after 3 cycles of chemotherapy (C3) as presented in (A), scheme was adapted from the scheme presented in *Improved T-cell Immunity Following Neoadjuvant Chemotherapy in Ovarian Cancer,Liu et al.,2022*. Single cell RNA-sequencing was performed on total PBMCS. The available dataset was kindly given to us and reanalysed to investigate *TCF7* expression in $CD8^+$ and $CD4^+$T cells. (B) comparison of $CD8^+$ T cell proportion at baseline and after C3 is shown. The comparison of the proportion of *TCF7* expressing $CD8^+$ T cells is shown in (C). The comparison between baseline and C3 concerning *TCF7*$^+$ *PDCD1*$^+$ (gene for PD1) $CD8^+$ T cells is shown in (D). (E) The comparison of $CD4^+$ T cell proportion at baseline and after C3 is shown. The comparison of the proportion of *TCF7* expressing $CD4^+$ T cells is shown in (F). The comparison between baseline and C3 concerning *TCF7*$^+$ *PDCD1*$^+$ $CD4^+$ T cells is shown in (G). After testing for normality for the graphs presented in (B) to (G). Statistically significant differences between groups were determined by a paired t test, **, $p \leq 0.01$. The expression level of *TCF7* in CD4 and $CD8^+$ T cells is shown in (H). for (H) Statistically significant differences between groups were one-sided Wilcoxon rank sum test****, $p \leq 0.0001$

We were then particularly interested in the phenotype of these *TCF7*$^{+}$ CD8^{+} T cells and investigate whether the increased expression of *TCF7* concerns only some CD8^{+} T cell subsets. Indeed, in mice, we observed a significant central memory expansion in tumour free mice. Therefore, we evaluated if *SELL*$^{+}$ (CD62L gene) and *CD44*$^{+}$ (gene for CD44) expressing CD8^{+} T cells showed an increase *TCF7* expression. CD8^{+} T cells were separated in twelve sub-clusters based on expression profile (fig 5.11 A). Among these subclusters, it seemed that *TCF7* expression were significantly increased after C3 in subsets 0, 2, 5, and 10 (fig 5.11 B,C). Among these four clusters, clusters 2 and 10 were co-expressing *CD44*$^{+}$ and *SELL*$^{+}$, indicating central memory characteristics (fig 5.11 D). Cluster 5 was showing naïve phenotype while cluster 0 showed neither of these three phenotypes (fig 5.11 D). It is possible that cycles of CarboTaxol induce central memory CD8^{+} T cells through the expression of *TCF7*[58].

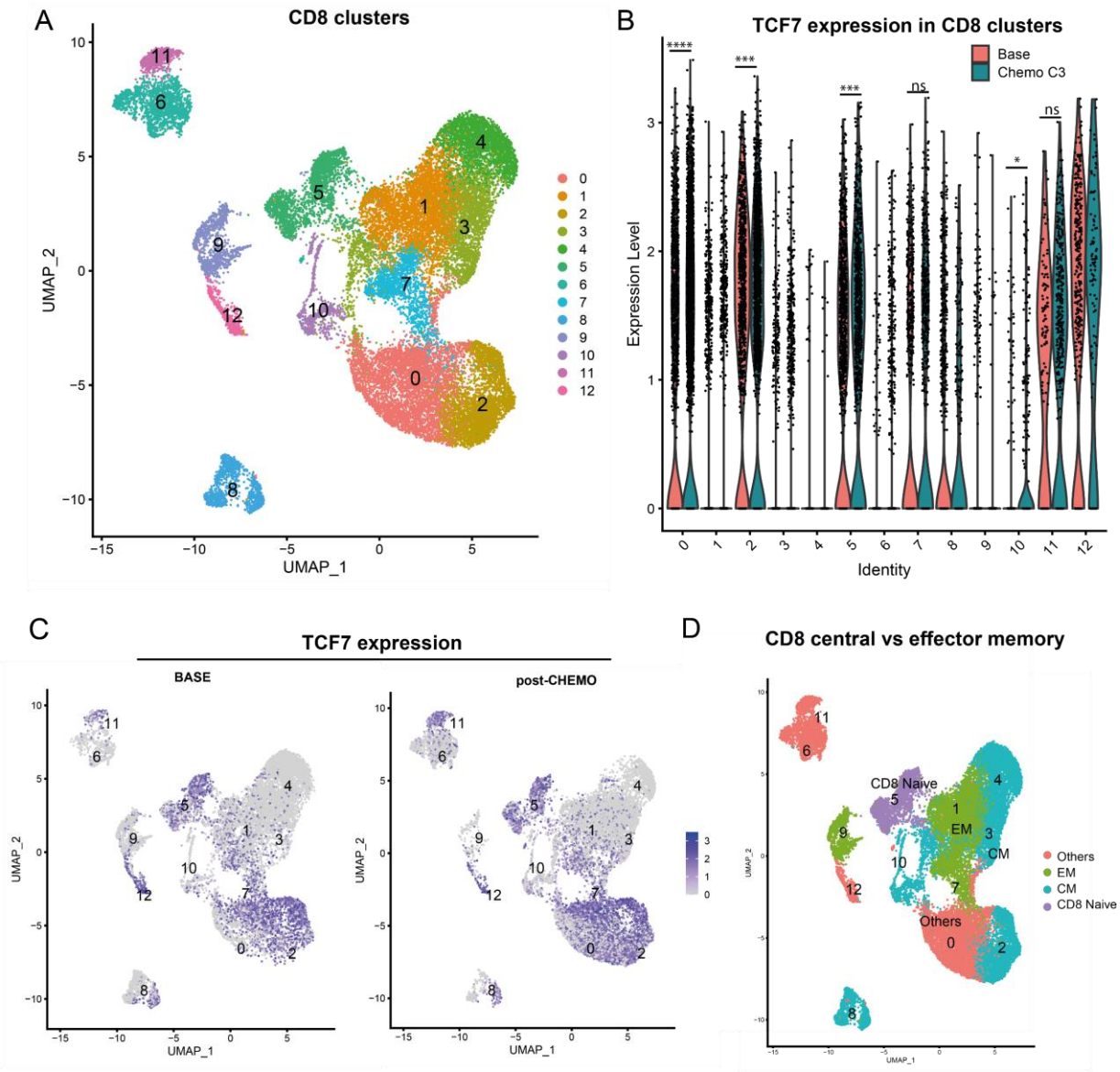


Figure 5.11 Carboplatin and paclitaxel increase TCF1 expression in Central memory CD8⁺ T cells in epithelial ovarian cancer patients.
Patients' blood was collected at baseline and after 3 cycles of chemotherapy (C3) as presented in figure 5.10 (A). Single cell RNA-sequencing was performed on total PBMCS. The available dataset was kindly given to us and reanalysed to investigate *TCF7* expression in $CD8^+$ and $CD4^+$T cells. (A) UMAP discriminating $CD8^+$ T cell sub-cluster based on gene expression profile is shown. (B) level of expression of *TCF7* at baseline and post C3 in these 12 different sub-clusters. Statistically significant differences between groups were determined by a paired t test, *, $p \leq 0.05$, **, $p \leq 0.01$, ****, $p \leq 0.0001$.(C) Level of expression of *TCF7* of these 12 subclusters is shown as an UMAP. (D) Clusters expressing the differential expression of *CD44* and *SELL* (gene for CD62L) are shown.

5.6 Discussion

5.6.1 New triple combination regimen efficacy and potential mechanism of action

In this chapter, we tested a new regimen of the triple combination, further corresponding to the schedule tested in the clinical trial, where anti-PD1 is given prior to ChAdOx1/MVA vaccination (fig 5.1). Indeed, when using immunomodulatory treatments, the therapeutic window is of major importance to raise the most efficient immune response [211]. It appears that the administration of pre-vac anti-PD1+vaccine does not support better tumour control (fig 5.2), survival (fig 5.3) and immunogenicity (fig 5.4) compared to the vaccine alone group. However, when this double treatment strategy was combined with CarboTaxol (triple pre-vac αPD1), we observed a better tumour control, survival and improved immunogenicity compared to vaccine alone or vaccine+chemotherapy group (fig 5.2, 5.3 and 5.4). CarboTaxol was able to rescue the synergy of the pre-vac anti-PD1 treatment combined with ChAdOx1/MVA. The triple combinations with pre-vac anti-PD1 displayed promising anti-tumour effects for clinical trials, similar to the triple combination with post-vac anti-PD1.

These results emphasised the importance of CarboTaxol in the synergistic effect observed with the triple combinations of treatments. We further investigated the impact of CarboTaxol on T cell phenotype in the context of the new regimen, pre-vac triple combination. 4 days post treatment, we were able to observe that $TCF1^+CD8^+$ T cells (fig 5.6 A) as well as $TCF1^+PD1^+CD8^+$ T cells (fig 5.6 B) were significantly expanded in the TME. The infiltration of precursor stem-like ($TCF1^+PD1^-$) and progenitor-exhausted stem-like cells ($TCF1^+PD1^+$) in the TME have previously been correlated with enhance response to checkpoint blockade therapy [62,277]. Furthermore, in the spleen and blood of mice treated with CarboTaxol, $TCF1^+PD1^-CD8^+$ T cells (fig 5.7) were also highly expanded. In the triple pre-vac combination group, the population of splenic and blood $TCF1^+PD1^-CD8^+$ T cells

were significantly expanded compared to the vaccine+pre-vac anti-PD1(fig 5.7 A,C). CarboTaxol might rescue the efficacy of the pre-vac anti-PD1+vaccine combination by inducing $CD8^+$ T cells with higher stemness properties[62,278].

One previous study has reported the induction of sub-primed T cells co-expressing $CD38^+$ and $PD1^+$ in the TME of mice treated with anti-PD1given prior to vaccination, compared to anti-PD1 given post-vaccination in a C57BL/6 TC-1 model [211]. We were interested to evaluate this population in our model. Similarly, we observed a significant increase in $CD38^+PD1^+CD8^+$ T cells in the TME of mice treated with pre-vac anti-PD1 alone or combined with the vaccine (fig 5.8 A,B). Surprisingly the other groups treated with CarboTaxol displayed an increase in $CD38^+PD1^+CD8^+$ T cells (fig 5.8 A,B). The function of CD38 in T cells is complex and not fully understood. We could hypothesise that these dysfunctional $CD8^+$ T cells are counter-balanced by the presence of $TCF1^+PD1^+$ and $TCF1^+CD8^+$ T cells in the TME [279,280]. This could explain why the pre-vac anti-PD1+vaccine group does not promote better immunogenicity while the vaccine+chemo group does improve the vaccine-induced immune response. Therefore, these data highlight the possible deleterious effect of $CD38^+CD8^+$ T cells for the vaccine efficacy. However, the expression of TCF1 induced by CarboTaxol may counterbalance the potentially deleterious effects of $CD38^+PD1^+CD8^+$ T cells.

In line with this hypothesis, the mice treated with the pre-vac triple combination did not show an increase in $CD38^+PD1^+CD8^+$ T cells (fig 5.8 A,B) but only $TCF1^+PD1^+$ and $TCF1^+PD1^-CD8^+$ T cells. Moreover, we investigated the proportions of $TCF1^+PD1^+$ expressing CD38 and observed a significant decrease in CD38 expression in those cells in the TME of triple pre-vac treated mice (fig 5.8 B). This could explain the difference between the vaccine+CarboTaxol group and the triple combination group which showed

the best synergistic effects in term of tumour control and survival. Indeed, the $CD38^{-}TCF1^{+}PD1^{+}CD8^{+}$ T cells could possibly be more efficient in controlling tumour growth than $CD38^{+}TCF1^{+}PD1^{+}$ T cells. Functional assay, confirming the activation, proliferation potential of $CD38^{-}TCF1^{+}PD1^{+}$ versus $CD38^{+}TCF1^{+}PD1^{+}$ will be necessary to confirm the decrease of function of $CD38^{+}TCF1^{+}$PD1+. Furthermore, we will need to explore why the triple pre-vac anti-PD1 combination did not induce $CD38^{+}PD1^{+}CD8^{+}$ T cells while pre-vac anti-PD1 and CarboTaxol respectively alone or in combination with the vaccine induced this population. To investigate that aspect, one group controlling for the combination of CarboTaxol+pre-vac anti-PD1 without the vaccine will have to be investigated.

Finally, previous studies have highlighted the effect of targeting MDSCs in order to improve checkpoint blockade efficacy[281,282]. Therefore, we also controlled the proportion of the $CD11b^{+}Ly6G^{+}$ populations in our model. As previously shown in chapter IV, CarboTaxol depleted this population in all the tested group, including the triple pre-vac anti-PD1 combination. The depletion in the triple pre-vac combination group was significant in the TME (fig 5.9 A), spleen (fig 5.9 B) and blood (fig 5.9 C) compared to the vaccine+pre-vac anti-PD1. Moreover, we observed a slightly increased infiltration of $CD11b^{+}Ly6G^{+}$ in the TME after pre-vac anti-PD1 alone or in combination with the vaccine compared to the control or vaccine alone groups (fig 5.9 A). Therefore, we cannot exclude the importance of $CD11b^{+}Ly6G^{+}$ depletion in the synergy observed in the triple pre-vac combination, nor the potential link between this depletion and TCF1 expression in $CD8^{+}$ T cells and/or $TCF1^{+}$ cell expansion, which will be the subject of future investigations.

5.6.2 Ovarian cancer patients display higher *TCF7* expression and increase proportion of *TCF7*+ CD8$^+$ T cells after 3 cycles of CarboTaxol

Positive clinical outcome as well as patient response to checkpoint blockade have also been correlated to the expression of *TCF7*[273] and the presence of stem-like or progenitor-exhausted stem-like cells[121,278]. Therefore, we were particularly interested in investigating *TCF7* expression in CD8$^+$ and CD4$^+$T cells in human patients after chemotherapy. Especially, the dosage of CarboTaxol cannot be completely translated from mouse to patients. We reanalysed available RNA-sequencing data from a study conducted in epithelial ovarian cancer patients to investigate *TCF7* expression[145]. In this study, patient blood was collected at baseline and after 3 cycles of Carboplatin+paclitaxel, enabling us to compare *TCF7* expression in T cells prior and post treatment. Very interestingly, we observed an increase in the average *TCF7* expression in CD8$^+$ T cells after C3 compared to baseline (fig 5.10 H). Furthermore, the *TCF7*+CD8$^+$ T cell population was significantly expanded after chemotherapy (fig 5.10C). Similar to what was observed in the blood of mice, the *TCF7*+*PDCD1*+ CD8$^+$ T cell population was not significantly expanded post treatment (fig 5.10 D). This increase in *TCF7* expression concerned only CD8$^+$ but not CD4$^+$T cells (fig 4.24). Min Liu *et al.* showed that CD8$^+$ T cells after the 3rd cycle of chemotherapy showed better activation and proliferation after viral antigen (FluA and CEF) stimulation, indicating that T cells after chemotherapy were more functional than before [145]. Furthermore, this enhanced T cell response was observed in both responders and partial responders (defined based on CA125 level, a protein over-expressed in ovarian cancer patients, that can be monitored in the blood). This study did not include non-responder to chemotherapy, it is therefore not possible to draw a direct link between CD8$^+$ T cell enhanced activity and the patients' response. Similarly, in the five patients' blood, analysed by RNA-sequencing, four were responders (patients 1,2,3,6) while one was a

partial responder (patient 7). Based on this limitation, we could not correlate the *TCF7* expression with the patients' response to chemotherapy.

We then scrutinised $CD8^+$ T cell sub-clusters to investigate whether the *TCF7* increased expression was in all or a fraction of the $CD8^+$ T cells. We were able to identify four sub-clusters among twelve with increased *TCF7* expression (fig 5.11 B,C). When looking at markers for central memory and effector memory phenotypes based on *CD44* and *SELL* expression we observed that two of the four subclusters with increased *TCF7* expression after chemotherapy (cluster 2 and 10) were central memory cells (fig 5.11 D). These data seem to correlate with our observations in mice where central memory $CD8^+$ T cell were expanded after CarboTaxol treatment. Clusters 0 were neither naïve, nor central memory nor effector memory while cluster 5 presented characteristic of a naïve phenotype.

Interestingly, these data suggest that the increased in $TCF7^+$ expression was observed in only some $CD8^+$ T cell subsets. The fact that this increased expression was observed in central memory cells correlates with the literature where TCF1 has been linked with the induction of Eomes[58], hence promoting central memory cells, through the WNT/β-Catenin pathway[58,283]. This also supports the fact that $TCF1^+CD8^+$T cell are prone to activation but keep a long-lived phenotype. Indeed, $TCF1^+$ cells have been described as memory-like cells with highly proliferative and with stemness characteristic[58,284]. Furthermore, the authors of these ovarian cancer patient study have highlighted a potential higher proportion of memory cells within the different $CD8^+$ clonotypes, although it was not significant[145]. Future investigations will focus on defining precisely the clusters 0, 2, 5 and 10. Furthermore, we are currently reanalysing RNA-sequencing data available from tumour biopsies in ovarian cancer patients treated with platinum-based chemotherapy[285]. These data could validate if the infiltration of stem-like and progenitor-exhausted stem-like $CD8^+$

T cells are expanded in the TME in ovarian cancer patients, like what was observed in our 15V4T3 DBA/2 tumour model.

Chapter VI: Summary and future work

6.1 Synergy of a triple combination of treatments: ChAdOx1/MVA, anti-PD1 and CarboTaxol

6.1.1 Summary

Chapter III presented the new combination of three immunomodulatory treatments: anti-PD1, CarboTaxol, and viral vector cancer vaccines, composed of ChAdOx1 and MVA, encoding the relevant antigens depending on the tumour model used. We tested this combination in both DBA/2 and C57BL/6 mice bearing 15V4T3 (P1A antigen) and TC-1 (E6-E7) tumours respectively.

When mice bear a substantial (>50mm^3), aggressive tumour, such as 15V4T3 or TC-1, ChAdOx/MVA vaccines displayed limited efficacy on their own. However, when combined with either anti-PD1 or CarboTaxol, the vaccines displayed improved tumour control and survival compared to the ChAdOx/MVA alone. Interestingly, the triple combination of these treatments demonstrated strong tumour control, survival, and high immunogenicity in both 15V4T3 DBA/2 and TC-1 C57BL/6 tumour models. Surprisingly, the addition of CarboTaxol, but not anti-PD1, promoted a higher specific CD8 immune response against P1A (DBA/2) or E6-E7 (C57BL/6) compared to the vaccine alone. Although the magnitude of the P1A-specific CD8$^+$ T cell response was not further increased by anti-PD1, it was sustained for longer, probably by limiting T cell exhaustion and promoting T cell activity. Therefore, the best synergy was observed when both anti-PD1 and CarboTaxol were combined with the vaccines. To further understand the mechanism behind this triple combination and particularly behind CarboTaxol-induced improved immunogenicity, we evaluated the TME, spleen and blood 5 days post boost. We did not see any long-term effects (day 12 post treatment) which could explain the increased magnitude of the P1A specific CD8$^+$ T cell response induced by chemotherapy in the vaccine+chemo and the triple combination groups. Interestingly, the triple combination

group displayed the highest proportion of $TCF1^+PD1^+$ and $TCF1^+PD1^-CD8$ T cells, which can be characterised as progenitor exhausted-stem-like and stem-like precursor T cells respectively and have a higher proliferation and differentiation potential than $TCF1^-$ T cells[62,283]. These populations were increased in the TME but not particularly in the spleen and blood. This highlights the importance of adding anti-PD1 to the vaccine+CarboTaxol to sustain the efficacy of the P1A specific immune response.

6.1.2 Limitations and future plans

To further confirm that anti-PD1 sustained the immune response when added to the vaccine+chemo, future investigations will explore the magnitude of the P1A-specific $CD8^+$ response of the triple combination at day 12 post boost in the spleen and dLNs and compare it to the response evaluated on day 5. One limitation for this new time point is the loss of the tumour in responders, which occurs mostly in the vaccine+chemo and triple combination groups, hence the need of exploring the dLNs. Indeed, most of the responders will be tumour free after day 6 post boost. The phenotype of T cells would be further explored at day 12 post boost, to evaluate the presence of $TCF1^+PD1^+$ and $TCF1^+PD1^-CD8^+$ T cells in blood, spleen and dLNs. Furthermore, dLNs have been shown to be a source for $TCF1^+PD1^+$ T cells, which then migrate in the TME. It would be of interest to further investigate if the increase of $TCF1^+PD1^+$ and $TCF1^+PD1^-CD8^+$ T cells in the TME of mice treated with the triple combination is due to the induction of a pool of these cells in dLNs[228,229].

6.2 CarboTaxol is an adjuvant for ChAdOx1/MVA: mechanism investigation.

6.2.1 Summary

To further investigate the mechanism behind the CarboTaxol-induced higher magnitude of the $CD8^+$ T cell response when combined with vaccine, we evaluated the immune landscape at day 4 post prime (i.e day 4 post CarboTaxol). The logic behind this time point was, firstly, the short half-life of chemotherapy, shown in both human and mice[255–257]. Moreover, publications have investigated CarboTaxol phenotype 72h post treatments[150]. Furthermore, we could not exclude the possibility of an effect of chemotherapy on the priming environment of the vaccine, which would lead to a better priming, hence an increased induction of P1A specific $CD8^+$ T cells.

We showed that CarboTaxol depleted $CD11b^+Ly6G^+$ cells (potential PMN-MDSCs) in the system, including BM, spleen and blood, and in the TME at 4 days post treatment. In the 15V4T3 DBA/2 tumour model, these cells showed slight immunosuppressive ability, suppressing the proliferation of naïve $CD8^+$ T cells. But regarding this limited effect, we decided to evaluate the cause-and-effect relationship between the depletion of $CD11b^+Ly6G^+$ and the synergistic effect observed between the vaccine and CarboTaxol, using an *in vivo* anti-GR1 antibody to deplete $CD11b^+Ly6G^+$ cells. Surprisingly, the vaccine+anti-GR1 did not recapitulate the effect of CarboTaxol on enhancing the vaccine efficacy. The vaccine+anti-GR1 treated mice did not display improved tumour control nor improved immunogenicity compared to the vaccine alone. Therefore, we concluded that $CD11b^+$ $Ly6G^+$ cell depletion was not the main cause of the vaccine and CarboTaxol synergy.

Subsequently, we investigated the potential effects of CarboTaxol on $CD8^+$ and $CD4^+$T cell phenotype and observed an increased TCF1 expression with over 95% of $CD8^+$ and

$CD4^+$T cells expressing TCF1 in the spleen and blood after CarboTaxol. This phenotype was observed in tumour bearing and tumour free mice and correlated with an expanded number of $TCF1^+PD1^-CD4^+$and $CD8^+$ T cells. In tumour free mice, we also observed an expansion of memory $CD44^+CD62L^+$ cells, indicating that these $TCF1^+PD1^-$ are not only naïve cells (defined as $CD44^+CD62L^+$) but also $CD44^+$. Furthermore, we observed an expansion of these stem-like cells as well as the progenitor exhausted stem-like $CD8^+$ T cells defined as $TCF1^+PD1^+CD8^+$ T cells in the TME of CarboTaxol treated mice, which have been correlated with better tumour control and prognosis in mouse studies and in patients[62,121,277,278]. Finally, this increased TCF1 expression on T cells in the TME, spleen and blood were highly negatively correlated with the $CD11b^+Ly6G^+$ cell depletion in all the organs evaluated even in tumour free mice, where $CD11b^+Ly6G^+$ cells are most likely neutrophils.

Two questions were then evaluated in parallel: Is TCF1 expression in T cells important in increasing the priming of the vaccine-induced immune response? Could the depletion of $CD11b^+Ly6G^+$ cells be the cause of $TCF1^+$ cell expansion or potential TCF1 increase expression?

To explore the first question, we evaluated the immunogenicity of the vaccine+chemo combination in tumour free mice, where TCF1 expression was increased too. We discovered that the vaccine immunogenicity was increased in the vaccine+CarboTaxol treated mice compared to the vaccine alone group. This increased immunogenicity occurred only when CarboTaxol was given with the prime, or up to 48h before the prime. When CarboTaxol was given further apart, we observed a loss of its adjuvant functions. Very interestingly, CarboTaxol was also able to enhance the boost vaccination efficacy

when given at the same time point of the MVA boost. This supports the fact that TCF1 expression and $TCF1^+$ cell expansion during priming might be of major importance[237,238].

Interestingly, $TCF1^+$ cell expansion in $CD8^+$ T cells correlates with Ly6G depletion, so we wondered if these 2 phenotypes were linked. We noticed a decrease of the environmental inflammation and particularly a decrease in the production of IL12/23(p40), which correlates with $CD11b^+Ly6G^+$ depletion. This phenotype has previously been described in the literature where macrophages, monocytes and DCs were shown to decrease their production in IL12/23(p40) as part of a mechanism to resolve inflammation. This decreased production was triggered by the phagocytosis of apoptotic neutrophils [248,250,251]. Carboplatin and Paclitaxel have been shown to trigger non-inflammatory cell death, called apoptosis, by inducing caspase-8 and caspase-3 activation, respectively[286,287]. Therefore, we hypothesised that the decrease in IL12/23(p40) is due to the phagocytosis of apoptotic neutrophils. This decrease would then trigger TCF1 expression, as IL12/23(p40) has been shown to block TCF1 induction through IL12 receptor/STAT4 in mice[227]. However, combining the vaccine with an anti-IL12/23(p40) neutralising antibody did not induce TCF1 expression. These results lead us to another hypothesis: IL12/23(p40) on its own might not be enough and other signals are in place. Potentially, the depletion of $Ly6G^+$ cells could trigger other signals, in part of the resolution of inflammation process[250]. Such resolution signals could be related to the secretion of WNT-3a by macrophages which has been observed during liver regeneration processes after injuries[261]. The WNT/β-Catenin pathway has been shown to generate memory $CD8^+$ T cells through the induction of TCF1 [275].

Alternatively, there may be no link between $CD11b^+Ly6G^+$ depletion and the TCF1 expression in T cells. Interestingly, paclitaxel has been shown to induce WNT/β-Catenin

as well as Notch pathways[262,263,267]. The Notch pathway has been described to induce TCF1 expression in thymic T cell[264–266]. Hence, it is not excluded that paclitaxel as part of CarboTaxol can directly activate these pathways on T cells. (See fig 6.1)

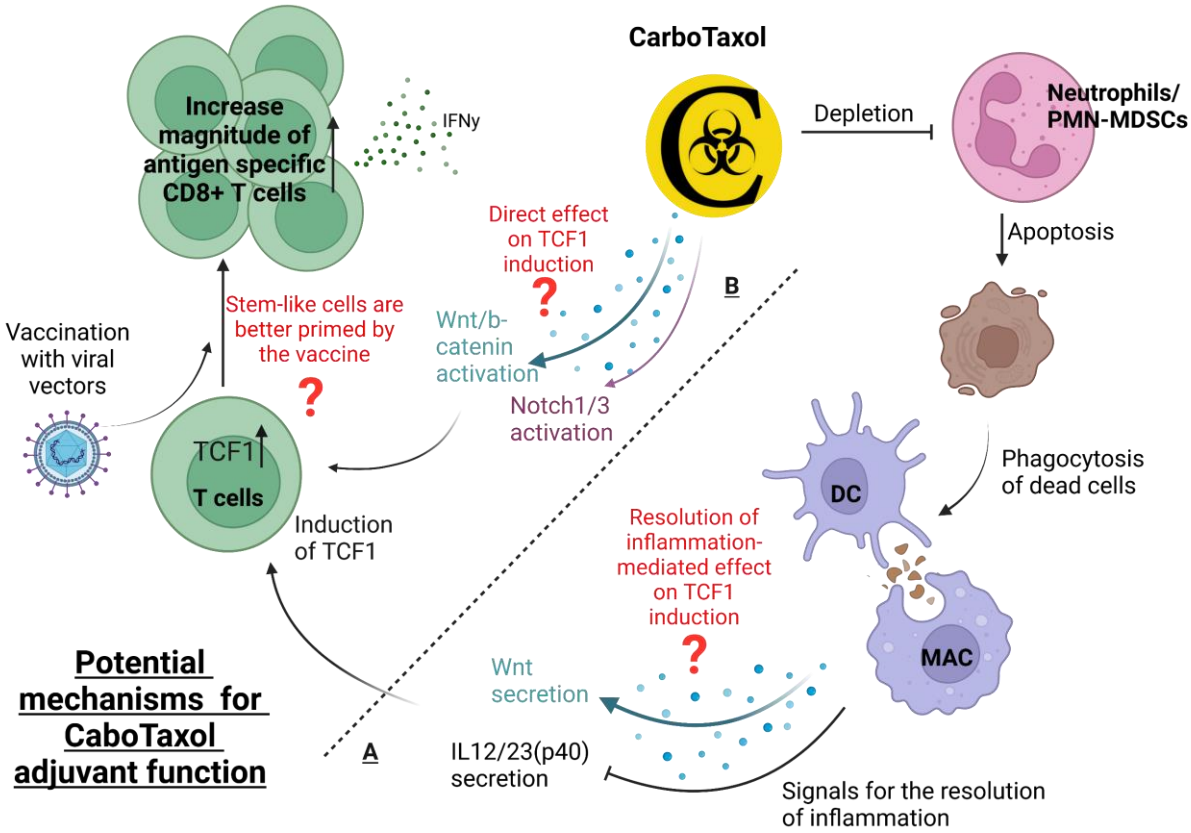


Figure 6.1 Potential mechanisms for CarboTaxol adjuvant function. (A) Indirect effect: CarboTaxol induces neutrophils/PMN-MDSCs apoptosis, hence the depletion observed from day 3 post CarboTaxol. DCs and macrophages will phagocyte neutrophils debris and in turn promote the resolution of inflammation. Resolution of inflammation go through the integration of different signals such as a decrease in IL12/23(p40) secretion, or an increase secretion of Wnt ligand. These signals either alone or more likely together will induce TCF1 expression in $CD8^+$ or $CD4^+$ T cell. **(B)** Alternatively, CarboTaxol could induce TCF1 through a more **direct effect:** induction of wnt/β-catenin signalling or Notch1/3 signalling on CD8 or CD4 T cells will increase the expression of TCF1.

6.2.2 Limitations and future plans

Future plans will further confirm the absence of effect of IL12/23(p40) on TCF1 expression. Moreover, we will explore the potential role of both Notch and WNT/β-Catenin pathways. However, these two pathways are comprised of many possible ligands and receptors. Determining which ones are involved in TCF1 expression and $TCF1^+$ cell expansion will be challenging to discover. Furthermore, these pathways display a very precise and sensitive spatio-temporal regulation which is particularly challenging to evaluate. Especially, in our model, several signals and immune cells are likely to be involved, it is therefore necessary to evaluate Notch and WNT/β-Catenin as part of *in vivo* and *ex vivo* experiments, where all the actors are considered.

In our study, we have highlighted the adjuvant effects of CarboTaxol and related it to its short-term effect on TCF1 expression in T cells. However, this was just a correlation, and to prove a cause-and-effect relationship between the increase proportion of $TCF1^+$ cells in T cells and CarboTaxol adjuvant effects, inhibiting TCF1 function will be necessary. One major limitation in understanding the CarboTaxol mechanism is that TCF1 is a transcription factor with no inhibitor developed to date. However, there is *Tcf7*-loxP mice available from Jackson laboratory. These mice can be crossed with CD8-restricted or CD4-restricted Cre, which will knock-out (KO) the expression of the long isoform of TCF1 in $CD8^+$ T cells or total T cells. The long isoform has been involved in the generation of $TCF1^+PD1^+$ cells in tumour models, as well as improving central memory generation after LCMV infection[247,276,288]. Alternatively, TCF1 KO mice have been developed by H.Clevers' group, where all TCF1 isoforms are targeted[289]. These mice competently generate effector T cells, despite a profound decrease in thymocytes development[227]. Interestingly, TCF1 KO mice were unable to generate memory or stem-like T cells after

vaccination or LCMV infection [227,284]. The use of these two models will be explored to confirm the importance of TCF1 in CarboTaxol adjuvant effect.

6.3 Importance of CarboTaxol in extending anti-PD1 therapeutic window: translational aspect of the triple combination

6.3.1 Summary

We investigated an early time point for anti-PD1, that mimics the clinical schedule that are now under testing in a clinical trial on NSCLC patients. Anti-PD1 was given prior to vaccination with or without CarboTaxol and compared with the vaccine+post-vac anti-PD1. Without CarboTaxol addition, the pre-vac anti-PD1 did not synergise with the vaccine and showed similar tumour growth control and immunogenicity to the vaccine alone. In contrast, the vaccine+post-vac anti-PD1 showed improved tumour control compared to the vaccine alone. Very interestingly, when vaccine+pre-vac anti-PD1 was combined with CarboTaxol the synergistic effect is rescued to the level of triple combination with post-vac anti-PD1 in term of tumour control, survival and immunogenicity. Whilst $CD8^+$ T cells with stem-like properties were absent after treatment with pre-vac anti-PD1+vaccine, the addition of CarboTaxol induced $TCF1^+PD1^-$ and $TCF1^+PD1^+$ T cells. Moreover, we observed an increase in $CD38^+PD1^+$ sub-primed and dysfunctional T cells in the vaccine+pre-vac anti-PD1[211]. Interestingly, $CD38^+PD1^+CD8^+$ T cells were decreased in the triple combination group compared to the respective double combination groups. Surprisingly, in the TME, $TCF1^+PD1^+$ cells were found to also express $CD38^+$ after chemotherapy, which potentially marks T cell dysfunctions. Interestingly, the proportion of $CD38^+$ cells among $TCF1^+PD1^+CD8^+$ T cells was significantly decreased in the triple combination group compared to the vaccine+chemo group. This supports the benefit of combining anti-PD1 with chemotherapy in promoting more competent and effective cells, even compared to vaccine+CarboTaxol. Therefore, the

triple combination is a very promising treatment in which CarboTaxol has a central role and allows for a more flexible therapeutic window for anti-PD1 therapy.

We next evaluated the impact of CarboTaxol on human samples. We got access to RNA-seq data from a published research article with the title "*Improved T-cell Immunity Following Neoadjuvant Chemotherapy in Ovarian Cancer"* by Miu *et al*. in 2022 [145]. The standard of care for ovarian epithelial cancer patients is the combination of a platinum-based chemotherapy, Carboplatin combined with paclitaxel in this study, given in several cycles 3 weeks apart from each other. Blood samples from these patients were evaluated by RNA-seq before the first cycle and after the third cycle of CarboTaxol. We re-analysed these data and evaluated the expression of *TCF7* in $CD8^+$ T cells and $CD4^+$T cells. We observed a significant increase of *TCF7*+ $CD8^+$ T cell proportion in the blood after 3 cycles of CarboTaxol compared to baseline. However, we did not see an impact on $TCF1^+CD4^+$T cell after CarboTaxol. *TCF7* average expression level was also significantly increased in $CD8^+$ T cells, but not in $CD4^+$T cells. We then investigated which subsets of $CD8^+$T cells displayed a higher *TCF7* expression after CarboTaxol. We noticed that four clusters showed an increase in *TCF7* expression, among which 2 had central memory characteristics and one had naïve characteristics which correlated with the literature[283,290]. Therefore, CarboTaxol has an impact on *TCF7* expression in cancer patients, which is really promising to test the triple combination therapy in clinical trial.

6.3.2 Future plans and limitations

Future work will involve the evaluation of $TCF1^+PD1^+CD38^+$ T cell functions in comparison to $TCF1^+PD1^+CD38^-$ $CD8^+$T cells. We will also explore why only the triple combination showed this decrease in $CD38^+PD1^+$ but not CarboTaxol nor anti-PD1 in combination with the vaccine on their own.

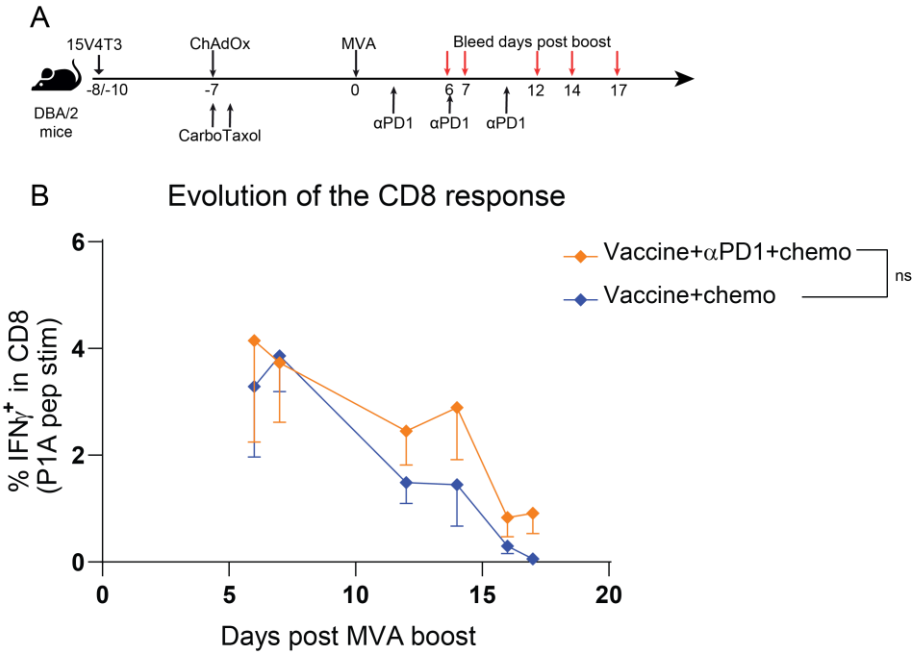
In parallel, we will further explore the RNA-seq dataset by investigating the phenotype of CD8 sub-cluster. Particularly, sub-cluster 0 did not present effector, central memory nor naïve characteristic. It is important to note that $CD44^+$ and $CD62L^+$ are not the best marker to discriminate memory and effector T cells in human, where memory T cells are usually characterised as $CD45RO^+CD45RA^-$[291]. So other markers will be evaluated as well as the top 50 genes of every sub-cluster showing higher expression of *TCF7* after chemotherapy. Finally, we will re-analyse the dataset from the article *"Longitudinal single-cell RNA-seq analysis reveals stress-promoted chemoresistance in metastatic ovarian cancer"* by Zhang *et al.*, published in 2022[285]. In this study, tumour samples of ovarian cancer patients were examined prior to platinum-based chemotherapy (biopsies) and after the third cycle of chemotherapy (debulking surgery). This will allow the investigation of $TCF1^+PD1^+CD8^+$ T cells, which are mainly found in the TME[62].

6.4 Project limitation: complexity of translating drugs to the clinic.

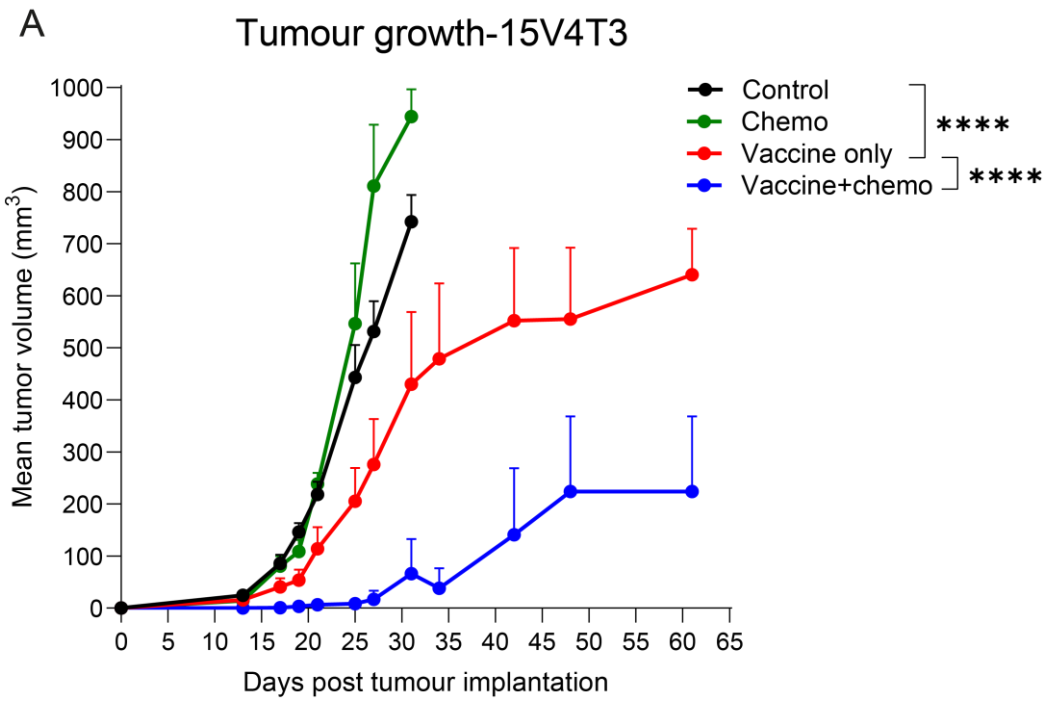
One main challenge and still a remaining question of this project is how to translate the dose of chemotherapy from mouse to cancer patients. Indeed, the literature has explored different doses and frequencies of chemotherapy used across different mouse strains. The MTD is strain, age, and chemotherapy dependent[292]. It is therefore complicated to have consistency across publications. Furthermore, the translation to the dose used in patients is unclear. One way of comparison could be to assess side effects, although mouse studies do not always report them. Cisplatin-treated mice, for example, has been shown to have similar side effects as human patients but each side effect was studied individually in various publications, rendering the comparison to human data difficult[293,294]. Here we used 40mg/kg of Carboplatin with 20mg/kg of paclitaxel, followed by another injection of paclitaxel at 20mg/kg the next day. This schedule was used together with vaccination and showed promising synergistic effects [150]. However, what is the corresponding dose in

patients? It has been shown that carboplatin MTD in mice is 85mg/kg, while paclitaxel MTD varies between 20-40 mg/kg between strains[212,295,296]. Therefore, we can argue that in our pre-clinical model we are using a more tolerable dose than the MTD. Importantly, we used only one cycle of these drugs, while patient regimen usually involves several cycles of chemotherapy at the MTD, separated by prolonged period of time to help the patient's recovery from adverse effects. Recently, clinical trials have investigated metronomic chemotherapy which is the frequent administration of low dose chemotherapy. This emerging regimen has higher tolerability, showed anti-angiogenic properties and better immune activation as well as better synergistic effect with immunotherapy[140,297–299]. Metronomic chemotherapy is not yet the standard of care in cancer patients but has shown very promising effects in triple negative breast cancer patients as well as NSCLC patients[140,300,301]. It would therefore be interesting to further explore the difference in synergy between different doses and different frequencies of CarboTaxol. Interestingly, preliminary results in our model using 2 cycles of chemotherapy still synergises with our vaccine and anti-PD1. Although, this will have to be repeated and further compared with metronomic regimens that are potentially less toxic and more immunogenic. Importantly, what would be the minimum dose of CarboTaxol to achieve an adjuvant effect? Moreover, exploring potential adjuvant effects from other types of chemotherapy will be important for future combinations with cancer vaccines. It is worth noting that the RNA-sequencing data in ovarian cancer patients treated at the MTD still revealed an increased *TCF7* expression such as what was observed in mice, which is promising for possible chemotherapy and vaccines combination in clinical trials.

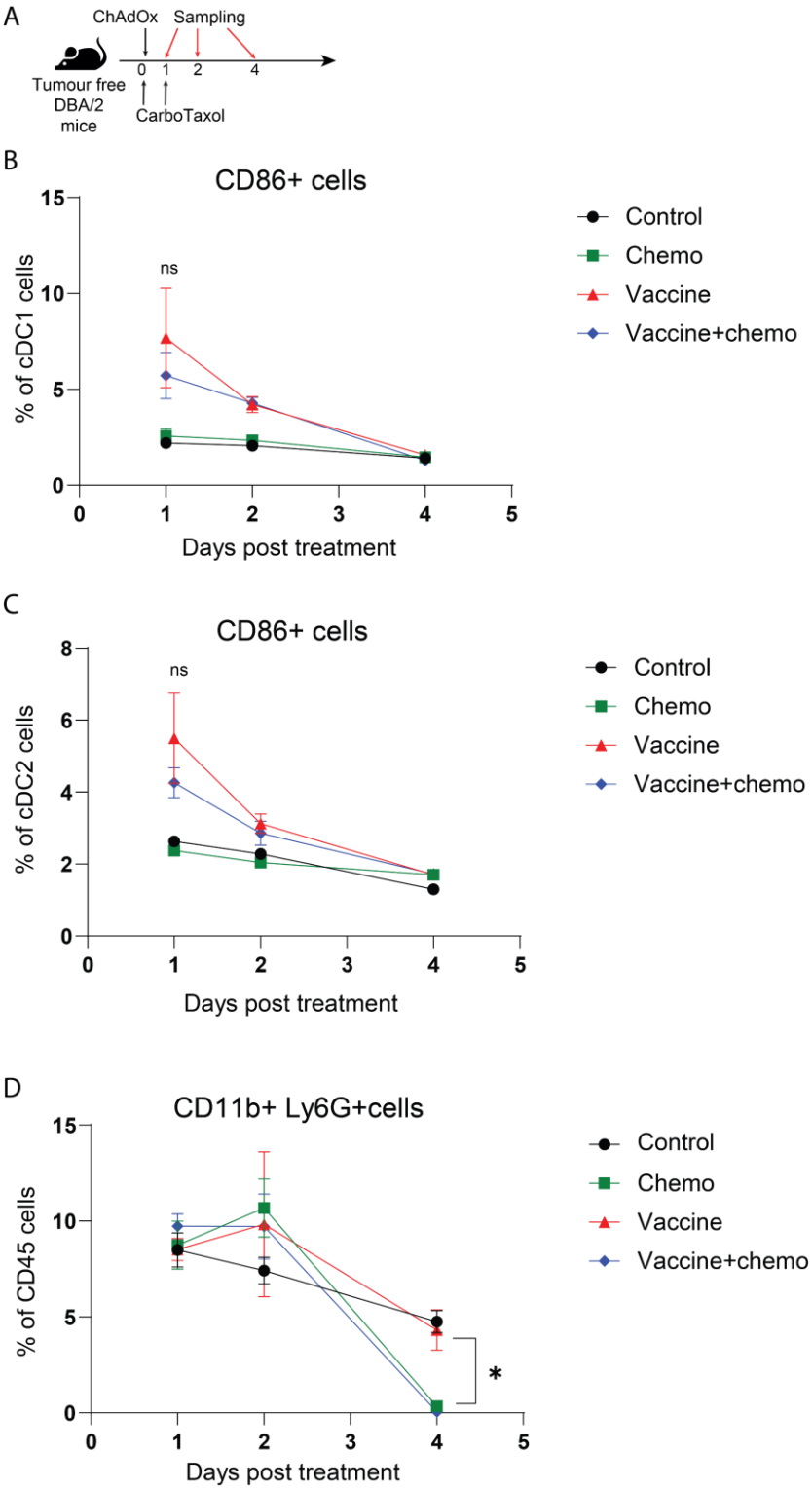
Appendix



Appendix Figure 1. Evolution of the magnitude of the P1A specific CD8 response overtime: comparison between Vaccine+CarboTaxol and Triple combination groups. (A)DBA/2 mice were implanted with $1x10^6$ 15V4T3 cells via s.c injections to initiate tumour growth. This figure combined results from different experiments where mice were treated with with 10^7 IU of ChAdOx1-Ii-P1A (ChAdOx) one week apart from 10^6 PFU of MVA-tpA-P1A. Mice were treated with carboplatin(40mg/kg) and paclitaxel (20mg/kg) on the day of the prime vaccination and 24h later with paclitaxel (20mg/kg) via i.p. The mice were also treated with anti-PD1 starting 3 days post boost for 3 i.p injections every 3rd day. The magnitude of the immune response was evaluated at the indicated days post boost. (B) PBMCs were harvested and stimulated with P1A peptides. The magnitude of IFNγ production was assessed in $CD8^+$ T cells. Each data point represents the mean± SEM of the response for each group (with n= 7 to 6 mice per groups). Mann-Whitney tests were performed to compare the mean of the 2 groups at each time point.



Appendix Figure 2. Prophylactic ChAdOx1/MVA-P1A combined with CarboTaxol promotes a better protection than vaccine alone against 15V4T3 in DBA/2 mice.
DBA/2 mice were implanted with $1x10^6$ 15V4T3 cells via s.c injections to initiate tumour growth 3 weeks after the MVA-tpa-P1A boost vaccination of the scheme presented in chapter 4 figure 4.24 (A). (A) Mean tumour growth data are presented as mean tumour volume (mm3) ± SEM. Data are representative of 3 independent experiments. Statistically significant differences between groups were determined by a two-way ANOVA followed by Tukey's post hoc test, ****, $p \leq 0.0001$.



Appendix Figure 3. Evolution of innate cell population after ChAdOx1 and CarboTaxol
(A) Scheme of treatment. DBA,2 mice were vaccinated via i.m with 10^7 IU of ChAdOx1-Ii-P1A or PBS sham and treated with carboplatin(40mg/kg) and paclitaxel (20mg/kg) and 24h later with paclitaxel (20mg/kg) via i.p. At Day 1, 2 and 4 post treatment, spleens were harvested and cDCs and $CD11b^+$ $Ly6G^+$ cells were analysed by flow cytometry. Evolution overtime of the proportion of cDC1 expressing CD86 is shown in (B) and the proportion of $CD86^+$ cells in cDC2 is shown in (C). Evolution of $CD11b^+$ $Ly6G^+$ proportion among $CD45^+$ cells is shown in (D). Data are representative of 1 experiment and mean for each group are shown. Each symbol represents the mean values at each time point (n=3 to 4 mice per groups). Statistically significant differences between groups were determined by a Kruskal-Wallis test with Dunn's multiple comparisons test,*, $p \leq 0.05$.

Table 23: Peptide sequences in P1A library used for T-cell stimulation assays.

Peptide No.	Amino Acids	Sequence
1	1-15	MSDNKKPDKAHSGSG
2	5-19	KKPDKAHSGSGGDGD
3	9-23	KAHSGSGGDGDGNRC
4	13-27	GSGGDGDGNRCNLLH
5	17-31	DGDGNRCNLLHRYSL
6	21-35	NRCNLLHRYSLEEIL
7	25-39	LLHRYSLEEILPYLG
8	29-43	YSLEEILPYLGWLVF
9	33-47	EILPYLGWLVFAVVT
10	37-51	YLGWLVFAVVTTSFL
11	41-55	LVFAVVTTSFLALQM
12	45-59	VVTTSFLALQMFIDA
13	49-63	SFLALQMFIDALYEE
14	53-67	LQMFIDALYEEQYER
15	57-71	IDALYEEQYERDVAW
16	61-75	YEEQYERDVAWIARQ
17	65-79	YERDVAWIARQSKRM
18	69-83	VAWIARQSKRMSSVD
19	73-87	ARQSKRMSSVDEDED
20	77-91	KRMSSVDEDEDDEDD
21	81-95	SVDEDEDDEDDEDDY
22	85-99	DEDDEDDEDDYYDDE
23	89-103	EDDEDDYYDDEDDDD
24	93-107	DDYYDDEDDDDDAFY
25	97-111	DDEDDDDDAFYDDED
26	101-115	DDDDAFYDDEDDEEE
27	105-119	AFYDDEDDEEEELEN
28	109-123	DEDDEEEELENLMDD
29	113-127	EEEELENLMDDESED
30	117-131	LENLMDDESEDEAEE
31	121-135	MDDESEDEAEEEMSV
32	125-139	SEDEAEEEMSVEMGA
33	129-143	AEEEMSVEMGAGAEE

34	133-147	MSVEMGAGAEEMGAG
35	137-151	MGAGAEEMGAGANCA
36	141-155	AEEMGAGANCACVPG
37	145-159	GAGANCACVPGHHLR
38	149-163	NCACVPGHHLRKNEV
39	153-167	VPGHHLRKNEVKCRM
40	157-171	HLRKNEVKCRMIYFF
41	161-175	NEVKCRMIYFFHDPN
42	165-179	CRMIYFFHDPNFLVS
43	169-183	YFFHDPNFLVSIPVN
44	173-187	DPNFLVSIPVNPKEQ
45	177-191	LVSIPVNPKEQMECR
46	181-195	PVNPKEQMECRCENA
47	185-199	KEQMECRCENADEEV
48	189-203	ECRCENADEEVAMEE
49	193-207	ENADEEVAMEEEEEE
50	197-211	EEVAMEEEEEEEEEE
51	201-215	MEEEEEEEEEEEEEE
52	205-219	EEEEEEEEEEEMGNP
53	209-223	EEEEEEEMGNPDGFS
54	210-224	EEEEEEMGNPDGFSP

REFERENCES

1. Ferlay J, E.M.L.F.C.M.M.L.P.M.Z.A.S.I.B.F. Global Cancer Observatory: Cancer Today. Lyon, France: International Agency for Research on Cancer(2020).

2. Sung, H., Ferlay, J., Siegel, R.L., Laversanne, M., Soerjomataram, I., Jemal, A., and Bray, F. (2021). Global Cancer Statistics 2020: GLOBOCAN Estimates of Incidence and Mortality Worldwide for 36 Cancers in 185 Countries. CA Cancer J Clin *71*, 209–249. 10.3322/caac.21660.

3. Hanahan, D., and Weinberg, R.A. (2011). Hallmarks of cancer: the next generation. Cell *144*, 646–674. 10.1016/J.CELL.2011.02.013.

4. Hanahan, D., and Weinberg, R.A. (2000). The hallmarks of cancer. Cell *100*, 57–70. 10.1016/S0092-8674(00)81683-9.

5. MacConaill, L.E., and Garraway, L.A. (2010). Clinical Implications of the Cancer Genome. Journal of Clinical Oncology *28*, 5219. 10.1200/JCO.2009.27.4944.

6. Pardoll, D. (2003). Does the immune system see tumors as foreign or self? Annu Rev Immunol *21*, 807–839. 10.1146/ANNUREV.IMMUNOL.21.120601.141135.

7. Decker, W.K., and Safdar, A. (2009). Bioimmunoadjuvants for the treatment of neoplastic and infectious disease: Coley's legacy revisited. Cytokine Growth Factor Rev *20*, 271–281. 10.1016/J.CYTOGFR.2009.07.004.

8. Old, L.J., and Boyse, E.A. IMMUNOLOGY OF EXPERIMENTAL TUMORS1,2.

9. Baldwin, R.W. (1955). Immunity to Methylcholanthrene-Induced Tumours in Inbred Rats Following Atrophy and Regression of the Implanted Tumours. British Journal of Cancer 1955 9:4 *9*, 652–657. 10.1038/bjc.1955.70.

10. FOLEY EJ. (1953). Antigenic properties of methylcholanthrene-induced tumors in mice of the strain of origin. . Cancer Res. .

11. Prehn, R.T.& M.J.M. (1957). Immunity to methylcholanthrene-induced sarcomas. Nat. Cancer Inst.

12. Burnet, M. (1957). Cancer: a biological approach. III. Viruses associated with neoplastic conditions. IV. Practical applications. Br Med J *1*, 841. 10.1136/BMJ.1.5023.841.

13. Grulich, A.E., van Leeuwen, M.T., Falster, M.O., and Vajdic, C.M. (2007). Incidence of cancers in people with HIV/AIDS compared with immunosuppressed

transplant recipients: a meta-analysis. Lancet *370*, 59–67. 10.1016/S0140-6736(07)61050-2.

14. Penn I. (1998). Occurrence of cancers in immunosuppressed organ transplant recipients. . Clin Transpl. .

15. Shankaran, V., Ikeda, H., Bruce, A.T., White, J.M., Swanson, P.E., Old, L.J., and Schreiber, R.D. (2001). IFNgamma and lymphocytes prevent primary tumour development and shape tumour immunogenicity. Nature *410*, 1107–1111. 10.1038/35074122.

16. Fridman, W.H. (2018). From Cancer Immune Surveillance to Cancer Immunoediting: Birth of Modern Immuno-Oncology. The Journal of Immunology *201*, 825–826.

17. Dunn, G.P., Old, L.J., and Schreiber, R.D. (2004). The Three Es of Cancer Immunoediting. https://doi.org/10.1146/annurev.immunol.22.012703.104803 *22*, 329–360. 10.1146/ANNUREV.IMMUNOL.22.012703.104803.

18. Chen, D.S., and Mellman, I. (2013). Oncology meets immunology: The cancer-immunity cycle. Immunity *39*, 1–10. 10.1016/j.immuni.2013.07.012.

19. Prager, I., and Watzl, C. (2019). Mechanisms of natural killer cell-mediated cellular cytotoxicity. J Leukoc Biol *105*, 1319–1329. 10.1002/JLB.MR0718-269R.

20. Garrido, F., and Algarra, I. (2001). MHC antigens and tumor escape from immune surveillance. Adv Cancer Res *83*, 117–158. 10.1016/S0065-230X(01)83005-0.

21. Aqbi, H.F., Wallace, M., Sappal, S., Payne, K.K., and Manjili, M.H. (2018). IFN-γ orchestrates tumor elimination, tumor dormancy, tumor escape and progression. J Leukoc Biol *103*, 1219–1223. 10.1002/JLB.5MIR0917-351R.

22. Fulda, S., and Debatin, K.M. (2002). IFNgamma sensitizes for apoptosis by upregulating caspase-8 expression through the Stat1 pathway. Oncogene *21*, 2295–2308. 10.1038/SJ.ONC.1205255.

23. Biswas, S.K., and Mantovani, A. (2010). Macrophage plasticity and interaction with lymphocyte subsets: Cancer as a paradigm. Nat Immunol *11*, 889–896. 10.1038/ni.1937.

24. Banchereau, J., and Steinman, R.M. (1998). Dendritic cells and the control of immunity. Nature *392*, 245–252. 10.1038/32588.

25. Granot, T., Senda, T., Carpenter, D.J., Matsuoka, N., Weiner, J., Gordon, C.L., Miron, M., Kumar, B. V., Griesemer, A., Ho, S.H., et al. (2017). Dendritic cells display subset and tissue-specific maturation dynamics over human life. Immunity *46*, 504. 10.1016/J.IMMUNI.2017.02.019.

26. Joffre, O.P., Segura, E., Savina, A., and Amigorena, S. (2012). Cross-presentation by dendritic cells. Nature Reviews Immunology 2012 12:8 *12*, 557–569. 10.1038/nri3254.

27. Noubade, R., Majri-Morrison, S., and Tarbell, K. V. (2019). Beyond CDC1: Emerging roles of DC crosstalk in cancer immunity. Front Immunol *10*, 1014. 10.3389/FIMMU.2019.01014/BIBTEX.

28. Gardner, A., de Mingo Pulido, Á., and Ruffell, B. (2020). Dendritic Cells and Their Role in Immunotherapy. Front Immunol *11*, 924. 10.3389/FIMMU.2020.00924/BIBTEX.

29. Diamond, M.S., Kinder, M., Matsushita, H., Mashayekhi, M., Dunn, G.P., Archambault, J.M., Lee, H., Arthur, C.D., White, J.M., Kalinke, U., et al. (2011). Type I interferon is selectively required by dendritic cells for immune rejection of tumors. J Exp Med *208*, 1989–2003. 10.1084/JEM.20101158.

30. Laoui, D., Keirsse, J., Morias, Y., Van Overmeire, E., Geeraerts, X., Elkrim, Y., Kiss, M., Bolli, E., Lahmar, Q., Sichien, D., et al. (2016). The tumour microenvironment harbours ontogenically distinct dendritic cell populations with opposing effects on tumour immunity. Nat Commun *7*. 10.1038/NCOMMS13720.

31. Kuhn, S., Yang, J., and Ronchese, F. (2015). Monocyte-Derived Dendritic Cells Are Essential for CD8+ T Cell Activation and Antitumor Responses After Local Immunotherapy. Front Immunol *6*, 23. 10.3389/FIMMU.2015.00584.

32. Sharma, M.D., Rodriguez, P.C., Koehn, B.H., Baban, B., Cui, Y., Guo, G., Shimoda, M., Pacholczyk, R., Shi, H., Lee, E.J., et al. (2018). Activation of p53 in Immature Myeloid Precursor Cells Controls Differentiation into Ly6c+CD103+ Monocytic Antigen-Presenting Cells in Tumors. Immunity *48*, 91-106.e6. 10.1016/j.immuni.2017.12.014.

33. Zoul, W., Machelon, V., Coulomb-L'Hermin, A., Borvakz, J., Nome, F., Isaeva, T., Wei, S., Krzysieks, R., Durand-Gasselin, I., Gordon, A., et al. (2001). Stromal-derived factor-1 in human tumors recruits and alters the function of plasmacytoid precursor dendritic cells. Nature Medicine 2001 7:12 *7*, 1339–1346. 10.1038/nm1201-1339.

34. DeNardo, D.G., and Ruffell, B. (2019). Macrophages as regulators of tumour immunity and immunotherapy. Nature Reviews Immunology 2019 19:6 *19*, 369–382. 10.1038/s41577-019-0127-6.

35. Boutilier, A.J., and Elsawa, S.F. (2021). Macrophage Polarization States in the Tumor Microenvironment. Int J Mol Sci *22*. 10.3390/IJMS22136995.

36. Muntjewerff, E.M., Meesters, L.D., and van den Bogaart, G. (2020). Antigen Cross-Presentation by Macrophages. Front Immunol *11*, 1276. 10.3389/FIMMU.2020.01276/BIBTEX.

37. Ostrand-Rosenberg, S., Sinha, P., Beury, D.W., and Clements, V.K. (2012). Cross-talk between myeloid-derived suppressor cells (MDSC), macrophages, and dendritic cells enhances tumor-induced immune suppression. Semin Cancer Biol *22*, 275. 10.1016/J.SEMCANCER.2012.01.011.

38. Blum, J.S., Wearsch, P.A., and Cresswell, P. (2013). Pathways of Antigen Processing. Annu Rev Immunol *31*, 443. 10.1146/ANNUREV-IMMUNOL-032712-095910.

39. Hammer, G.E., Gonzalez, F., James, E., Nolla, H., and Shastri, N. (2007). In the absence of aminopeptidase ERAAP, MHC class I molecules present many unstable and highly immunogenic peptides. Nat Immunol *8*, 101–108. 10.1038/NI1409.

40. Boulanger, D.S.M., Douglas, L.R., Duriez, P.J., Kang, Y., Dalchau, N., James, E., and Elliott, T. (2022). Tapasin-mediated editing of the MHC I immunopeptidome is epitope specific and dependent on peptide off-rate, abundance, and level of tapasin expression. Front Immunol *13*, 956603. 10.3389/FIMMU.2022.956603/BIBTEX.

41. van Hateren, A., and Elliott, T. (2021). The role of MHC I protein dynamics in tapasin and TAPBPR-assisted immunopeptidome editing. Curr Opin Immunol *70*, 138–143. 10.1016/J.COI.2021.06.016.

42. Landsverk, O.J.B., Bakke, O., and Gregers, T.F. (2009). MHC II and the endocytic pathway: regulation by invariant chain. Scand J Immunol *70*, 184–193. 10.1111/J.1365-3083.2009.02301.X.

43. Joffre, O.P., Segura, E., Savina, A., and Amigorena, S. (2012). Cross-presentation by dendritic cells. Nature Reviews Immunology 2012 12:8 *12*, 557–569. 10.1038/nri3254.

44. Mant, A., Chinnery, F., Elliott, T., and Williams, A.P. (2012). The pathway of cross-presentation is influenced by the particle size of phagocytosed antigen. Immunology *136*, 163–175. 10.1111/J.1365-2567.2012.03558.X.

45. Smith-Garvin, J.E., Koretzky, G.A., and Jordan, M.S. (2009). T cell activation. Annu Rev Immunol *27*, 591–619. 10.1146/ANNUREV.IMMUNOL.021908.132706.

46. Pham, N.L.L., Badovinac, V.P., and Harty, J.T. (2011). Differential role of "signal 3" inflammatory cytokines in regulating CD8 T cell expansion and differentiation in vivo. Front Immunol *2*, 4. 10.3389/FIMMU.2011.00004/BIBTEX.

47. Taraban, V.Y., Rowley, T.F., O'brien, L., Chan, H.T.C., Haswell, L.E., Green, M.H.A., Tutt, A.L., Glennie, M.J., and Al-Shamkhani, A. (2002). Expression and costimulatory effects of the TNF receptor superfamily members CD134 (OX40) and CD137 (4-1BB), and their role in the generation of anti-tumor immune responses. 10.1002/1521-4141.

48. Bansal-Pakala, P., Halteman, B.S., Cheng, M.H.-Y., and Croft, M. (2004). Costimulation of CD8 T cell responses by OX40. J Immunol *172*, 4821–4825. 10.4049/JIMMUNOL.172.8.4821.

49. Laheurte, C., Dosset, M., Vernerey, D., Boullerot, L., Gaugler, B., Gravelin, E., Kaulek, V., Jacquin, M., Cuche, L., Eberst, G., et al. (2019). Distinct prognostic value of circulating anti-telomerase CD4+ Th1 immunity and exhausted PD-1+/TIM-3+ T cells in lung cancer. British Journal of Cancer 2019 121:5 *121*, 405–416. 10.1038/s41416-019-0531-5.

50. Raskov, H., Orhan, A., Christensen, J.P., and Gögenur, I. (2020). Cytotoxic CD8+ T cells in cancer and cancer immunotherapy. British Journal of Cancer 2020 124:2 *124*, 359–367. 10.1038/s41416-020-01048-4.

51. Oh, D.Y., and Fong, L. (2021). Cytotoxic CD4+ T cells in cancer: Expanding the immune effector toolbox. Immunity *54*, 2701–2711. 10.1016/j.immuni.2021.11.015.

52. Donnarumma, T., Young, G.R., Merkenschlager, J., Eksmond, U., Bongard, N., Nutt, S.L., Boyer, C., Dittmer, U., Le-Trilling, V.T.K., Trilling, M., et al. (2016). Opposing Development of Cytotoxic and Follicular Helper CD4 T Cells Controlled by the TCF-1-Bcl6 Nexus. Cell Rep *17*, 1571–1583. 10.1016/J.CELREP.2016.10.013.

53. Śledzińska, A., Vila de Mucha, M., Bergerhoff, K., Hotblack, A., Demane, D.F., Ghorani, E., Akarca, A.U., Marzolini, M.A.V., Solomon, I., Vargas, F.A., et al. (2020). Regulatory T Cells Restrain Interleukin-2- and Blimp-1-Dependent Acquisition of Cytotoxic Function by CD4+ T Cells. Immunity *52*, 151-166.e6. 10.1016/j.immuni.2019.12.007.

54. Wu, T., Shin, H.M., Ashley, E., Gattinoni, L., Mcgavern, D.B., and Schwartzberg Correspondence, P.L. (2015). TCF1 Is Required for the T Follicular Helper Cell Response to Viral Infection. CellReports *12*, 2099–2110. 10.1016/j.celrep.2015.08.049.

55. Basu, A., Ramamoorthi, G., Albert, G., Gallen, C., Beyer, A., Snyder, C., Koski, G., Disis, M.L., Czerniecki, B.J., and Kodumudi, K. (2021). Differentiation and Regulation of TH Cells: A Balancing Act for Cancer Immunotherapy. Front Immunol *12*, 669474. 10.3389/FIMMU.2021.669474.

56. Tay, R.E., Richardson, E.K., and Toh, H.C. (2020). Revisiting the role of CD4+ T cells in cancer immunotherapy—new insights into old paradigms. Cancer Gene Therapy 2020 28:1 *28*, 5–17. 10.1038/s41417-020-0183-x.

57. Dolina, J.S., Van Braeckel-Budimir, N., Thomas, G.D., and Salek-Ardakani, S. (2021). CD8+ T Cell Exhaustion in Cancer. Front Immunol *12*, 2880. 10.3389/FIMMU.2021.715234/BIBTEX.

58. Paley, M.A., and Wherry, E.J. (2010). TCF-1 Flips the Switch on Eomes. Immunity *33*, 145–147. 10.1016/j.immuni.2010.08.008.

59. Zhang, J., Lyu, T., Cao, Y., and Feng, H. (2021). Role of TCF-1 in differentiation, exhaustion, and memory of CD8+ T cells: A review. FASEB J *35*. 10.1096/FJ.202002566R.

60. Zhao, X., Shan, Q., and Xue, H.H. (2021). TCF1 in T cell immunity: a broadened frontier. Nature Reviews Immunology 2021 22:3 *22*, 147–157. 10.1038/s41577-021-00563-6.

61. Weber, B.N., Chi, A.W.S., Chavez, A., Yashiro-Ohtani, Y., Yang, Q., Shestova, O., and Bhandoola, A. (2011). A critical role for TCF-1 in T-lineage specification and differentiation. Nature 2011 476:7358 *476*, 63–68. 10.1038/nature10279.

62. Siddiqui, I., Schaeuble, K., Chennupati, V., Fuertes Marraco, S.A., Calderon-Copete, S., Pais Ferreira, D., Carmona, S.J., Scarpellino, L., Gfeller, D., Pradervand, S., et al. (2019). Intratumoral Tcf1+PD-1+CD8+ T Cells with Stem-like Properties Promote Tumor Control in Response to Vaccination and Checkpoint Blockade Immunotherapy. Immunity *50*, 195-211.e10. 10.1016/J.IMMUNI.2018.12.021.

63. Masopust, D., and Schenkel, J.M. (2013). The integration of T cell migration, differentiation and function. Nat. Rev. Immunol. *13*, 309–320. 10.1038/nri3442.

64. Bjorkdahl, O., Barber, K.A., Brett, S.J., Daly, M.G., Plumpton, C., Elshourbagy, N.A., Tite, J.P., and Thomsen, L.L. (2003). Characterization of CC-chemokine receptor 7 expression on murine T cells in lymphoid tissues. Immunology *110*, 170. 10.1046/J.1365-2567.2003.01727.X.

65. van der Woude, L.L., Gorris, M.A.J., Halilovic, A., Figdor, C.G., and de Vries, I.J.M. (2017). Migrating into the Tumor: a Roadmap for T Cells. Trends Cancer *3*, 797–808. 10.1016/J.TRECAN.2017.09.006.

66. Mullins, I.M., Slingluff, C.L., Lee, J.K., Garbee, C.F., Shu, J., Anderson, S.G., Mayer, M.E., Knaus, W.A., and Mullins, D.W. (2004). CXC chemokine receptor 3 expression by activated CD8+ T cells is associated with survival in melanoma patients with stage III disease. Cancer Res *64*, 7697–7701. 10.1158/0008-5472.CAN-04-2059.

67. Zhang, L., Conejo-Garcia, J.R., Katsaros, D., Gimotty, P.A., Massobrio, M., Regnani, G., Makrigiannakis, A., Gray, H., Schlienger, K., Liebman, M.N., et al. (2003). Intratumoral T cells, recurrence, and survival in epithelial ovarian cancer. N Engl J Med *348*, 203–213. 10.1056/NEJMOA020177.

68. Zhang, Y., Guan, X.Y., and Jiang, P. (2020). Cytokine and Chemokine Signals of T-Cell Exclusion in Tumors. Front Immunol *11*, 3093. 10.3389/FIMMU.2020.594609/BIBTEX.

69. Kohli, K., Pillarisetty, V.G., and Kim, T.S. (2021). Key chemokines direct migration of immune cells in solid tumors. Cancer Gene Therapy 2021 29:1 *29*, 10–21. 10.1038/s41417-021-00303-x.

70. Pan, J., Burdick, M.D., Belperio, J.A., Xue, Y.Y., Gerard, C., Sharma, S., Dubinett, S.M., and Strieter, R.M. (2006). CXCR3/CXCR3 ligand biological axis impairs RENCA tumor growth by a mechanism of immunoangiostasis. J Immunol *176*, 1456–1464. 10.4049/JIMMUNOL.176.3.1456.

71. Mikucki, M.E., Fisher, D.T., Matsuzaki, J., Skitzki, J.J., Gaulin, N.B., Muhitch, J.B., Ku, A.W., Frelinger, J.G., Odunsi, K., Gajewski, T.F., et al. (2015). Non-redundant requirement for CXCR3 signalling during tumoricidal T-cell trafficking across tumour vascular checkpoints. Nat Commun *6*. 10.1038/NCOMMS8458.

72. Fowell, D.J., and Kim, M. (2021). The spatio-temporal control of effector T cell migration. Nature Reviews Immunology 2021 21:9 *21*, 582–596. 10.1038/s41577-021-00507-0.

73. Coulie, P.G., Van Den Eynde, B.J., Van Der Bruggen, P., and Boon, T. (2014). Tumour antigens recognized by T lymphocytes: at the core of cancer immunotherapy. Nat Rev Cancer *14*, 135–146. 10.1038/NRC3670.

74. Kawakami, Y., Eliyahu, S., Sakaguchi, K., Robbins, P.F., Rivoltini, L., Yannelli, J.R., Appella, E., and Rosenberg, S.A. (1994). Identification of the immunodominant peptides of the MART-1 human melanoma antigen recognized by the majority of HLA-A2-restricted tumor infiltrating lymphocytes. J Exp Med *180*, 347–352. 10.1084/JEM.180.1.347.

75. Schumacher, T.N., and Schreiber, R.D. (2015). Neoantigens in cancer immunotherapy. Science (1979) *348*, 69–74. 10.1126/SCIENCE.AAA4971.

76. Lambert, P.F., and Sugden, B. (2006). Cancer issue: Viruses and Human Cancer. Yale J Biol Med *79*, 115. 10.1016/B978-0-323-47674-4.00012-8.

77. Weon, J.L., and Potts, P.R. (2015). The MAGE protein family and cancer. Curr Opin Cell Biol *37*, 1. 10.1016/J.CEB.2015.08.002.

78. Scanlan, M.J., Gure, A.O., Jungbluth, A.A., Old, L.J., and Chen, Y.T. (2002). Cancer/testis antigens: an expanding family of targets for cancer immunotherapy. Immunol Rev *188*, 22–32. 10.1034/J.1600-065X.2002.18803.X.

79. Van Eynde, B. Den, Hainaut, P., Hérin, M., Knuth, A., Lemoine, C., Weynants, P., Van Bruggen, P. Der, Fauchet, R., and Boon, T. (1989). Presence on a human melanoma of multiple antigens recognized by autologous CTL. Int J Cancer *44*, 634–640. 10.1002/IJC.2910440413.

80. Chen, Y.T., Scanlan, M.J., Sahin, U., Türeci, Ö., Gure, A.O., Tsang, S., Williamson, B., Stockert, E., Pfreundschuh, M., and Old, L.J. (1997). A testicular antigen aberrantly expressed in human cancers detected by autologous antibody screening. Proc Natl Acad Sci U S A *94*, 1914–1918. 10.1073/PNAS.94.5.1914.

81. Van Der Bruggen, P., Traversari, C., Chomez, P., Lurquin, C., De Plaen, E., Van Den Eynde, B., Knuth, A., and Boon, T. (1991). A gene encoding an antigen recognized by cytolytic T lymphocytes on a human melanoma. Science *254*, 1643–1647. 10.1126/SCIENCE.1840703.

82. Almeida, L.G., Sakabe, N.J., de Oliveira, A.R., Silva, M.C.C., Mundstein, A.S., Cohen, T., Chen, Y.T., Chua, R., Gurung, S., Gnjatic, S., et al. (2009). CTdatabase: a knowledge-base of high-throughput and curated data on cancer-testis antigens. Nucleic Acids Res *37*. 10.1093/NAR/GKN673.

83. Sarma, S., Guo, Y., Guilloux, Y., Lee, C., Bai, X.F., and Liu, Y. (1999). Cytotoxic T lymphocytes to an unmutated tumor rejection antigen P1A: Normal development but restrained effector function in vivo. Journal of Experimental Medicine *189*, 811–820. 10.1084/jem.189.5.811.

84. Smith, C.C., Selitsky, S.R., Chai, S., Armistead, P.M., Vincent, B.G., and Serody, J.S. (2019). Alternative tumour-specific antigens. Nature Reviews Cancer 2019 19:8 *19*, 465–478. 10.1038/s41568-019-0162-4.

85. Kassiotis, G. (2014). Endogenous retroviruses and the development of cancer. J Immunol *192*, 1343–1349. 10.4049/JIMMUNOL.1302972.

86. M, S., S, S., E, K., K, R., G, D., I, L., M, B., B, B., D, N.-H., and N, M.-L. (1995). Human endogenous retrovirus K10: expression of Gag protein and detection of antibodies in patients with seminomas. J Virol *69*, 414–421. 10.1128/JVI.69.1.414-421.1995.

87. Cherkasova, E., Scrivani, C., Doh, S., Weisman, Q., Takahashi, Y., Harashima, N., Yokoyama, H., Srinivasan, R., Linehan, W.M., Lerman, M.I., et al. (2016). Detection of an Immunogenic HERV-E Envelope with Selective Expression in Clear Cell Kidney Cancer. Cancer Res *76*, 2177–2185. 10.1158/0008-5472.CAN-15-3139.

88. Ng, K.W., Boumelha, J., Enfield, K.S.S., Almagro, J., Cha, H., Pich, O., Karasaki, T., Moore, D.A., Salgado, R., Sivakumar, M., et al. (2023). Antibodies against endogenous retroviruses promote lung cancer immunotherapy. Nature 2023 616:7957 *616*, 563–573. 10.1038/s41586-023-05771-9.

89. Barczak, W., Carr, S.M., Liu, G., Munro, S., Nicastri, A., Lee, L.N., Hutchings, C., Ternette, N., Klenerman, P., Kanapin, A., et al. (2023). Long non-coding RNA-derived peptides are immunogenic and drive a potent anti-tumour response. Nat Commun *14*, 1078. 10.1038/s41467-023-36826-0.

90. Laumont, C.M., Vincent, K., Hesnard, L., Audemard, É., Bonneil, É., Laverdure, J.P., Gendron, P., Courcelles, M., Hardy, M.P., Côté, C., et al. (2018). Noncoding regions are the main source of targetable tumor-specific antigens. Sci Transl Med *10*. 10.1126/SCITRANSLMED.AAU5516/SUPPL_FILE/AAU5516_TABLES_S1_TO_S18.XLSX.

91. Li, F., Li, C., Cai, X., Xie, Z., Zhou, L., Cheng, B., Zhong, R., Xiong, S., Li, J., Chen, Z., et al. (2021). The association between CD8+ tumor-infiltrating lymphocytes and the clinical outcome of cancer immunotherapy: A systematic review and meta-analysis. EClinicalMedicine *41*, 101134. 10.1016/J.ECLINM.2021.101134.

92. Liu, S., Lachapelle, J., Leung, S., Gao, D., Foulkes, W.D., and Nielsen, T.O. (2012). CD8 +lymphocyte infiltration is an independent favorable prognostic indicator in basal-like breast cancer. Breast Cancer Research *14*, 1–14. 10.1186/BCR3148/TABLES/4.

93. Schulze, A.B., Evers, G., Görlich, D., Mohr, M., Marra, A., Hillejan, L., Rehkämper, J., Schmidt, L.H., and Heitkötter, B. (2020). Tumor infiltrating T cells influence prognosis in stage I–III non-small cell lung cancer. J Thorac Dis *12*, 1824. 10.21037/JTD-19-3414A.

94. Axelrod, M.L., Cook, R.S., Johnson, D.B., and Balko, J.M. (2019). Biological consequences of MHC-II expression by tumor cells in cancer. Clinical Cancer Research *25*, 2392–2402. 10.1158/1078-0432.CCR-18-3200/74844/AM/BIOLOGICAL-CONSEQUENCES-OF-MAJOR.

95. Weigelin, B., den Boer, A.T., Wagena, E., Broen, K., Dolstra, H., de Boer, R.J., Figdor, C.G., Textor, J., and Friedl, P. (2021). Cytotoxic T cells are able to efficiently eliminate cancer cells by additive cytotoxicity. Nature Communications 2021 12:1 *12*, 1–12. 10.1038/s41467-021-25282-3.

96. Chin, Y.E., Kitagawa, M., Kuida, K., Flavell, R.A., and Fu, X.Y. (1997). Activation of the STAT signaling pathway can cause expression of caspase 1 and apoptosis. Mol Cell Biol *17*, 5328–5337. 10.1128/MCB.17.9.5328.

97. Fridman, W.H., Petitprez, F., Meylan, M., Chen, T.W.W., Sun, C.M., Roumenina, L.T., and Sautès-Fridman, C. (2021). B cells and cancer: To B or not to B? Journal of Experimental Medicine *218*. 10.1084/JEM.20200851/211614.

98. Niogret, J., Berger, H., Rebe, C., Mary, R., Ballot, E., Truntzer, C., Thibaudin, M., Derangère, V., Hibos, C., Hampe, L., et al. (2021). Original research: Follicular helper-T cells restore CD8+-dependent antitumor immunity and anti-PD-L1/PD-1 efficacy. J Immunother Cancer *9*, 2157. 10.1136/JITC-2020-002157.

99. Zitvogel, L., Tesniere, A., and Kroemer, G. (2006). Cancer despite immunosurveillance: immunoselection and immunosubversion. Nature Reviews Immunology 2006 6:10 *6*, 715–727. 10.1038/nri1936.

100. Labani-Motlagh, A., Ashja-Mahdavi, M., and Loskog, A. (2020). The Tumor Microenvironment: A Milieu Hindering and Obstructing Antitumor Immune Responses. Front Immunol *11*. 10.3389/FIMMU.2020.00940.

101. Hiam-Galvez, K.J., Allen, B.M., and Spitzer, M.H. (2021). Systemic immunity in cancer. Nature Reviews Cancer 2021 21:6 *21*, 345–359. 10.1038/s41568-021-00347-z.

102. Garg, A.D., Martin, S., Golab, J., and Agostinis, P. (2013). Danger signalling during cancer cell death: origins, plasticity and regulation. Cell Death & Differentiation 2014 21:1 *21*, 26–38. 10.1038/cdd.2013.48.

103. Lin, A., Schildknecht, A., Nguyen, L.T., and Ohashi, P.S. (2010). Dendritic cells integrate signals from the tumor microenvironment to modulate immunity and tumor growth. Immunol Lett *127*, 77–84. 10.1016/J.IMLET.2009.09.003.

104. Lin, J.H., Huffman, A.P., Wattenberg, M.M., Walter, D.M., Carpenter, E.L., Feldser, D.M., Beatty, G.L., Furth, E.E., and Vonderheide, R.H. (2020). Type 1 conventional dendritic cells are systemically dysregulated early in pancreatic carcinogenesis. Journal of Experimental Medicine *217*. 10.1084/JEM.20190673/151817.

105. Gabrilovich, D.I., and Nagaraj, S. (2009). Myeloid-derived suppressor cells as regulators of the immune system. Nat Rev Immunol *9*, 162–174. 10.1038/NRI2506.

106. Bronte, V., Brandau, S., Chen, S.H., Colombo, M.P., Frey, A.B., Greten, T.F., Mandruzzato, S., Murray, P.J., Ochoa, A., Ostrand-Rosenberg, S., et al. (2016). Recommendations for myeloid-derived suppressor cell nomenclature and characterization standards. Nature Communications 2016 7:1 *7*, 1–10. 10.1038/ncomms12150.

107. Bayik, D., Zhou, Y., Park, C., Hong, C., Vail, D., Silver, D.J., Lauko, A., Roversi, G., Watson, D.C., Lo, A., et al. (2020). Myeloid-derived suppressor cell subsets

drive glioblastoma growth in a sex-specific manner. Cancer Discov *10*, 1210. 10.1158/2159-8290.CD-19-1355.

108. Seidel, J.A., Otsuka, A., and Kabashima, K. (2018). Anti-PD-1 and Anti-CTLA-4 Therapies in Cancer: Mechanisms of Action, Efficacy, and Limitations. Front Oncol *8*, 86. 10.3389/FONC.2018.00086.

109. Wing, K., Onishi, Y., Prieto-Martin, P., Yamaguchi, T., Miyara, M., Fehervari, Z., Nomura, T., and Sakaguchi, S. (2008). CTLA-4 control over Foxp3+ regulatory T cell function. Science *322*, 271–275. 10.1126/SCIENCE.1160062.

110. Paluskievicz, C.M., Cao, X., Abdi, R., Zheng, P., Liu, Y., and Bromberg, J.S. (2019). T regulatory cells and priming the suppressive tumor microenvironment. Front Immunol *10*, 2453. 10.3389/FIMMU.2019.02453/BIBTEX.

111. Groth, C., Hu, X., Weber, R., Fleming, V., Altevogt, P., Utikal, J., and Umansky, V. (2019). Immunosuppression mediated by myeloid-derived suppressor cells (MDSCs) during tumour progression. Br J Cancer *120*, 16–25. 10.1038/S41416-018-0333-1.

112. Corzo, C.A., Cotter, M.J., Cheng, P., Cheng, F., Kusmartsev, S., Sotomayor, E., Padhya, T., McCaffrey, T. V., McCaffrey, J.C., and Gabrilovich, D.I. (2009). Mechanism regulating reactive oxygen species in tumor-induced myeloid-derived suppressor cells. J Immunol *182*, 5693–5701. 10.4049/JIMMUNOL.0900092.

113. Griffioen, A.W. (2008). Anti-angiogenesis: making the tumor vulnerable to the immune system. Cancer Immunology, Immunotherapy *57*, 1553. 10.1007/S00262-008-0524-3.

114. Schouppe, E., Mommer, C., Movahedi, K., Laoui, D., Morias, Y., Gysemans, C., Luyckx, A., De Baetselier, P., and Van Ginderachter, J.A. (2013). Tumor-induced myeloid-derived suppressor cell subsets exert either inhibitory or stimulatory effects on distinct CD8+ T-cell activation events. Eur J Immunol *43*, 2930–2942. 10.1002/EJI.201343349.

115. Vuillefroy de Silly, R., Dietrich, P.Y., and Walker, P.R. (2016). Hypoxia and antitumor CD8+ T cells: An incompatible alliance? Oncoimmunology *5*. 10.1080/2162402X.2016.1232236.

116. Chang, C.H., Qiu, J., O'Sullivan, D., Buck, M.D., Noguchi, T., Curtis, J.D., Chen, Q., Gindin, M., Gubin, M.M., Van Der Windt, G.J.W., et al. (2015). Metabolic competition in the tumor microenvironment is a driver of cancer progression. Cell *162*, 1229. 10.1016/J.CELL.2015.08.016.

117. Sharpe, A.H., and Pauken, K.E. (2017). The diverse functions of the PD1 inhibitory pathway. Nature Reviews Immunology 2017 18:3 *18*, 153–167. 10.1038/nri.2017.108.

118. Salmaninejad, A., Valilou, S.F., Shabgah, A.G., Aslani, S., Alimardani, M., Pasdar, A., and Sahebkar, A. (2019). PD-1/PD-L1 pathway: Basic biology and role in cancer immunotherapy. J Cell Physiol *234*, 16824–16837. 10.1002/jcp.28358.

119. Das, M., Zhu, C., and Kuchroo, V.K. (2017). Tim-3 and its role in regulating anti-tumor immunity. Immunol Rev *276*, 97. 10.1111/IMR.12520.

120. Sakuishi, K., Apetoh, L., Sullivan, J.M., Blazar, B.R., Kuchroo, V.K., and Anderson, A.C. (2010). Targeting Tim-3 and PD-1 pathways to reverse T cell exhaustion and restore anti-tumor immunity. J Exp Med *207*, 2187. 10.1084/JEM.20100643.

121. Fang, X., Wu, G., Hua, J., Zhao, P., Shan, M., Wang, N., Zeng, Y., Ding, T., Zhu, H., Zhu, X., et al. (2022). TCF-1+ PD-1+ CD8+T cells are associated with the response to PD-1 blockade in non-small cell lung cancer patients. J Cancer Res Clin Oncol *148*, 2653–2660. 10.1007/S00432-021-03845-7.

122. Monu, N.R., and Frey, A.B. (2012). Myeloid-Derived Suppressor Cells and anti-tumor T cells: a complex relationship. Immunol Invest *41*, 595. 10.3109/08820139.2012.673191.

123. Huang, B., Pan, P.Y., Li, Q., Sato, A.I., Levy, D.E., Bromberg, J., Divino, C.M., and Chen, S.H. (2006). Gr-1+CD115+ immature myeloid suppressor cells mediate the development of tumor-induced T regulatory cells and T-cell anergy in tumor-bearing host. Cancer Res *66*, 1123–1131. 10.1158/0008-5472.CAN-05-1299.

124. Nishikawa, H., and Koyama, S. (2021). Mechanisms of regulatory T cell infiltration in tumors: implications for innovative immune precision therapies. J Immunother Cancer *9*, e002591. 10.1136/JITC-2021-002591.

125. Nakamura, H., and Maeda, H. (2022). Cancer Chemotherapy. Fundamentals of Pharmaceutical Nanoscience, 401–427. 10.1007/978-1-4614-9164-4_15.

126. de Sousa, G.F., Wlodarczyk, S.R., and Monteiro, G. (2014). Carboplatin: molecular mechanisms of action associated with chemoresistance. Brazilian Journal of Pharmaceutical Sciences *50*, 693–701. 10.1590/S1984-82502014000400004.

127. Kampan, N.C., Madondo, M.T., McNally, O.M., Quinn, M., and Plebanski, M. (2015). Paclitaxel and Its Evolving Role in the Management of Ovarian Cancer. Biomed Res Int *2015*. 10.1155/2015/413076.

128. Schiff, P.B., Fant, J., and Horwitz, S.B. (1979). Promotion of microtubule assembly in vitro by taxol. Nature *277*, 665–667. 10.1038/277665A0.

129. Zitvogel, L., Apetoh, L., Ghiringhelli, F., and Kroemer, G. (2008). Immunological aspects of cancer chemotherapy. Nat Rev Immunol *8*, 59–73. 10.1038/NRI2216.

130. Opzoomer, J.W., Sosnowska, D., Anstee, J.E., Spicer, J.F., and Arnold, J.N. (2019). Cytotoxic chemotherapy as an immune stimulus: A molecular perspective on turning up the immunological heat on cancer. Front Immunol *10*, 1654. 10.3389/FIMMU.2019.01654/BIBTEX.

131. Van Der Most, R.G., Currie, A.J., Cleaver, A.L., Salmons, J., Nowak, A.K., Mahendran, S., Larma, I., Prosser, A., Robinson, B.W.S., Smyth, M.J., et al. Cyclophosphamide Chemotherapy Sensitizes Tumor Cells to TRAIL-Dependent CD8 T Cell-Mediated Immune Attack Resulting in Suppression of Tumor Growth. 10.1371/journal.pone.0006982.

132. Obeid, M., Tesniere, A., Ghiringhelli, F., Fimia, G.M., Apetoh, L., Perfettini, J.L., Castedo, M., Mignot, G., Panaretakis, T., Casares, N., et al. (2006). Calreticulin exposure dictates the immunogenicity of cancer cell death. Nature Medicine 2006 13:1 *13*, 54–61. 10.1038/nm1523.

133. Tesniere, A., Schlemmer, F., Boige, V., Kepp, O., Martins, I., Ghiringhelli, F., Aymeric, L., Michaud, M., Apetoh, L., Barault, L., et al. (2009). Immunogenic death of colon cancer cells treated with oxaliplatin. Oncogene 2010 29:4 *29*, 482–491. 10.1038/onc.2009.356.

134. Kim, W.S., Kim, H., Kwon, K.W., Im, S.H., Lee, B.R., Ha, S.J., and Shin, S.J. (2016). Cisplatin induces tolerogenic dendritic cells in response to TLR agonists via the abundant production of IL-10, thereby promoting Th2- and Tr1-biased T-cell immunity. Oncotarget *7*, 33765. 10.18632/ONCOTARGET.9260.

135. Wu, J., and Waxman, D.J. (2014). Metronomic cyclophosphamide schedule-dependence of innate immune cell recruitment and tumor regression in an implanted glioma model. Cancer Lett *353*, 272–280. 10.1016/J.CANLET.2014.07.033.

136. Fabian, K.P., Wolfson, B., and Hodge, J.W. (2021). From Immunogenic Cell Death to Immunogenic Modulation: Select Chemotherapy Regimens Induce a Spectrum of Immune-Enhancing Activities in the Tumor Microenvironment. Front Oncol *11*, 3215. 10.3389/FONC.2021.728018/BIBTEX.

137. Wu, J., and Waxman, D.J. (2018). Immunogenic chemotherapy: Dose and schedule dependence and combination with immunotherapy. Cancer Lett *419*, 210. 10.1016/J.CANLET.2018.01.050.

138. Jia, L., and Waxman, D.J. (2013). Thrombospondin-1 and pigment epithelium-derived factor enhance responsiveness of KM12 colon tumor to metronomic cyclophosphamide but have disparate effects on tumor metastasis. Cancer Lett *330*, 241–249. 10.1016/J.CANLET.2012.11.055.

139. Chen, C.S., Doloff, J.C., and Waxman, D.J. (2014). Intermittent Metronomic Drug Schedule Is Essential for Activating Antitumor Innate Immunity and Tumor Xenograft Regression. Neoplasia *16*, 84-W27. 10.1593/NEO.131910.

140. Cazzaniga, M.E., Cordani, N., Capici, S., Cogliati, V., Riva, F., and Cerrito, M.G. (2021). Metronomic Chemotherapy. Cancers (Basel) *13*. 10.3390/CANCERS13092236.

141. Lake, R.A., and Robinson, B.W.S. (2005). Immunotherapy and chemotherapy — a practical partnership. Nature Reviews Cancer 2005 5:5 *5*, 397–405. 10.1038/nrc1613.

142. Chang, C.L., Hsu, Y.T., Wu, C.C., Lai, Y.Z., Wang, C., Yang, Y.C., Wu, T.C., and Hung, C.F. (2013). Dose-dense chemotherapy improves mechanisms of antitumor immune response. Cancer Res *73*, 119–127. 10.1158/0008-5472.CAN-12-2225/650650/AM/DOSE-DENSE-CHEMOTHERAPY-IMPROVES-MECHANISMS-OF.

143. Byrd-Leifer, C.A., Block, E.F., Takeda, K., Akira, S., and Ding, A. (2001). The role of MyD88 and TLR4 in the LPS-mimetic activity of Taxol. Eur J Immunol *31*, 2448–2457. 10.1002/1521-4141(200108)31:8<2448::aid-immu2448>3.0.co;2-n.

144. Carson, W.E., Shapiro, C.L., Crespin, T.R., Thornton, L.M., and Andersen, B.L. (2004). Cellular immunity in breast cancer patients completing taxane treatment. Clin Cancer Res *10*, 3401–3409. 10.1158/1078-0432.CCR-1016-03.

145. Liu, M., Tayob, N., Penter, L., Sellars, M., Tarren, A., Chea, V., Carulli, I., Huang, T., Li, S., Cheng, S.C., et al. (2022). Improved T-cell Immunity Following Neoadjuvant Chemotherapy in Ovarian Cancer. Clin Cancer Res *28*, 3356–3366. 10.1158/1078-0432.CCR-21-2834.

146. de Goeje, P.L., Poncin, M., Bezemer, K., Kaijen-Lambers, M.E.H., Groen, H.J.M., Smit, E.F., Dingemans, A.M.C., Kunert, A., Hendriks, R.W., and Aerts, J.G.J.V. (2019). Induction of Peripheral Effector CD8 T-cell Proliferation by Combination of Paclitaxel, Carboplatin, and Bevacizumab in Non-small Cell Lung Cancer Patients. Clin Cancer Res *25*, 2219–2227. 10.1158/1078-0432.CCR-18-2243.

147. Yan, Y., Dronca, R.S., Liu, X., Markovic, S., and Dong, H. (2018). Effect of paclitaxel and carboplatin on tumor-reactive T cells and the efficacy of PD-1 blockade. https://doi.org/10.1200/JCO.2017.35.7_suppl.65 *35*, 65–65. 10.1200/JCO.2017.35.7_SUPPL.65.

148. Katsumata, N., Yasuda, M., Takahashi, F., Isonishi, S., Jobo, T., Aoki, D., Tsuda, H., Sugiyama, T., Kodama, S., Kimura, E., et al. (2009). Dose-dense paclitaxel once a week in combination with carboplatin every 3 weeks for advanced ovarian cancer: a phase 3, open-label, randomised controlled trial. The Lancet *374*, 1331–1338. 10.1016/S0140-6736(09)61157-0.

149. Lutsiak, M.E.C., Semnani, R.T., De Pascalis, R., Kashmiri, S.V.S., Schlom, J., and Sabzevari, H. (2005). Inhibition of CD4(+)25+ T regulatory cell function implicated in enhanced immune response by low-dose cyclophosphamide. Blood *105*, 2862–2868. 10.1182/BLOOD-2004-06-2410.

150. Welters, M.J., Van Der Sluis, T.C., Van Meir, H., Loof, N.M., Van Ham, V.J., Van Duikeren, S., Santegoets, S.J., Arens, R., De Kam, M.L., Cohen, A.F., et al. (2016). Vaccination during myeloid cell depletion by cancer chemotherapy fosters robust T cell responses. Sci Transl Med *8*. 10.1126/SCITRANSLMED.AAD8307.

151. Vincent, J., Mignot, G., Chalmin, F., Ladoire, S., Bruchard, M., Chevriaux, A., Martin, F., Apetoh, L., Rébé, C., and Ghiringhelli, F. (2010). 5-Fluorouracil selectively kills tumor-associated myeloid-derived suppressor cells resulting in enhanced T cell-dependent antitumor immunity. Cancer Res *70*, 3052–3061. 10.1158/0008-5472.CAN-09-3690.

152. Suzuki, E., Kapoor, V., Jassar, A.S., Kaiser, L.R., and Albelda, S.M. (2005). Gemcitabine selectively eliminates splenic Gr-1+/CD11b+ myeloid suppressor cells in tumor-bearing animals and enhances antitumor immune activity. Clin Cancer Res *11*, 6713–6721. 10.1158/1078-0432.CCR-05-0883.

153. Wu, C., Tan, X., Hu, X., Zhou, M., Yan, J., and Ding, C. (2020). Tumor microenvironment following Gemcitabine treatment favors differentiation of immunosuppressive Ly6Chigh myeloid cells. J Immunol *204*, 212. 10.4049/JIMMUNOL.1900930.

154. Chan, T.S., Hsu, C.C., Pai, V.C., Liao, W.Y., Huang, S.S., Tan, K.T., Yen, C.J., Hsu, S.C., Chen, W.Y., Shan, Y.S., et al. (2016). Metronomic chemotherapy prevents therapy-induced stromal activation and induction of tumor-initiating cells. Journal of Experimental Medicine *213*, 2967–2988. 10.1084/JEM.20151665.

155. Corrigan-Curay, J., Kiem, H.-P., Baltimore, D., O'Reilly, M., Brentjens, R.J., Cooper, L., Forman, S., Gottschalk, S., Greenberg, P., Junghans, R., et al. (2014). T-Cell Immunotherapy: Looking Forward. Molecular Therapy *22*, 1564–1574. 10.1038/mt.2014.148.

156. Sadelain, M., Brentjens, R., and Rivière, I. (2013). The basic principles of chimeric antigen receptor design. Cancer Discov *3*, 388–398. 10.1158/2159-8290.CD-12-0548/42970/P/THE-BASIC-PRINCIPLES-OF-CHIMERIC-ANTIGEN-RECEPTOR.

157. Maude, S.L., Frey, N., Shaw, P.A., Aplenc, R., Barrett, D.M., Bunin, N.J., Chew, A., Gonzalez, V.E., Zheng, Z., Lacey, S.F., et al. (2014). Chimeric Antigen Receptor T Cells for Sustained Remissions in Leukemia. N Engl J Med *371*, 1507. 10.1056/NEJMOA1407222.

158. Schuster, S.J., Svoboda, J., Chong, E.A., Nasta, S.D., Mato, A.R., Anak, Ö., Brogdon, J.L., Pruteanu-Malinici, I., Bhoj, V., Landsburg, D., et al. (2017). Chimeric Antigen Receptor T Cells in Refractory B-Cell Lymphomas. New England Journal of Medicine *377*, 2545–2554. 10.1056/NEJMOA1708566/SUPPL_FILE/NEJMOA1708566_DISCLOSURES.PDF.

159. Yang, J.C., and Rosenberg, S.A. (2016). Adoptive T-Cell Therapy for Cancer. Adv Immunol *130*, 279–294. 10.1016/BS.AI.2015.12.006.

160. Brudno, J.N., and Kochenderfer, J.N. (2019). Recent advances in CAR T-cell toxicity: Mechanisms, manifestations and management. Blood Rev *34*, 45–55. 10.1016/J.BLRE.2018.11.002.

161. Furzer, J., Gupta, S., Nathan, P.C., Schechter, T., Pole, J.D., Krueger, J., and Pechlivanoglou, P. (2020). Cost-effectiveness of Tisagenlecleucel vs Standard Care in High-risk Relapsed Pediatric Acute Lymphoblastic Leukemia in Canada. JAMA Oncol *6*, 393–401. 10.1001/JAMAONCOL.2019.5909.

162. Kruger, S., Ilmer, M., Kobold, S., Cadilha, B.L., Endres, S., Ormanns, S., Schuebbe, G., Renz, B.W., D'Haese, J.G., Schloesser, H., et al. (2019). Advances in cancer immunotherapy 2019 - latest trends. J Exp Clin Cancer Res *38*. 10.1186/S13046-019-1266-0.

163. Larkin, J., and Gore, M. (2008). Malignant melanoma (metastatic). BMJ Clin Evid *2008*.

164. Larkin, J., Chiarion-Sileni, V., Gonzalez, R., Grob, J.-J., Rutkowski, P., Lao, C.D., Cowey, C.L., Schadendorf, D., Wagstaff, J., Dummer, R., et al. (2019). Five-Year Survival with Combined Nivolumab and Ipilimumab in Advanced Melanoma. New England Journal of Medicine *381*, 1535–1546. 10.1056/NEJMOA1910836/SUPPL_FILE/NEJMOA1910836_DATA-SHARING.PDF.

165. Rotte, A. (2019). Combination of CTLA-4 and PD-1 blockers for treatment of cancer. Journal of Experimental & Clinical Cancer Research 2019 38:1 *38*, 1–12. 10.1186/S13046-019-1259-Z.

166. Michot, J.M., Bigenwald, C., Champiat, S., Collins, M., Carbonnel, F., Postel-Vinay, S., Berdelou, A., Varga, A., Bahleda, R., Hollebecque, A., et al. (2016). Immune-related adverse events with immune checkpoint blockade: A comprehensive review. Eur J Cancer *54*, 139–148. 10.1016/j.ejca.2015.11.016.

167. Au, L., Hatipoglu, E., Robert de Massy, M., Litchfield, K., Beattie, G., Rowan, A., Schnidrig, D., Thompson, R., Byrne, F., Horswell, S., et al. (2021). Determinants of anti-PD-1 response and resistance in clear cell renal cell carcinoma. Cancer Cell *39*, 1497-1518.e11. 10.1016/J.CCELL.2021.10.001.

168. Marin-Acevedo, J.A., Dholaria, B., Soyano, A.E., Knutson, K.L., Chumsri, S., and Lou, Y. (2018). Next generation of immune checkpoint therapy in cancer: new developments and challenges. J Hematol Oncol *11*. 10.1186/S13045-018-0582-8.

169. Law, A.M.K., Valdes-Mora, F., and Gallego-Ortega, D. (2020). Myeloid-Derived Suppressor Cells as a Therapeutic Target for Cancer. Cells *9*. 10.3390/CELLS9030561.

170. Ko, J.S., Zea, A.H., Rini, B.I., Ireland, J.L., Elson, P., Cohen, P., Golshayan, A., Rayman, P.A., Wood, L., Garcia, J., et al. (2009). Sunitinib mediates reversal of myeloid-derived suppressor cell accumulation in renal cell carcinoma patients. Clin Cancer Res *15*, 2148–2157. 10.1158/1078-0432.CCR-08-1332.

171. Mirza, N., Fishman, M., Fricke, I., Dunn, M., Neuger, A.M., Frost, T.J., Lush, R.M., Antonia, S., and Gabrilovich, D.I. (2006). All-trans-retinoic acid improves differentiation of myeloid cells and immune response in cancer patients. Cancer Res *66*, 9299–9307. 10.1158/0008-5472.CAN-06-1690.

172. Guha, P., Gardell, J., Darpolor, J., Cunetta, M., Lima, M., Miller, G., Espat, N.J., Junghans, R.P., and Katz, S.C. (2019). STAT3 inhibition induces Bax-dependent apoptosis in liver tumor myeloid-derived suppressor cells. Oncogene *38*, 533–548. 10.1038/S41388-018-0449-Z.

173. De Santo, C., Serafini, P., Marigo, I., Dolcetti, L., Bolla, M., Del Soldato, P., Melani, C., Guiducci, C., Colombo, M.P., Iezzi, M., et al. (2005). Nitroaspirin corrects immune dysfunction in tumor-bearing hosts and promotes tumor eradication by cancer vaccination. Proc Natl Acad Sci U S A *102*, 4185–4190. 10.1073/PNAS.0409783102.

174. Serafini, P., Meckel, K., Kelso, M., Noonan, K., Califano, J., Koch, W., Dolcetti, L., Bronte, V., and Borrello, I. (2006). Phosphodiesterase-5 inhibition augments endogenous antitumor immunity by reducing myeloid-derived suppressor cell function. J Exp Med *203*, 2691–2702. 10.1084/JEM.20061104.

175. Tumeh, P.C., Harview, C.L., Yearley, J.H., Shintaku, I.P., Taylor, E.J.M., Robert, L., Chmielowski, B., Spasic, M., Henry, G., Ciobanu, V., et al. (2014). PD-1 blockade induces responses by inhibiting adaptive immune resistance. Nature *515*, 568–571. 10.1038/NATURE13954.

176. Liu, J., Fu, M., Wang, M., Wan, D., Wei, Y., and Wei, X. (2022). Cancer vaccines as promising immuno-therapeutics: platforms and current progress. Journal of Hematology & Oncology 2022 15:1 *15*, 1–26. 10.1186/S13045-022-01247-X.

177. Tran, T., Blanc, C., Granier, C., Saldmann, A., Tanchot, C., and Tartour, E. (2018). Therapeutic cancer vaccine: building the future from lessons of the past. Semin Immunopathol. 10.1007/s00281-018-0691-z.

178. Corbière, V., Chapiro, J., Stroobant, V., Ma, W., Lurquin, C., Lethé, B., Van Baren, N., Van Den Eynde, B.J., Boon, T., and Coulie, P.G. (2011). Antigen spreading contributes to MAGE vaccination-induced regression of melanoma metastases. Cancer Res *71*, 1253–1262. 10.1158/0008-5472.CAN-10-2693/649561/AM/ANTIGEN-SPREADING-CONTRIBUTES-TO-MAGE-VACCINATION.

179. McAuliffe, J., Chan, H.F., Noblecourt, L., Ramirez-Valdez, R.A., Pereira-Almeida, V., Zhou, Y., Pollock, E., Cappuccini, F., Redchenko, I., Hill, A.V.S., et al. (2021). Heterologous prime-boost vaccination targeting MAGE-type antigens promotes tumor T-cell infiltration and improves checkpoint blockade therapy. J Immunother Cancer *9*, e003218. 10.1136/JITC-2021-003218.

180. Shibata, T., Lieblong, B.J., Sasagawa, T., and Nakagawa, M. (2019). The promise of combining cancer vaccine and checkpoint blockade for treating HPV-related cancer. Cancer Treat Rev *78*, 8–16. 10.1016/j.ctrv.2019.07.001.

181. Cappuccini, F., Stribbling, S., Pollock, E., Hill, A.V.S., and Redchenko, I. (2016). Immunogenicity and efficacy of the novel cancer vaccine based on simian adenovirus and MVA vectors alone and in combination with PD-1 mAb in a mouse model of prostate cancer. Cancer Immunology, Immunotherapy *65*, 701–713. 10.1007/S00262-016-1831-8/FIGURES/6.

182. Hollingsworth, R.E., and Jansen, K. (2019). Turning the corner on therapeutic cancer vaccines. npj Vaccines 2019 4:1 *4*, 1–10. 10.1038/s41541-019-0103-y.

183. Saxena, M., van der Burg, S.H., Melief, C.J.M., and Bhardwaj, N. (2021). Therapeutic cancer vaccines. Nature Reviews Cancer 2021 21:6 *21*, 360–378. 10.1038/s41568-021-00346-0.

184. Cheever, M.A., and Higano, C.S. (2011). PROVENGE (Sipuleucel-T) in prostate cancer: the first FDA-approved therapeutic cancer vaccine. Clin Cancer Res *17*, 3520–3526. 10.1158/1078-0432.CCR-10-3126.

185. Gilbert, S.C. (2012). T-cell-inducing vaccines – what's the future. Immunology *135*, 19. 10.1111/J.1365-2567.2011.03517.X.

186. Rollier, C.S., Reyes-Sandoval, A., Cottingham, M.G., Ewer, K., and Hill, A.V.S. (2011). Viral vectors as vaccine platforms: deployment in sight. Curr Opin Immunol *23*, 377–382. 10.1016/J.COI.2011.03.006.

187. van Montfoort, N., van der Aa, E., and Woltman, A.M. (2014). Understanding MHC Class I Presentation of Viral Antigens by Human Dendritic Cells as a Basis for Rational Design of Therapeutic Vaccines. Front Immunol *5*. 10.3389/FIMMU.2014.00182.

188. Albert, M.L., Sauter, B., and Bhardwaj, N. (1998). Dendritic cells acquire antigen from apoptotic cells and induce class I-restricted CTLs. Nature *392*, 86–89. 10.1038/32183.

189. Dolan, B.P., Gibbs, K.D., and Ostrand-Rosenberg, S. (2006). Dendritic cells cross-dressed with peptide MHC class I complexes prime CD8+ T cells. J Immunol *177*, 6018–6024. 10.4049/JIMMUNOL.177.9.6018.

190. Capone, S., D'Alise, A.M., Ammendola, V., Colloca, S., Cortese, R., Nicosia, A., and Folgori, A. (2014). Development of chimpanzee adenoviruses as vaccine vectors: challenges and successes emerging from clinical trials. http://dx.doi.org/10.1586/erv.13.15 *12*, 379–393. 10.1586/ERV.13.15.

191. Ewer, K.J., O'Hara, G.A., Duncan, C.J.A., Collins, K.A., Sheehy, S.H., Reyes-Sandoval, A., Goodman, A.L., Edwards, N.J., Elias, S.C., Halstead, F.D., et al. (2013). Protective CD8+ T-cell immunity to human malaria induced by chimpanzee adenovirus-MVA immunisation. Nat Commun *4*, 2836. 10.1038/ncomms3836.

192. Nwanegbo, E., Vardas, E., Gao, W., Whittle, H., Sun, H., Rowe, D., Robbins, P.D., and Gambotto, A. (2004). Prevalence of neutralizing antibodies to adenoviral serotypes 5 and 35 in the adult populations of The Gambia, South Africa, and the United States. Clin Diagn Lab Immunol *11*, 351–357. 10.1128/CDLI.11.2.351-357.2004.

193. Ersching, J., Hernandez, M.I.M., Cezarotto, F.S., Ferreira, J.D.S., Martins, A.B., Switzer, W.M., Xiang, Z., Ertl, H.C.J., Zanetti, C.R., and Pinto, A.R. (2010). Neutralizing antibodies to human and simian adenoviruses in humans and New-World monkeys. Virology *407*, 1–6. 10.1016/J.VIROL.2010.07.043.

194. Colloca, S., Barnes, E., Folgori, A., Ammendola, V., Capone, S., Cirillo, A., Siani, L., Naddeo, M., Grazioli, F., Esposito, M.L., et al. (2012). Vaccine vectors derived from a large collection of simian adenoviruses induce potent cellular immunity across multiple species. Sci Transl Med *4*. 10.1126/SCITRANSLMED.3002925.

195. Dicks, M.D.J., Spencer, A.J., Edwards, N.J., Wadell, G., Bojang, K., Gilbert, S.C., Hill, A.V.S., and Cottingham, M.G. (2012). A Novel Chimpanzee Adenovirus Vector with Low Human Seroprevalence: Improved Systems for Vector Derivation and Comparative Immunogenicity. PLoS One *7*, e40385. 10.1371/JOURNAL.PONE.0040385.

196. Volz, A., and Sutter, G. (2017). Modified Vaccinia Virus Ankara: History, Value in Basic Research, and Current Perspectives for Vaccine Development. Adv Virus Res *97*, 187–243. 10.1016/BS.AIVIR.2016.07.001.

197. Reyes-Sandoval, A., Berthoud, T., Alder, N., Siani, L., Gilbert, S.C., Nicosia, A., Colloca, S., Cortese, R., and Hill, A.V.S. (2010). Prime-boost immunization with

adenoviral and modified vaccinia virus Ankara vectors enhances the durability and polyfunctionality of protective malaria CD8+ T-cell responses. Infect Immun *78*, 145–153. 10.1128/IAI.00740-09.

198. Alharbi, N.K., Padron-Regalado, E., Thompson, C.P., Kupke, A., Wells, D., Sloan, M.A., Grehan, K., Temperton, N., Lambe, T., Warimwe, G., et al. (2017). ChAdOx1 and MVA based vaccine candidates against MERS-CoV elicit neutralising antibodies and cellular immune responses in mice. Vaccine *35*, 3780–3788. 10.1016/J.VACCINE.2017.05.032.

199. Chinnakannan, S.K., Cargill, T.N., Donnison, T.A., Ansari, M.A., Sebastian, S., Lee, L.N., Hutchings, C., Klenerman, P., Maini, M.K., Evans, T., et al. (2020). The Design and Development of a Multi-HBV Antigen Encoded in Chimpanzee Adenoviral and Modified Vaccinia Ankara Viral Vectors; A Novel Therapeutic Vaccine Strategy against HBV. Vaccines (Basel) *8*. 10.3390/VACCINES8020184.

200. McMahon, M., Arunkumar, G.A., Liu, W.C., Stadlbauer, D., Albrecht, R.A., Pavot, V., Aramouni, M., Lambe, T., Gilbert, S.C., and Krammer, F. (2019). Vaccination With Viral Vectors Expressing Chimeric Hemagglutinin, NP and M1 Antigens Protects Ferrets Against Influenza Virus Challenge. Front Immunol *10*. 10.3389/FIMMU.2019.02005.

201. Gilbert, S.C., Schneider, J., Hannan, C.M., Hu, J.T., Plebanski, M., Sinden, R., and Hill, A.V.S. (2002). Enhanced CD8 T cell immunogenicity and protective efficacy in a mouse malaria model using a recombinant adenoviral vaccine in heterologous prime-boost immunisation regimes. Vaccine *20*, 1039–1045. 10.1016/S0264-410X(01)00450-9.

202. Cappuccini, F., Bryant, R., Pollock, E., Carter, L., Verrill, C., Hollidge, J., Poulton, I., Baker, M., Mitton, C., Baines, A., et al. (2020). Safety and immunogenicity of novel 5T4 viral vectored vaccination regimens in early stage prostate cancer: a phase I clinical trial. J Immunother Cancer *8*. 10.1136/JITC-2020-000928.

203. Sorensen, M.R., Holst, P.J., Pircher, H., Christensen, J.P., and Thomsen, A.R. (2009). Vaccination with an adenoviral vector encoding the tumor antigen directly linked to invariant chain induces potent CD4(+) T-cell-independent CD8(+) T-cell-mediated tumor control. Eur J Immunol *39*, 2725–2736. 10.1002/EJI.200939543.

204. Halbroth, B.R., Sebastian, S., Poyntz, H.C., Bregu, M., Cottingham, M.G., Hill, A.V.S., and Spencer, A.J. (2018). Development of a Molecular Adjuvant to Enhance Antigen-Specific CD8+ T Cell Responses. Sci Rep *8*. 10.1038/S41598-018-33375-1.

205. Esposito, I., Cicconi, P., D'Alise, A.M., Brown, A., Esposito, M., Swadling, L., Holst, P.J., Bassi, M.R., Stornaiuolo, M., Mori, F., et al. (2020). MHC class II invariant chain-adjuvanted viral vectored vaccines enhances T cell responses in

humans. Sci Transl Med *12*, 7715. 10.1126/SCITRANSLMED.AAZ7715/SUPPL_FILE/AAZ7715_SM.PDF.

206. Emens, L.A., and Middleton, G. (2015). The Interplay of Immunotherapy and Chemotherapy: Harnessing Potential Synergies. Cancer Immunol Res *3*, 436. 10.1158/2326-6066.CIR-15-0064.

207. Melief, C.J.M., Welters, M.J.P., Vergote, I., Kroep, J.R., Kenter, G.G., Ottevanger, P.B., Tjalma, W.A.A., Denys, H., Van Poelgeest, M.I.E., Nijman, H.W., et al. (2020). Strong vaccine responses during chemotherapy are associated with prolonged cancer survival. Sci Transl Med *12*. 10.1126/SCITRANSLMED.AAZ8235.

208. Reinhard, K., Rengstl, B., Oehm, P., Michel, K., Billmeier, A., Hayduk, N., Klein, O., Kuna, K., Ouchan, Y., Wöll, S., et al. (2020). An RNA vaccine drives expansion and efficacy of claudin-CAR-T cells against solid tumors. Science *367*, 446–453. 10.1126/SCIENCE.AAY5967.

209. Al-Haideri, M., Tondok, S.B., Safa, S.H., maleki, A.H., Rostami, S., Jalil, A.T., Al-Gazally, M.E., Alsaikhan, F., Rizaev, J.A., Mohammad, T.A.M., et al. (2022). CAR-T cell combination therapy: the next revolution in cancer treatment. Cancer Cell Int *22*, 1–26. 10.1186/S12935-022-02778-6/TABLES/4.

210. Paz-Ares, L., Luft, A., Vicente, D., Tafreshi, A., Gümüş, M., Mazières, J., Hermes, B., Çay Şenler, F., Csőszi, T., Fülöp, A., et al. (2018). Pembrolizumab plus Chemotherapy for Squamous Non–Small-Cell Lung Cancer. New England Journal of Medicine *379*, 2040–2051. 10.1056/NEJMOA1810865/SUPPL_FILE/NEJMOA1810865_DATA-SHARING.PDF.

211. Verma, V., Shrimali, R.K., Ahmad, S., Dai, W., Wang, H., Lu, S., Nandre, R., Gaur, P., Lopez, J., Sade-Feldman, M., et al. (2019). PD-1 blockade in subprimed CD8 cells induces dysfunctional PD-1+CD38hi cells and anti-PD-1 resistance. Nature Immunology 2019 20:9 *20*, 1231–1243. 10.1038/s41590-019-0441-y.

212. Wolpoe, M.E., Lutz, E.R., Ercolini, A.M., Murata, S., Ivie, S.E., Garrett, E.S., Emens, L.A., Jaffee, E.M., and Reilly, R.T. (2003). HER-2/neu-Specific Monoclonal Antibodies Collaborate with HER-2/neu-Targeted Granulocyte Macrophage Colony-Stimulating Factor Secreting Whole Cell Vaccination to Augment CD8+ T Cell Effector Function and Tumor-Free Survival in Her-2/ neu - Transgenic Mice . The Journal of Immunology *171*, 2161–2169. 10.4049/jimmunol.171.4.2161.

213. Moschella, F., Valentini, M., Aricò, E., Macchia, I., Sestili, P., D'Urso, M.T., Alessandri, C., Belardelli, F., and Proietti, E. (2011). Unraveling cancer chemoimmunotherapy mechanisms by gene and protein expression profiling of

responses to cyclophosphamide. Cancer Res *71*, 3528–3539. 10.1158/0008-5472.CAN-10-4523.

214. Schlom, J. (2012). Therapeutic Cancer Vaccines: Current Status and Moving Forward. JNCI Journal of the National Cancer Institute *104*, 599. 10.1093/JNCI/DJS033.

215. Haen, S.P., Löffler, M.W., Rammensee, H.G., and Brossart, P. (2020). Towards new horizons: characterization, classification and implications of the tumour antigenic repertoire. Nature Reviews Clinical Oncology 2020 17:10 *17*, 595–610. 10.1038/s41571-020-0387-x.

216. Lonchay, C., Van Der Bruggen, P. Der, Connerotte, T., Hanagiri, T., Coulie, P., Colau, D., Lucas, S., Van Pel, A., Thielemans, K., Van Baren, N., et al. (2004). Correlation between tumor regression and T cell responses in melanoma patients vaccinated with a MAGE antigen. Proceedings of the National Academy of Sciences *101*, 14631–14638. 10.1073/PNAS.0405743101.

217. Jiang, Y., Li, Y., and Zhu, B. (2015). T-cell exhaustion in the tumor microenvironment. Cell Death & Disease 2015 6:6 *6*, e1792–e1792. 10.1038/cddis.2015.162.

218. Wang, X., Bao, Z., Zhang, X., Li, F., Lai, T., Cao, C., Chen, Z., Li, W., Shen, H., and Ying, S. (2017). Effectiveness and safety of PD-1/PD-L1 inhibitors in the treatment of solid tumors: a systematic review and meta-analysis. Oncotarget *8*, 59901. 10.18632/ONCOTARGET.18316.

219. Wang, X., Teng, F., Kong, L., and Yu, J. (2016). PD-L1 expression in human cancers and its association with clinical outcomes. Onco Targets Ther *9*, 5023. 10.2147/OTT.S105862.

220. Wu, M., Huang, Q., Xie, Y., Wu, X., Ma, H., Zhang, Y., and Xia, Y. (2022). Improvement of the anticancer efficacy of PD-1/PD-L1 blockade via combination therapy and PD-L1 regulation. Journal of Hematology & Oncology 2022 15:1 *15*, 1–58. 10.1186/S13045-022-01242-2.

221. Langer, C.J., Gadgeel, S.M., Borghaei, H., Papadimitrakopoulou, V.A., Patnaik, A., Powell, S.F., Gentzler, R.D., Martins, R.G., Stevenson, J.P., Jalal, S.I., et al. (2016). Carboplatin and pemetrexed with or without pembrolizumab for advanced, non-squamous non-small-cell lung cancer: a randomised, phase 2 cohort of the open-label KEYNOTE-021 study. Lancet Oncol *17*, 1497. 10.1016/S1470-2045(16)30498-3.

222. Wang, Z., Till, B., and Gao, Q. (2017). Chemotherapeutic agent-mediated elimination of myeloid-derived suppressor cells. Oncoimmunology *6*. 10.1080/2162402X.2017.1331807.

223. Hanoteau, A., Henin, C., Svec, D., Bisilliat Donnet, C., Denanglaire, S., Colau, D., Romero, P., Leo, O., van den Eynde, B., and Moser, M. (2017). Cyclophosphamide treatment regulates the balance of functional/exhausted tumor-specific CD8+ T cells. Oncoimmunology *6*. 10.1080/2162402X.2017.1318234.

224. Bhat, P., Leggatt, G., Waterhouse, N., and Frazer, I.H. (2017). Interferon-γ derived from cytotoxic lymphocytes directly enhances their motility and cytotoxicity. Cell Death Dis *8*, e2836. 10.1038/CDDIS.2017.67.

225. Lethé, B., van den Eynde, B., van Pel, A., Corradin, G., and Boon, T. (1992). Mouse tumor rejection antigens P815A and P815B: two epitopes carried by a single peptide. Eur J Immunol *22*, 2283–2288. 10.1002/EJI.1830220916.

226. Jung, S., and Baek, J.H. (2021). The Potential of T Cell Factor 1 in Sustaining CD8+ T Lymphocyte-Directed Anti-Tumor Immunity. Cancers (Basel) *13*, 1–17. 10.3390/CANCERS13030515.

227. Danilo, M., Chennupati, V., Silva, J.G., Siegert, S., and Held, W. (2018). Suppression of Tcf1 by Inflammatory Cytokines Facilitates Effector CD8 T Cell Differentiation. Cell Rep *22*, 2107–2117. 10.1016/J.CELREP.2018.01.072.

228. Schenkel, J.M., Herbst, R.H., Canner, D., Li, A., Hillman, M., Shanahan, S.L., Gibbons, G., Smith, O.C., Kim, J.Y., Westcott, P., et al. (2021). Conventional type I dendritic cells maintain a reservoir of proliferative tumor-antigen specific TCF-1+ CD8+ T cells in tumor-draining lymph nodes. Immunity *54*, 2338-2353.e6. 10.1016/J.IMMUNI.2021.08.026.

229. Connolly, K.A., Kuchroo, M., Venkat, A., Khatun, A., Wang, J., William, I., Hornick, N.I., Fitzgerald, B.L., Damo, M., Kasmani, M.Y., et al. (2021). A reservoir of stem-like CD8+ T cells in the tumor-draining lymph node preserves the ongoing antitumor immune response. Sci Immunol *6*, 7836. 10.1126/SCIIMMUNOL.ABG7836/SUPPL_FILE/SCIIMMUNOL.ABG7836_TABLE_S2.ZIP.

230. Anani, W., and Shurin, M.R. (2017). Targeting Myeloid-Derived Suppressor Cells in Cancer. In (Springer, Cham), pp. 105–128. 10.1007/978-3-319-67577-0_8.

231. Gabrilovich, D.I., and Nagaraj, S. (2009). Myeloid-derived-suppressor cells as regulators of the immune system. Nat Rev Immunol *9*, 162. 10.1038/NRI2506.

232. Caldwell, R.B., Toque, H.A., Narayanan, S.P., and Caldwell, R.W. (2015). Arginase: an old enzyme with new tricks. Trends Pharmacol Sci *36*, 395–405. 10.1016/j.tips.2015.03.006.

233. Fleming, V., Hu, X., Weber, R., Nagibin, V., Groth, C., Altevogt, P., Utikal, J., and Umansky, V. (2018). Targeting Myeloid-Derived Suppressor Cells to Bypass

Tumor-Induced Immunosuppression. Front Immunol *9*. 10.3389/FIMMU.2018.00398.

234. Clavijo, P.E., Friedman, J., Robbins, Y., Moore, E.C., Smith, E., Zauderer, M., Evans, E.E., and Allen, C.T. (2019). Semaphorin4D inhibition improves response to immune-checkpoint blockade via attenuation of MDSC recruitment and function. Cancer Immunol Res *7*, 282–291. 10.1158/2326-6066.CIR-18-0156.

235. Sun, L., Clavijo, P.E., Robbins, Y., Patel, P., Friedman, J., Greene, S., Das, R., Silvin, C., Van Waes, C., Horn, L.A., et al. (2019). Inhibiting myeloid-derived suppressor cell trafficking enhances T cell immunotherapy. JCI Insight *4*. 10.1172/JCI.INSIGHT.126853.

236. Yang, J., Yan, C., Vilgelm, A.E., Chen, S.C., Ayers, G.D., Johnson, C.A., and Richmond, A. (2021). Targeted deletion of CXCR2 in myeloid cells alters the tumor immune environment to improve antitumor immunity. Cancer Immunol Res *9*, 200–213. 10.1158/2326-6066.CIR-20-0312.

237. Stemberger, C., Neuenhahn, M., Gebhardt, F.E., Schiemann, M., Buchholz, V.R., and Busch, D.H. (2009). Stem cell-like plasticity of naïve and distinct memory CD8+ T cell subsets. Semin Immunol *21*, 62–68. 10.1016/J.SMIM.2009.02.004.

238. Jeannet, G., Boudousquié, C., Gardiol, N., Kang, J., Huelsken, J., and Held, W. (2010). Essential role of the Wnt pathway effector Tcf-1 for the establishment of functional CD8 T cell memory. Proc Natl Acad Sci U S A *107*, 9777–9782. 10.1073/PNAS.0914127107/SUPPL_FILE/PNAS.200914127SI.PDF.

239. Chandrasekaran, S., Funk, C.R., Kleber, T., Paulos, C.M., Shanmugam, M., and Waller, E.K. (2021). Strategies to Overcome Failures in T-Cell Immunotherapies by Targeting PI3K-δ and –γ. Front Immunol *12*, 3406. 10.3389/FIMMU.2021.718621/BIBTEX.

240. Vankerckhoven, A., Baert, T., Riva, M., De Bruyn, C., Thirion, G., Vandenbrande, K., Ceusters, J., Vergote, I., and Coosemans, A. (2021). Type of chemotherapy has substantial effects on the immune system in ovarian cancer. Transl Oncol *14*, 101076. 10.1016/J.TRANON.2021.101076.

241. Rose, S., Misharin, A., and Perlman, H. (2012). A novel Ly6C/Ly6G-based strategy to analyze the mouse splenic myeloid compartment. Cytometry Part A *81 A*, 343–350. 10.1002/cyto.a.22012.

242. Ye, Z., Gould, T.M., Zhang, H., Jin, J., Weyand, C.M., and Goronzy, J.J. (2021). The GSK3β-β-catenin-TCF1 pathway improves naive T cell activation in old adults by upregulating miR-181a. npj Aging and Mechanisms of Disease 2021 7:1 *7*, 1–9. 10.1038/s41514-021-00056-9.

243. Yi, L., and Yang, L. (2022). Stem-like T cells and niches: Implications in human health and disease. Front Immunol *13*, 4624. 10.3389/FIMMU.2022.907172/BIBTEX.

244. Jiang, W., He, Y., He, W., Wu, G., Zhou, X., Sheng, Q., Zhong, W., Lu, Y., Ding, Y., Lu, Q., et al. (2020). Exhausted CD8+T Cells in the Tumor Immune Microenvironment: New Pathways to Therapy. Front Immunol *11*. 10.3389/FIMMU.2020.622509.

245. van Loosdregt, J., and Coffer, P.J. (2018). The Role of WNT Signaling in Mature T Cells: T Cell Factor Is Coming Home. The Journal of Immunology *201*, 2193–2200. 10.4049/JIMMUNOL.1800633.

246. Harbour, S.N., Maynard, C.L., Zindl, C.L., Schoeb, T.R., and Weaver, C.T. (2015). Th17 cells give rise to Th1 cells that are required for the pathogenesis of colitis. Proc Natl Acad Sci U S A *112*, 7061–7066. 10.1073/PNAS.1415675112/-/DCSUPPLEMENTAL.

247. Gullicksrud, J.A., Li, F., Xing, S., Zeng, Z., Peng, W., Badovinac, V.P., Harty, J.T., and Xue, H.-H. (2017). Differential Requirements for Tcf1 Long Isoforms in CD8+ and CD4+ T Cell Responses to Acute Viral Infection. J Immunol *199*, 911–919. 10.4049/JIMMUNOL.1700595.

248. Xie, C.B., Jane-Wit, D., and Pober, J.S. (2020). Complement Membrane Attack Complex: New Roles, Mechanisms of Action, and Therapeutic Targets. American Journal of Pathology *190*, 1138–1150. 10.1016/J.AJPATH.2020.02.006.

249. Boivin, G., Faget, J., Ancey, P.B., Gkasti, A., Mussard, J., Engblom, C., Pfirschke, C., Contat, C., Pascual, J., Vazquez, J., et al. (2020). Durable and controlled depletion of neutrophils in mice. Nature Communications 2020 11:1 *11*, 1–9. 10.1038/s41467-020-16596-9.

250. Cartwright, J.A., Lucas, C.D., and Rossi, A.G. (2019). Inflammation Resolution and the Induction of Granulocyte Apoptosis by Cyclin-Dependent Kinase Inhibitor Drugs. Front Pharmacol *10*. 10.3389/FPHAR.2019.00055.

251. Stark, M.A., Huo, Y., Burcin, T.L., Morris, M.A., Olson, T.S., and Ley, K. (2005). Phagocytosis of apoptotic neutrophils regulates granulopoiesis via IL-23 and IL-17. Immunity *22*, 285–294. 10.1016/j.immuni.2005.01.011.

252. Liu, Q., and Muruve, D.A. (2003). Molecular basis of the inflammatory response to adenovirus vectors. Gene Therapy 2003 10:11 *10*, 935–940. 10.1038/sj.gt.3302036.

253. Zhu, J., Huang, X., and Yang, Y. (2012). Myeloid-Derived Suppressor Cells Regulate Natural Killer Cell Response to Adenovirus-Mediated Gene Transfer. J Virol *86*, 13689. 10.1128/JVI.01595-12.

254. Quinn, K.M., Zak, D.E., Costa, A., Yamamoto, A., Kastenmuller, K., Hill, B.J., Lynn, G.M., Darrah, P.A., Lindsay, R.W.B., Wang, L., et al. (2015). Antigen expression determines adenoviral vaccine potency independent of IFN and STING signaling. J Clin Invest *125*, 1129–1146. 10.1172/JCI78280.

255. McKeage, M.J. (1995). Comparative Adverse Effect Profiles of Platinum Drugs. Drug Saf *13*, 228–244. 10.2165/00002018-199513040-00003.

256. Siddik, Z.H., Jones, M., Boxall, F.E., and Harrap, K.R. (1988). Comparative distribution and excretion of carboplatin and cisplatin in mice. Cancer Chemother Pharmacol *21*, 19–24. 10.1007/BF00262732.

257. Siddik, Z.H., Newell, D.R., Boxall, F.E., and Harrap, K.R. (1987). The comparative pharmacokinetics of carboplatin and cisplatin in mice and rats. Biochem Pharmacol *36*, 1925–1932. 10.1016/0006-2952(87)90490-4.

258. Fu, C., and Jiang, A. (2018). Dendritic Cells and CD8 T Cell Immunity in Tumor Microenvironment. Front Immunol *9*, 3059. 10.3389/FIMMU.2018.03059/BIBTEX.

259. Jiao, J., Dragomir, A.-C., Kocabayoglu, P., Rahman, A.H., Chow, A., Hashimoto, D., Leboeuf, M., Kraus, T., Moran, T., Carrasco-Avino, G., et al. (2014). Central role of conventional dendritic cells in regulation of bone marrow release and survival of neutrophils. J Immunol *192*, 3374–3382. 10.4049/JIMMUNOL.1300237.

260. Saito, Y., Komori, S., Kotani, T., Murata, Y., and Matozaki, T. (2022). The Role of Type-2 Conventional Dendritic Cells in the Regulation of Tumor Immunity. Cancers (Basel) *14*. 10.3390/CANCERS14081976.

261. Boulter, L., Govaere, O., Bird, T.G., Radulescu, S., Ramachandran, P., Pellicoro, A., Ridgway, R.A., Seo, S.S., Spee, B., Van Rooijen, N., et al. (2012). Macrophage derived Wnt signalling opposes Notch signalling in a Numb mediated manner to specify HPC fate in chronic liver disease in human and mouse. Nat Med *18*, 572. 10.1038/NM.2667.

262. Resham, K., and Sharma, S.S. (2019). Pharmacological interventions targeting Wnt/β-catenin signaling pathway attenuate paclitaxel-induced peripheral neuropathy. Eur J Pharmacol *864*, 172714. 10.1016/J.EJPHAR.2019.172714.

263. Fu, Q., Chen, Z., Gong, X., Cai, Y., Chen, Y., Ma, X., Zhu, R., and Jin, J. (2015). β-Catenin expression is regulated by an IRES-dependent mechanism and stimulated by paclitaxel in human ovarian cancer cells. Biochem Biophys Res Commun *461*, 21–27. 10.1016/J.BBRC.2015.03.161.

264. Besseyrias, V., Fiorini, E., Strobl, L.J., Zimber-Strobl, U., Dumortier, A., Koch, U., Arcangeli, M.L., Ezine, S., MacDonald, H.R., and Radtke, F. (2007). Hierarchy

of Notch–Delta interactions promoting T cell lineage commitment and maturation. J Exp Med *204*, 331. 10.1084/JEM.20061442.

265. Felli, M.P., Maroder, M., Mitsiadis, T.A., Campese, A.F., Bellavia, D., Vacca, A., Mann, R.S., Frati, L., Lendahl, U., Gulino, A., et al. (1999). Expression pattern of Notch1, 2 and 3 and Jagged1 and 2 in lymphoid and stromal thymus components: distinct ligand–receptor interactions in intrathymic T cell development. Int Immunol *11*, 1017–1025. 10.1093/INTIMM/11.7.1017.

266. Shi, J., Fallahi, M., Luo, J.L., and Petrie, H.T. (2011). Nonoverlapping functions for Notch1 and Notch3 during murine steady-state thymic lymphopoiesis. Blood *118*, 2511. 10.1182/BLOOD-2011-04-346726.

267. Li, D.Y., Gao, S.J., Sun, J., Zhang, L.Q., Wu, J.Y., Song, F.H., Liu, D.Q., Zhou, Y.Q., and Mei, W. (2022). Notch signaling activation contributes to paclitaxel-induced neuropathic pain via activation of A1 astrocytes. Eur J Pharmacol *928*, 175130. 10.1016/J.EJPHAR.2022.175130.

268. A Trial of ChAdOx1 and MVA Vaccines Against MAGE-A3 and NY-ESO-1 - Full Text View - ClinicalTrials.gov https://clinicaltrials.gov/ct2/show/NCT04908111.

269. Chang, R.B., and Beatty, G.L. (2020). The interplay between innate and adaptive immunity in cancer shapes the productivity of cancer immunosurveillance. J Leukoc Biol *108*, 363. 10.1002/JLB.3MIR0320-475R.

270. Cannizzo, E.S., Bellistrì, G.M., Casabianca, A., Tincati, C., Iannotti, N., Barco, A., Orlandi, C., Monforte, A.D.A., and Marchetti, G. (2015). Immunophenotype and Function of CD38-Expressing CD4+ and CD8+ T Cells in HIV-Infected Patients Undergoing Suppressive Combination Antiretroviral Therapy. J Infect Dis *211*, 1511–1513. 10.1093/INFDIS/JIU634.

271. Chen, P.M., Katsuyama, E., Satyam, A., Li, H., Rubio, J., Jung, S., Andrzejewski, S., Becherer, J.D., Tsokos, M.G., Abdi, R., et al. (2022). CD38 reduces mitochondrial fitness and cytotoxic T cell response against viral infection in lupus patients by suppressing mitophagy. Sci Adv *8*, 4271. 10.1126/SCIADV.ABO4271/SUPPL_FILE/SCIADV.ABO4271_SM.PDF.

272. Kareva, I., Waxman, D.J., and Klement, G.L. (2015). Metronomic chemotherapy: an attractive alternative to maximum tolerated dose therapy that can activate anti-tumor immunity and minimize therapeutic resistance. Cancer Lett *358*, 100. 10.1016/J.CANLET.2014.12.039.

273. Sade-Feldman, M., Yizhak, K., Bjorgaard, S.L., Ray, J.P., de Boer, C.G., Jenkins, R.W., Lieb, D.J., Chen, J.H., Frederick, D.T., Barzily-Rokni, M., et al. (2018). Defining T Cell States Associated with Response to Checkpoint Immunotherapy in Melanoma. Cell *175*, 998-1013.e20. 10.1016/J.CELL.2018.10.038.

274. Zhu, Y., Wang, W., and Wang, X. (2015). Roles of transcriptional factor 7 in production of inflammatory factors for lung diseases. J Transl Med *13*, 1–13. 10.1186/S12967-015-0617-7/FIGURES/7.

275. Zhao, D.-M., Yu, S., Zhou, X., Haring, J.S., Held, W., Badovinac, V.P., Harty, J.T., and Xue, H.-H. (2010). Constitutive activation of Wnt signaling favors generation of memory CD8 T cells. J Immunol *184*, 1191–1199. 10.4049/JIMMUNOL.0901199.

276. Ma, J., Wang, R., Fang, X., and Sun, Z. (2012). β-catenin/TCF-1 pathway in T cell development and differentiation. J Neuroimmune Pharmacol *7*, 750–762. 10.1007/S11481-012-9367-Y.

277. Kurtulus, S., Madi, A., Escobar, G., Klapholz, M., Nyman, J., Christian, E., Pawlak, M., Dionne, D., Xia, J., Rozenblatt-Rosen, O., et al. (2019). Checkpoint blockade immunotherapy induces dynamic changes in PD-1−CD8+ tumor-infiltrating T cells. Immunity *50*, 181. 10.1016/J.IMMUNI.2018.11.014.

278. Tabanelli, V., Melle, F., Motta, G., Mazzara, S., Fabbri, M., Agostinelli, C., Calleri, A., Corvo, M. Del, Fiori, S., Lorenzini, D., et al. (2022). The identification of TCF1+ progenitor exhausted T cells in THRLBCL may predict a better response to PD-1/PD-L1 blockade. Blood Adv *6*, 4634–4644. 10.1182/BLOODADVANCES.2022007046.

279. Piedra-Quintero, Z.L., Wilson, Z., Nava, P., and Guerau-de-Arellano, M. (2020). CD38: An Immunomodulatory Molecule in Inflammation and Autoimmunity. Front Immunol *11*, 3111. 10.3389/FIMMU.2020.597959/BIBTEX.

280. Li, W., Liang, L., Liao, Q., Li, Y., and Zhou, Y. (2022). CD38: An important regulator of T cell function. Biomedicine & Pharmacotherapy *153*, 113395. 10.1016/J.BIOPHA.2022.113395.

281. Wu, Y., Yi, M., Niu, M., Mei, Q., and Wu, K. (2022). Myeloid-derived suppressor cells: an emerging target for anticancer immunotherapy. Molecular Cancer 2022 21:1 *21*, 1–19. 10.1186/S12943-022-01657-Y.

282. Li, T., Liu, T., Zhu, W., Xie, S., Zhao, Z., Feng, B., Guo, H., and Yang, R. (2021). Targeting MDSC for Immune-Checkpoint Blockade in Cancer Immunotherapy: Current Progress and New Prospects. https://doi.org/10.1177/11795549211035540 *15*. 10.1177/11795549211035540.

283. Pais Ferreira, D., Silva, J.G., Wyss, T., Fuertes Marraco, S.A., Scarpellino, L., Charmoy, M., Maas, R., Siddiqui, I., Tang, L., Joyce, J.A., et al. (2020). Central memory CD8+ T cells derive from stem-like Tcf7hi effector cells in the absence of cytotoxic differentiation. Immunity *53*, 985-1000.e11. 10.1016/J.IMMUNI.2020.09.005.

284. Utzschneider, D.T., Charmoy, M., Chennupati, V., Pousse, L., Ferreira, D.P., Calderon-Copete, S., Danilo, M., Alfei, F., Hofmann, M., Wieland, D., et al. (2016). T Cell Factor 1-Expressing Memory-like CD8+ T Cells Sustain the Immune Response to Chronic Viral Infections. Immunity *45*, 415–427. 10.1016/J.IMMUNI.2016.07.021.

285. Zhang, K., Erkan, E.P., Jamalzadeh, S., Dai, J., Andersson, N., Kaipio, K., Lamminen, T., Mansuri, N., Huhtinen, K., Carpén, O., et al. (2022). Longitudinal single-cell RNA-seq analysis reveals stress-promoted chemoresistance in metastatic ovarian cancer. Sci Adv *8*, 1831. 10.1126/SCIADV.ABM1831/SUPPL_FILE/SCIADV.ABM1831_DATA_S1_AND_S2.ZIP.

286. Khing, T.M., Choi, W.S., Kim, D.M., Po, W.W., Thein, W., Shin, C.Y., and Sohn, U.D. (2021). The effect of paclitaxel on apoptosis, autophagy and mitotic catastrophe in AGS cells. Scientific Reports 2021 11:1 *11*, 1–19. 10.1038/s41598-021-02503-9.

287. Shen, B., Mao, W., Ahn, J.C., Chung, P.S., and He, P. (2018). Mechanism of HN-3 cell apoptosis induced by carboplatin: Combination of mitochondrial pathway associated with Ca2+ and the nucleus pathways. Mol Med Rep *18*, 4978. 10.3892/MMR.2018.9507.

288. Liu, Y., Debo, B., Li, M., Shi, Z., Sheng, W., and Shi, Y. (2021). LSD1 inhibition sustains T cell invigoration with a durable response to PD-1 blockade. Nature Communications 2021 12:1 *12*, 1–16. 10.1038/s41467-021-27179-7.

289. Verbeek, S., Izon, D., Hofhuis, F., Robanus-Maandag, E., Te Riele, H., Watering, M. Van De, Oosterwegel, M., Wilson, A., Robson MacDonald, H., and Clevers, H. (1995). An HMG-box-containing T-cell factor required for thymocyte differentiation. Nature 1995 374:6517 *374*, 70–74. 10.1038/374070a0.

290. Zhou, X., Yu, S., Zhao, D.M., Harty, J.T., Badovinac, V.P., and Xue, H.H. (2010). Differentiation and Persistence of Memory CD8+ T Cells Depend on T Cell Factor 1. Immunity *33*, 229–240. 10.1016/j.immuni.2010.08.002.

291. Farber, D.L., Yudanin, N.A., and Restifo, N.P. (2013). Human memory T cells: generation, compartmentalization and homeostasis. Nature Reviews Immunology 2013 14:1 *14*, 24–35. 10.1038/nri3567.

292. Warncke, U.O., Toma, W., Meade, J.A., Park, A.J., Thompson, D.C., Caillaud, M., Bigbee, J.W., Bryant, C.D., and Damaj, M.I. (2021). Impact of Dose, Sex, and Strain on Oxaliplatin-Induced Peripheral Neuropathy in Mice. Frontiers in Pain Research *2*, 17. 10.3389/FPAIN.2021.683168.

293. Perše, M. (2021). Cisplatin mouse models: Treatment, toxicity and translatability. Biomedicines *9*. 10.3390/BIOMEDICINES9101406/S1.

294. Aston, W.J., Hope, D.E., Nowak, A.K., Robinson, B.W., Lake, R.A., and Lesterhuis, W.J. (2017). A systematic investigation of the maximum tolerated dose of cytotoxic chemotherapy with and without supportive care in mice. BMC Cancer *17*, 1–10. 10.1186/S12885-017-3677-7/FIGURES/4.

295. Falah, M., Rayan, M., and Rayan, A. (2019). A Novel Paclitaxel Conjugate with Higher Efficiency and Lower Toxicity: A New Drug Candidate for Cancer Treatment. International Journal of Molecular Sciences 2019, Vol. 20, Page 4965 *20*, 4965. 10.3390/IJMS20194965.

296. Jandial, D.D., Messer, K., Farshchi-Heydari, S., Pu, M., and Howell, S.B. (2009). Tumor platinum concentration following intraperitoneal administration of cisplatin versus carboplatin in an ovarian cancer model. Gynecol Oncol *115*, 362. 10.1016/J.YGYNO.2009.08.028.

297. Biziota, E., Mavroeidis, L., Hatzimichael, E., and Pappas, P. (2017). Metronomic chemotherapy: A potent macerator of cancer by inducing angiogenesis suppression and antitumor immune activation. Cancer Lett *400*, 243–251. 10.1016/j.canlet.2016.12.018.

298. Chen, C.A., Ho, C.M., Chang, M.C., Sun, W.Z., Chen, Y.L., Chiang, Y.C., Syu, M.H., Hsieh, C.Y., and Cheng, W.F. (2010). Metronomic chemotherapy enhances antitumor effects of cancer vaccine by depleting regulatory T lymphocytes and inhibiting tumor angiogenesis. Molecular Therapy *18*, 1233–1243. 10.1038/mt.2010.34.

299. Wu, J., and Waxman, D.J. (2015). Metronomic cyclophosphamide eradicates large implanted GL261 gliomas by activating antitumor Cd8+ T-cell responses and immune memory. Oncoimmunology *4*, e1005521. 10.1080/2162402X.2015.1005521.

300. Cazzaniga, M.E., Dionisio, M.R., and Riva, F. (2017). Metronomic chemotherapy for advanced breast cancer patients. Cancer Lett *400*, 252–258. 10.1016/J.CANLET.2016.12.019.

301. Wong, N.S., Buckman, R.A., Clemons, M., Verma, S., Dent, S., Trudeau, M.E., Roche, K., Ebos, J., Kerbel, R., DeBoer, G.E., et al. (2010). Phase I/II trial of metronomic chemotherapy with daily dalteparin and cyclophosphamide, twice-weekly methotrexate, and daily prednisone as therapy for metastatic breast cancer using vascular endothelial growth factor and soluble vascular endothelial growth factor receptor levels as markers of response. J Clin Oncol *28*, 723–730. 10.1200/JCO.2009.24.0143.